Università degli Studi della Calabria

Dipartimenti di Fisica e Chimica

Dottorato Internazionale di Ricerca in
"Scienze e Tecnologie delle Mesofasi e dei Materiali Molecolari"
(STM^3) - Dottorato Internazionale - XIX° ciclo

Tesi di Dottorato

Innovative Electro-Optic and Photonic Effects in Liquid Crystals

Supervisore
Prof. N. Scaramuzza
Prof. G. Strangi

Coordinatore
Prof. M. Longeri

Candidato
Dott. Valentin Barna

Anno Accademico 2005-2006

Contents

Introduction - Outline of the Thesis

As the title announces, the thesis explores some interesting phenomena in liquid crystalline materials physics.

The research activity performed during the Ph.D course was focused on three major topics which are to be discussed individually in the following chapters of this thesis.

Chapter I is an introduction to liquid crystals and illustrates some of their main physical properties.

In Chapter II it is presented and characterized a novel physical phenomenon of ultra-fast electro-optic switching in symmetric\asymmetric nematic liquid crystal cells containing thin duromer films deposited by plasma polymerization technique. A detailed introduction to plasma polymerization technique and to the features of this process is followed by a description of the the experimental investigations. It was found a suitable choice of materials, cell geometries, surface treatments and special ways of applying the electric field that led to a very low switch off response time (of only 0.3-1 ms) which is as fast as that at switch on. Experimental evidences support the concept that a very important role is played by the delocalized electrons in polyaniline-nematogen cyanobiphenyls interaction. On this basis, a model is proposed to explain this unusual elecro-optic behaviour.

Chapter III discusses the design and attributes of distributed feedback organic microstructures for lasing devices.

The first part consists in an overview of the 1D, 2D and 3D photonic crystals properties together with the most interesting phenomena and processes endorsed by these systems such as Bragg diffraction and photonic bandgaps ,distributed feedback (DFB), spontaneous emission and the Purcell effect.

Experimental investigations included the study of light emission properties from confined helixed liquid crystals doped with fluorescent guest molecules in PoLiCryPS structure and in fiber-like cylindrical microcavities.

An ultralow-threshold color-tunable microlaser array was created by embedding dye-doped helixed liquid crystals in holographically sculptured polymeric microchannels (PoLiCryPS) while having directional control on the lasing emission, a fine wavelength tunability and the control over the emission intensity.

The confinement of dye doped helixed liquid crystal in cylindrical microcavities gives rise to a 3D periodical superstructure where the two naturally preferred helical directions (axial and radial) create spontaneously. Low-threshold highly directional laser action was demonstrated both for radial and axial directions. Along with the expected band edge modes it was found that long-lived spectrally narrow laser defect modes survive within the central region of the stop band. This complex system keeps the advantage of a 3D blue phase-like matrix while providing a wider thermal operating range and laser action wavelength tunability.

In Chapter IV a new physical process, dealing with random laser action in a partially ordered, optically anisotropic nematic liquid crystal with long-range dielectric tensor fluctuations is presented and characterized.

The beginning of the chapter presents an outline for the main physical concepts which govern the random lasing world such as Anderson localization of light, enhanced backscattering and gain in random media.

A complete description of the random lasing phenomena and weak localization of light in nematic liquid crystals together with a comparison of the laser action for systems with different order degree (fully disordered semiconductor powders, self-ordered cholesterics and partially ordered nematic liquid crystals) is carried out for the experimental section of the chapter. It is found that weakly localized light waves inside dye doped nematic samples are responsible for amplification of light inside such systems while the resonance frequencies are selected through interference phenomena of the counter-propagating light waves within the localized loops.

Also, it is briefly presented the first experimental evidence of random lasing in free standing and freely suspended dye doped nematic liquid crystal films together with a summary of some of the most interesting experimental results for these systems.

Chapter I

Introduction to liquid crystals

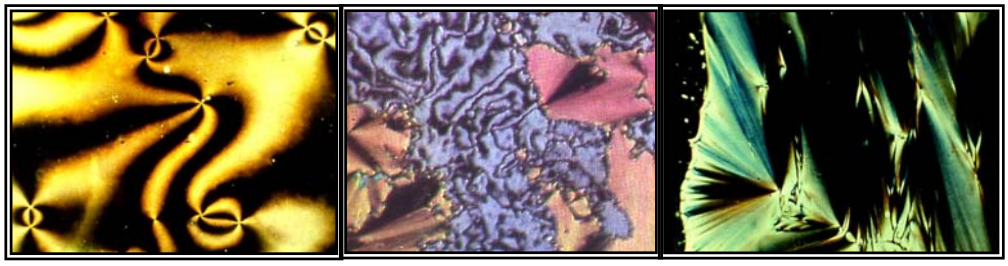

Chapter I

Introduction to liquid crystals

1.1. Introduction to Liquid Crystals

The major part of matter that forms nature can be found in one of the three different states of aggregation: solid, liquid and gas phase. However, there exist some materials which can also be found in the "fourth" one. These materials do not show a direct phase transition from the solid into the liquid phase but rather a cascade of transitions involving new phases.

Condensed matter which exhibit intermediate thermodynamic phases between the crystalline solid and simple liquid state are called liquid crystals or mesophases. Since they look like a liquid and exhibit anisotropic dielectric, magnetic, and optical properties, typical for a crystal, these phases are called liquid crystalline. The main characteristic of these mesophases is that they share properties with the solid as well as the liquid state of matter.

The discovery of liquid crystals goes back to the late nineteenth century, the year 1888, when an Austrian botanist, Friedrich Reinitzer, observed that the material known as cholesteryl benzoate had a two-stage melting. By heating the material, it went from the solid state to an opaque liquid. Then, by further increase of temperature it changed into a transparent liquid. It turned out later that this was the first report on matter we know today as liquid crystals.

After careful microscopic investigation and discussions with Reinitzer, O. Lehman published the first paper on liquid crystals: "*Über fliessende Kristalle"*, Zs. Phys. Chem. 4, 510-514 (1889). At that time, Lehmann thought that he dealt with a real birefringent crystal, but a very unstable one that "it could not even sustain its own weight" [1,2]. However, after 15 years of extensive studies Lehman came to the conclusion that he dealt with liquid crystals. In 1904 he published the first book on liquid crystals ("Die Flüssige Kristalle" – Leipzig) containing the results of his optical studies of anisotropic liquids.

1.2. Classification

Liquid crystals can be classified according to:

(i) their mean of formation: thermotropic (change of temperature and pressure), lyotropic (change of the molecular concentration in water and some other solvents), carbonized (change of polymerization degree), rare special mechanisms (formation of chain structures in some inorganic substances).

The most important categories are thermotropic liquid crystals and lyotropic liquid crystals. These two types of liquid crystals are distinguished by the mechanisms that drive their self-organization, but they are also similar in many ways.

Thermotropic transactions occur in most liquid crystals, and they are defined by the fact that the transitions to the liquid crystalline state are induced thermally. That means that one can arrive at the liquid crystalline state by raising the temperature of a solid and/or lowering the temperature of a liquid. Thermotropic liquid crystals can be classified into two types: enantiotropic liquid crystals, which can be changed into the liquid crystal state from either lowering the temperature of a liquid or raising of the temperature of a solid, and monotropic liquid crystals, which can only be changed into the liquid crystal state from either an increase in the temperature of a solid or a decrease in the temperature of a liquid, but not both. In general, thermotropic

mesophases occur because of anisotropic dispersion forces between the molecules and because of packing interactions.

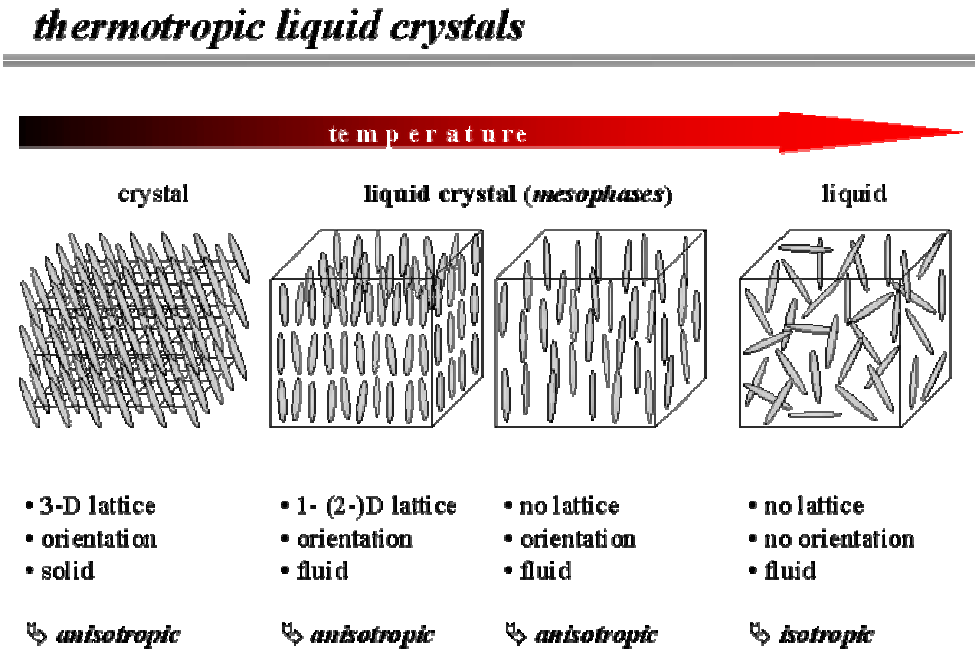

Fig.1.1. Liquid crystalline mesophases between the solid and isotropic liquid phase.

In contrast to thermotropic mesophases, lyotropic liquid crystal transitions occur with the influence of solvents, not by a change in temperature. Lyotropic mesophases occur as a result of solvent-induced aggregation of the constituent mesogens into micellar structures. Lyotropic mesogens are typically amphiphilic, meaning that they are composed of both lyophilic (solvent-attracting) and lyophobic (solvent-repelling) parts. This causes them to form into micellar structures in the presence of a solvent, since the lyophobic ends will stay together as the lyophilic ends extend outward, toward the solution. As the concentration of the solution is increased and the solution is cooled, the micelles increase in size and eventually coalesce. This separates the newly formed liquid crystalline state from the solvent. While thermotropics are presently mostly used for technical applications, lytropics are important for biological systems (e.g. membranes).

(ii) molecular shape

calamitic: 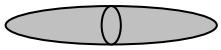 discotic: 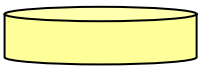 banana: 

etc.

A very large number of chemical compounds are known to exhibit one or several liquid crystalline phases. Despite significant differences in chemical composition, these molecules have some common features in chemical and physical properties. There are two types of thermotropic liquid crystals: discotics and rod-shaped molecules. Discotics are flat disc-like molecules consisting of a core of adjacent aromatic rings. This allows for two dimensional columnar ordering. Rod-shaped molecules have an elongated, anisotropic geometry which allows for preferential alignment along one spatial direction.

(iii) optical properties (uniaxial, biaxial, helical);

(iv) chemical classes (biphenyls, Schiff bases, pyrimidines, tolanes, etc).

(v) the symmetry of a liquid crystalline phase which determines physical properties of the phase.

This classification is a generalization of the one suggested by G.Friedel [3].
Below there is a short description of the most important liquid crystalline phases.

1.3. Liquid Crystalline Phases

Isotropic phase

In the isotropic phase the molecules are randomly aligned and exhibit no long range order [4]. The isotropic phase has a low viscosity and will often appear to be very clear. There is no long range positional or orientational order of the molecules, although this sort of order may exist on very short length scales of order tens of Angstroms, corresponding to a few molecular distances.

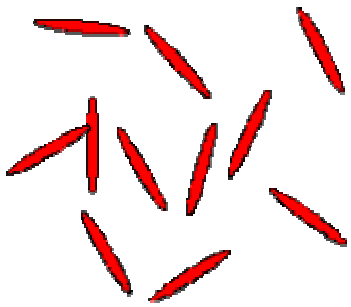

Fig.1.2. Diagram showing the random orientation of molecules in the isotropic phase.

For all practical purposes, the isotropic phase macroscopically appears to be like any other isotropic liquid such as water.

Nematic phase

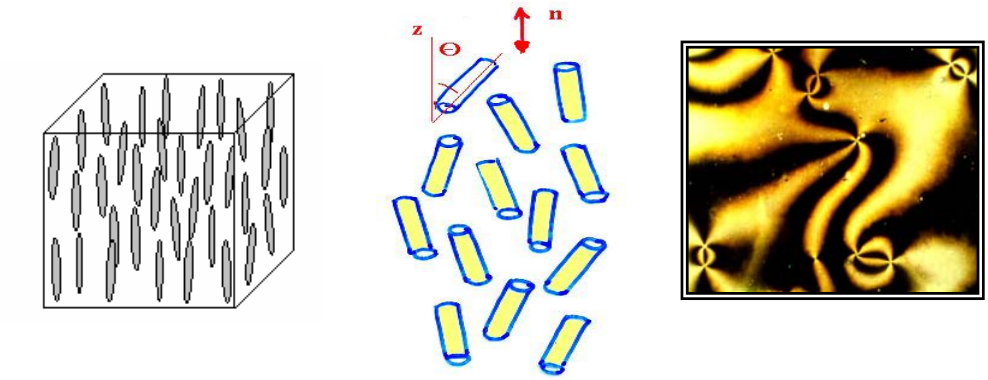

(a) (b)

Fig.1.3. (a) Diagram showing the orientation of molecules in the nematic liquid crystalline phase. (b) Picture showing a typical nematic texture with point disclinations, the nuclei of divergent brushes or threads.

The simplest case, in which the molecules possess only orientational order but no positional long range order is the nematic phase (coming from the greek word nema which means thread). The name of this phase has been given with respect to thread-like textures observed under polarizing microscope. Nematic phase is the first one which is obtained when cooling down from isotropic. The orientations of the molecules are largely "frozen" such that the particles point on average in the same direction. This direction of preferred alignment can be described by a unit vector, the so-called nematic director $\vec{n}$. The orientation of individual molecules may differ from this direction, so that the director must be more correctly defined as the symmetry axis of the orientational distribution. In nematics the distribution function is rotationally symmetric around the director (i.e. they are uniaxial). Usually, the nematic liquid crystals are invariant for an inversion of $\vec{n}$ (meaning that $\vec{n}$ and $-\vec{n}$ states are indistinguishable). The nematic symmetry is present even when the constituent molecules are polar because the molecules form antiparallel pairs to minimize the intermolecular interaction energy (usually originating from Van der Waals force). As consequence of the existence of this privileged axis of orientation, there is a macroscopic anisotropy in many material properties, such as dielectric constants and refractive indices.

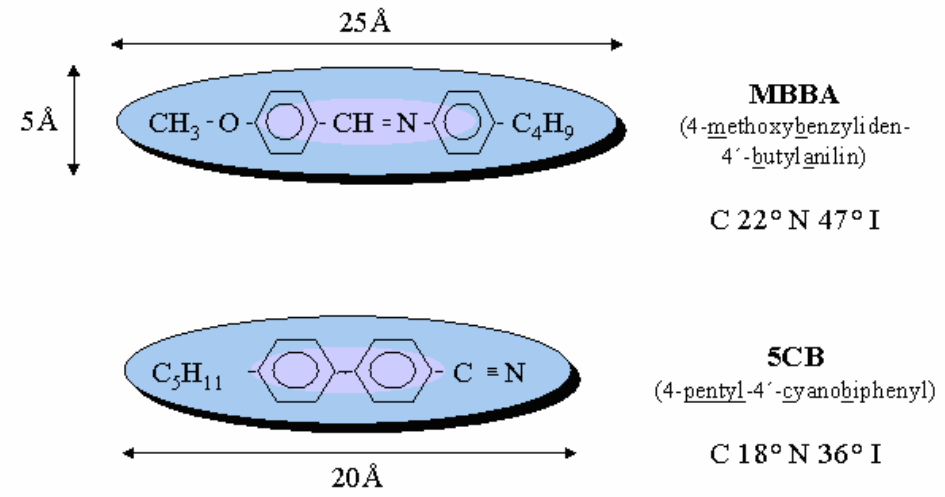

Fig.1.4. Structure of MBBA and 5CB nematic liquid crystals.

In the above figure one can observe the chemical structure for two of the most prominent representatives of rod-like molecules which exhibit liquid crystalline order. MBBA was the first room temperature liquid crystal synthesized in 1969, whereas 5CB was the first member of the optically and chemically stable cyanobiphenyls, one of the most applicable family of liquid crystals, discovered in 1973. Both compounds show the nematic phase at room temperature. The transition temperatures between crystalline (C), nematic (N), and isotropic (I) state are given in Celsius (Fig.1.4).

The nematic phase is the phase which is used in many liquid crystal devices (i.e. the "twisted nematic" cell), because the average orientation may be manipulated with an electric field, and the polarization of light will follow the molecular orientation as it changes through a cell. Typical response times are in the millisecond range.

Smectic A phase

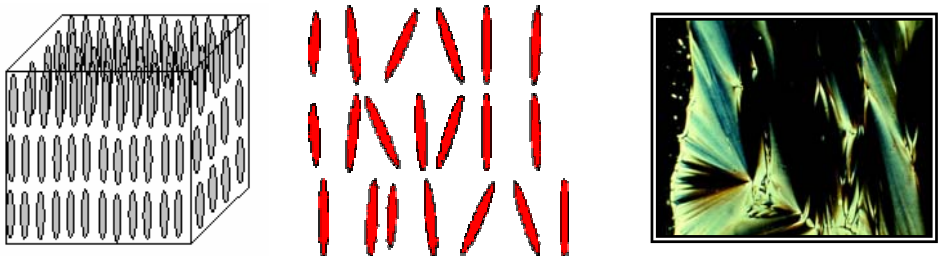

(a) (b)

Fig.1.5. (a) Diagram showing the orientation of molecules in the Smectic A phase. (b) Typical texture of the Smectic A phase - the so-called "fans" consisting of "focal-conic" domains originated from the layered structure.

Apart from the long range orientational order of nematics, the smectic phase has also a unidimensional positional order; the molecules being constrained between parallel plains called "smectic planes". There is no correlation between molecular positions in the neighbouring layers. Smectic A phase is often considered a two dimensional liquid (freedom of molecular motion within the layer) and a quasi one-dimensional solid (hindered translation from one layer to the next). The viscosity is rather high, and this phase is generally not useful for devices [4].

(Tilted) Smectic C phase

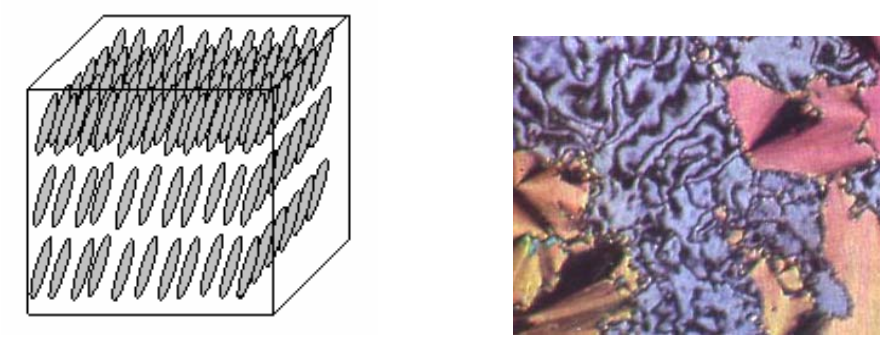

(a) (b)

Fig.1.6. (a) Diagram showing the orientation of molecules in the Smectic C phase. (b) Typical texture of the Smectic C phase.

The difference between the Smectic A and the Smectic C phase is the fact that the LC molecules are tilted with respect to the layers, and the system is now "biaxial" in character.

Smectic B phase

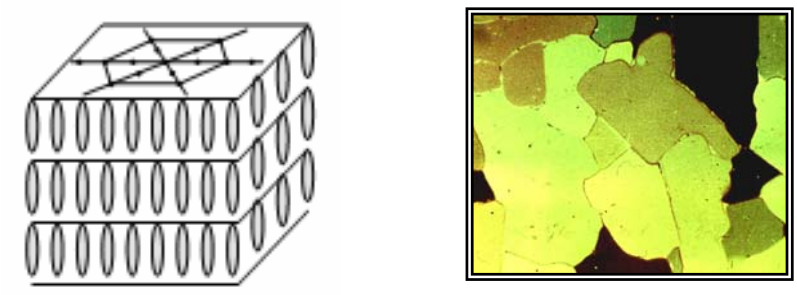

(a) (b)

Fig.1.7. (a) Diagram showing the orientation of molecules in the Smectic B phase. (b) Typical mosaic texture of the Smectic B phase.

The Smectic B phase is characterised by the hexagonal arrangement of the molecules inside the smectic plains.

Chiral nematic or cholesteric phase

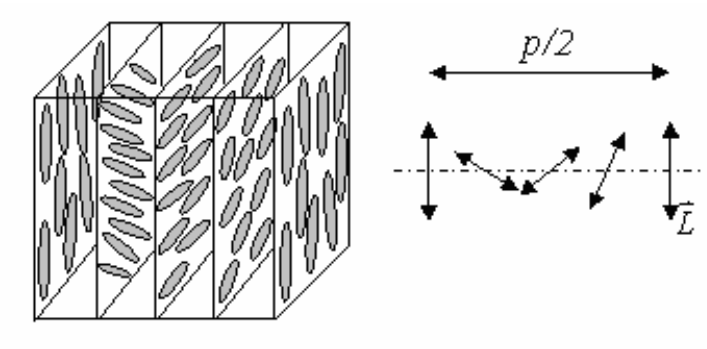

Fig.1.8. Diagram showing the typical orientation of molecules in the cholesteric phase.

The term chirality comes from the Greek word for "hand". Chirality means lack of mirror symmetry. W.H. Thomson (Lord Kelvin) defines chirality as follows: "any geometrical figure has chirality if its image in a plane mirror cannot be brought into coincidence with itself". Unfortunately, there is no quantitative definition. In this phase, the structure of the optically active molecules causes them to be arranged in a twisted way, forming a helical superstructure. The twist can be left or right handed depending on the conformation of the molecule. The cholesteric pitch p represents the length along the twist axis corresponding to a full turn of the nematic director.

Other interesting liquid crystalline phases include the Smectic C* ferroelectric, Smectic C_A , Blue phases etc.

1.4. Liquid Crystal Textures

The term texture refers to the orientation of liquid crystal molecules in the vicinity of a surface [4]. Each liquid crystal mesophase can form its own characteristic textures, which are useful in identification. If mesogenic materials are confined between closely spaced plates with rubbed surfaces and oriented with rubbing directions parallel, the entire (ideal case) liquid crystal sample can be oriented in a planar texture, as shown in the following diagram. Mesogens can also be oriented normal to a surface with the use of appropriate surfactants, or in the presence of an electric field applied normal to the surface (in the case of a material with positive dielectric anisotropy), giving rise to the homeotropic texture, as illustrated below. Other sample geometries such as twisted and super twisted alignments are often employed in display applications.

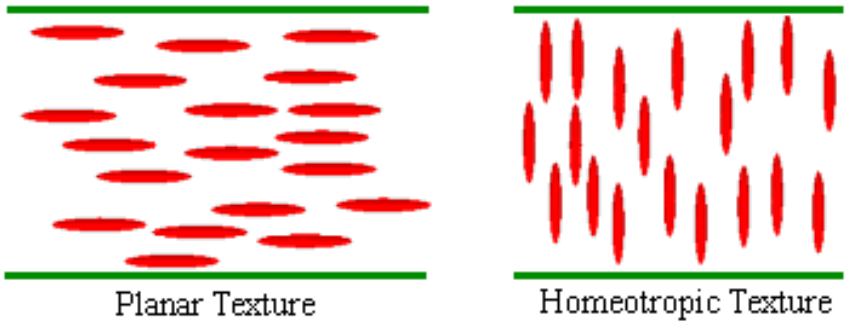

Fig.1.9. Planar and homeotropic textures for a nematic liquid crystal.

1.5. Order Parameter in Nematic Liquid Crystals

A nematic liquid crystal has orientational order and no positional long range order. To be able to analyse quantitatively the degree of order inside the system one makes use of a scalar value called Order Parameter (S). In order to define this factor let us consider a rod like molecule of nematic liquid crystal placed in a Cartesian laboratory

frame of coordinates (x,y,z). We denote by $\vec{n}$ the z axis of our frame while the main axis of the molecule is given by the vector $\vec{a}$.

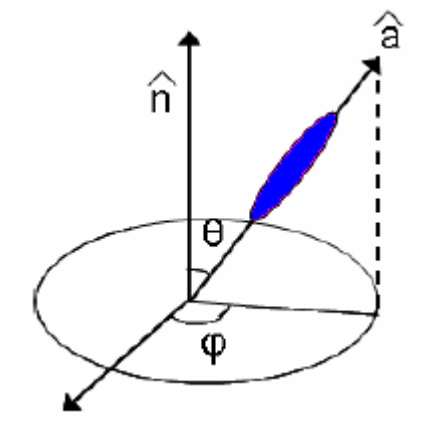

Fig.1.10. Geometry used for defining the order parameter.

Taking into account the polar and azimuthal orientations we can write :

$$a_x = \sin\theta\cos\varphi$$

$$a_y = \sin\theta\sin\varphi$$

$$a_z = \cos\theta\,.$$

The degree of alignment of the rod-like molecule can be described by a distribution function $f(\theta,\varphi)d\Omega$, giving the probability of finding molecules in a small solid angle of $d\Omega = \sin\theta d\theta d\varphi$ around the direction (θ,φ). Though, it is desirable to characterize the alignment of the molecules not by using the full function $f(\theta,\varphi)$ but rather by one related numerical parameter. For conventional nematics $f(\theta,\varphi)$ satisfies the following conditions:

(i) $f(\theta,\varphi)$ is independent of φ; it has complete cylindrical symmetry about $\vec{n}$;

(ii) f(θ) = f(π − θ); the direction $\vec{n}$ is equivalent to -$\vec{n}$ because of the symmetry of the molecular system with respect to the director's inversion and to the cylindrical symmetry of the nematic phase respect to $\vec{n}$.

If the function f(θ) is expanded in terms of orthonormal functions, like the Legendre polynomials, the first non vanishing term that reflects the above conditions is the second Legendre polynomial given by $1/2< 3\cos^2 \theta - 1 >$ where the brackets denote an average over all θ.

The order parameter is therefore usually defined as [5]:

$$S = \frac{1}{2}\left\langle 3\cos^2 \vartheta - 1 \right\rangle = \int \frac{1}{2}(3\cos^2 \vartheta - 1) f(\vartheta) d\Omega \qquad (1.1)$$

where θ is the angle between the director and the long axis of each molecule.
In the isotropic phase, because of the complete orientational disorder (molecules are oriented completely random or $<\cos^2 \theta> = 1/3$) the order parameter is S=0. In the case of an ideal nematic liquid crystal, the molecules align perfectly parallel to the director (or θ=0), therefore S=1. One can consider the case when all the molecules are in the plane perpendicular to the principal axis $\vec{n}$. In this case, for all of them θ=π/2, $<\cos^2 \theta >=0$, resulting in S = -1/2. It would still be a nematic phase, but such nematics have not been found yet.
In some cases is useful to consider also the fourth Legendre polynomial:

$$S_4 = <P_4(\cos\vartheta)> \equiv (1/8)<35\cos^4\vartheta - 30\cos^2\vartheta + 3> \qquad (1.2).$$

The parameter S_2 can be found from the anisotropy of magnetic susceptibility, optical dichroism and birefringence, NMR, etc. The determination of higher order parameters requires for more sophisticated techniques. For instance, S_4 can be found from Raman scattering of light, from luminescence or other two-wave interaction optical experiments. Data on S_6, S_8 are not available at present.

Typically, the order parameter in liquid crystal phases ranges from 0.3 to 0.9 and this value is temperature dependent owing to the kinetic motion of the molecules.

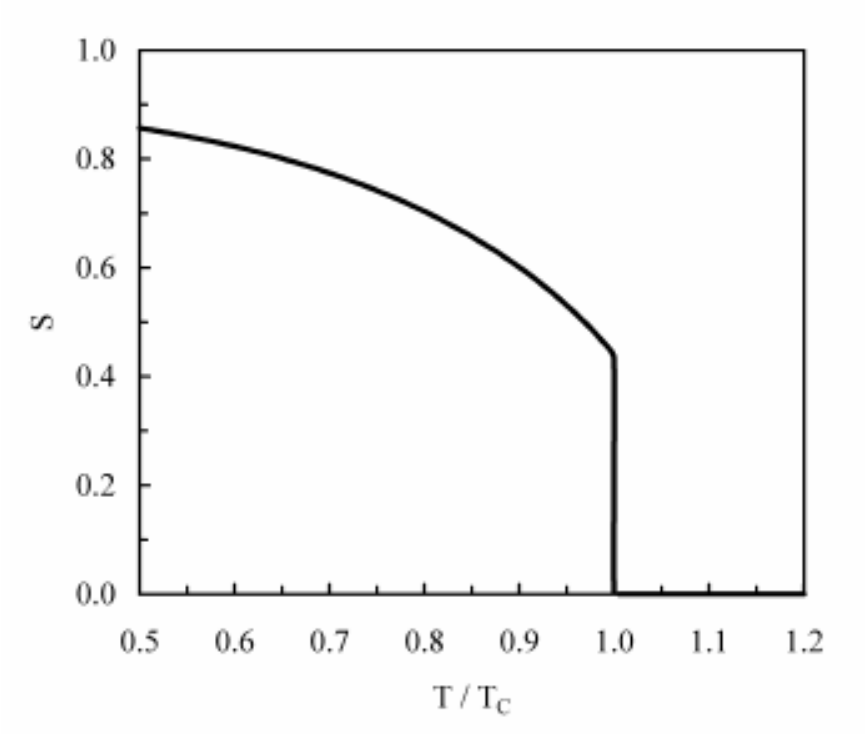

Fig.1.11. The order parameter as a function of temperature, according to Maier-Saupe mean field theory.

1.6. Continuum Theory and Liquid Crystal Deformations

In an ideal nematic single crystal the molecules are aligned along an average direction, called the director, denoted by $\vec{n}$ or $n(\vec{r})$ where $\vec{r}$ is a position vector in the sample. However, on account of constraints imposed by limiting surfaces of the sample and by external fields there is distortion of the perfect alignment. The order parameter then varies from point to point inside the sample. Nevertheless, if this variation is small, the order parameter can be safely assumed to be constant. A continuum theory is based on the assumption that this is true and considers only liquid crystals' elastic energy.

Any deviation from the average direction of orientation costs elastic energy, $\int F_e dV$, where F_e is the elastic energy density and the integration is over the volume of the liquid crystal. A vector field, with all its local variations, is known if we know its divergence $\nabla \cdot n$ and curl $\nabla \times n$, everywhere in addition to boundary conditions.

In 1928, Oseen [6], followed by DeGennes showed that the elastic energy density in the bulk (i.e. discarding surface effects) can be written in the diagonal form:

$$F_e = \frac{1}{2}K_{11}(\nabla \cdot n)^2 + \frac{1}{2}K_{22}(n \cdot \nabla \times n)^2 + \frac{1}{2}K_{33}(n \times \nabla \times n)^2 \qquad (1.3)$$

where K_{11}, K_{22} and K_{33} are called Frank's elastic constants corresponding to the three types of distortions - splay, twist and bend. It is found that for most liquid crystals K_{11}, K_{22} and K_{33} are in the order of 10^{-11} N and K_{33} is usually larger than K_{22} and K_{11}.

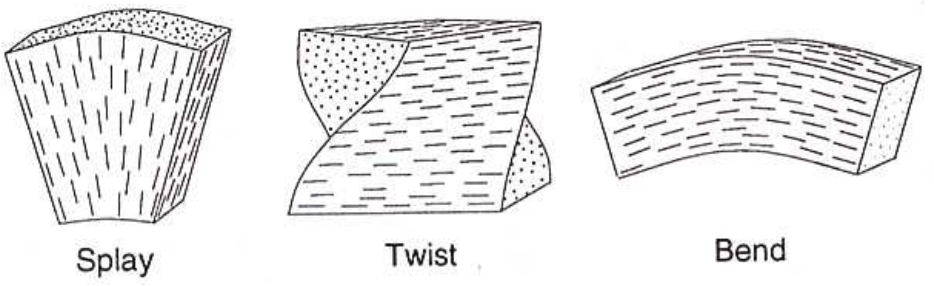

Fig.1.12. Common distortions in liquid crystals.

The relation shows that the elastic energy is a quadratic form in three curvature deformations or strains (called splay, twist, bend) which can be treated independently. The splay is described by a scalar (pure divergence) $\nabla \cdot n$, the twist is described by a pseudoscalar (it changes sign on reflection in a plane parallel to the twist axis or when we go from a right handed reference frame to a left handed reference frame), which is the component of $\nabla \times n$ along the director $|\nabla \times n|_{||}$, whereas the bend is described by a vector with the component of $\nabla \times n$ perpendicular to the director $|\nabla \times n|_{\perp}$.

The condition imposed by Oseen in the derivation of the elastic energy was that F_e must be even in n; this comes from the fact that n and -n are indistinguishable.

If we define the z-axis along the director, then:

$$[\nabla \cdot n]^2 = \left[\left(\frac{\partial n_x}{\partial x} \right)_{y,z} + \left(\frac{\partial n_y}{\partial y} \right)_{x,z} \right]^2 \qquad (1.4)$$

$$[n \cdot (\nabla \times n)]^2 = \left[\left(\frac{\partial n_y}{\partial x} \right)_{y,z} - \left(\frac{\partial n_x}{\partial y} \right)_{x,z} \right]^2 \qquad (1.5)$$

$$\left| n \times (\nabla \times n) \right|^2 = \left(\frac{\partial n_x}{\partial z} \right)^2_{x,y} + \left(\frac{\partial n_y}{\partial z} \right)^2_{x,y} \qquad (1.6)$$

Each of the above equations describes a different type of deformation, namely, splay, twist, and bend, respectively. K_{11}, K_{22} and K_{33} are then called splay, twist, and bend constants. For most calamitic nematics, these constants it is found that $0.5 < K_{33}/ K_{11} < 3.0$ and $0.5 < K_{22}/ K_{11} < 0.8$.

1.7. Birefringence

As a result of orientational order, most physical properties of liquid crystals are anisotropic and must be described by second rank tensors. Examples are the heat diffusion, the magnetic susceptibility, the dielectric permittivity or optical birefringence. Additionally, there are new physical qualities, which do not appear in simple liquids, for example elastic or frictional torques (rotational viscosity) acting on static or dynamic director deformations, respectively.

Remarkable features of liquid crystals with respect to applications are due to their anisotropic optical properties [4]. Nematics and SmAs are uniaxial, SmCs weakly biaxial. Cholesterics give rise to Bragg reflections if the helix pitch is in the magnitude of the light wavelength (which will be discussed later). As mentioned, these properties are carried by a fluid, soft material, and therefore are extremely sensitive against external perturbations.

When light propagates through a liquid crystal, the anisotropy of the phase causes light polarised along the director (also known as extraordinary ray) to propagate at a velocity different than light polarised perpendicular to the director (ordinary ray).

The indices of refraction along the two directions can be defined as $n_e = c/v_{//}$ and $n_o = c/v_{\perp}$. This gives rise to birefringence in liquid crystals. The birefringence of a material is characterised by $\Delta n = n_e - n_o$. Birefringent media can be classified in uniaxial and biaxial media. The uniaxial media have $n_e > n_o$ (positive uniaxial media) or $n_o > n_e$ (negative uniaxial media). The greatest part of thermotropic uniaxial mesophases show a positive birefringence while the nematic phase shows only positive birefringence.

One can define the optical path in a medium, since for the above two wave components travelling at different speeds, the difference in optical paths will lead to a change in the polarization state of the emerging (output) beam. A phase shift between the two components will accumulate as the wave travels across the liquid crystal. The optical path, for a wave travelling a distance d in a crystal of refractive index n, is nd. Thus, the optical path difference between the two wave components mentioned above

will be $d(n_e - n_o) = d\Delta n$. The resulting phase difference (also known as optical retardation α) between the two components is given by $(2\pi/\lambda)d\Delta n$.

Molecules that form liquid crystals are usually uniaxial rod-like, but by bending them a new liquid-crystal phase — a biaxial nematic — should form.
This other nematic phase is predicted to occur at lower temperatures than the uniaxial nematic. In this instance, the molecular short axes tend to be aligned over large distances as well, giving a phase with three directors, about which three molecular axes tend to align. The phase has two optical axes (directions along which the optical properties appear to be cylindrically symmetric), hence its description as 'biaxial' [7].

The design of molecules with sufficient biaxiality is a difficult task. There are many forms that the molecules could take, in addition to the lozenge, that deviate from a cylindrical shape. For example, a series of molecular shapes could be formed by linking rod-like, disc-like and semicircular moieties together (Fig.1.13b). Such molecules would be long enough to exhibit a nematic phase and to deviate sufficiently from cylindrical symmetry to give a biaxial nematic. Indeed, the first claimed discovery of a biaxial nematic was for a compound formed of spoon-like molecules, and similar claims soon followed for cross-shaped and bone-shaped molecules.

One design not previously explored was that of a V-shaped molecule, formed simply by bending a rod-like molecule. Such boomerang-like molecules should form a biaxial nematic (Fig.1.13c) and, more importantly, theory has indicated how the stability of the elusive phase should depend on the angle between the two arms.
Although such molecules should certainly exhibit biaxial nematics, the problem lies in identifying the symmetry of the nematic phase unambiguously [8].

Orientational order and hence birefringence can be manipulated easily (i.e. with the help of rather weak magnetic, electric or optical fields), leading to huge magneto-optical, electro-optical effects. The most successful application are liquid crystal displays well-known from wrist watches, pocket calculators or flat screens of laptop computer which take advantage of electro-optical effects.

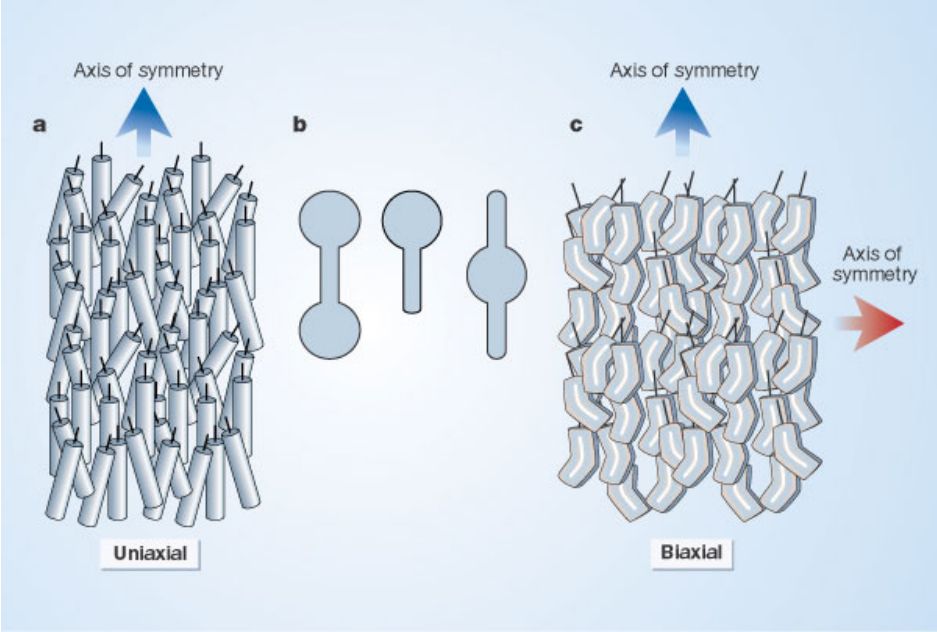

Fig.1.13. Rod-like molecules can organize themselves so that their long axes are aligned. (a) uniaxial nematic phase, characterized by a single optic axis, known as the director. (b) for molecules whose shape deviates from the cylindrical form, a second nematic phase should exist. This is the biaxial nematic phase, with two optic axes. (c) this kind of phase seems to have been found now for boomerang-shaped molecules.

More recently, it turned out that orientational order can be also affected by optical fields leading to rather sensitive optical effects and nonlinear optical properties which are extremely important (i.e. for all-optical switching and other photonic devices in future optical information technologies).

1.8. The Dielectric Anisotropy

The shape anisotropy of liquid crystals manifests itself in many physical properties of liquid crystals [9]. When electric/magnetic fields are applied to the liquid crystal, the phase responds differently, depending on the direction of application of the field. Significant reorientation of molecules can be achieved with low field values; a property that is exploited in majority of the technological applications of liquid crystals. This is possible because some liquid crystal molecules possess permanent

dipole moments due to the delocalisation of electrons comprising the molecules. It is also possible to have induced electric dipoles in the presence of an electric field. In general, molecules possess a dipole moment both along and across the long axis of the molecule. The molecules reorient so that the larger of the two dipoles lie along the electric field. The ratio of the polarisation to electric field gives the dielectric constant and this is a measure of how easily a material is polarised by an electric field. The dielectric anisotropy is defined as:

$$\Delta\varepsilon = \varepsilon_{//} - \varepsilon_{\perp} \qquad (1.7)$$

which is a measure of the difference between the dielectric constant parallel to the long axis of the molecule ($\varepsilon_{//}$) and that perpendicular to the long axis of the molecule ($\varepsilon_{\perp}$).

1.9. Frederiks Transition in Nematic Liquid Crystals

A consequence of the anisotropy of the diamagnetic and dielectric susceptibilities is that the free energy of an ensemble of nematic liquid crystal molecules in an external magnetic or electric field has a minimum for a well defined orientation of the molecular axes (of the director) relative to the field. With positive values $\Delta\chi$ and $\Delta\varepsilon$ the director tends to align itself along the field; with negative values a perpendicular alignment is induced. If in the initial state the directions of the field and the director of the liquid crystal do not correspond to the condition of minimum free energy, then with a sufficiently strong field, capable of overcoming the elastic forces of the nematic liquid crystal, a reorientation of the director will occur, resulting in a configuration of lower free-energy. This effect was discovered and studied in detail by V.K.Frederiks in the early 1930s [10].

When a nematic liquid crystal is under the influence of an applied electric field, the resulting polarization (dipole moment per unit volume) is:

$$\vec{P} = \varepsilon_0 \vec{\chi} \cdot \vec{E} \qquad (1.8)$$

where ε_0 is the permitivity of free space and $\vec{\chi}$ is the susceptibility tensor. We can define the electric displacement as:

$$\vec{D} = \varepsilon_0 \vec{E} + \vec{P} \qquad (1.9)$$

or

$$\vec{D} = \vec{\varepsilon} \cdot \vec{E} \qquad (1.10)$$

where

$$\vec{\varepsilon} = \varepsilon_0 (\vec{1} + \vec{\chi}) \qquad (1.11)$$

and $\vec{1}$ is the unit tensor .

The permitivity anisotropy being:

$$\Delta\varepsilon = \varepsilon_{//} - \varepsilon_{\perp},$$

which decreases as temperature increases and one approaches the transition to isotropic phase. $\Delta\varepsilon$ is zero above the clearing point.

The figure below shows the three basic configurations in the study of the Frederiks effect. These correspond to the Splay (S), Bend (B) and Twist (T) deformations in nematic liquid crystals.

Let us consider the theory of the Frederiks transition in the simplest case and make the following simplifying assumptions [11]:

(i) the difference in Frank's elastic constants is ignored ($K_{11} = K_{22} = K_{33}$);

(ii) the field direction is selected along one of the principal axis of the liquid crystal; in this case we consider conditions presented in Fig.1.14a with the field in the z direction;

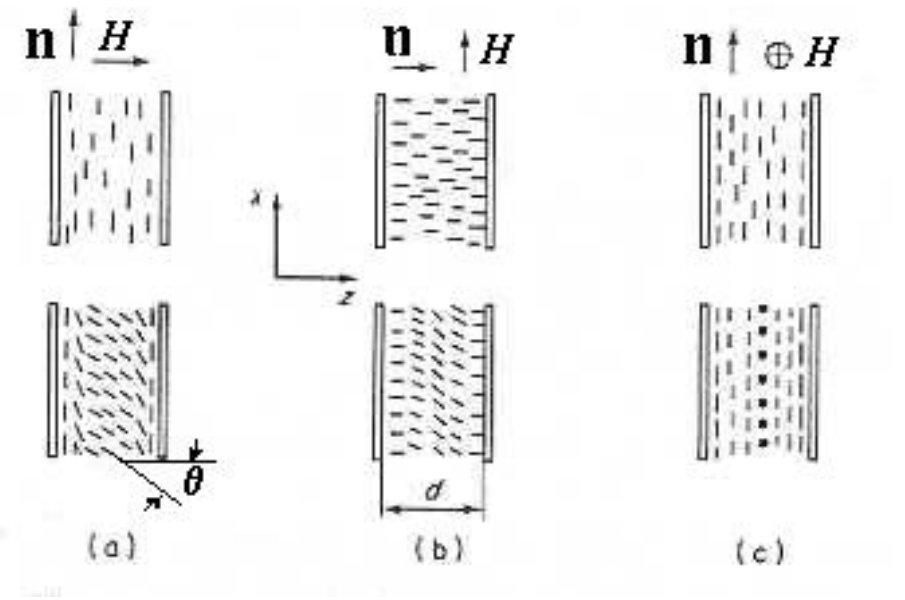

Fig.1.14. Geometry for observing the (a) Splay deformation, (b) Bend deformation and (c) Twist deformation. One can notice the initial orientation of the LC molecules (above) and the deformations when the field exceeds the threshold value (below).

(iii) an infinitely strong boundary anchoring of the LC molecules is assumed; $\theta|_{z=0} = 0$, $\theta|_{z=d}=0$;

(iv) a steady-state situation is considered - the transient flow of the nematic (backflow) that occurs even in the case of the magnetic field is ignored;

(v) the electric conductivity is disregarded and the value $\Delta\varepsilon > 0$ is considered small with respect to the average dielectric permitivity. As a consequence, the field inside the sample is taken as being uniform.

By using Frank's energy,

$$F_e = \frac{1}{2}K_{11}(\nabla \cdot n)^2 + \frac{1}{2}K_{22}(n \cdot \nabla \times n)^2 + \frac{1}{2}K_{33}(n \times \nabla \times n)^2 \qquad (1.12)$$

the free energy of a layer of thickness d is obtained, with allowance for the term

$$\frac{\Delta\varepsilon}{4\pi}\left(\vec{n} \cdot \vec{E}\right)^2 = -\frac{\Delta\varepsilon}{4\pi}E^2\cos^2\psi = -\frac{\Delta\varepsilon}{4\pi}E^2\sin^2\theta \qquad (1.13)$$

which describes the interaction of the field with the dielectrically anisotropic medium (ψ is the angle between the director and the field, $\theta = \pi/2-\psi$ is the angle between the director and the direction x of its initial orientation).

Therefore, we obtain the free energy as being:

$$F = \frac{1}{2}\int_0^d \left[K\left(\frac{\delta\theta}{\delta z}\right)^2 - \frac{\Delta\varepsilon}{4\pi}E^2\sin^2\theta \right] dz \qquad (1.14).$$

A second order differential equation (Euler's equation) is obtained which expresses the extremum condition for F:

$$\frac{\partial^2\theta}{\partial z^2} + \frac{\Delta\varepsilon E^2}{4\pi K}\sin\theta\cos\theta = 0 \qquad (1.15).$$

After integration, minimization and expansion in series we obtain the first two terms of the equation:

$$E = \left(\frac{4\pi K}{\Delta\varepsilon}\right)^{\frac{1}{2}}\frac{\pi}{d}\left(1 + \frac{1}{4}\sin^2\theta_m + \ldots\right) \qquad (1.16).$$

Thus, a deformation with $\theta_m \neq 0$ occurs only in fields exceeding the threshold $E > E_0$, where

$$E_0 = \frac{\pi}{d}\left(\frac{4\pi K}{\Delta\varepsilon}\right)^{\frac{1}{2}} \qquad (1.17).$$

In this simple case, the threshold voltage ($U_0 = E_0 d$) of the Frederiks transition is not dependent on the thickness of the layer. This is because in a thicker layer, for a given θ_m of the director at the centre, the deformation is of longer wavelength and so requires a lower field strength to overcome the elastic forces.

References

[1].F. Reinitzer, Montash Chem. 9, 421 (1888).

[2].O. Lehmann, Z. Krist. 18, 464 (1890).

[3].G. Friedel, Ann Phys Paris, 18, 273 (1922).

[4].Case Western Reserve University (CWRU) Liquid Crystal site – Prof.

C.Rosenblatt.

[5].P. G. DeGennes, J. Prost., The Physics of Liquid Crystals, Oxford University Press, Clarendon Oxford (1993).

[6].C.W. Oseen, Arkiv Mat. Astron Fysik 21A, 1 (1928).

[7].G. R. Luckhurst, Nature, 430, 413-414 (2004).

[8]. Y. Galerne, Mol. Cryst. Liq. Cryst. 323, 211−229 (1998).

[9].L. Liebert, Liquid Crystals, New York, Academic Press, (1978).

[10].V. Freedericks, V. Zolina, Zh.Russ.Fiz-Khim.Ova., Chast.Fiz.,62,457 (1930).

[11].L. M. Blinov, Electro-optical and magneto-optical properties of liquid crystals, New York: John Wiley & Sons Limited, (1983).

Chapter II

Plasma Polymerization and Fast Electro-Optic Switching in Nematic Liquid Crystals

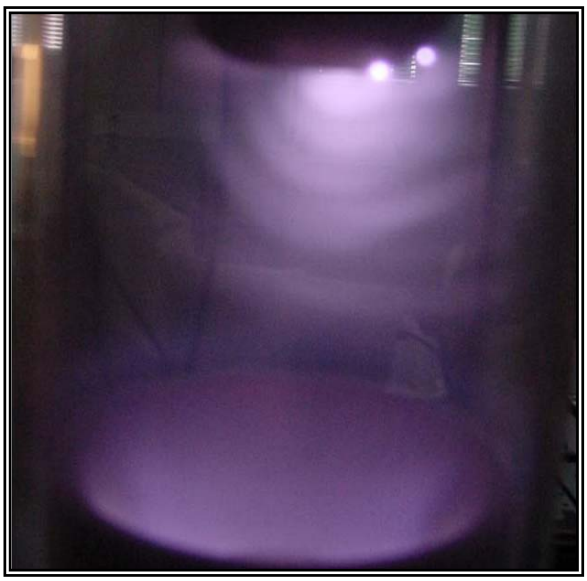

Chapter II

Plasma Polymerization and Fast Electro-Optic Switching in Nematic Liquid Crystals

2.1. Introduction to Plasma

Plasma is typically an ionized gas, and is usually considered to be a distinct phase of matter in contrast to solids, liquids, and gases because of its unique properties. Ionized means that at least one electron has been dissociated from a proportion of the atoms or molecules. The free electric charges make the plasma electrically conductive so that it responds strongly to electromagnetic fields.

This fourth state of matter was first identified in a discharge tube (or Crookes tube), and so described by Sir William Crookes in 1879 (he called it "radiant matter"). The nature of the Crookes tube, "cathode ray" matter was subsequently identified by English physicist Sir J.J. Thomson in 1897, and dubbed "plasma" by Irving Langmuir in 1928 [1], perhaps because it reminded him of a blood plasma. Langmuir wrote:

“Except near the electrodes, where there are sheaths containing very few electrons, the ionized gas contains ions and electrons in about equal numbers so that the resultant space charge is very small. We shall use the name plasma to describe this region containing balanced charges of ions and electrons”.

Plasma typically takes the form of neutral gas-like clouds or charged ion beams, but may also include dust and grains (called dusty plasmas) [2]. They are typically formed by heating and ionizing a gas, stripping electrons away from atoms, thereby enabling the positive and negative charges to move freely.

In addition, there are a large amount of excited molecular conditions, that under delivery from electro-magnetic radiation turns back to the ground state, which leads to the characteristic luminance of the plasma.

When a solid is heated it undergoes a phase change to liquid, which on heating transforms into a gas. When a gas is heated it breaks into ions, electrons and neutrals. This excited gaseous state called plasma is the most abundant state of matter in the universe.

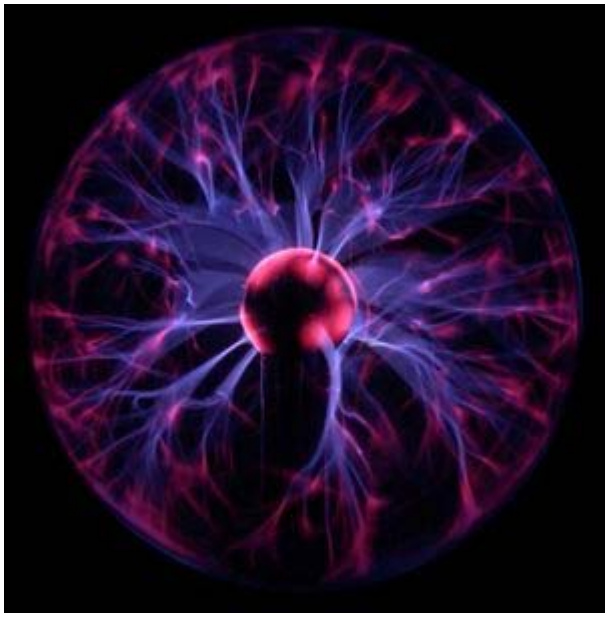

Fig.2.1. A plasma lamp, illustrating some complex phenomena of plasma, including filamentation. The colors are a result of the relaxation of electrons in excited states to lower energy states after they have recombined with ions. These processes emit light in a spectrum characteristic of the gas being excited.

The required energy by the origination of plasma can have very different sources. Just like in nature, plasma occurs for example on the sun as well as in lightnings and flames; but also in the atmospheric phenomenon known as polar light. By far the most

frequent type of technical production of plasma is the concentrated irradiation of electronic fields.

In the laboratory, plasma can be produced if sufficient energy can be provided to excite the gaseous particles. Plasma has been generated by combustion, flames, electrical discharge, controlled nuclear reactions, shocks, etc. Since plasma loses energy to its environment mainly by radiation and conduction to the walls, in order to maintain the plasma state continuously in a laboratory apparatus, energy must be supplied as fast as it is lost. Of the various means to maintain plasma state continuously for relatively long periods of time, the most obvious and common method is by means of an electrical discharge. For this reason, most experimental work, particularly in the study of polymerization, has been carried out using some kind of electric discharge. Plasma formation is initiated by free electrons which are present in the gas. The applied electric field accelerates these electrons, which leads to collisions with neutrals and subsequent scattering. Occasionally, sufficient energy is imparted by electron-neutral collisions to ionize the molecules. This process produces ions and more electrons. The process avalanches until a steady state determined by the production and scavenging of electrons is reached. In this way, the plasma state is achieved.

Although plasma is loosely described as a quasi-neutral collection of charged particles, a more rigorous definition requires three criteria to be satisfied [3]:

(i). The plasma approximation. Charged particles must be close enough together that each particle influences many nearby charged particles, rather than just the interacting with the closest particle (these collective effects are a distinguishing feature of plasma). The plasma approximation is valid when the number of electrons within the sphere of influence (called the Debye sphere whose radius is the Debye screening length) of a particular particle is large. The average number of particles in the Debye sphere is given by the plasma parameter Λ.

When speaking about the plasma parameter one considers the bulk plasma. The plasma parameter is a number, usually denoted by capital Λ, which measures the average number of electrons contained within a Debye sphere (a sphere of radius the Debye

length) in plasma. It is defined as $\Lambda = (4\pi\ n\ \lambda_D^3)\ /3$, where n is the number density of particles, and λ_D is the Debye length.

In plasma physics, the Debye length (named after the Dutch physical chemist Peter Debye) is the scale over which mobile charge carriers (i.e. electrons) screen out electric fields in plasmas and other conductors:

$$\lambda_D = \sqrt{\frac{\varepsilon_0 k / q_e^2}{n_e / T_e + \sum_{ij} j^2 n_{ij} / T_i}} \qquad (2.1)$$

where,

λ_D is the Debye length,
ε_0 is the permittivity of free space,
k is Boltzmann's constant,
q_e is the charge on an electron,
T_e and T_i are the temperatures of the electrons and ions, respectively,
n_e is the density of electrons,
n_{ij}'is the density of atomic specie i, with positive ionic charge jq_e,

The ion term is often dropped, the resulting formula for the Debye length being

$$\lambda_D = \sqrt{\frac{\varepsilon_0 k T_e}{n_e q_e^2}} \qquad (2.2)$$

although this is only valid when the ions are much colder than the electrons.

In other words, the Debye length is the distance over which significant charge separation can occur. In space plasmas, where the electron density is relatively low, the Debye length may reach macroscopic values, such as in the Magnetosphere, Solar wind, Interstellar medium and Intergalactic medium.

Taking into account a Maxwell-Boltzmann distribution with three degrees of freedom , $\langle E \rangle = (3/2)(k_B T)$, 1 degree Kelvin corresponds to cca. 8.6×10^{-5} eV.

Plasma	**Density** $n_e(m^3)$	**Electron temperature** T(K)	**Magnetic field** B(T)	**Debye length** $\lambda_D(m)$
Gas discharge	10^{16}	10^4	--	10^{-4}
Ionosphere	10^{12}	10^3	10^{-5}	10^{-3}
Magnetosphere	10^7	10^7	10^{-8}	10^2
Solar core	10^{32}	10^7	--	10^{-11}
Solar wind	10^6	10^5	10^{-9}	10
Interstellar medium	10^5	10^4	10^{-10}	10
Intergalactic medium	1	10^6	--	10^5

Fig.2.2. Table presenting possible values for the Debye length in different media.

In a low density plasma, localized space charge regions may build up large potential drops over distances of the order of some tens of the Debye lengths. Such regions have been called electric double layers. An electric double layer is the simplest space charge distribution that gives a potential drop in the layer and a vanishing electric field on each side of the layer.

One of the criteria which determines whether a collection of charged particles can rigorously be named plasma is that $\Lambda>>1$. When this is the case, collective electrostatic interactions dominate over binary collisions, and the plasma particles can be treated as if they only interact with a smooth background field, rather than through pairwise interactions (collisions).

(ii). Bulk interactions. The Debye screening length is short compared to the physical size of the plasma. This criterion means that interactions in the bulk of the plasma are more important than those at its edges, where boundary effects may take place.

(iii). Plasma frequency. The electron plasma frequency (measuring plasma oscillations of the electrons) is large compared to the electron-neutral collision frequency (measuring frequency of collisions between electrons and neutral particles). When this condition is valid, plasmas act to shield charges very rapidly - quasineutrality is another defining property of plasmas.

If we consider a neutral plasma, consisting of a gas of positively charged ions and negatively charged electrons, then, if there is a displacement by a tiny amount of all the electrons with respect to the ions, the Coulomb force pulls back, acting as a restoring force.
If the electrons are cold, then the charge density oscillates at the plasma frequency:

$$\omega_{pe} = \sqrt{\frac{ne^2}{m\varepsilon_0}} \qquad (2.3)$$

where n is the density of electrons, e is the electric charge, m is the mass of the electron, and ε_0 is the permittivity of free space. The formula is derived under the approximation that the ion mass is infinite. This is generally a good approximation, as the electrons are so much lighter than ions.

2.1.1. Types of Plasmas

Temperature is one way of classifying plasmas [4]. The most important temperatures that characterize plasma are:

(i). The gas temperature, which characterizes the translatory energy of the gas;

(ii) The excitation temperature, which characterizes the energy of the excited particles in the plasma;

(iii) The ionization temperature, which characterizes the ionization energy;

(iv) The dissociation temperature, which characterizes the dissociation energy;

(v) The radiation temperature, which characterizes the radiation energy.

Complete thermodynamic equilibrium cannot be achieved in the plasma as the radiation temperature cannot equal the temperature in the plasma bulk. However, local thermodynamic equilibrium (LTE) can be reached in laboratory environment.
Based on the presence or absence of this local thermodynamic equilibrium, laboratory and industrial plasmas are of two types:

(i) Thermal Plasma
When there is existence of LTE, the plasma is called thermal plasma. LTE can exist when the heavy particles are very energetic, at temperatures of the order of 10^6-10^8 K and when the pressure is atmospheric, even at temperatures as low as 6000 K.

(ii) Cold Plasma
In low-pressure discharges, LTE is not achieved. In this case, the electron temperature is much higher than that of the heavy particles. The electron temperatures can reach values as high as 10^4-10^5 K, while the gas temperature can be as low as room temperature. This non equilibrium characteristic allows the cold plasma to have physical and chemical reactions at relatively low temperatures.
Cold Plasmas are generated by means of Radio Frequency (RF), DC and microwave excitation.

2.1.2. Plasma Processing

When a substrate is kept in plasma, one of the following processes take place:

(i) Activation or more correctly Modification:
When a substrate comes in contact with plasma, the molecules, monomers or radicals can be adsorbed onto the surface. These adsorbed species may react with atoms or radicals from the plasma and form compounds. This leads to "activation" of the surface. The processes are changing the polymer structure and elemental composition within a few molecular layers, exchanging carbon-hydrogen-bondings by functional groups. The type of introduced functional groups depends on the process gas. These groups are used to provide better adhesion, wettability, biocompatibility or more inert properties of the surface.
For example, if a substrate like polyethylene is exposed to inert gas or non-hydrocarbon plasma, the surface will be activated by species from these gases, thereby incorporating moieties that were not initially present.

(ii) Sputtering.
When a substrate is placed in plasma, it is negatively biased with respect to the plasma. Owing to this, the positive ions are accelerated towards the surface. If the ion has sufficient energy, it can knock out an atom from the surface. This process is called "sputtering". Sputtering is used extensively to clean surfaces. Organic contaminants like cutting oil, skin oil, mold releases, etc., are sputtered from the surface when inert and oxygen plasmas are used. These contaminants undergo repeated scission in plasma till their molecular weight becomes so low that they can boil away in the vacuum.

(iii) Deposition.
When complex molecules are introduced in plasma, they fragment and react with themselves to form a film on the surface of a substrate. This is called as plasma enhanced chemical vapour deposition (PECVD).

(+) The advantages of Plasma Processing are:

(1) Environmentally benign process, as it does not have any residues;
(2) It is a room temperature process;
(3) Plasma polymers can be deposited on a wide variety of substrates;
(4) Uniform pinhole free films can be deposited;
(5) Films have excellent adherence to the substrate;

(-) Disadvantages of Plasma Processing are:

(1) The deposited films have low abrasion resistance;
(2) Owing to very low deposition rates, only very thin films can be deposited economically on high production items;
(3) All the surfaces "seen" by the plasma are coated. This makes reactor cleaning essential for consistent results;
(4) Retrofitting equipment is expensive.

2.2. Plasma Polymerization

2.2.1. Polymers in History

The compounds known as polymers are comprised of tens, hundreds, thousands, up to millions of separate smaller molecules, known as monomers. The term polymer stems from the Greek language where poly means multiple and mer means parts. The chemical reaction binding monomer molecules together covalently is called polymerization.
Since the discovery of natural rubber and the synthetic route to polyethylene, polymers have become an important type of material with properties that are easily manipulated, for instance by altering the chemical nature of the monomer, the number of monomers per chain and processing conditions [5]. Although some very well known polymers are

mass produced, such as polystyrene, polyvinyl chloride, poly(methyl methacrylate) - PMMA and polyethylene, some polymers are specially tailor made and show remarkable properties.

An alternative term that is used for polymers is macromolecule.

Synthetic polymers are actually only part of the larger group of macromolecules that also include biomacromolecules, such as DNA and proteins, but also semi-synthetic and inorganic polymer (natural silicates). Semi-synthetic macromolecules, such as vulcanized natural rubber, follow from a chemical reaction with a natural macromolecule.

The versatility of polymers is clearly indicated by the many applications polymers are used for, such as rubber tires, bulletproof vests, plastic cutlery, soda bottles, household plastic, computer parts, organic technology (solar cells and light emitting diodes), and so on.

Polymers are commonly regarded as modern and purely synthetic materials.

However, polymers actually have a rich history and are found widely in nature. Nature has formed her own brands of polymer, such as the blueprint of life (DNA), proteins, tar, wood and timber and many more. Natural rubber was discovered and extracted from the trees by the Aztecs in 1600 BC. It is believed that the Aztecs used balls of natural rubber in ritual games and figurines in worship. Modern man rediscovered natural rubber in the 18th century. In the mid 19th century, uncured rubber was used as a water repelling additive to coatings applied to textiles. But it wasn't until the chemical treatment of natural rubber, that the great potential of natural rubber was realized. By vulcanization of natural rubber, a discovery by Goodyear and Hancock, a durable material was obtained that could be moulded in any desired shape and dimension prior to vulcanization. Vulcanized rubber deforms under a heavy load, but recovers entirely and returns to its original shape when the load is removed. Comparing rubbers to modern materials, such as steel, it is obvious that rubbers can be extended to several times their initial length and recover completely, whereas steel only allows reversible deformation of a few percent.

Celluloid and Bakelite were the first successful plastics. John Wesley Hyatt introduced Celluloid in 1869 as a surrogate for ivory in billiard balls, that had become increasingly difficult to obtain. The chemical reaction involved within the formation of

Celluloid had already been known since 1832. Henri Braconnot added nitric acid to starch or wood fibers, thereby converting the cellulose in the fibers to the unstable and highly explosive salt cellulose nitrate. Camphor stabilized Celluloid was used up to the 1950s as photographic material in stills, movies and X-ray films. Due to the hazardous circumstances of manufacturing and processing Celluloid, the production was eventually discontinued. Bakelite was synthesized in 1907 by Leo Baekeland and was applied in many household and technical applications, such as insulation for electrical wiring and housing for electrical appliances. Bakelite is formed by the condensation polymerization of phenol and formaldehyde. Phenol-formaldehyde (phenolic) resins are still used today as adhesives for composite wood products.

With the increasing application of rubbers and plastics and the continuing innovation that followed the inventions of Celluloid, Bakelite and the serendipitous discovery of polyethylene in 1930, engineering plastics with on-demand physical and chemical properties became a reality.

The majority of polymers used today are thermoplastics. Thermoplastic behaviour is a consequence of the absence of chemical cross-links. Thermoplastics are liquefied and easily moulded upon heating and return to their glassy or semi-crystalline solid state when cooled. Thermoplastic polymers are easily processed and reprocessed or recycled. Among the many examples of the thermoplastics are Cellulose, polyethylene (PE), polystyrene (PS), polymethyl methacrylate (PMMA), polyamid (PA), polycarbonate (PC) and polyvinyl chloride (PVC).

Natural rubbers are a typical example of a group known as thermoset polymers.

Upon irreversible chemical or thermal curing, individual polymer chains are physically interconnected, thereby forming a polymer chain network that assumes the shape of the mould. Thermoset polymers are not easily recycled or reprocessed. Examples of thermoset plastics are Bakelite, polyester and epoxy resins (used in fibre reinforced composites).

Polymers & Properties

On the molecular level, a polymer, or macromolecule, can be considered as chain-like, where the chain is not stretched completely, but folded like a coil. A polymer is made up of a repetition of subunits, also known as monomers. If a single type of monomers

is used, homopolymers are obtained. A polymerization with two different monomer units yields copolymers and that of three different monomers gives terpolymers. The monomers are connected by covalent chemical bonds and thereby form a chain. The chemical and physical properties of any polymer depends on the choice of monomer(s), the composition of the polymer, the length of the chains, the distribution in the chain length (i.e. the variation in chain length), purity and the method of processing (polymerization technique).

2.2.2. Plasma Polymerization

Plasma polymerization is the deposition of thin films on substrate surfaces from organic monomers by means of plasma. Plasma polymers have been observed since the early nineteenth century in the form of oily products on electrode surfaces and walls of reactors, when working with electric discharges in a glass reactor [6-9]. However, these were thought of as annoying by-products of electric discharge process. It was not until the late twentieth century that the specific characteristics of these films were studied and their reaction mechanisms elucidated [10-14].

Plasma polymerization is different from conventional polymerization in the fact that it may be characterized as elemental or atomic polymerization [15]. This is because in glow discharge polymerization the monomer structure is not retained, but the original monomer molecules serve as a source of elements for the formation of large molecules. Thus, plasma polymer is not usually identified from the starting material. The polymerization mechanisms and structure of the plasma polymer is deduced from the breakdown of monomer molecules based on the strength of their chemical bonds.

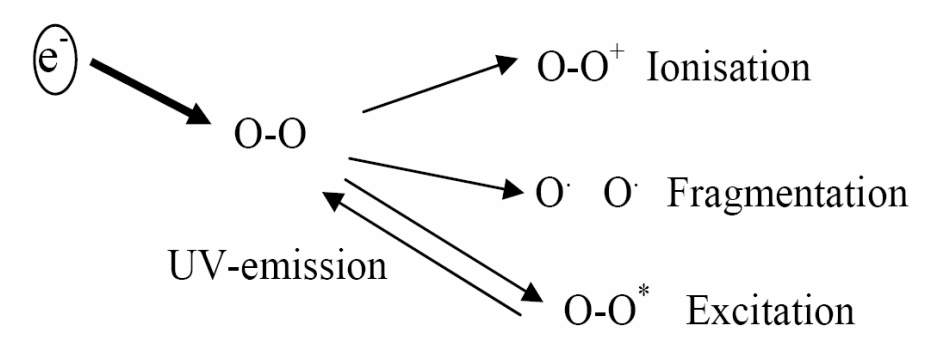

Fig.2.3. Elemental processes in a plasma.

Unlike conventional polymerization, most of the reactions in plasma polymerization are one-step reactions between two reactive species. Some other reactions are between activated species and a molecule, which are essentially the same as the propagation reaction of the conventional addition polymerization. Such reactions can proceed in a chain mechanism if the reacting molecule has the appropriate molecular structure. However, even in such cases the formation of polymerization is because of the very low ceiling-temperature of addition polymerization in vacuum.

Plasma polymerization is usually initiated and generated in the vapour phase during the plasma process. As polymerization proceeds, the growing polymer can not remain in the vapour phase and diffuses to a surface. Reactive species in the gas phase, such as ions and free radicals, may simultaneously interact with surfaces inside the plasma reactor that have been activated by the impact of the glow discharge to form ions or free radicals from the surface molecules of substrates. As the ions and free radicals do not distinguish between the various substrates, they interact and form polymers on all the substrates, including the walls of the reactor. Plasma polymer film deposition and growth steps on that surface may follow [16].

The homogeneous polymerization in the plasma phase and heterogeneous polymerization at the surface of the growing film can be summarized by the reaction scheme proposed originally by Poll et al. [17] and illustrated in Fig.2.4. As shown in this figure, the gaseous precursor monomers can polymerize in the plasma and deposit as a film (reaction path 1, characterized by a rate $k1$), be converted in the plasma into

reactive products (path 2), or be converted in non-reactive products (path 4). The reactive products can convert into depositing polymer film (path 3) or can be converted to non-reactive products (path 5). Degradation of the formed polymer film can occur to form non-reactive products (path 6).

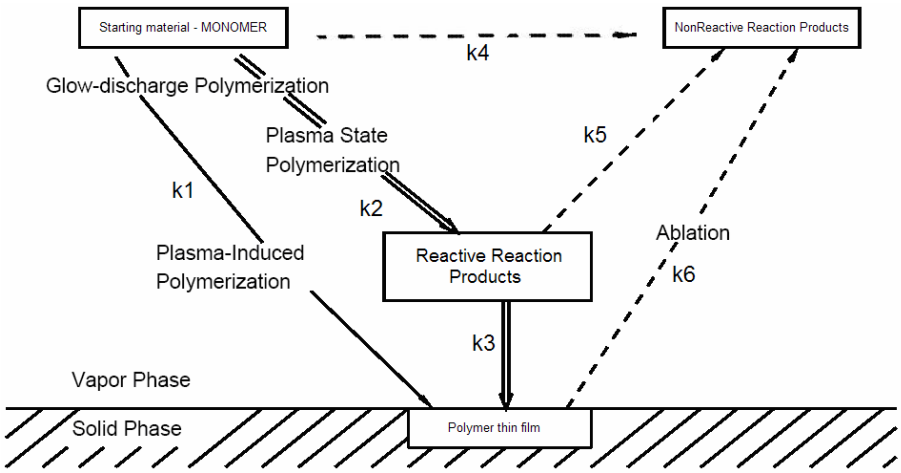

Fig.2.4. Diagram of plasma polymerization. Solid line - polymer deposition path; broken line - volatile product formation path.

Path 1, by which the monomer is directly polymerized into the growing film, is also called plasma induced polymerization. This is essentially a conventional molecular polymerization process, triggered in this case by reactive plasma species.

Plasma induced polymerization can take place only if the original monomer contains polymerizable functional groups, such as double, triple, or cyclic bonds [18].

Deposition of a polymer film through path 2 and 3 is considered as being plasma polymerization. In plasma polymerization, the intermediate reactive products can be ions, excited molecules, and free radicals not necessarily preserving the original monomer. The monomer does not need to have polymerizable groups in order to to undergo plasma polymerization.

As the monomer molecules in plasma, for the most part, become shattered into reactive particles, there remain at most, only partially preserved chemical structures of the output gases in the product, which results in cross-linked and disordered structure (Fig.2.5). Structural preservation and cross-linking gradients can be controlled through

process parameters, such as pressure, working gas-flow and applied electrical output; so that one can also construct so called gradient layers (i.e with increasing degree of crosslinking over the thickness).

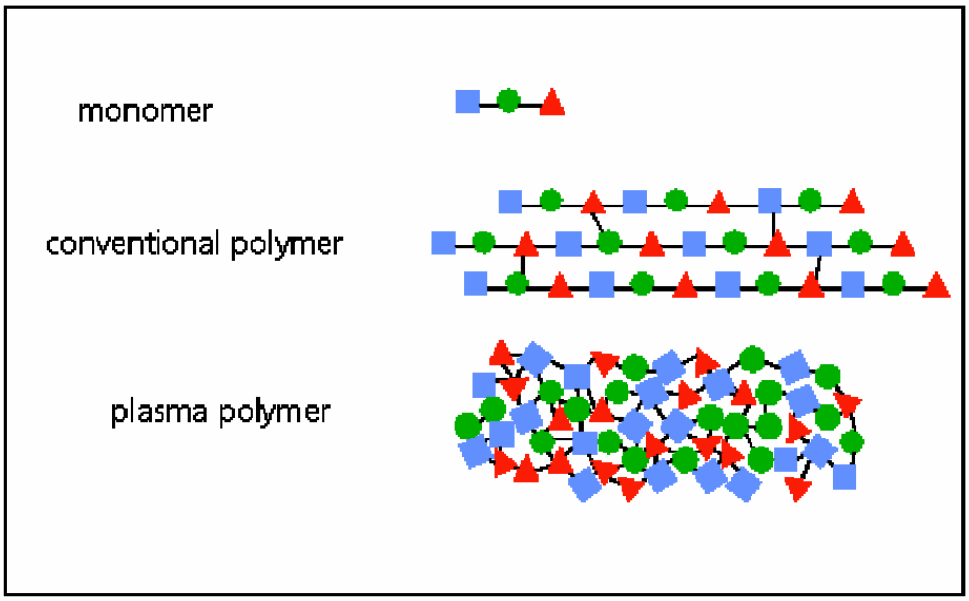

Fig.2.5. Comparison between the structures of plasma polymers and conventional polymers.

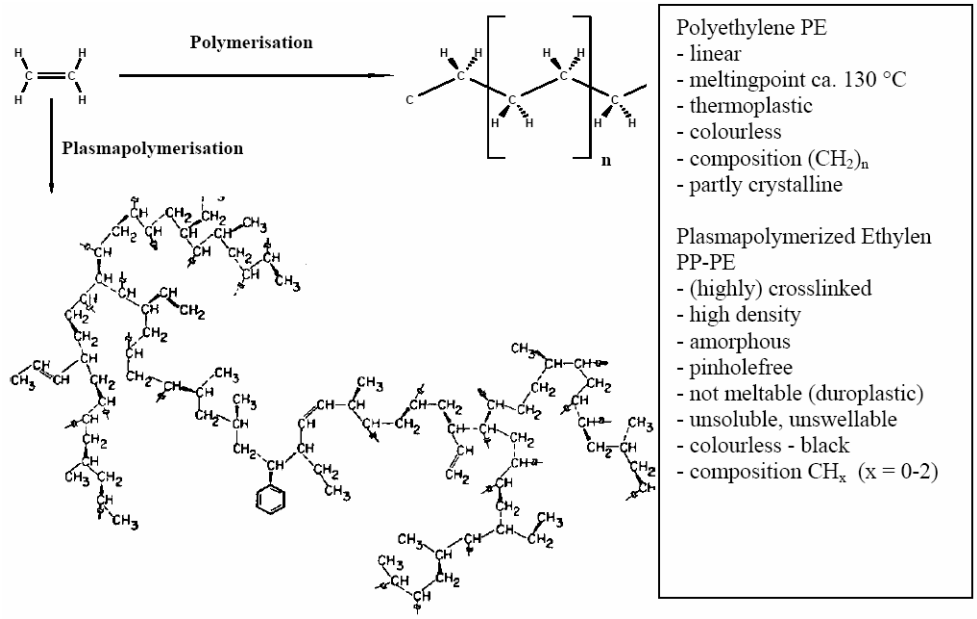

Fig.2.6. Polymer vs. Plasma Polymer.

The variety of obtainable plasma polymer layers can be increased if we mix the monomer with gases, which are typically used for modification processes (Fig.2.7) . The result will be a modified plasma polymer layer, which combines the principal advantages of the plasma polymer with the functionality of a plasma modified surface [19-25].

Oxygen O_2	Modification of polymers Cleaning, degreasing and hydrophilisation
Hydrogen H_2	Cleaning of metals Reduction of oxidized layers

Hydrocarbons Ethylene, Ethane, Acetylene, Methane	Polymerisation
CF_4, SF_6	Etching

Noble gases He, Ne, Ar	Activation and degreasing
Nitrogen N_2	Activation of polymers
N_2O, CO_2, NH_3, ..	Modification

Fluorcarbons C_2F_4, C_2F_6,...	Hydrophobisation Polymerisation
Si-organic reagents HMDSO, TMS, ...	Polymerisation

Fig.2.7. Commonly used gases for plasma surface deposition and plasma treatment.

2.2.3. Criteria of Monomer Choice

The selection criteria of a suitable chemical precursor for coating applications are that the precursor [26]:

(i) is stable at room temperature;

(ii) has low vaporization temperature and high saturation of vapour pressure;

(iii) can generate vapour that is stable at low temperature (i.e. before decomposing or reacting at a higher temperature);

(iv) has suitable deposition rate. Low deposition rates for thin film applications (e.g. semiconductor industry) and high deposition rates for thick coating applications;

(v) undergoes decomposition/chemical reaction at a temperature below the melting temperature and phase transformation of the substrate depending on the engineering applications;

(vi) has low toxicity, explosivity and inflammable for safety of handling chemicals and disposing of the unreacted precursor. This is especially desirable for large scale industrial applications;

(vii) is cost-effective for thin film or coating deposition;

(viii) is readily available at high purity electronic grade commercially.

2.2.4. Processing Factors of Glow Discharge Polymerization

It is extremely important to recognize the difference between polymer-forming plasmas and nonpolymer-forming plasmas in order to understand the true meaning of the processing factors of glow discharge polymerization. Not all glow discharges yield polymer deposition. For instance, plasmas of Ar**,** Ne, 0_2, N_2 and air are typical nonpolymer-forming plasma. The significance of polymerforming plasmas, such as glow discharges of acetylene, ethylene, styrene, benzene, etc., is that a considerable portion or the majority of molecules of starting material leave the gas (plasma) phase and deposit as a solid polymer.

In contrast to polymer-forming plasmas, the total number of gas phase molecules in nonpolymer-forming plasmas do not change. Only a portion of gas molecules repeat the process of being ionized, excited, and quenched. However, the total number of gas molecules remains constant. This situation can be visualized by the pressure change that occurs before, during, and after the glow discharge. In the case of a nonpolymer-forming plasma, no pressure change is observed unless a material which reacts with excited species of plasma is placed in the discharge system [27,28]. The system pressure of a polymer-forming plasma changes as soon as discharge is initiated. The

pressure change is dependent on the characteristic nature of the starting material, which is related to the product gas formation. With starting materials that yield very little product gas (i.e. acetylene, benzene, styrene, etc.) the system pressure drops to nearly zero when a high polymerization yield is obtained. In other words, an efficient plasma polymerization is an excellent vacuum pump, whereas a nonpolymer-forming plasma has no characteristic of this nature [29-34].

Unfortunately, most fundamental work on the plasma state was done with nonpolymer-forming plasmas, and the concept of the operational parameters used in such studies cannot be applied directly to polymer-forming plasmas.

Characteristic polymer deposition by glow discharge polymerization occurs onto surfaces exposed to (directly contacting) the glow. Some deposition of polymer occurs on surfaces in nonglow regions (but the deposition rate is orders of magnitude smaller). The surface on which a polymer deposits could be an electrode surface, a wall surface, or a substrate surface suspended in the glow region.

Another important factor that must be considered in dealing with operational factors of glow discharge polymerization is that it is system dependent.

Consequently, polymer deposition rates are dependent on the ratio of surface to volume of glow. Therefore, other operational parameters such as flow rate, system pressure, and discharge power are insufficient parameters for the complete description of glow discharge polymerization. Such parameters serve as empirical means of describing operational conditions of glow discharge polymerization in a particular system, but they should not be taken beyond this limitation.

The following operational factors are, however, important. More other factors influence glow discharge polymerization in an interrelated manner. Therefore, any single feature should not be taken as an independent variable of the process.

2.2.5. Parameters of Plasma Polymerization

2.2.5.1. Modes of Electric Discharge. Plasma Reactor Categories.

Although a number of methods can be used to generate plasma, the methods utilized in plasma polymerization of organic compounds are more or less limited to some kind of electric discharge. This is perhaps due to the fact that organic compounds decompose at high temperatures and "hot plasma" cannot be used for polymer synthesis. Another factor is that electric discharge is the most practical means for creating and maintaining "low-temperature plasma" in a laboratory.

Electric discharge can be obtained in a number of ways, and numerous combinations of factors involved in the design of a reaction vessel are given in the literature. Basically, however, the combination of two major factors (i.e. type of electric power source and mode of coupling) will cover nearly all practical cases.

For glow discharge polymerization, the location of the surface on which plasma polymer is deposited also plays an important role. The reactors may be characterized by discharge with internal or external electrodes (Fig.2.8), may be characterized by discharge with external electrodes [35,36]. All inductively coupled discharges are called "electrodeless" glow discharge, since electrodes are not employed. The discharge power of the plasma plays an important role as higher discharge power increase the ions energy.

	Power Source	**Mode of Coupling**	**Location of Substrate Surface**
1	DC	Capacitive	On an electrode surface (cathode)
2	DC	Capacitive	In between electrodes
3	AC	Capacitive	On an electrode surface
4	AC	Capacitive	In between electrodes
5	RF	Capacitive	On an electrode surface
6	RF	Capacitive	In between electrodes
7	AC and RF	Capacitive,external	In between electrodes

		electrodes	
8	AC and RF	Capacitive,external electrodes	In tail flame
9	RF	Inductive	Inside RF coil
10	RF	Inductive	In tail flame
11	Microwave	Inductive	In the coupling region
12	Microwave	Inductive	In tail flame

Fig.2.8. Factors of plasma polymerization reactors.

2.2.5.2 Plasma Reactor Types

The main categories of reactor designs (based on the used electrical sources) are presented below [37].

There are three types of plasma reactors for plasma polymerization of organic monomers. Radio frequency (RF) (usually 13.56M Hz) and microwave (MW) (2.45G Hz) are mainly used when the substrates are insulating materials. DC reactors, which have a direct current source, are simpler than the other two categories and are the best ones for electric conductive substrates. The substrates can act as electrodes of the DC reactor.

Currently, the RF reactor is the most popular plasma reactor, because the MW reactor is too complicated and DC has some restrictions about the substrates.

DC Plasma Reactor

In DC plasma reactors, the plasma is sustained between two parallel plate electrodes as shown in Fig.2.9, and the electric power is supplied to excite the plasma in the abnormal discharge mode. The distances between the electrodes and the pressure in the reactor have to satisfy Paschen's law [38].

$$V_b = \frac{C_1(pd)}{C_2 + \ln(pd)} \qquad (2.4)$$

where,

p is the pressure of the gas;

d is the distance between electrodes;

C_1 and C_2 are constants that depend on the nature of the gas;

V_b is the breakdown voltage.

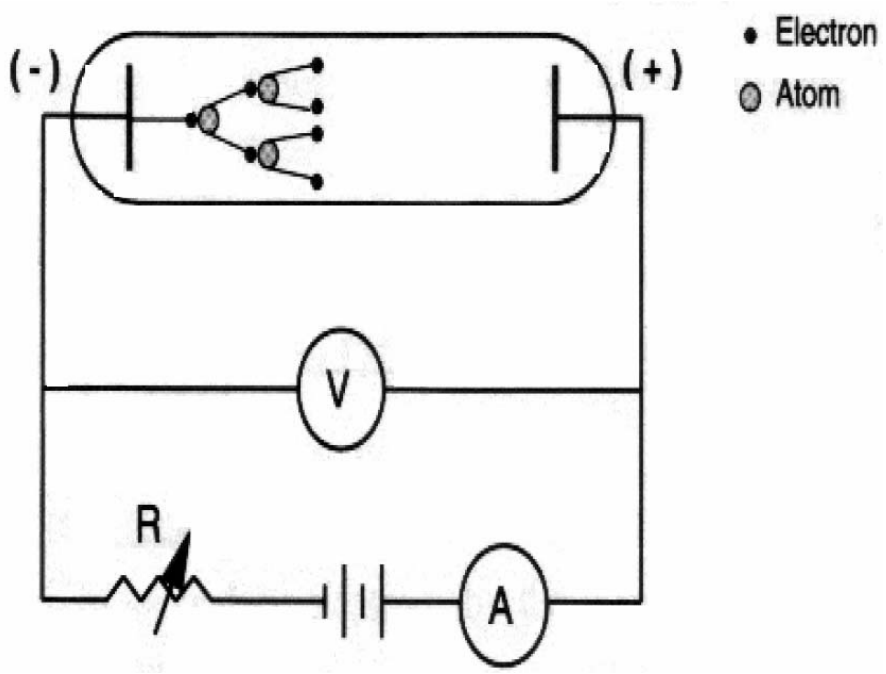

Fig.2.9. Diagram of a DC Plasma Reactor.

The power supplies used to sustain DC plasma can generally be used in a constant voltage, constant current, or constant power mode. The power supplies should be able to control the preset value in each mode. The excitation and sustainment of a DC plasma require the use of electrically conductive electrodes and samples. However, electrically insulating films may deposit locally on the surface of the electrodes or

samples due to contaminants formed in the plasma. In such cases, local dielectric breakdown normally occurs, causing arcing that results in spikes of high currents.
The power supply must be able to withstand these spikes and return to normal operation without shutting off. Nevertheless, it must also be able to distinguish between the transient arcing currents and shorts that may occur between the electrodes and grounded surfaces. This feature, called arc suppression, must be a characteristic of a DC power supply of a plasma reactor.

RF Plasma Reactor

RF discharges have many advantages over DC discharges, which explains the wider use of RF plasma as compared to DC plasma:

(i). RF plasma can be excited and sustained using either conductive or nonconductive electrodes, while DC discharges require the electrodes to be conductive throughout the process;

(ii). RF plasma can be sustained with internal as well as external electrodes, while DC discharges require the electrodes to be inserted inside the reactor and be in direct contact with the plasma. Use of external electrodes is sometimes required when the gases of the discharge are corrosive or when it is necessary to reduce contamination of the plasma with the material of the electrodes;

(iii). RF plasmas are characterized by higher ionization efficiencies than the DC plasma;

(iv). RF plasma can be sustained at lower gas pressures than DC plasma;

(v). In RF plasma the energy of the ions bombarding the sample is controlled by the negative bias, which can be adjusted over a wide range of values. Samples placed on

the cathode of the DC discharge are exposed to bombardment of high-energy ions that are accelerated at voltages that have to be above the minimal breakdown voltage. This can cause damage to sensitive substrates.

A typical RF-plasma system is shown in Fig.2.10. These kinds of reactors couple the RF power to two parallel electrodes inserted inside the reactor. The coupling is done through special RF vacuum feedthroughs. One electrode is often grounded together with the walls of the reactor. This arrangement is also called a diode or parallel plate reactor. This is the most common approach in the design of industrial RF plasma reactors, but it is not suitable for some specific processes (use of powders etc).

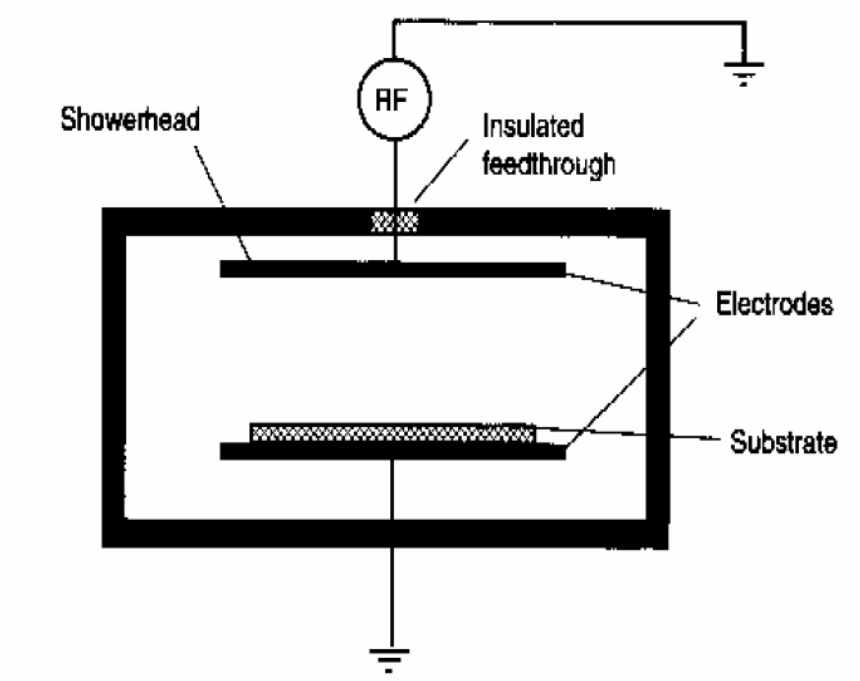

Fig.2.10.Diagram of a RF plasma reactor.

Microwave Plasma Reactor

Microwave plasmas are sustained by power supplies operating at a frequency of 2.45 GHz. This frequency, which is commonly used for industrial or home heating applications, makes suitable power supplies readily available. The excitation of the plasma by microwaves is similar to the excitation with RF, while differences result from the ranges of frequencies.

In a typical microwave plasma the strength of the electric field is about E~30V/cm; therefore, in a collisionless situation, the corresponding maximum energy acquired by an electron during one cycle is about 0.03eV [39]. This energy is far too small to sustain a plasma. Therefore microwave discharges are more difficult to be sustained at low pressures (< 1torr) compared with the DC or RF discharges.

In a collisional discharge, the absorption of microwave power is a function of the collision frequency of the electrons with the heavy species and is therefore dependent on the pressure in the discharge. For a microwave frequency of 2.45GHz, efficient microwave absorption in helium, for example, occurs at 5-10 torr [40]. For other gases, the optimum pressure for microwave discharge is in the range 0.5-10 torr.

While the RF glow discharge can be made to extend virtually throughout the entire reactor, whose dimensions are much smaller than the wavelength of the RF field (~22 m at 13.56MHz), the microwave plasma has its greatest glow because of the coupling microwave cavity and diminishes rapidly outside it, because of the much smaller wavelength of the microwave (X=12.24 cm for a frequency of 2.45GHz). In the microwave plasma, the magnitude of the electric field can vary within the reactor, which now has dimensions of the same order of magnitude as the wavelength. One can thus find active species from the discharge still persisting into a region free of the glow of the plasma, that is, in afterglow.

Microwaves are easily absorbed or reflected by most materials and cannot be transmitted via cables, like RF energy, without significant losses. Special coaxial cables can be used to transmit low-power (<200 W) microwaves. The coax consists of two concentric conductors separated by a dielectric. For higher-power levels, specially designed wave-guides have to be used. The cross sections of the conductors of the

coax or the waveguide are determined by the wavelength of the microwave. A microwave power supply system is illustrated in Fig.2.11 and consists of:

1. A filtered, low-ripple microwave power supply of constant frequency but variable power;

2. A circulator, whose role is to protect the power supply from large reflected power which may result from an impedance mismatched microwave applicator;

3. Meters for monitoring both the incident and reflected power;

4. A variable, manual or automatic, impedance matching of the applicator with the plasma, at different and variable discharge conditions; an impedance mismatch will cause the microwave to reflect instead of propagate into the plasma.

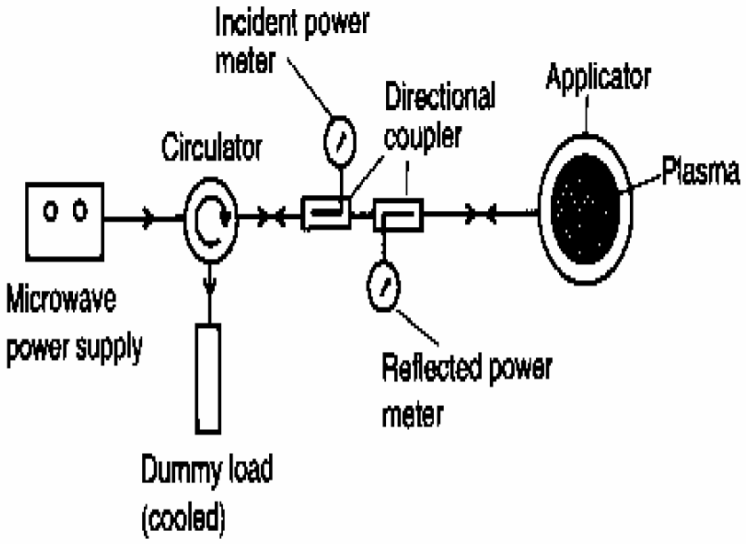

Fig.2.11. Diagram of a microwave power system for cold plasma excitation.

2.2.5.3. System Pressure

The system pressure is perhaps the most misunderstood and mistreated parameter regarding the glow discharge polymerization phenomenon. This misunderstanding comes from the lack of distinction between nonpolymer-forming and polymer-forming plasmas. As mentioned earlier, efficient glow discharge polymerization is an excellent pump. Consequently, the polymerization itself changes the system pressure. Another factor contributing to the misunderstanding is the failure to recognize the effect of product gas. In many cases, the system pressure observed before glow discharge, P_0, is cited as though it represents the system pressure during glow discharge polymerization, P_g. In some cases P_g can be adjusted with respect to P_0 by controlling the pumping rate. Since P_g is dependent on the production rate of product gas, such an operation is not always possible. Furthermore, in view of the etching effect of the product-gas plasma which is highly dependent on the amount and nature of product gas, such an operation does not seem to have any advantage or significance in controlling the process.

The following points may clarify the meaning of system pressure in glow discharge polymerization:

(i). The system pressure before glow discharge, P_0, at a given flow rate is entirely dependent on the pumping rate [30-33]. The higher the pumping rate, the lower is the value of P_0;

(ii). The pumping rate of a system is dependent on the nature of the gas and is particularly important when a liquid nitrogen trap or a turbomolecular pump is employed in a vacuum system. These are excellent pumps for most organic vapours (starting material of glow discharge polymerization) and some gases; however, they offer virtually no pumping action for H_2, which is the main product gas when hydrogen-containing compounds are used as the starting material;

(iii). As far as the gas phase is concerned, glow discharge polymerization acts as an additional pump;

(iv). Glow discharge polymerization changes the gas phase from the starting material to the product gas;

(v). Consequently, the system pressure with the glow discharge on, P_g, is largely determined by the pumping efficiency of the product gas, the efficiency of the polymerization, and the production rate of the product gas.

(vi). Therefore, there is no unique relationship between P_g and P_0. In a system where the polymerization yield is maintained at nearly 100%, P_g is determined by the flow rate but not by the value of P_0.

Since the velocity and the ionization of gas molecules are dependent on pressure [41] the value of P_g (but not P_0) is important in controlling the distribution of polymer deposition and the properties of polymers formed in glow discharge polymerization. Nevertheless, P_g cannot be considered as a manipulable processing factor. The value of P_g can be manipulated to a certain extent, but it is largely determined by the nature of the starting material (i.e. gas production rate).

A change in pressure also changes the volume and intensity of the plasma, which not only changes the relative position of the polymer-collecting surface in the plasma but also the ratio of polymer collected on the surface to the total amount of polymers formed. The discussion of polymer deposition rate has a meaning only when the ratio mentioned above is close to unity or at least does not change significantly within the range of experimental conditions.

Therefore, the dependence of polymer deposition rate on the pressure should be interpreted only in the context that the pressure is an empirical controlling factor of plasma reactor.

2.2.5.4. Flow Rate and Other Factors

Flow rate determines the amount of gas available for plasma polymerization per unit time and can also be used to determine the deposition rate of plasma polymer [42].

The flow of a monomer is generally given by the volume of the gas at standard temperature and pressure per unit time. In the case of low flow rate and low pressure the diffusion of gases is more important than the flow, whereas in the case of higher flow rate and higher pressure the flow plays the more important role. The resident time of monomer molecules in the plasma is dependent on the length of plasma in the direction of displacement (consequently, the volume of plasma) and the mass flow velocity [43].

In the diffusion-dominant case, nearly all monomer molecules coming into the reaction chamber may polymerize; consequently, the apparent rate of polymer deposition is controlled by the monomer feed-in rate (flow rate).

Nevertheless, the deposition rate increases (in the low-flow-rate region) nearly linearly proportionally to the monomer flow rate. As the flow rate increases, the resident time of the monomer in the plasma decreases [44]; as a result, the rate of polymer deposition as well as the yield of polymerization both decrease with increasing flow rate as shown in Fig. 2.12.

It should be noted here that all these observations were made at a fixed discharge wattage. As mentioned earlier, none of the parameters such as discharge power, flow rate, and system pressure can be treated as an independent parameter. All factors influence the glow discharge polymerization in an interrelated manner, and such a plot merely represents the slicing of a threedimensional profile at a fixed plane.

The following aspects should be taken into consideration when one considers the dependence of polymer deposition on operational factors such as pressure, discharge power, and flow rate.

(i). The total volume and intensity of plasma changes as the operational factors vary. Therefore, the ratio of plasma volume to the total volume of the system also changes.

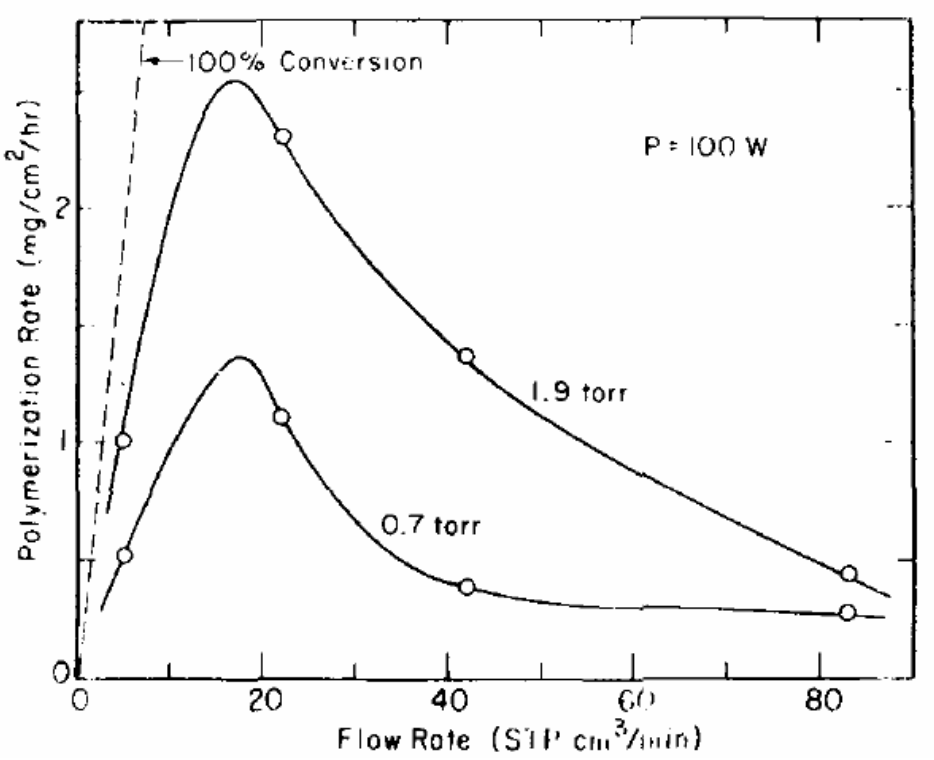

Fig.2.12. Effect of monomer flow rate on the rate of polymer deposition.

(ii). The surface on which polymer exclusively deposits may change with operational factors. If the polymer deposition rate is measured with a substrate placed on the inside surface of an electrode, it may lead to a dramatic decrease in the polymer deposition rate at lower pressures. However, it may simply be due to the shift of the polymer deposition surface at lower pressure when the polymer starts to deposit more on the other side of the electrode and also on the wall of the chamber.

(iii). The medium in which glow discharge polymerization occurs is not homogeneous. Therefore, the location of the polymer deposition surface and the type of glow to which the surface is exposed are very important factors.

Other important parameters for a plasma deposition include: the discharge power, geometrical factors of the plasma reactor, nonpolymerizable gas, distribution of polymer deposition etc.

2.2.6. Creation of Chemically Reactive Species in a DC Discharge

The foundation of the chemistry of plasma polymerization and of plasma treatment of material surfaces is based on the chemical reactions of reactive species created by the dissociations of organic molecules caused by the impact of electrons, ions, and excited neutral species in the plasma. Although the primary species created by the ionization of organic molecules or fragmented moieties may not play the dominant role, it is quite clear that the whole process does not proceed without the ionization process. Therefore, it is important to recognize the fundamental step of ionization in a gas discharge system. For this purpose, we shall consider the simplest case of ionization of argon in a DC glow discharge This model is used in explaining the fundamentals of a glow discharge [45].

In a DC discharge plasma polymerization reactor, a constant voltage is applied between a cathode and an anode, and the luminous glow develops near the cathode surface. The maximum of the electric field exists near the surface of the cathode, and the acceleration of electrons mainly takes place in this region. The ionization of an argon atom occurs when an electron gains sufficient energy to ionize the atom. Therefore, the ionization of argon takes place in the vicinity of the cathode glow. The electron temperature (T_e) rises as electrons are accelerated in the electric field. During this process, the number of electrons is relatively small. When the electron temperature reaches the maximum level as a function of the distance, T_e starts to drop significantly, but the number of electrons starts to increase as electrons are pulled towards the anode. The positively charged argon ions will be pulled towards the negatively charged cathode surface and cause the emission of secondary electrons, which will be accelerated while travelling in the cathode fall region. Beyond the cathode fall region, very little electric field exists and no significant acceleration of an electron occurs. The major portion of the negative glow is filled with a large number of electrons, whose energy is not high enough to ionize a significant amount of argon but high enough to create argon atoms in various excited states.

When speaking about organic molecules instead, the consequence of ionization is much more complex than the simple case of the argon glow discharge presented above. However, the movement of electrons can be considered to be similar to the case shown

for argon glow discharge. As so far as plasma chemical vapour deposition (PCVD) is concerned, the location where the creation of reactive species occurs and its relative position to the substrate surface, on which plasma polymers are deposited, are important factors to be considered.

The well-characterized DC glow discharge is more or less limited to the discharge of inert gases. When an organic gas, instead of an inert gas, is used in the same discharge reactor, a nearly completely different phenomenon occurs, in which the deposition of material occurs and the composition of the gas phase changes continuously as deposition proceeds.

This difference can be further illustrated by an example for glow discharge of argon and of acetylene.

Let us consider a closed system (i.e. argon or acetylene). In this case, the discharge is completely different and can be summarized in the following way. The glow discharge of argon can be maintained indefinitely, and diagnostic measurements such as electron temperature measurement and emission spectroscopy could be carried out in such a steady glow discharge. In contrast to this situation, the glow discharge of acetylene extinguishes within a few seconds to a few minutes depending on the size of the tube and the system pressure. This is because acetylene forms polymers and deposits on the walls of the reactor. In the process of plasma polymerization of acetylene, very little hydrogen, or any gaseous species, is created, and the plasma polymerization acts as a vacuum pump. When the system pressure decreases beyond a certain threshold value, the discharge cannot be maintained.

A similar situation can be also seen in a flowsystem discharge. Again, argon discharges can be maintained indefinitely under a steady-state flow of argon under a given pressure. This is not the case with acetylene glow discharges. At a relatively low flow rate and when the pumping rate is not controlled to adjust the pressure change (i.e. under full pumping capacity), the acetylene is consumed (by plasma polymerization) faster than it is replenished by the flow of acetylene. As a result, the system pressure decreases, and the glow discharge extinguishes. In a flow-system, however, acetylene is fed into the system continuously at a given flow rate, and the system pressure increases as soon as the glow discharge extinguishes. As the system pressure increases back to the pressure, where breakdown of the gas phase could occur

under the applied voltage, glow discharge is ignited again, but the re-ignited glow discharge follows the same path of the first discharge. As a consequence of these processes, the glow discharge occurs as a self-pulsating intermittent discharge. A significant difference between glow discharge of an inert gas such as argon and that of an organic compound such as acetylene is the fundamental step of creating excited or reactive species.

The direct ionization of the entire molecule is rather an unlikely event. The ionization would occur with fragmented moieties in the case of organic gases. Species that contribute to the deposition of materials in the cathode region are mainly created by the electron impact dissociation in the cathode dark space. Ions are pulled to the cathode surface by the electric field. As the energy increases, as an ion travels towards the cathode, neutral species (including the monomer) are dissociated by the ion impact dissociation. The polymer forming (reactive) species thus created in the dark space near the cathode are not photon-emitting species [46].

Polymer-forming species thus created in the cathode region of a DC discharge, presumably free radicals and cation-free radicals, are deposited on the cathode surface and form a solid film by reacting with the substrate surface and each other.

In order to maintain glow discharge, however, the secondary electrons must be emitted from the cathode surface. This means that the secondary electrons must come out of the cathode surface, which could be sufficiently covered by the deposited plasma polymer. The emission of secondary electrons from the surface of dielectric materials is a well-known phenomenon. In the case of plasma polymers, it can be understood that the surface state electrons, which are responsible for the contact electrification of the polymer surfaces (static charges), could be emitted as the secondary electrons to sustain the glow discharge. An ultrathin layer of plasma polymer (up to cca. 100 nm) is electrically conducting as evidenced by the fact that a plasma coated metal plate can be coated by the electrochemical deposition of paint (E-coating) []. Thus the plasma polymer layer remains at the same electrical potential of the cathode (within a limited thickness) and the work function for the secondary electron emission does not increase significantly.

Another important factor is the negative glow in a DC discharge, which is observed in the plasma polymerization process. The negative glow constitutes the main body of

glow in which plasma polymerization of organic vapours generally occurs in high-frequency discharges. The negative glow in a DC discharge should also cause plasma polymerization of an organic vapour. The mechanisms of the creation of polymer-forming species in the negative glow must be significantly different from that for the cathodic polymerization described above. While the ionization is essential for sustaining the glow discharge, the reactive neutral species (free radicals), which can be considered as the byproducts of the ionization, are dominant species that control the deposition of an organic compound in plasma [47]. The difference in the deposition kinetics in the negative glow and in the cathode dark space, strongly indicates that the cathodic deposition is not the deposition of species that are created in the negative glow and enhanced by the electric field in the cathode fall.

The formation of reactive species and the deposition of materials in the cathode region can be called as cathodic polymerization and those occurring in the rest of the space will be named plasma polymerization. According to this distinction of two processes, the cathodic polymerization takes place in the "dark" space, and the plasma polymerization occurs in the "glow". The "dark" and the "glow" regions refer to the location where the plasma polymerization process takes place. Polymerization does not emit photons because the excess energy is dissipated in the chemical reactions to form polymers. Polymerization and photon-emission are both deactivation processes of excited species and compete with each other in the plasma process.

In a DC discharge, a relatively smaller amount of deposition occurs on the anode surface than what occurs on the cathode. Experiments involving plasma polymerization in DC discharge show that the anode deposition pattern has the shape of the cathode (i.e. a rectangular cathode produces a rectangular-shape deposition on a larger square anode). The deposition on the anode surface is not pressure dependent. Research tests demonstrate that in the case when a floating substrate is placed between the cathode and the anode, the deposition on the anode shows the shadow of the substrate. The size of the shadow, in which no deposition is observed, is proportional to the size of the substrate that is placed in front of the. These results indicate that the anode is a passive surface as far as the plasma polymerization is concerned. The deposition does not change from the floating substrate placed between cathode and

anode, which receives deposition by the "glow" plasma polymerization in the negative glow region.

In plasma polymerization, the activation (formation of the reactive species) and deactivation (deposition of materials) are coupled, because the power input is directly applied to monomer gases and the polymerization occurs generally in the glow region of a reactor. Mainly, the activation of an organic molecule for the "glow" polymerization starts at the boundary of the glow. The supply of the monomer into the glow volume is a crucially important factor because the monomer is consumed in the glow by depositing polymers and the numbers of polymer-forming species in the glow decreases.

2.2.7. The Competitive Ablation and Polymerization (CAP) Principle. Plasma Sensitivity of Elements in Plasma Polymerization and Plasma Treatment

The Competitive Ablation and Polymerization (CAP) principle [47] is a basic concept that relates the ablation of materials in plasma (gases and solids exposed to plasma) to the deposition of a solid from the plasma phase. Plasma polymerization and plasma treatment cannot be explicated without considering the fragmentation of molecules in both the gas and solid phases. The principle was established by merging two separate observations made in two different plasma processes aimed at mutually opposing objectives. Dr. Eric Kay's group at IBM was working on the etching of Si by perfluorocarbon plasmas. Dr. H. Yasuda's group at the Research Triangle Institute was working on the plasma polymerization of perfluorocarbons. In the etching study, it was found that when hydrogen was present in a perfluorocarbon plasma etching system, a deposition of materials, instead of etching, was observed [48]. In the plasma polymerization study, it was found that a decrease in the weight of a substrate, rather than a weight increase, was observed when the power-input level was raised above a threshold value [49]. The implication of these findings is that ablation and polymerization could occur in a competitive manner in either plasma etching or plasma

polymerization, and the balance depends on the overall system conditions of the plasma.

Therefore, what happens in a plasma process cannot be determined in an a priori manner based only on the nature of the plasma gas or on the objective of the process. A plasma etching process, such as the pre treatment of an alloy substrate, could result in the deposition of a polymer, and a plasma polymerization process could etch a substrate material. The plasma-sensitivity series of elements involved determines the balance between ablation and polymerization by influencing the fragmentation pattern of molecules in the plasma environment. Plasma sensitivity refers to the fragmentation tendency of materials and surfaces that come into contact with plasma, which contains various energetic species including ions, electrons, excited species, meta-stables and chemically reactive species. Bombardment with energetic species such as electron-beams, ion-beams, or X-rays causes much more severe fragmentation than contact with plasma. Plasma sensitivity refers to the latter case rather than sensitivity to ionizing radiation. The plasma sensitivity series orders the sensitivity of elements to a plasma, in a manner similar to the expression for the ionization of metals in solution by the galvanic series. Nowadays, however, there is no clear plasma sensitivity table established. Nevertheless, there are some trends that seem related to the plasma sensitivity series. These are behaviours in terms of weight loss rates when polymeric materials are exposed to plasmas [50]. It is important to recognize that the ionization of a molecule, particularly an organic one, does not follow the same process applicable to a simple mono-atomic gas. The bond energies which link elements are much smaller than the ionization energies of mono-atomic gases used as carrier gases in low-temperature plasma processes. As a result, the creation of a plasma state of an organic molecule, by itself or with a carrier gas, causes fragmentation of the molecule.

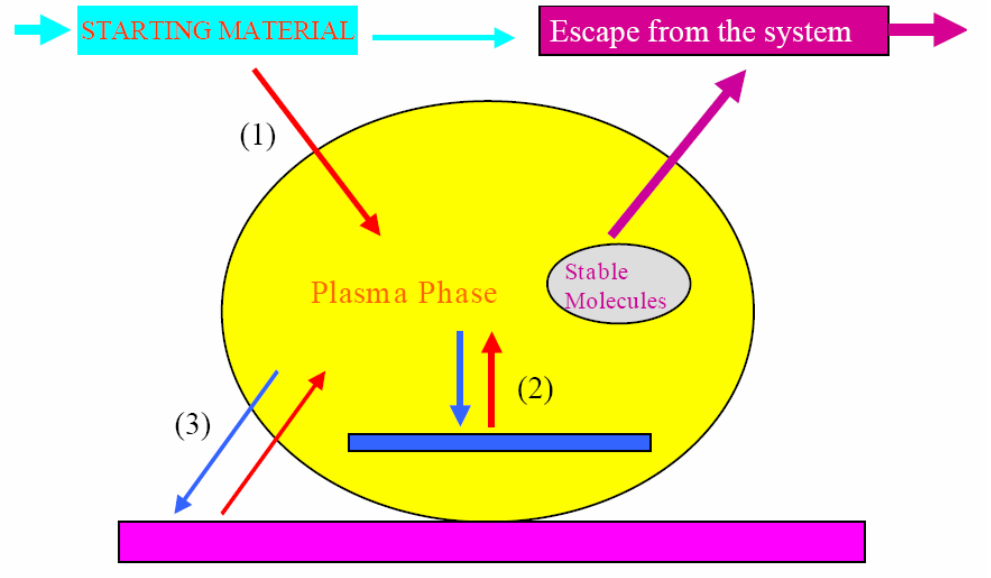

Fig.2.13. Schematic diagram of the Competitive Ablation and Polymerization (CAP) principle: (1) ablation of monomer to form reactive species, (2) deposition of plasma polymer and ablation of solid including plasma polymer deposition in plasma phase, (3) deposition to and ablation from nonsubstrate surfaces (in and out of plasma phase).

The schematic diagram of the CAP [51] principle is presented in Fig.2.13. In this scheme, there are four major processes necessary to complete the mass balance in the reactor: (1) monomer feed-in, (2) ablation, (3) material deposition, and (4) escape from the system (pump out). The formation of reactive species is an ablation process, because, in general, a considerable amount of fragmentation of the monomer (starting material) occurs. Material deposition occurs via plasma formation of reactive species. But, this it is not a simple step of forming a polymeric material from a set of reactive species. The reactive species do not necessarily originate from the monomer, because the ablation process can and does contribute. Gaseous reactive species can originate from the once deposited material (plasma polymer) and also from the reactor walls or any other solid surfaces that are in contact with the plasma. The following important steps that constitute the CAP principle can be considered:

(i). Ablation - which is fragmentation, is involved in every process (i.e. monomer to reactive species, plasma polymer to reactive species, wall surface to reactive species and escape of fragmented species from the system). Fragmentation of molecules is the primary effect of plasma exposure of a material.

(ii). The reactive species are created not only by fragmentation of the monomer but also by fragmentation of the plasma polymer formed and of materials existing on the various surfaces that come into contact with the plasma.

(iii). The escaping species consist of "non-polymerforming" stable species and some "un-reacted" monomer depending on system conditions (such as power input level, flow rate, flow pattern, pumping rate, shape and size of reactor etc).

(iv). The species that do not contribute to polymer formation are basically stable molecules, such as H_2, HF, and SiF_4. When these species are created in a plasma, the balance between deposition and ablation shifts. However, the manner in which the balance shifts is dependent on the specific system. The formation of stable escaping species is crucially important in determining the nature of the depositing materials.

In order to elucidate the mechanisms by which a polymeric material deposits and also those by which the surface modification of a polymeric material by plasma proceeds it is essential to understand the CAP principle [51].

2.2.8. Plasma Treatments and Summary

Plasma polymerization processes were noticed for the first time it the beginning of the last century when the deposition of some organic compounds on the walls of a discharge generated in acetylene was observed. Considered to be a "mystery" of the electrical discharges,

researches in the field of plasma polymerization had an impressive development during the last two decades. Plasma polymerization is now regarded to be one of the main branches of the polymer science and of plasma chemistry.

In plasma polymerization processes, the monomer does not need to have a double bond, an aromatic structure or a unsaturated bond in order to be able to form polymers. Practically all the carbon (or silicon) compounds can be polymerized in plasma. Due to the high energies (compared to the binding energy of molecules) of the plasma species (electrons, ions, excited species) the modification of the initial structure of the monomer is expected and new compounds are obtained. Because of this behaviour, plasma polymerization mechanism is also named "Plasma Atomic Polymerization". The plasma polymers are characterized by an three-dimensional (network) structure and not by a one-dimensional chain structure like the usual thermo-plastic polymers. Also, plasma polymers don't have unique repeating units. In the frame of this main characteristic of a polymer, plasma polymers are not polymers, but macromolecular compounds obtained in plasma. A more adequate name for them could be amorphous carbon (or silicon) materials. By changing the plasma conditions one can perform a partial or a total break of the initial structure of the monomers and consequently the properties and structure of plasma polymers can be drastically modified. Many types of deposits can be achieved starting from powders and oils to insoluble and wear resistant (thin) films.

The polymers obtained by conventional chemistry methods are produced on large industrial scale and have a huge number of applications in the field of textile industry, plastic materials and electric insulators. Due to the

uniformity of the polymeric chain they have good strength to weight ratio as well as excellent plastic and elastic properties. Conventional polymer manufacturing methods represent a major revolution in the field of the material technology allowing the production of macromolecular compounds having the desired chemical, optical, and electrical properties and presenting excellent mechanical properties. However, most of the polymers obtained by using the methods of conventional chemistry are characterized by a low corrosion resistance and a high degree of solubility. [52-58]

In fact, plasma polymerization can be considered to be not a regular polymerization technique, but an efficient method for depositing of (thin) polymeric films or a tool for changing of surface structure starting from carbon compounds. Properties of plasma polymeric films are very different, covering a broad field of applications (films for improving adhesion and compatibility at the interface, wear resistant films, thin films used in membrane separation processes, hydrophobic films for optical applications, organo-metallic films for microelectronics, films used for biocompatible materials) [59-65].

Plasma finecleaning Plasma etching	Plasma modification	Plasmapolymerisation
- Removing of thin organic layers (release agents, adsorbance layers) - Reduction of oxized layers - Photoresist stripping - Plasmaetching	Increase of - wettability - adhesive strength for bonding, printing, painting and vulcanisation primers - adhesive strength of metallization - hydrophobic properties	deposition of thin layers with properties like: - hydrophilic - adhesion promoting - biocompatibility - diffusionbarrier - antifogging - scratch resistant

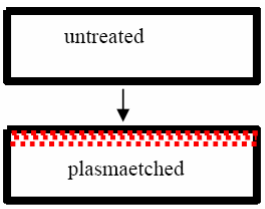

+ easy process
+ good hydrophilisation
+ nearly no aging
- strong degradation of the polymers
- hydrophilic layer only weak bounded (WBL)
- typically not useful for achieving good adhesion properties
- not suitable for fluidic applications

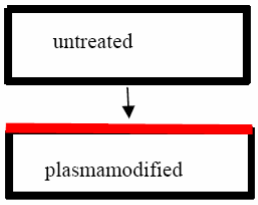

+ easy process
~ sucess extremly dependant ohne correct chosen paramters (especially the process gas)
~ good wettability seldom a useful criteria for good adhesion properties
- for most polymers, short lifetimes are observed
- result dependent from composition of the substrate
- no temperature stability

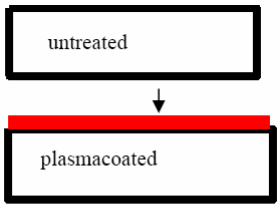

+ good results for all typical used polymers
+ not dependent on the type of substrate
+ reduced degradation
+ excellent aging behavior
+ excellent temperature stability
+ good coherence between wettability and adhesion

In another category of plasma-organic compounds interactions one can include the surface plasma treatments. This technique changes the surface properties of a conventional polymer, with the purpose of generating polar groups, reactive species and crosslinking of the surface molecules, allowing to improve wettability, adhesion, wear resistance and chemical reactivity.

There are categories of plasma – monomer interactions (Plasma Assisted Polymerization) in which the plasma is not directly involved in forming the polymeric structures. In this particular case, plasma is used only as initiator and as a catalyst for the conventional polymerization processes, either in gas or or in liquid phase. The main advantage of Plasma Assisted Polymerization is represented by the very high degree of the polymerization that is conferred to the polymers obtained with this method.

2.3. Polyaniline Thin Films Obtained via Plasma Polymerization Technique

Chemical and electrochemical polymerizations are common methods used to obtain polyaniline thin films on different types of substrates [66,67]. However, the technique of plasma polymerization is increasingly being used as an alternative for obtaining polymer thin films [68]. Polymer thin films obtained by plasma polymerization technique are different from those obtained by the conventional technique. The properties of these films can be tailored according to requirements by varying the deposition parameters like pressure, applied voltage, monomer flow rate and time of polymerization. Pinhole free, chemically inert, thermally stable and of of uniform thickness polymer thin films can be deposited by employing plasma polymerization technique [69,70].

Aniline is considered as a starting monomer to produce conducting polymers, as homopolymer or by doping with anions. Polyaniline (PANI) is usually obtained in solution by direct oxidation of aniline or by electrochemical oxidation [71]. This process is used to obtain linear PANI and sometimes is combined with simultaneous doping methods to increase its conductivity. Linear PANI is an electric insulating polymer but can be converted to a semiconductor by doping the compound with halogens and other anions. Crosslinked PANI shows similar behaviour with lower values of conductivity. Films of PANI are difficult to synthesize by conventional chemical methods because they form powders when recovered from the starting acid solution. Some PANI films over insulating substrates have been prepared by chemical oxidation using very dilute aqueous solutions of aniline [72]. Thin films of around 1 micron in thickness of chemically synthesized PANI have also been prepared by thermal and/or vacuum evaporation of the polymer powder [73]. Paloheimo et al. [74] recently used the layer-by-layer self-assembly method for fabricating thin films of PANI.

Another method of PANI film synthesis, less commonly used, is by plasma polymerization. The chemical reactions are promoted by excitation and/or ionization produced by collisions of the monomer molecules with the electrons immersed in a plasma generated by electric discharges. The best suited plasma for polymerization is

the glow discharge. In this process the polymerization occurs without the presence of other reagents, such as the oxidant agent and the solvent in the liquid phase, giving a product without major contamination. The reactions can also be combined with other compounds looking for specific characteristics in the final polymer. There is not much information about PANI synthesized with this technique. Bhat and Joshi [75] synthesized PANI by plasma polymerization using the RF inductive coupling mechanism. The plasma polymerization method has also been used to synthesize other conducting polymers [76-78].

The figure below presents the four idealized oxidation states of PANI: leucoemeraldine, emeraldine, pernigraniline and emeraldine salt. Different structures result in different electrical behaviors of the material [79].

Emeraldine salt is a partially oxidized compound, protonated, with electrical conducting characteristics. Leucoemeraldine is a reduced compound with low electrical conductivity characteristics. There are no double bonds between the aromatic rings and the N–H groups. Emeraldine base is an insulating compound, partially oxidized with few N–H groups in the main chain. Emeraldine changes from insulator to conductor when it is protonated with proton donor acids, such as HCl. This change is one of the most interesting properties of PANIs. The structure of emeraldine PANI can be changed to emeraldine salt by removing an electron from the N–H group. Pernigraniline is a fully oxidized compound without conducting characteristics. There are no N–H groups in the structure. The level of protonation in the structure causes dramatic changes in the conductivity. Another factor that affects conductivity in doped PANIs is moisture. It is known that moisture increases the conductivity in doped PANIs by changing the electrostatic interaction between anions and positive charges.

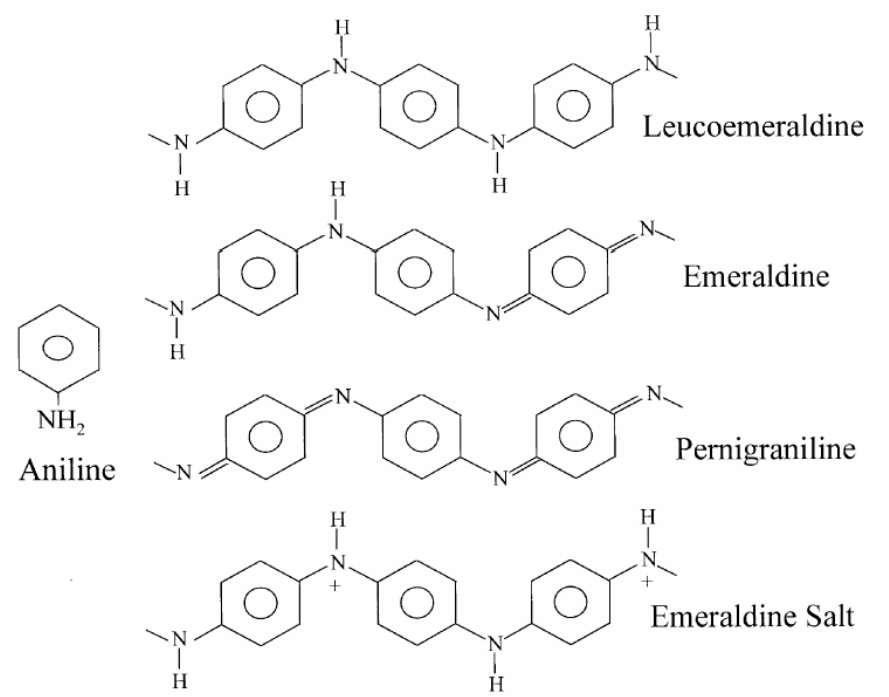

Fig.2.14. Representation of various oxidation states of Polyaniline.

Various thin polymer films were deposited via plasma polymerization technique in a DC plasma glow discharge reactor (Fig.2.15). The special geometry of the electrodes conferred an uniform deposition of the polymer films onto a ITO (indium Tin Oxide) Glass substrate.

The experimental conditions for the deposition of the polymeric films were the following: system pressure $5x10^{-2}$ – 0.5 Torr (measured with a thermal conductivity Pirani gauge), applied voltage up to 2KV, discharge current up 20mA, distance between electrodes in the range 15-30cm.

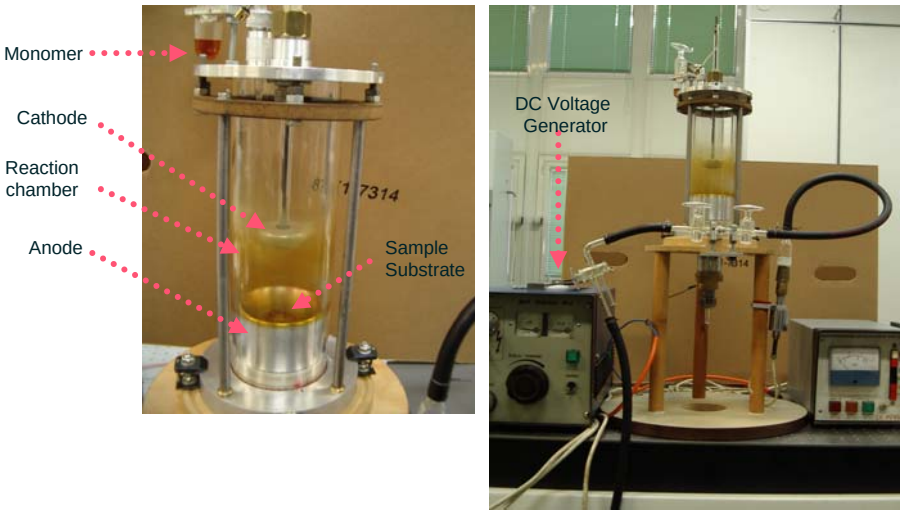

Fig.2.15. Plasma Glow Discharge Reactor for Plasma Polymerization.

Fig.2.16. Glow Discharge polymerization inside the DC Reactor.

The polymerization period varied between 20 and 240 seconds in function of the used monomer, the flow rate and applied voltage in base of the desired film thickness.

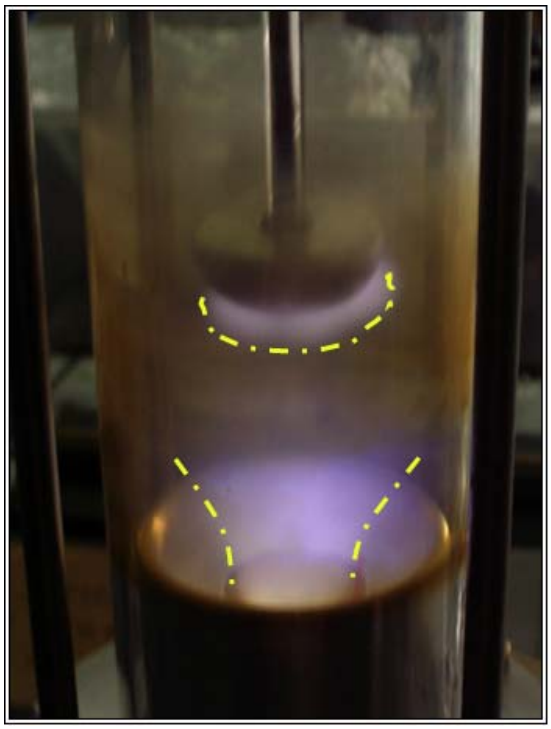

Fig.2.17. The special geometry of the electrodes ensures an uniform deposition of the polymer films.

In a flow-system, the monomer was is fed into the system continuously at a given flow rate, while the system pressure slowly decreased. The blue-violet glow discharge colour inside the reactor chamber shows that the polymerization occurred in the space between the electrodes (glow polymerization) (Fig.2.16). At the end of the deposition, upon closure of the monomer container, the glow discharge occurs as a self-pulsating intermittent discharge while the remaining monomer (inside the plasma chamber) is deposited onto the substrate. Polyaniline (PANI), poly- (*o*-anisidine), polypyrrole, and polythiophene polymer thin films were obtained via glow plasma polymerization (starting from vapours of respective monomers) (Fig.2.18) [80-82].

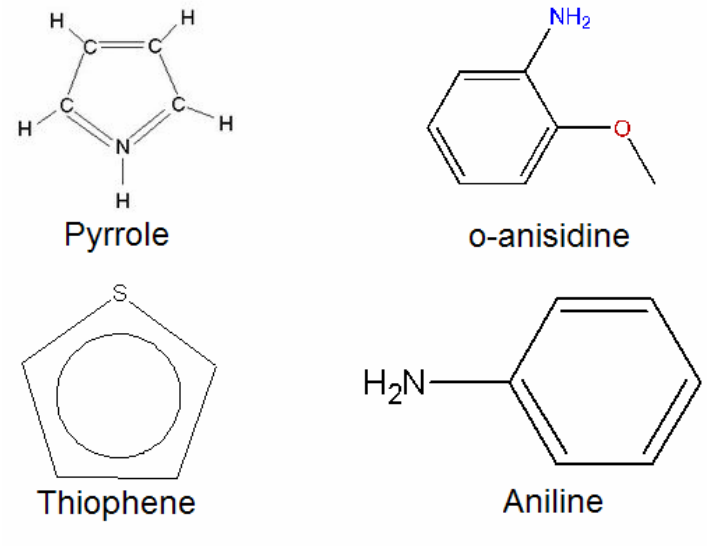

Fig.2.18. Structure of different monomers used in glow plasma polymerization.

The thickness and topography of the films was investigated using ellipsometric and scanning electron microscopy techniques.

Atomic force microscopy measurements reveal a relatively uniform film topology for a PANI thin polymer film, as in can be observed from Fig.2.19.

By preparing a sample and then making a deep cut in the polymeric film or by partially covering the substrate during deposition it was possible to estimate the thickness of the film. The obtained results were verified by ellipsometric measurements (using a VASE Instrument).

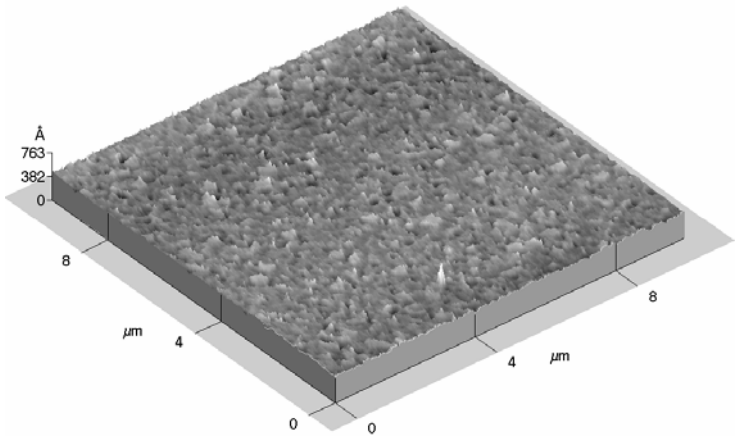

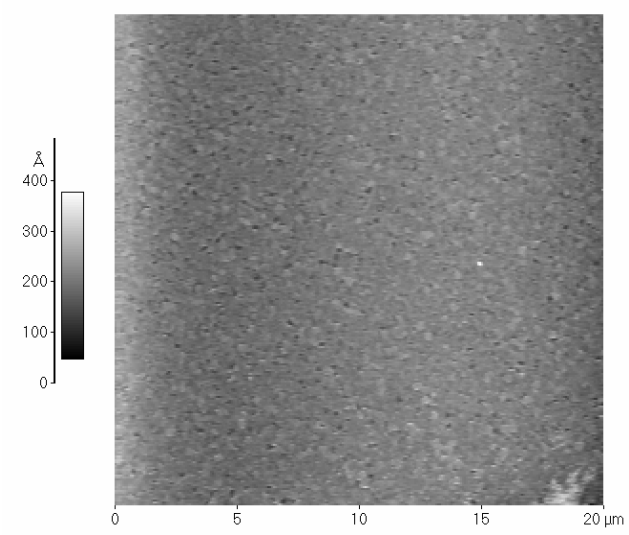

Fig.2.19. Polyaniline thin polymer film deposited via plasma polymerization. 3D (top) and 2D (bottom) mapping of the surface using the AFM.

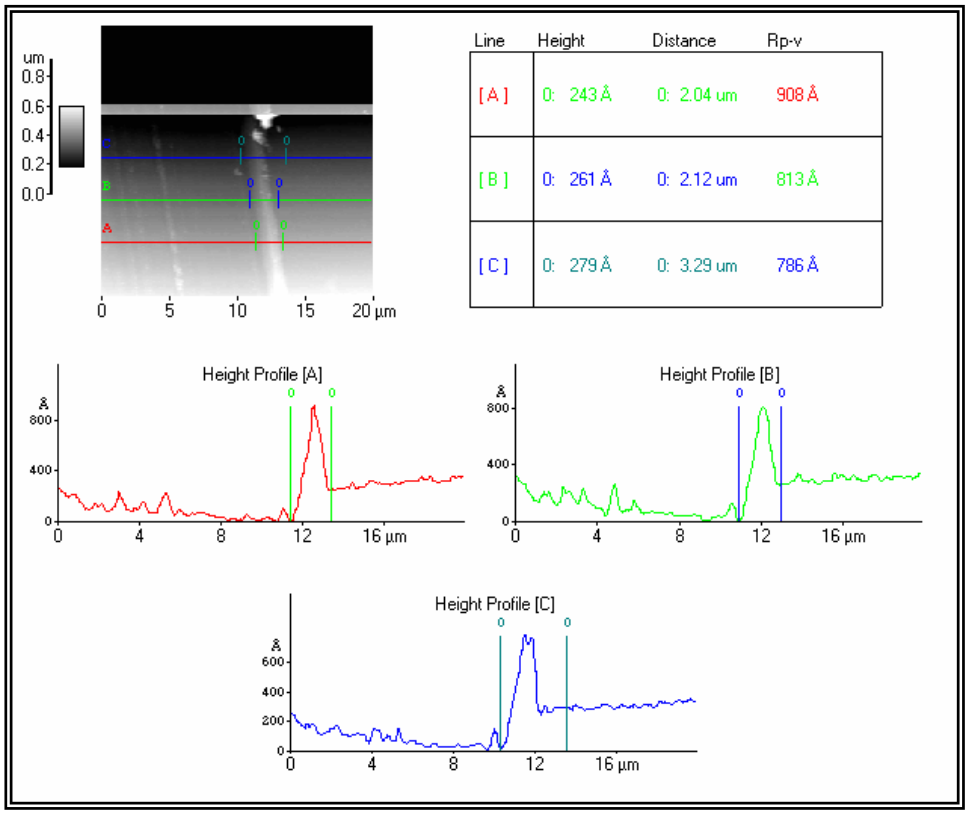

Fig.2.20. AFM thickness measurements on a PANI substrate.

By changing the experimental parameters of the deposition we were able to obtain polymeric films ranging from 50A up to 200 nm in thickness.
The yellowish colour of the PANI thin film, as well as the strong yellow colour of the interior of the plasma reactor indicate that plasma obtained PANI consists mainly of leucoemeraldine base (i.e. the most reduced form) (Fig.2.14).

2.4. Fast Electro-Optic Switching in Nematic Liquid Crystals Cells. Experimental Results.

Organic thin films have recently received a great deal of interest due to their extensive applications in the fields of mechanics, electronics and optics. Applications include chemical, physical and biological sensors, microelectronic devices, non-linear optical and molecular devices. Ultrathin polymer films can be mainly prepared in two ways: one includes wet processes like Langmuir-Blodgett, spreading, dipping or solvent casting methods; the other is dry processing, such as physical vapour deposition and chemical vapour deposition. Of these methods, the chemical vapour deposition methods, such as plasma polymerization, are frequently used to make polymer thin and ultrathin films.
During the last decades plasma has been extensively investigated due to the possible application in technology, synthesis and processing of polymeric materials and spectroscopy.
Plasma polymerization is a unique technique used to fabricate polymer films (ranging from 20A up to several microns in thickness) from a variety of organic and organometallic starting materials. Plasma polymerized films are pinhole-free and highly crosslinked, thermally stable, chemically inert and mechanically tough. Furthermore, such films are often highly coherent and adherent to a variety of substrates including conventional polymer, glass and metal surfaces. Due to these excellent properties they have been undertaken very actively in the last few years for a variety of applications such as anticorrosive surfaces, permselective membranes, protective coatings, scratch resistant coatings, chemical barrier coatings, electronic and

optical devices (electrical resistors humidity sensors, optical filters), biomedical materials and adhesion promoters.

In this chapter it is presented and characterized a very interesting phenomenon of electro-optic switching in asymmetrical nematic liquid crystal cells having as one-side boundary a thin film of plasma polymerized polymer.

The electric conductivity in ordered phases of pentylcyanobiphenyls (5CB) or hexylcyanobiphenyls (6CB) across phenyl rings $\sigma_\perp$ (i.e. perpendicular to the nematic director n) is much higher than along n ($\sigma_\parallel$). Typically, $\sigma_\parallel \sim 6 \times 10^{-8}$ S/m while $\sigma_\perp \sim 9 \times 10^{-7}$ S/m, leading to a relative anisotropy of:

$$\sigma_a = \frac{\sigma_{ll} - \sigma_\perp}{(\sigma_{ll} + 2\sigma_\perp)/3} \approx -135\% \qquad (2.5).$$

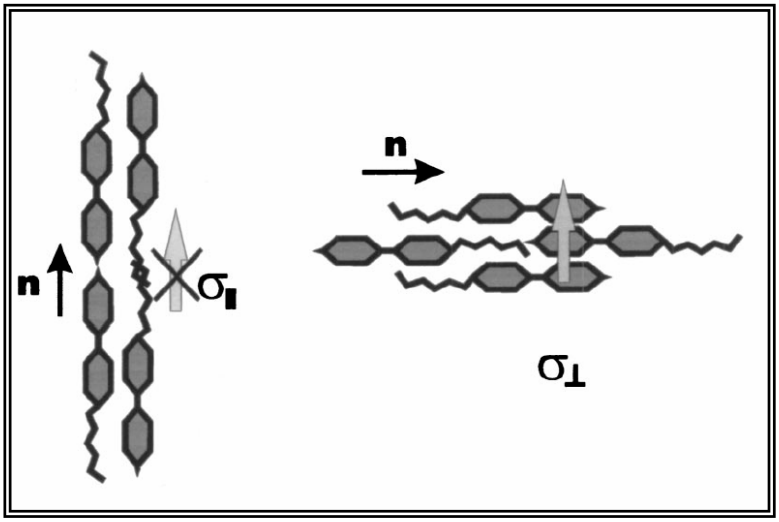

Fig.2.21. Parallel and perpendicular values of the conductivity tensor in nematic biphenyls. In the parallel case the alkyl tails do not favour electronic transport from one molecule to the other.

This large negative anisotropy has been explained by considering the contribution to the electric conduction of delocalized π electrons [83]. This type of conduction

anisotropy has also been seen and explained in the case of discotic liquid crystals [84-87]. Using the strong dielectric anisotropy of nematic liquid crystal molecules, all nematic liquid crystal displays (LCD) presently in use are based on texture changes in thin films of a nematic material under the application of a suitable external electric field (either DC or AC).

The easiest way to describe the molecular alignment in a nematic layer is by the director n, which represents an average of the molecular long axis orientations in a very small (yet macroscopic) volume. In the absence of the electric field the equilibrium configuration of the director n is imposed only by the limiting surfaces. An electric field applied across this layer tends to rotate the director parallel to the field (in the case of positive dielectric anisotropy), eventually resulting a new configuration (texture) as a balance between the dielectric torque in the bulk and the restoring torques of the surfaces [88,89]. Changes in nematic textures directly influence the transmission of linearly polarized light through the film. Usually, starting with unpolarized light (for instance from a microscope bulb), a linear polarizer is placed in front of the nematic cell to create a polarized beam that traverses the cell and passes through another polarizer (analyzer) placed after the cell, having the polarizing direction at 90° with respect to the first one (i.e. crossed polarizers). In a planar cell the director in the nematic film lies everywhere in planes parallel to the surfaces (and perpendicular to the light beam). In a homogeneously oriented planar cell the director is also parallel everywhere to a plane that contains the light beam. If this plane is also parallel to one of the directions of the polarizers, the transmitted light is blocked, but it increases when rotating this plane until it is 45° to either direction of the polarizers. If the director is everywhere perpendicular to the surfaces (parallel to the light beam), the light is always blocked (homeotropic cell). Starting with a uniform planar configuration at 45° with respect to the crossed polarizers, a strong enough electric field across the cell can induce a homeotropic texture (director perpendicular to the surfaces) that blocks the light.

So, switching on and off the electric field turns off and on the transmitted light. This is the well-known Freedericksz transition (presented in Chapter I). It was intensely studied because it is the principal mechanism that allows functioning of LCDs. One characteristic of the Freedericksz transition in uniform planar cells is its threshold

character; that is, the planar configuration does not turn to homeotropic until a certain voltage value is surpassed. Another one refers to the characteristic switch on and switch off times. Namely, when switching on the field, the strong dielectric torque turns the director to the homeotropic configuration very fast, whereas switching it off is followed by a relaxation of the director to the initial planar texture in a much longer time. The torque due to the anchoring properties of the surfaces normally is not so large as the dielectric torque. The characteristic time at switching the field on is the order of milliseconds, whereas that at switching the field off could be as large as seconds. In the later case, the system slowly changes the refraction index anisotropy, leading to interference fringes and the transmitted light intensity oscillates. In such a situation, the refreshing frequency of a LCD would be less than 1 Hz, truly unacceptable for nonstatic displays.

To overcome these drawbacks, a strong (infinite) anchoring should be used but this, in turn, asks for larger local electric fields obtained only with thin film transistors (TFT).

We have obtained experimental evidence that very fast relaxation times appear, apparently, without very strong anchoring energies (and TFTs) [90]. Apart from their practical importance, these experiments confirm that more elaborate considerations regarding interactions within nematic liquid crystal devices are necessary to explain them [91-92].

Experimental Set-up.

In order to build a sample, capillary cells were made out of two glass plates ITO coated and filled with 5CB or 6CB. To avoid interpretation problems arising from the threshold character of Freedericksz transition in uniform planar cells, we have used hybrid alignment in the sample. Such a cell has one plate (surface) that imposes homeotropic alignment, the other one giving planar alignment. It is known that a bare ITO surface that had been immersed for a very short time (about 10 s) in a sulfochromic mixture (900 mL of H_2SO_4, 200 g of $K_2Cr_2O_7$, 80 mL of H_2O) gives homeotropic alignment. The planar alignment was induced by another plate coated with plasma polymer on top of the ITO side. Different plasma polymer films were

used: polyaniline (PANI), poly- (*o*-anisidine), polypyrrole, and polythiophene. The film thickness was estimated to be between 200 and 300 Å.

By using appropriate Mylar spacers, the thickness of the capillary liquid crystal film was 19 μm.

Without an electric field applied, a hybrid cell configuration has a director field n bending continuously in a plane perpendicular to surfaces from parallel to the polymer-coated surface to perpendicular to the bare ITO surface. If the bending plane lies at 45° to the cross polarizers directions, the light passes through the cell, although with a transmitted intensity lower than was the case with planar cells. An applied electric field has no effect on the liquid crystal molecules already perpendicular to the bare ITO surface, but forces the other molecules to align parallel to the field. The electric field increases the homeotropic character of the cell, resulting in the diminishing of the transmitted light. High enough fields succeed in overpassing the planar anchoring at PANI surface, making the cell almost homeotropic, thus blocking the light. Because on one side of the cell n has homeotropic orientation, in a hybrid cell the Freedericksz transition does not show any threshold voltage. In the following figure the two above mentioned configurations are presented.

The transmitted light has been converted to an electric current by a fast photodiode. This signal has been displayed on a CRT of a very fast digital oscilloscope and saved in digital form for subsequent processing. On each sample several spots were individuated that provided maximum transmission light; the local director was then at 45° to the crossed polarizers. For a better alignment we have also tried rubbing but the procedure could have ruined the thin plasma polymer film.

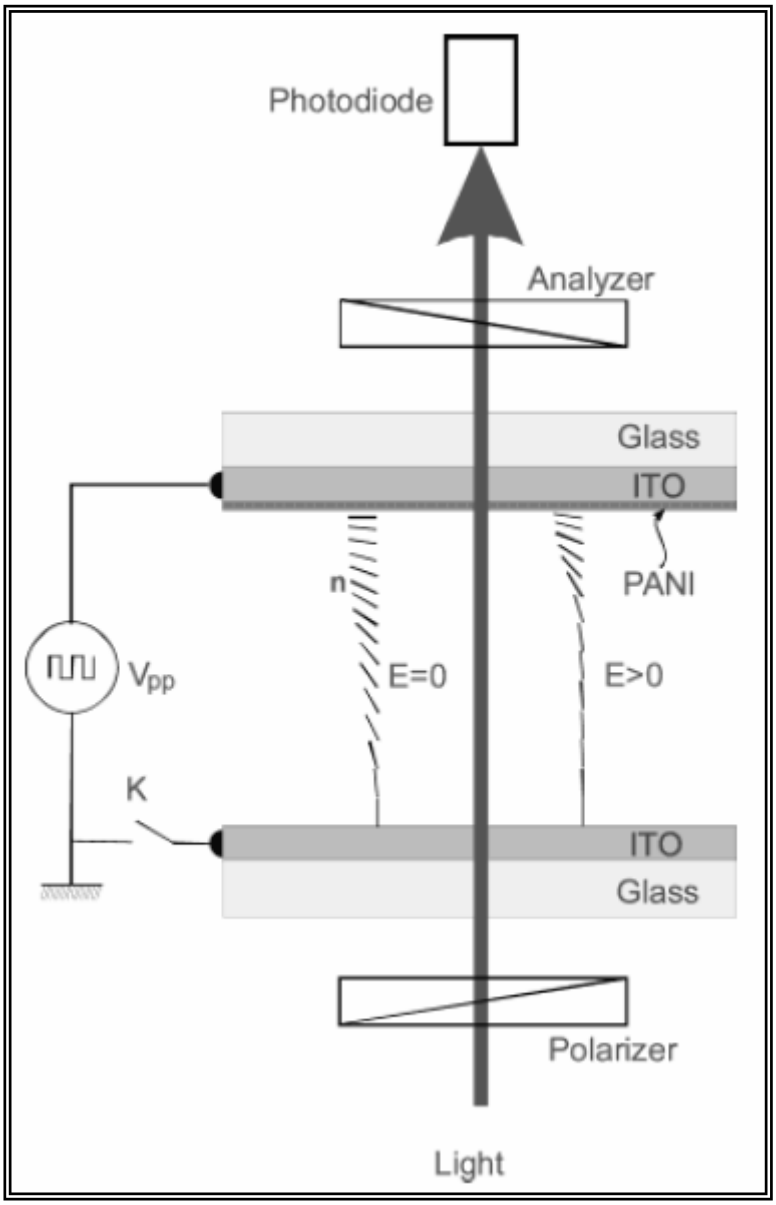

Fig.2.22. Sketch of the experimental setup. Polarizers and analyzers are crossed. Without applied electric field (left) there is a larger planar orientation than with an electric field (right).

The presented measurements were performed without rubbing. When a strong enough voltage across the sample is switched on, the transmitted light is blocked. Switching the voltage off, the liquid crystal relaxes back to the hybrid structure with a certain characteristic time and with oscillations of the transmitted light intensity. We have used both monochromatic light (He- Ne laser, 632) and "white" light (the bulb of the microscope).

Results

In figure 2.23 one may see a striking difference between the switch on characteristic time (at the instant 9 s) and the switch off time (at the instant 1 s) as well as the electro-optic oscillations. (t_{off} corresponds to the rise-up of the recorded curve and t_{on} corresponds to the fall down of the curve).

We have found some particular experimental conditions in which this behaviour is completely changed. As mentioned earlier, the electro-optic effect appears either when applying a dc voltage or an ac voltage. We have used square pulsed voltages from 50 Hz up to 15 kHz with various amplitudes from 10 to 130 Vpp. The voltage was provided by a function generator and amplified by a linear amplifier; both of them generated electric signals referred to a common ground, the cell itself being not grounded separately but floating. As the cell is not symmetric, there are two possibilities of applying the voltage: either the signal (phase) to the polymer coated ITO layer and the uncoated ITO layer to the ground, or vice versa. Switching the voltage off could also be done in two ways: interrupting the phase or interrupting the ground.

In figure 2.23, looking at the switch off part, one can observe the complete disappearance of the oscillations, remaining only the first rise-up characteristic of 2-3 ms, practically the same as the characteristic time at switch on. The plot also presents a higher transmission in the off state than the relaxed transmission for the standard behaviour (about 1.5 times higher, comparing the amplitudes between on and off states). Of the four possibilities mentioned above, the anomalous effect shown in figure 2.23 corresponds to the case when the phase was applied to the polymer side while the ground was switched off the other side.

The atypical effect has also been seen with symmetric planar cells that were made with two similarly polyaniline coated plates, the same thickness and the same liquid crystal. In this case there are, of course, only two possibilities: either switching off the phase or the ground.

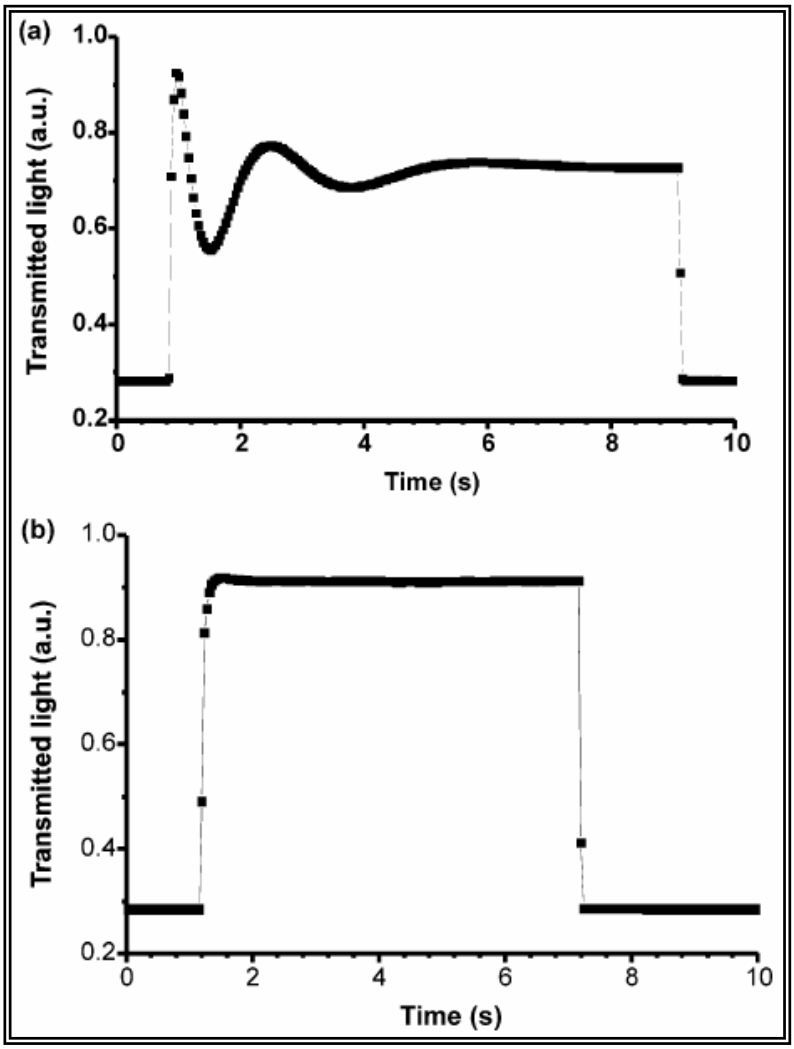

Fig.2.23. *Transmitted light versus time. Hybrid cell, 5CB, 19 μm thick. Planar orientation with PANI (thickness 300 Å). Phase on PANI, 80 Vpp, 5 kHz. Time separation between points 800 μs. (a) Switching off phase at instant 1 s and switching back on at 9 s. (b) Switching off ground at instant 1 s and switching it on at 7 s.*

In Figure 2.24, corresponding to switching off the ground, one can see an abrupt rise-up behaviour, whereas in figure 2.24a, corresponding to switching off the phase, one sees the oscillations. Also, in the former case the relaxed transmitted light has a higher intensity than in the later case.

Another set of experiments done with the hybrid cells consisted of first switching off the ground (attached to uncoated ITO side) and then the phase. In figure 2.25 there are two plots describing the intensity of transmitted light as function of the amplitude of square pulses when the phase is on and when the phase is off (the ground being always

off). With the phase off (that is, the cell completely insulated electrically) the transmitted light, of course, does not depend on the amplitude of the pulses.

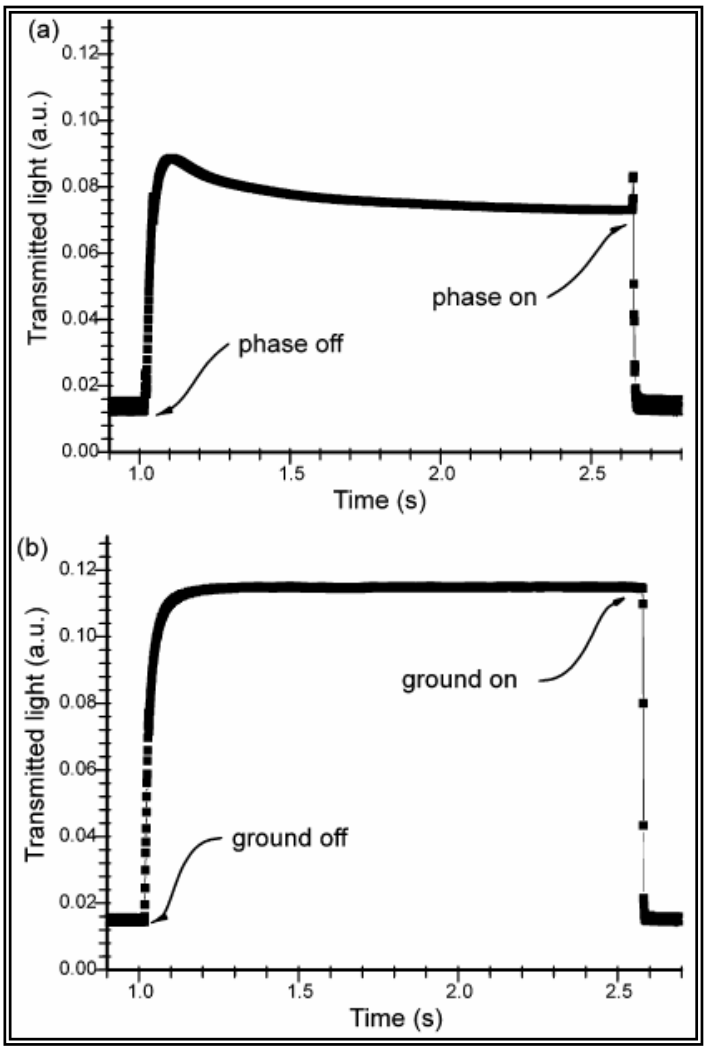

Fig.2.24. Transmitted light versus time. Planar cell, 5CB, 19 µm thick. Both plates PANI, 300 Å thick. Square pulsed voltage 80 Vpp, 5 kHz. (a) Switching phase off and on. (b) Switching ground off and on.

With the phase on, first at small amplitudes, the transmitted light is smaller than when the phase is off. Beyond a certain amplitude (60 V_{pp}) the transmitted light increases and then decreases but is always higher compared to the phase off. Then, from 140 V_{pp} on, the transmitted light with phase on is slightly smaller compared to phase off. Some recorded curves are presented in figure 2.25. It is by now clear that the anomalous

effect should be linked to specific mechanisms appearing to the ITO/PANI/liquid crystal interfaces when the phase is applied to that side. No such effect has been reported with the standard polymer coating that gives planar alignment. We also checked this with good commercial cells that use polyimide for planar alignment and did not see any anomalous effect even in a wider range of frequencies or voltage amplitudes.

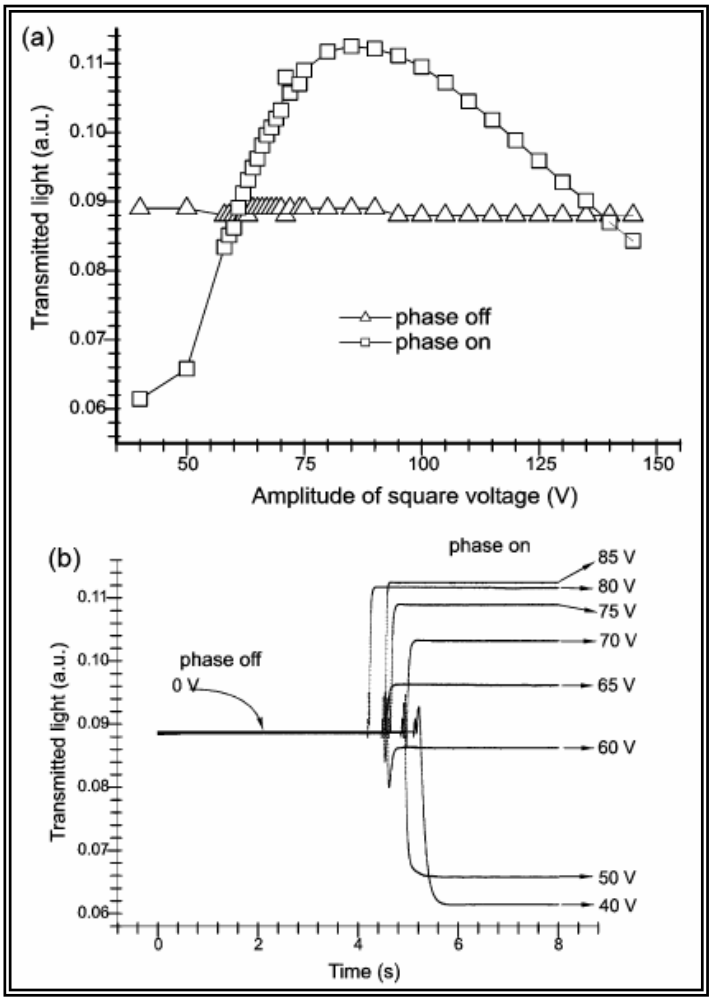

Fig.2.25. Hybrid cell. Phase on PANI, uncoated ITO floating. (a) Transmitted light versus voltage amplitude of phase (at 5 kHz). Triangles: phase off (electric insulation). Squares: Phase on. (b) Transmitted light versus time for different voltage amplitudes of phase.

It was normal to presume that the electronic processes at the interfaces should depend on the polarity of the signal. To check this, we have measured the steady current across the cell for both polarities of the applied voltage (the ground being always on the uncoated ITO side).

In figure 2.26 it is plotted the current versus time for ±65 V amplitude having applied to the ample a square wave of 6 mHz and 130 V_{pp}. It is easy to see that the conduction for negative voltage is more than twice as large as for positive voltage. Figure 2.26b presents a plot of saturation currents for various positive and negative voltages. Beyond a certain threshold, almost the same for positive and negative polarities, the cell presents rectifying properties. The positive current is limited (<2.5 μA) whereas the negative current increases linearly (absolute values).

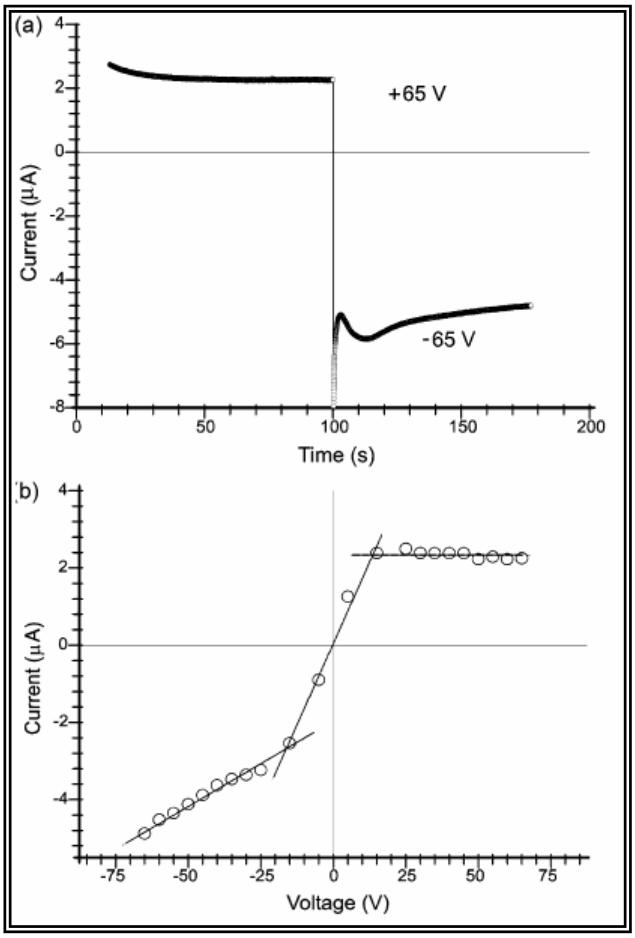

Fig.2.26. Electric conduction of a hybrid cell; 5CB 19 µm, PANI 300 Å. (a) Current versus time (130 Vpp). (b) Current versus voltage.

Last, but not the least, present the measured values of the relaxation time versus voltage amplitude for several frequencies (Fig.2.27a) and versus frequency for several voltage amplitudes (Fig.2.27b) are presented. Beyond certain values, for both frequencies and voltages, the transmitted light behaviour is similar to that shown in figure 2.23b (even the small shoulder visible in figure 2.23b disappears at larger voltage amplitudes). If the threshold values are not surpassed the behaviour is similar to that shown in figure 2.23a. The relaxation time was measured on a figure 2.23b type curve on the rising part of it between 10% and 90% of the total amplitude. For figure 2.23a type curves the 90% point was substituted with the abscissas of the first deepest minimum.

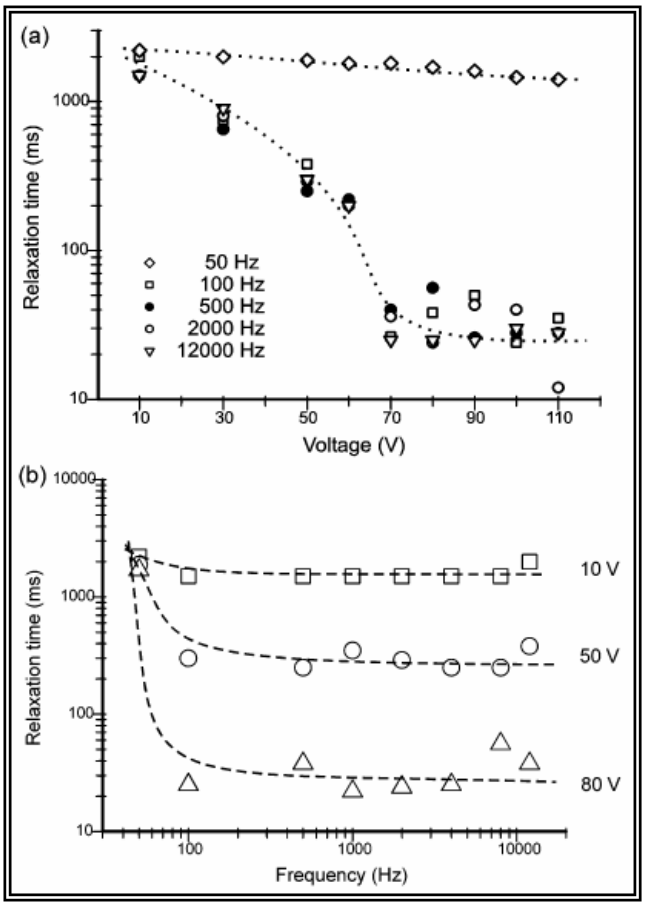

Fig.2.27. Relaxation times for a hybrid cell. (a) Relaxation time versus amplitude (different frequencies). (b) Relaxation time versus frequency (three voltage amplitudes).

The plots in figure 2.27 were obtained for a hybrid cell, using one PANI-coated ITO side and 19 μm thick 5CB liquid crystal layer. The PANI thickness was about 300 Å. Many other similar plots were obtained varying either the thickness of the polymer or the chemical nature of it or the liquid crystal (6CB instead of 5CB). The plots are similar but not identical; that is, the relaxation times and/or threshold values can vary from sample to sample. As far as PANI is concerned, we have observed that polymer thickness of about 300 Å gives the best (shortest) relaxation time and the smaller threshold values (for both frequency and voltage). Thinner or thicker polymer layers present poorer characteristics. Yet, the shortest relaxation time of all has been observed for a cell coated with poly(o-anisidine) instead of PANI ($t_{off} \sim 2$ ms) but, at this stage, we cannot conclude that poly(o-anisidine) is "better" than PANI; it might just happen that the thickness of poly(o-anisidine) and/or plasma reactor conditions concur to produce a successful result. In this respect, more systematic work remains to be done.

Effect of Annealing on Dielectric Loss

The most important factors preventing the widespread application of plasma polymerized thin films in microelectronics technology are high dielectric loss and the instability of dielectric parameters when subjected to ambient conditions []. High dielectric loss in plasma polymerized films is due to the high concentration of free radicals. To reduce the free radical concentration, thermal annealing of these films was carried out for periods of time ranging from couple of minutes up to several hours. Dielectric loss is reduced in the post treated polyaniline thin films. Below graphics clearly show the effects of post-treatment of plasma polymerized aniline thin films. Electro-optic samples prepared with this annealed PANI films show an even faster switch-off time for the nematic liquid crystal. In some cases, the switch-off time goes as low as 350-400 μs (one order of magnitude lower than in the case of the sample with the non-annealed PANI thin film).

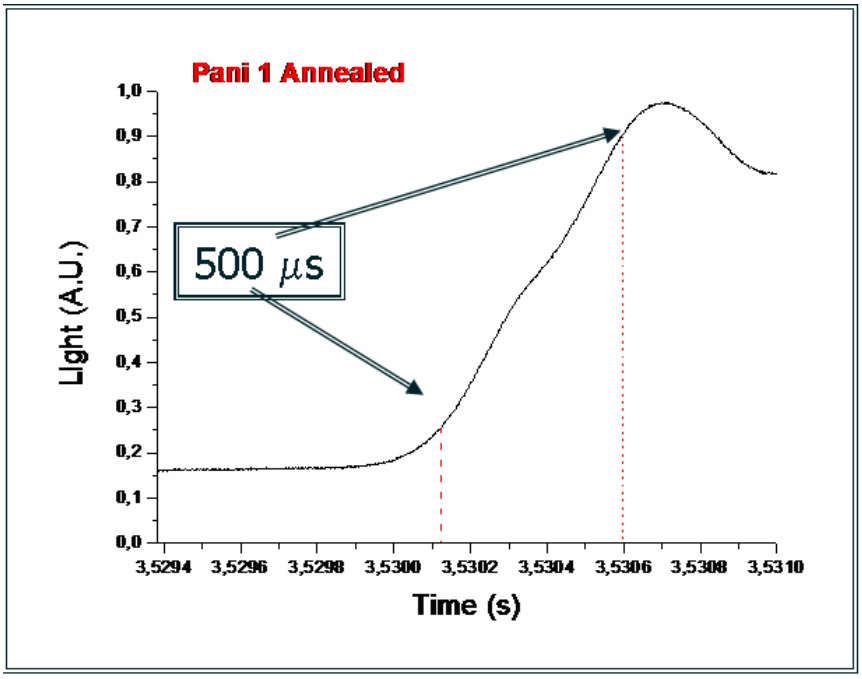

Fig.2.28. Transmitted light versus time. Switching off the ground. (Phase on PANI) Hybrid cell, 5CB, 19 µm thick. Planar orientation with annealed PANI (thickness 400 Å).

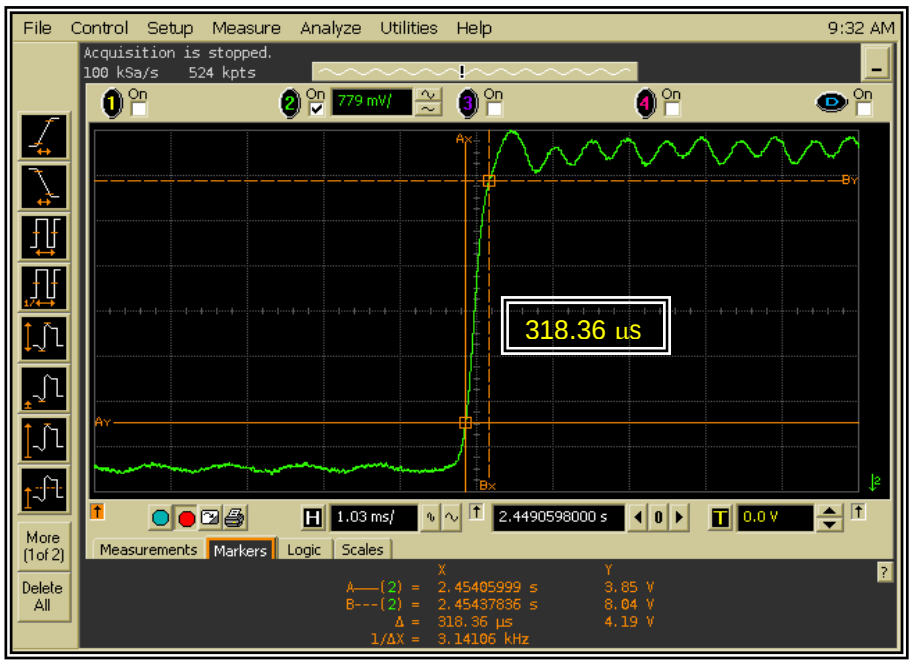

Fig.2.29. Transmitted light versus time. Switching off the ground. (Phase on PANI) Hybrid cell, 5CB, 19 µm thick. Planar orientation with annealed PANI (thickness 300 Å).

Model and Conclusions

Let us sum up the most relevant experimental facts just presented:

(i) In the first place, the atypical effect has been observed only with PANI or polymers akin containing aromatic carbon rings;

(ii) The effect appears only when the phase is applied to the polymer coated side of the cell;

(iii) The simple presence of the phase on that side, even without an electric field applied within the bulk of the cell (the ground being switched off) increases the light transmission; that is, the planar alignment, within a large range of voltage amplitudes;

(iv) The effect appears only with ac voltage (although most of the experiments have been performed with squared pulsed voltages, the effect can be seen also with sine voltages);

(v) There are voltage and frequency thresholds;

(vi) The cell has an asymmetric electric conduction, the higher current arising when the polymer side is negatively polarized.

All these facts suggest that delocalized π electrons should play an important role, as they are common both to polymers and to liquid crystals that contain phenyl rings (like 5CB or 6CB). As a matter of fact, we have also checked the effect with another liquid crystal (pentyl-5-cyclohexyl-5'-cyano-phenyl) that possesses only one aromatic ring per molecule. Although the effect can be seen, it is weaker (i.e. the relaxation times and threshold values are longer and higher). The almost planar disposal of aromatic rings in the PANI layer contributes essentially to the planar anchoring properties of this polymer. Van der Waals dispersion attraction between PANI phenyl rings and

those of 5CB and 6CB strengthen this anchoring, due to the larger polarizability of π electrons. The same π electrons contribute to the electric conductivity anisotropy of these liquid crystals, as mentioned earlier.

Let us imagine, succinctly, a mechanism that could explain the above-mentioned experimental facts.

With the ITO/PANI side negative, electrons tunnel the thin ITO/PANI interface, traverse the PANI layer by fast and reversible charging of it, and enter liquid crystal reducing the aromatic rings that contain electron-withdrawing cyano groups. Due to asymmetric current-voltage characteristic (Fig.2.26), one way to take advantage of the peculiar properties of the ITO/ PANI/cyanobiphenyl interface is to use alternating voltage. When using ac voltage, for each negative pulse on the ITO/PANI side, electrons are injected across the polymer, forming a charge distribution. Due to diffusion in the liquid crystal (and the reservoir character of π delocalized states) and to the affinity of liquid crystal molecules to electrons, when the positive pulse is on, not all the electrons tunnel back trough the polymer to ITO. Therefore, on each cycle, charges accumulate at the polymer-liquid crystal interface. The accumulated charge sets in a counter-field that raises the barrier to further tunneling, on one hand, and on the other hand, some of this charge can reach the other electrode (uncoated ITO) in a time interval equal to the characteristic discharge time, RC, of the capacitor. With typical values of over 10 MΩ for R and 1 nF for C this time is about 10 ms. If the frequency of the applied voltage is higher than 100 Hz, a steady negative charge will build up in the proximity of the ITO/PANI interface. This steady charge is localized on liquid crystal molecules, increasing their polarizability and also the attractive van der Waals interaction when two neighbouring molecules have aromatic rings face to face. The charge also tends to spread away from the interface to minimize the local electrostatic energy. This energy could diminish faster if the local configuration of nematic molecules is planar. The larger is the planar layer, the smaller will be the extra electrostatic energy. Both higher $\sigma_{\perp}$ conductivity and higher polarizability would act to increase the planar alignment.

This planar alignment is, nevertheless, just a mere tendency. The electric field inside the cell has a stronger, opposite effect, eventually the cell being oriented

homeotropically. Now, switching the voltage off, the electric field disappears very fast because it is due to the charges accumulated on the two conducting ITO layers that form the capacitor. If the phase is on the polymer side, the injection of electrons continues until the negative potential of the now uniformly charged cell raises the tunneling barrier. At this time, the two contributions to higher anchoring can manifest without being counterbalanced by a strong uniform field inside the bulk.

This model is justified by the experimental facts presented above. For instance, the differences between figures 2.23a,b can now be understood easily. Keeping the phase on the uncoated ITO layer and switching off the ground from the polymer side, the injection of electrons is quite small and entirely reversible. No charge accumulates at the interface. The anchoring strength is not increased, and the relaxation is slow. It also presents oscillations, the explanation of which was done many years ago considering the slow change of the refractive index leading to interference fringes. In figure 2.23b the now higher anchoring gives a shorter relaxation time, higher transmitted intensity and no oscillations. In fact, the lack of oscillations is due to the shorter relaxation time; it is not an artifact, because the recording system (photodiode and digital oscilloscope) was set to a smaller time resolution (similar to the physiological resolution of the human eye).

Probably, the shortening of relaxation times and lack of oscillations-although very important from the application point of view-do not constitute the best evidence of the role of delocalized electrons in increasing the planar alignment. A better one is given by the experiments presented in Fig.2.25. In these experiments we started first with the insulated cell (that is the uncoated ITO side is floating and the phase on the PANI side is switched off) and recorded the transmitted light. When the phase is switched on, the transmitted light increases, meaning that the planar alignment within the cell is better. Yet, this increase is present only when the amplitude of the square pulses lies within the range 60-140 V_{pp}. Why only in this region? If the voltage is smaller than 60 V_{pp}, the injection of electrons through the polyaniline is small and the planar effect is also small. The charges on the ITO layer can easily follow the change of the phase polarity (even at 15 kHz) because the ITO layer has a small resistance (20 Ω/□) and small capacitance. Either for a negative or a positive pulse there will be a negative or positive superficial charge on the very thin ITO layer that creates an (alternating)

electric field normal to the surface and penetrating the polymer layer into the liquid crystal. The same dielectric torque as in the case of the electro-optic effect tends to orient the liquid crystal molecules perpendicular to the surface, thus decreasing the planar order. These two competing effects are balanced at a threshold value of cca. 60 V_{pp}. In fact, both the charge accumulation at the interface and the strength of the electric field in the vicinity of the ITO surface increase with the amplitude of the pulses. Whereas the electric field increases proportional to the pulse amplitude ($E = \sigma/\varepsilon\varepsilon_0$, and the superficial charge density σ is proportional to the amplitude $|V|$), the accumulated charge depends on the tunneling probability that increases exponentially with the amplitude (yet, only for negative pulses). We should expect the transmitted light to saturate for higher and higher voltage amplitudes. Fig. 2.23a does not present such a behaviour. This is due to the fact that a larger amount of tunneled electrons are localized on aromatic rings of molecules that are transformed into labile negative ions. When such a negatively charged ring faces a neutral parallel ring of another molecule, the attractive van der Waals interaction, both dispersion and mostly dipole induced, is larger than between two neutral rings. If, instead, the negatively charged ring faces another negatively charged ring, the now even higher van der Waals attraction is surpassed by the Coulombic repulsion between like charges. The higher is the accumulated charge at the interface, the larger is the probability that one negative molecular ion face another negative ion instead of a neutral molecule. This is another effect that hinders the planar order in the cell.

Although we do not have accurate data concerning the influence of the polymer thickness on the increase of planar order, qualitatively we have seen that very thick polymer films give a worse result. Probably this is one of the reasons for which we did not see the anomalous effect when solution cast polyaniline films are used. We have not succeeded in making a film as thin as when using plasma polymerization. Of course, the thicker is the polymer film the smaller is the tunneling probability and, therefore, the smaller is the steady accumulated charge. Though very interesting in themselves, these effects could also lead to important technological consequences. An immediate idea consists of building pixel matrixes with one large ITO electrode covered with the appropriate polymer film on one side and an array of multiplexed pixels on the bare ITO plate. These pixels could be done in the standard way, by

etching the ITO surface. All these pixels on the uncoated ITO are connected to the ground of a variable frequency voltage supply, the phase being on the polymer side. An electronic procedure can be used to interrupt the connection to the ground of each pixel, when desired. New experimental work and theoretical considerations could lead to displays operating at a higher frequency and with a better contrast ratio.

Further planned investigations also include research studies for better understanding of the role of the plasma polymer layer thickness on the switching time of the nematic LCs, the influence of the annealing process as well as the use of other glow discharge plasma polymers deposited under various conditions.

References

[1]. I. Langmuir, "Oscillations in ionized gases," Proc. Nat. Acad. Sci. U.S., vol. 14, (1928).

[2]. G. Morfill et al, Focus on Complex (Dusty) Plasmas, New J. Phys., 5, (2003).

[3]. Goldston, Rutherford, Introduction to Plasma Physics, Institute of Physics Publishing, Philadelphia, (1997).

[4]. A. Grill, Cold Plasma in Materials Fabrication: from fundamentals to applications, IEEE Press, New Jersey, 1994.

[5]. S.Harkema, Capillary Instabilities in Thin Polymer Films Mechanism of Structure Formation and Pattern Replication", Univ.Gro (2006).

[6]. A. Brewer, R. Kveck, J. Phys. Chem., 35, 1293, (1931).

[7]. J.Austin, J.Black, J. Am. Chem. Soc., 4552, 52, (1930).

[8]. E.Lindner, A.Davis, J. Phys. Chem., 35, 3649 (1931).

[9]. Stewart R.L, Phys. Rev., 45, 488 (1934).

[10]. Goodman J, J. Polym. Sci., 44, 551 (1960).

[11]. Stuart M, Nature, 199, 59 (1963).

[12]. Bradley A, Hammes J P, J. Electrochem Soc., 110, 15 (1963).

[13]. Bradley A, Trans. Faraday Soc., 61, 773 (1965).

[14]. Bashara N.M, Day C.T, J. Appl. Phys., 35, 3498 (1964).

[15]. Yasuda H, Plasma Polymerization, Academic Press, Orlando (1985).

[16]. Yasuda H., Plasma Polymerization - Kinetic and Mechanisteic Aspects, Academic Press, Orlando, Florida, (1985).

[17]. Poll H. U., Artz M., Wickleder K. H., Eur. Polym. J., 12, 505 (1976).

[18]. Yasuda H, Thin Film processes, eds. Kern W. and Vossen J. L, New York, Academic Press, 361, (1978).

[19]. Vautrin-Ul C, Boisse-Laporte C, Chausse A, Leprince P, Messsina R, Progress in Organic Coatings, 38, 9 (2000).

[20]. Yasuda H K, Yu Q S, Reddy CM, Moffitt C E, Wieliczka D M, J. of Appl. Polym. Sci, 85 1387, (2002).

[21]. Ooij W J, Zhang N, Guo S, Fundamentals and Applied Aspects of Chemically Modified Surfaces, The Royal Society of Chemistry, (1999).

[22]. Zeuner M, Neumann H, Meichsner J, Vacuum, 48, 443(1997).

[23]. T.F. Wang, T.J. Lin, D.J. Yang, J.A. Antonelli, H.K. Yasuda, Prog. Org. Coat. 28 (1996).

[24]. H.K. Yasuda, T.F. Wang, D.L. Cho, T.J. Lin, J.A. Antonelli, Prog. Org. Coat. 30 (1996).

[25]. C.M. Reddy, Q.S. Yu, C.E. Moffitt, D.M. Wieliczka, R. Johnson, J.E. Deffeyes, H.K. Yasuda, Corrosion, 56, (2000).

[26]. Lili Vescan C, Handbook of thin film process technology, Bristol (UK), Institute of Physics, (1995).

[27]. Yasuda, H., Bumgarner, M. O., and Hillman, J., J. Appl. Polym. Sci. 19,531 (1975).

[28]. Yasuda, H., Marsh, H. C., and Tsai, J., J. Appl. Polym. Sci. 19,2157 (1975).

[29]. Yasuda, H., and Hirotsu, T.. J. Polym. Sci. Polym. Chem. Ed. 15,2749, (1977).

[30]. Yasuda, H., and Hirotsu, T., J. Polym. Sci. Polym. Chem. Ed. 16,229, (1978).

[31]. Yasuda, H., and Hirotsu, T. J. Polym. Sci. Polym. Chem. Ed. 16, 313, (1978).

[32]. Yasuda, H., and Hirotsu, T. J. Polym. Sci. Polym. Chem. Ed. 16,743, (1978).

[33]. Yasuda, H., and Hirotsu, T. J. Polym. Sci. Polym. Chem. Ed. 16,2587, (1978).

[34]. Yasuda, H., and Hirotsu, T. J. Appl. Polym. Sci. 22, 1195, (1978).

[35]. Westwood,A. R. Eur. Polym. J. 7,363, (1971).

[36]. Westwood,A. R. Eur. Polym. J. 7,377, (1971).

[37]. Y. Lin and H. Yasuda, J. Appl. Polym. Sci., 60, 543 (1996).

[38]. Cecchi J. L., Handbook of Plasma Processing Technology, eds. Stephen M. Rossnagel, Jerome J. Cuomo, and Willian D. Westwood, Park Ridge, NJ: Noyes publication, (1990).

[39]. Chapman I. B., Glow Discharge Processes: Sputtering and Plasma Etching, New York: J. Wiley &Sons, (1980).

[40]. Amussen J., Handbook of Plasma processing technology, eds. Stephen M. Rossnagel, Jerome J. Cuomo, and Willianm D. Westwood, Park Ridge, NJ: Noyes Publications, (1990).

[41]. Bell, A. T., J. Macromol. Sci. Chem. 10(3), 309, (1976).

[42]. Yasuda, H., and Lamaze,C. E. J. Appl. Polym. Sci. 17, 1519, (1973).

[43]. Yasuda, H., and Lamaze, C. E. J. Appl. Polym. Sci. 17, 1533, (1973).

[44]. Kobayashi, H., Bell, A. T., and Shen, M. Macromolecules 7,277, (1974).

[45]. H. Yasuda, Nuclear Instruments and Methods in Physics Research A, 515 (2003).

[46]. Q.S. Yu, H.K. Yasuda, Plasma Chem. Plasma Process 18 461, (1998).

[47]. H. Yasuda, Plasma Polymerization, Academic Press, Orlando, FL (1985).

[48]. E. Kay, Invited Paper, International Round Table on Plasma Polymer Treatment, IUPAC Symposium, Plasma Chemistry, Limoges, France (1977).

[49]. H. Yasuda, T. Hsu, J. Polym. Sci., Polym. Chem. Ed. 16 415, (1978).

[50]. T. Yasuda, M. Gazicki, H. Yasuda, J. Appl. Polym. Sci., Appl. Polym. Symp. 38 201, (1984).

[51]. H. Yasuda, T. Yasuda, J. Polym. Sci., Polym. Chem. Ed. 38 943, (2000).

[52]. P.V. Hinman, A.T. Bell and M. Shen, J. Auu1.Polvm. Sci.. 23, 3651 (1979).

[53]. D.L. Cho and H. Yamada, Proceedings of the ACS D ivision of Polvmeric Materials. 57, 599 (1987).

[54]. H. Yasuda and M. Gazicki, Biomaterials 3, 68 (1982).

[55]. R. Hollahan and A.T. Bell, Techniaues and Aplications of Plasma Chemistry, John Wiley and Sons, (1984).

[56]. S . Hattori, J. Tamano, M. Yasuda, M. Ieda, S. Morita, K. Yoneda and S. Ishibashi, Thin Solid Films 85, 189 - 194 (1981).

[57]. Y. Osada, A. Mizumoto and H. Tsuruta, J. Macromo1. Sci. Chem. A 24, 403 - 413 (1987).

[58]. P.K. Tien, G. Smolinski and R.J. Martin, Appl. Optics. 11 (3), 637, (1972).

[59]. A. Moshonov, Y. Avni, J. Appl. Polym. Sci. 25, 771 (1980).

[60]. N. Inagaki and H. Yasuda, J. Auul. Polvm. Sci. 26, 3333 (1983).

[61]. N. Ingaki, S. Kondo, M. Hirata and H. Urushibata, J. Appl. Polym. Sci., 30, 3385 (1985).

[62]. A.M. Wrobel, M.R. Wertheimer, J. Dib and H.P. Schreiber, J. Macromol. Sci.-Chem., A14(3), 321 (1980).

[63]. Y. Inoue, H. Sugimura and O. Takai, Thin Solid Films 345, 90 (1999).

[64]. Y. Segui and B. Ai, J.Appl. Polym. Sci., 20, 1611 (1976).

[65].. Inagaki N., Tasaka S.and Abe H., J. of Appl. Polym. Sci., 46, 595 (1992).

[66]. C.H. McCoy, I.M. Lorkoviv, M.S. Wrighton, J. Am. Chem. Soc. 117, 6934, (1995).

[67]. M. Karakisla, M. Sacak, U. Akbulut, J. Appl. Polym. Sci. 59 1347, (1996).

[68]. H. Yasuda, Plasma Polymers, Academic Press, New York, (1989).

[69]. N.P. Chermisinoff, Handbook of Polymer Science and Technology, vol. 4, Marcel Dekker, New York, (1989).

[70]. C.J. Mathai et al., Materials Letters, 57, (2003).

[71]. E.M. Genie`s, A. Boyle, M. Łapkowski and C. Tsintavis, Synth. Met., 36 (1990).

[72]. K.F. Schoch, W.A. Byers and L.J. Buckley, Synth. Met., 72, 13–23, (1995).

[73]. T.L. Porter, K. Caple and G. Caple, J. Vac. Sci. Technol. A, 12, 2441–2445, (1994).

[74]. J. Paloheimo, J. Laasko,H. Isotalo andH. Stub, Synth.Met., 68, 249–257, (1995).

[75]. N.V. Bhat and N.V. Joshi, Plasma Chem. Plasma Process., 4, 151–161, (1994).

[76]. X. Xie, J.U. Thiele, R. Steiner and P. Oelhafen, Synth.Met., 63, 221–224, (1994).

[77]. K. Tanaka, Y. Matsuura, S. Nishio and T. Yamabe, Synth. Met., 65, 81–84, (1994).

[78]. M. Grunwald, H.S.Munro and T.Wilhelm, Synth.Met., 41–43 (1991).

[79]. G.J. Cruz et al., Synthetic Metals 88, 213–218 (1997).

[80]. Mathai C. J., Saravanan S., Anantharaman M. R., Venkitachalam S., Jayalekshmi S. J., Phys. D: Appl. Phys., 35, (2002).

[81]. Ayad M. et al, Synth. Met., 132, (2003).

[82]. Long Y. Z.et al., Physics B, 325, (2002).

[83]. Alexe-Ionescu A. L., Ionescu A. Th., Barna E. S., Scaramuzza, N., Strangi G., J. Phys. Chem. B, 107, (2003).

[84]. Boden N. et al, Phys. Rev. B, 52, (1995).

[85]. Van de Craats A. M. et al, Adv. Mater., 11, (1999).

[86]. Cornil J. et al, Adv. Mater., 13, (2001).

[87]. Cornil J. et al. Adv. Mater., 14, 726-729 (2002).

[88]. De Gennes P. G., Prost J., The Physics of Liquid Crystals, Clarendon Press, Oxford, U.K., (1993).

[89]. Blinov L. M.,Chigrinov V. G., Electrooptic Effects in Liquid Crystal Materials, Springer, New York, (1994).

[90]. Alexe-Ionescu A. L., Ionescu A. Th., Barna E. S., Barna V., Scaramuzza N., Italian patent No. TO2003A000490. (2003).

[91]. A.L.Ionescu, A.Ionescu, E.S.Barna, V. Barna, N. Scaramuzza, Appl. Phys. Lett. Vol 84(1), (2004).

[92]. A.L.Ionescu, A.Ionescu, E.S.Barna, V.Barna, N. Scaramuzza, J.Phys.Chem.B 108(26), (2004).

Chapter III

Colour-Tunable Organic DFB Microcavity Lasers

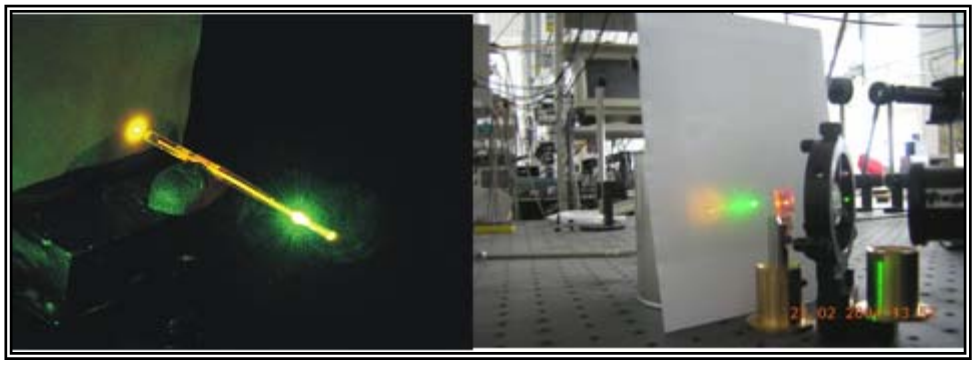

Chapter III

Colour-Tunable Organic DFB Microcavity Lasers

3.1. Introduction. Light in Free Space and Interaction with Matter.

A person can see things because they emit or scatter light that is subsequently absorbed in our eyes. Emission, absorption and scattering of light are examples of interactions of light with matter. These phenomena occur and materialize to the eye as a colour appearance of an object. If a colour appearance of an object is created by absorbance of specific wavelengths, the wavelengths that are not absorbed determine the colour of appearance; white materials do not absorb visible wavelengths whereas black material absorbs all visible wavelengths. Emission of light by substances such as pigments that are present in the material, can also cause the colour appearance of an object. In nature and every day life many examples of absorption and emission are encountered: (i) a paint is red because the pigment perylene, present inside, absorbs green light and emits red light; (ii) grass is green since the chlorophyll absorbs blue and red light and emits green light.

The appearance of a blue sky is explained by a completely different phenomenon: light scattering. Particles that are smaller than the wavelength of light and present in the sky cause the blue part of the emitted spectrum of the sun to be scattered more than the red part of the spectrum, causing a blue appearance. This phenomenon is also called Rayleigh scattering.

A colour appearance can, however, also result from reflectance of specific colours from the physical structure of the material. Due to constructive interference from a plane, a thin layer, or a collection of ordered lattice planes in the material, light with a certain wavelength is reflected causing appearance of a colour. If such a structure is illuminated with white light, the light is reflected under different angles and the incident white light is split up into its spectral colours. This phenomenon is also known as iridescence. A thin layer of oil on water is a beautiful example of this iridescence, the light is reflected from the front side and the backside of the oil layer since there is a change in refractive index at both sides; from air to oil and from oil to water. The reflected waves interfere constructively and cause a rainbow-like colour appearance. Other examples of iridescence in nature are butterfly wings or fish-scales. The following figure shows how the butterfly wings reflecting blue-greenish colours due to the wing structure consisting of discrete multilayers of cuticle (tough but flexible, non-mineral covering of an organism) and air. It also displays a rainbowfish with a hue of colours. Because of a structure of periodically varying refractive index of air and chitine the incident light is Bragg diffracted and the reflected light appears in a rainbow of colours.

It should be noted that the colour of appearance can additionally be caused by the presence of some pigments. Both colour expressions can occur simultaneously. Other examples of iridescence caused by constructive interference that occur in nature are the feathers of hummingbirds, reptiles, insects or certain minerals.

If in addition to iridescence, also, some random scattering takes place, due to (for example) imperfections, the phenomenon of constructive interference is called opalescence.

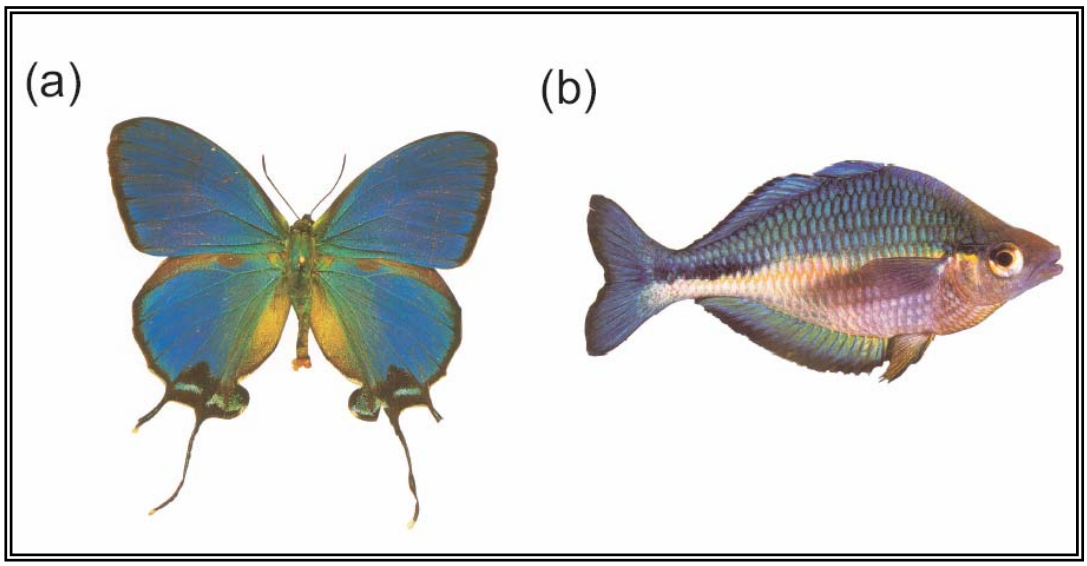

Fig.3.1. Examples of iridescence caused by interference from multilayer structures with periodically varying refractive indices.

The iridescence has then a milky appearance. In nature, opalescence is widely known as having the name of the gemstone opal. Figure 3.2 shows two examples of such natural opalescence. In the case of the shells the opalescent appearance is caused by alternating layers of anorganic, calcium carbonate, and organic, conchiolin, material. These materials are formed due to seasonal fluctuations. In figure 3.2b a photograph of a noble opal is shown where all colours of the rainbow are present. The microscopic structure of these opals consist of periodically arranged glass spheres, organized in a three-dimensional (3D) ordering.

According to classical optics, light is a name for those electromagnetic waves that happen to be visible for the human eye. Electromagnetic waves can be described as the solutions of Maxwell's equations. In free space, solutions of Maxwell's equations correspond to plane waves that move in straight lines. In many experiments, especially those involving interference, light appears to be a wave indeed. In other experiments, light can best be understood as a stream of particles (called photons). This two-sided nature of light can nowadays be described consistently in one theory, namely in the quantum theory of

light (or quantum electrodynamics).

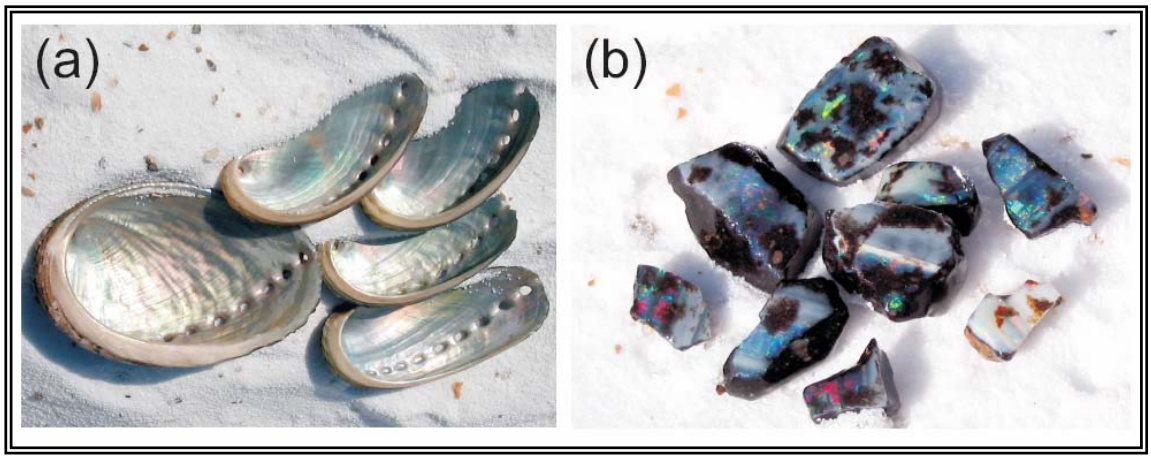

Fig.3.2. Examples of natural opalescence. (a) Shells. (b)Opal gems.

When the field interacts with matter, the properties of the electromagnetic field are changed [1]. In air, for instance, light travels just a bit slower than in free space, because the interactions with the air molecules take some time. The factor 1.0003 by which the light is slower is the refractive index of air. If one looks even more precisely, one finds that air shows frequency dispersion: different colours move at different speeds. Violet light has a refractive index of 1.000298 and red light is faster with a refractive index of 1.000291 [2].

Light can be described as a wavelength λ or as a frequency ω in electromagnetic oscillations per unit time and has typical length scales of λ = 400-1000 nm, corresponding to frequencies of ω = 3-7,5 THz (1THz = 10^{12} s^{-1}). For comparison computers nowadays have processors that work at a clock speed of up to ω =5 GHz (1GHz = $10^{9}s^{-1}$). If the frequencies of light are considered to be the (maximum) speed with which light can be manipulated, it illustrates that studying light interaction and transport is an excited subject to investigate.

Light is crucial to many biological, physical and chemical processes. An example of a chemical reaction that is induced by light is the photosynthesis in plants, where light energy is converted into chemical energy. Carbondioxide and water are converted into adenosine tri phosphate (ATP) and oxygen under influence of light – known as process of photosynthesis. Many other examples prove that light is not only essential

for life on earth, but also show the importance for humans to manipulate light. Mankind is continuously trying to imitate nature (or"to use nature as a source of inspiration").
Whereas nature is able to convert light into energy with a high efficiency, researchers are still trying to harvest solar energy in an efficient way by the use of the basic chemistry of photosynthesis. Aspects such as self-cleaning, utilization of the complete sunlight spectrum and lifetime of solar cells are nowadays high priority topics. This example clearly illustrates that if light can manipulated, it would be interesting for a variety of research fields such as (photo) chemistry, biology, and physics.

In this chapter we will discuss and investigate structures, the so-called photonic crystals, that are engineered to show interference effects, while in addition scattering effects also take place. Due to the strong interaction of these photonic crystals with light, they exhibit characteristics that can influence the emission of certain light sources. Here, we discuss the possibility of these photonic structures to manipulate light by investigating the properties of emission (fluorescence and stimulated emission) from dye-doped photonic structures.

3.2. Bragg Diffraction

Bragg diffraction plays a prominent role in optical experiments on photonic crystals. It occurs whenever there is constructive interference of waves reflected from a set of lattice planes, as illustrated in Fig.3.3.

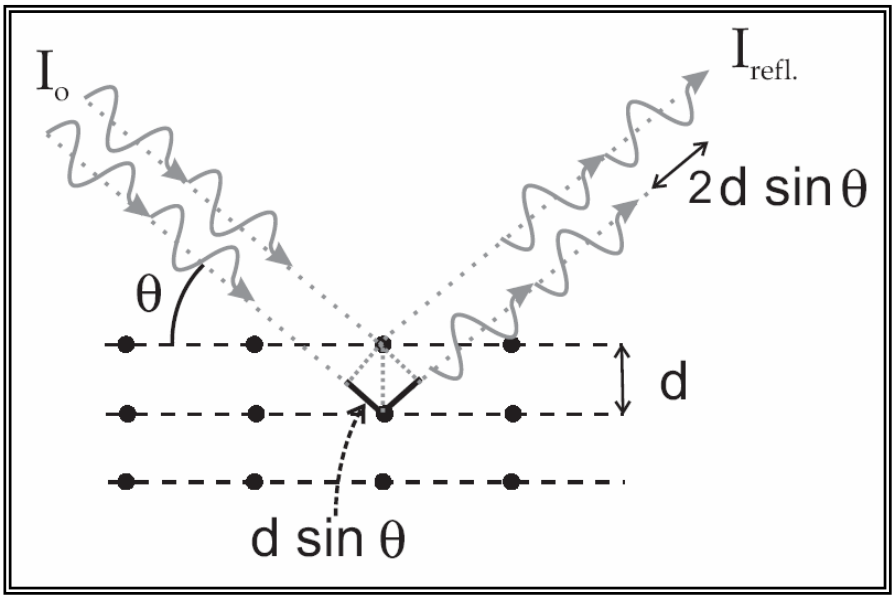

Fig.3.3. The principle of Bragg diffraction from lattice planes. Incident waves are diffracted at the lattice planes and constructively interfere if the path length difference is exactly an integer number of 2d sinθ .

A set of crystal planes acts like a mirror if the Bragg condition, $m\lambda = 2d \cos \theta$, is met, where m is an integer number (the order of the reflection), λ the wavelength of the incident waves, d the lattice spacing and θ the angle of incidence between the beam and the lattice plane. When the path length difference of these reflected waves is equal to an integer number of wavelengths m, the waves constructively interfere and the wave with that certain wavelength is amplified. In figure 3.3 the scattered or reflected waves from the crystal planes have a path length difference of 2d sinθ and interfere constructively after they are reflected from the lattice planes.

Constructive interference of reflected waves was first described by Sir Lawrence Bragg. Bragg reflection of electromagnetic radiation was first studied for X-rays that are diffracted by atomic crystals [3] and later for optical waves in layered media and gratings [4-8].

3.3. Photonic Crystals and Photonic Bandgaps

3.3.1. General Considerations

The concept of wave transport in complex media, in particular the propagation of electromagnetic waves in dielectric periodic structures represents a topic of great interest in various fields of scientific research. Periodic structured materials, namely "photonic crystals" that strongly localize light, are finding applications in many technological areas, providing an intriguing stage for controlling radiation fields [9-11].

Photonic crystals are periodic dielectric or metallo-dielectric structures that are designed to affect the propagation of electromagnetic waves (EM) in the same way as the periodic potential in a semiconductor crystal affects the electron motion by defining allowed and forbidden electronic energy bands.

Photonic crystals were introduced by Yablonovitch [12] and John [13] and have attracted a huge interest because of their remarkable potential confirmed in fundamental physics and emerging applications [14-18].

The optical properties of photonic materials are governed by a refractive index spatial modulation, on length scales comparable to wavelengths of light, similar to the periodic potential for an electron in a crystal. This variation of the dielectric constant gives rise to Bragg selective reflection effect, within a certain frequency band, allowing the confinement, manipulation and guiding of light photons in such ordered structures. Analogous to the energy gap in semiconductors, periodic photonic crystals exhibit stop bands, representing forbidden windows for the electromagnetic wave propagation within a given frequency range [12].

Photonic band gaps were first predicted in 1987 by the two physicists working independently: Eli Yablonovitch, at Bell Communications Research in New Jersey, and John Sajeev of the University of Toronto. An array of 1mm holes mechanically drilled in a slab of material with refractive index 3.6, latter to be known as Yablonovite, was found to prevent microwaves from propagating in any direction. Despite this remarkable success, it took more than a decade to fabricate photonic crystals that work in the near-infrared (780-3000 nm) and visible (450-750 nm) ranges of the spectrum and forbid light propagation in all directions. The main challenge was

to find suitable materials and technologies to fabricate structures that are about a thousandth the size of the Yablonovite.

In a periodic structure, the appearance of the bandgap can be explained as due to coherent Bragg scattering of the coupled waves inside the photonic crystal (PC). If a crystal is sufficiently well ordered that the reflections from many lattice planes interfere constructively, then the Bragg reflection will be very strong, close to 100%. In this case, the associated extinction will be very large, increasing with the sample thickness. Light cannot propagate in the direction of a Bragg reflection: the Bragg reflections correspond to the stop bands in the photonic structure. The wavelength λ and angle θ then do not need to conform to Bragg's law exactly: the interference still will be constructive for the limited number of lattice planes involved. As a consequence, the Bragg reflections extend over a range of frequencies, corresponding to the width of the stop bands.

In order to understand better light propagation in a photonic crystal let us compare that to the carrier transport in a semiconductor. The similarity between electromagnetic waves in a PCs and de-Broglie electronic waves propagating in a crystalline solid has been utilized to develop certain theories of photonic crystals. This resemblance first arises in differential equations describing wave motion in both media. For electrons in semiconductor materials the Schrodinger equation reads as:

$$\left(-\frac{\nabla^2}{2}+V(r)\right)\Psi(r)=E\Psi(r) \qquad (3.1)$$

In a semiconductor crystal the atoms are arranged in a periodic lattice, and moving carriers experience a periodic atomic lattice potential

$$V(r+a)=V(r) \qquad (3.2)$$

where a is a lattice constant. Then, there exists a wavevector k in the reciprocal lattice such that $\Psi(r)$ can be written as:

$$\Psi(r)=e^{ikr}u_k(r) \qquad (3.3)$$

where $u_k(r + a) = u_k(r)$ is a periodic function on the lattice.

This expression is known as Bloch's theorem. Substituting this into the above equation one finds the eigenfunctions $u_k(r)$ and eigenvalues E_k. The periodic potential causes formation of allowed energy bands separated by gaps. In perfect bulk semiconductor crystals no electrons or holes can be found in these energy gaps. The situation also holds for photons travelling through periodic structures.

3.3.2. 1D Photonic Crystal Situation. The Photonic Parameter

Let us consider a 1D photonic crystal (Fig.3.4) consisting of alternate layers having indices of refraction n_1 and n_2. An incident wave with a wavelength that is equal to the periodicity in refractive index in the crystal illuminates the structure. Since the incident wave has a wavelength that corresponds with the lattice spacing of the crystal as in Bragg's law (i.e. $\lambda = 2d$), the wave is reflected. The incident and reflected wave have identical wavelengths and interfere with each other while travelling in opposite directions, and they build up a so-called standing wave.

Standing wave (1) has its antinodes in n_1 and nodes in n_2 and is predominantly in n_1 while in standing wave (2) predominantly is in the material n_2. Both standing waves have identical wavelengths but mainly exist in a different medium, n_1 or n_2. Since the frequency of light ω is equal to

$$\omega = \frac{c}{n} k = \frac{c}{n} \frac{2\pi}{\lambda} \qquad (3.4)$$

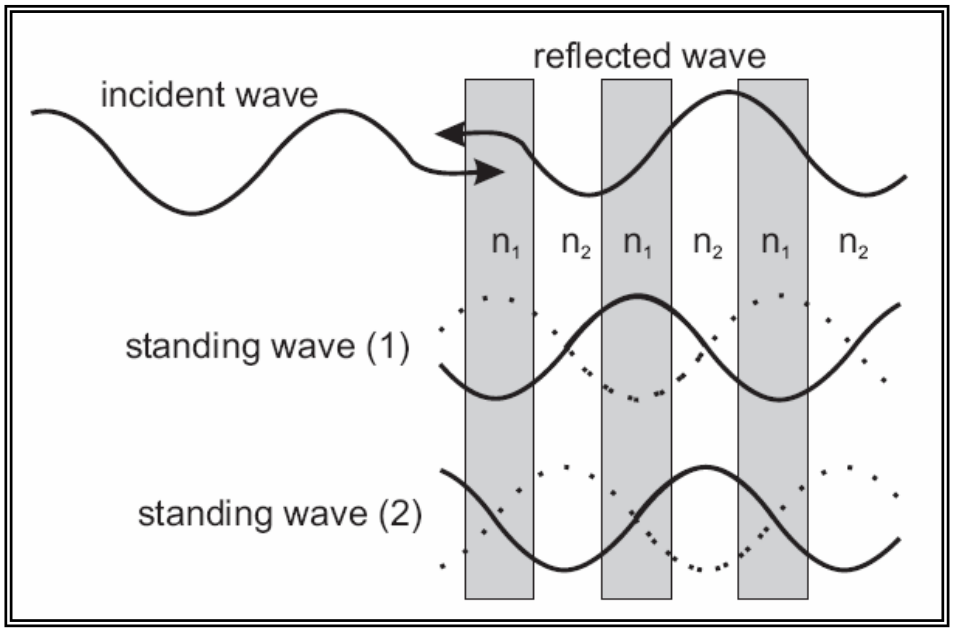

Fig.3.4. Scheme demonstrating light propagation in one-dimensional crystals with periodically varying refractive indices.

where c is the speed of light, n the refractive index and λ the wavelength, both standing waves have a different frequency. Wave vector k represents the number of periods per length along a certain direction. Generally it can be said that in a crystal with periodically varying refractive indices, there are two frequencies at a given wavelength at the Bragg condition.

Because to these two different frequencies at the Bragg condition, a stop gap opens up as displayed in figure, where the higher frequency corresponds to the wave in n_{low} and the lower frequency to the wave in n_{high}.

The wave vector on the x-axis is directed along the direction of the wave propagation and inversely proportional to the wavelength. At π/a, where a is the lattice constant, a ”forbidden” frequency range is developed. In this frequency range, light with a wavelength corresponding to a/λ cannot exist in the crystal and is therefore excluded.

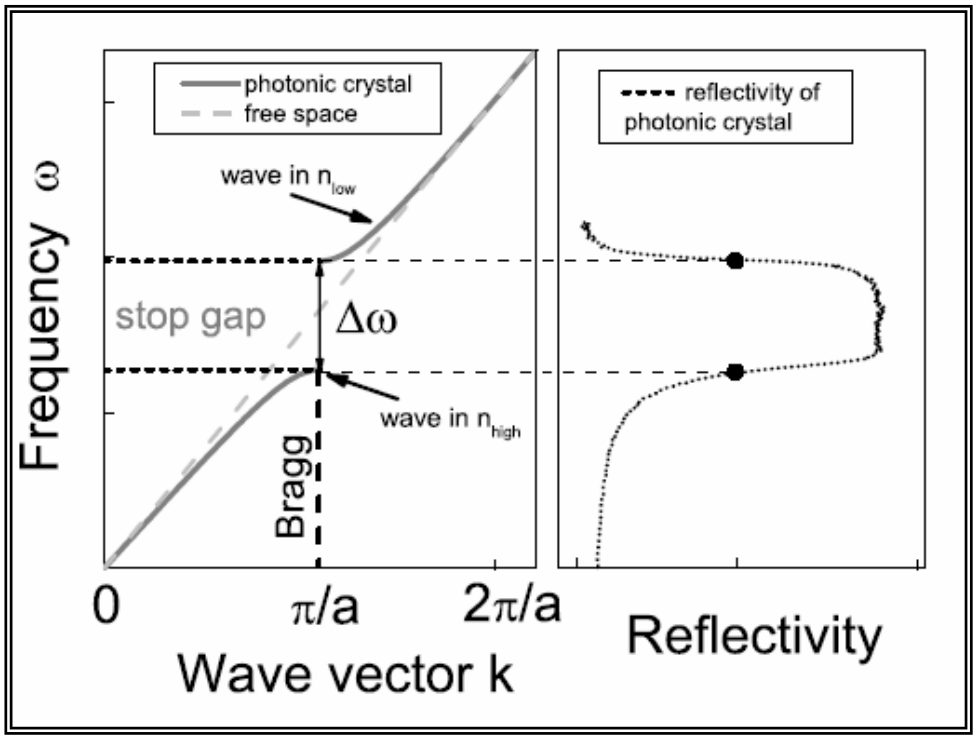

Fig.3.5. Scheme of a bandgap structure. At the Bragg condition there are two standing waves, one in n_{high} , and one in n_{low}. For comparison the frequency behavior of a homogeneous dielectric is also plotted, where the relation with the wave vector is linear (dashed line). In the right side the reflectivity peak of the photonic crystal. The reflected light appearing in the spectrum is excluded from the crystal and corresponds to the frequencies of the stopband.

When no periodicity in refractive index is present, which is the case in free space or vacuum, the behavior of frequency with wavelength is linear (being plotted in figure as a dashed line). In the right side of figure a reflectivity peak from a photonic crystal is plotted. At the position of the stop gap a peak manifests; the light with this frequency and along this direction cannot enter the crystal and is reflected. The width of the stop gap (i.e. the width of the reflectivity peak, denoted as Δω) is a very important measure for photonic crystals. This width is indicated in the figure with an arrow. To classify the interaction strength of photonic crystals with light, the photonic parameter Ψ is defined as:

$$\Psi = \frac{\Delta\omega}{\omega} \propto 3\phi \frac{m^2 - 1}{m^2 + 2} \tag{3.5}$$

where Δω, ω, φ and m are respectively the width and the center frequency of the stop gap, the volume fraction of the high index material and the refractive index contrast between the low and high index material. The photonic parameter or photonic strength mainly describes the polarizability per volume. This parameter was introduced by Vos et al [19,20]. in 1996. The photonic parameter is strongly influenced by the refractive index contrast m and the volume fraction of the high index material φ. A high refractive index contrast results in a wide stop gap and thus a large photonic strength. It is possible to adjust the positions of these bandgaps by changing the size of the periodic layers or by variation of the refractive index.

3.3.3. Photonic Crystals with 1D, 2D or 3D Directional Periodicity

The simplest form of a photonic crystal is a one-dimensionally periodic structure, such as a multilayer film (a Bragg mirror); electromagnetic wave propagation in such systems was first studied by Lord Rayleigh in 1887, who showed that any such one-dimensional system has a band gap. 1D-periodic systems continued to be studied extensively, and appeared in applications from reflective coatings to distributed feedback (DFB) lasers. 2D-periodic optical structures, without band gaps, received limited study in the 1970s and 1980s. The possibility of two- and three-dimensionally periodic crystals with corresponding two- and three-dimensional band gaps was not suggested until 100 years after Rayleigh, by Eli Yablonovitch and Sajeev John (1987), and such structures have since seen growing interest by a number of research groups around the world. With applications including LEDs, optical fiber, nanoscopic lasers, ultrawhite pigment, radio frequency antennas and reflectors, and photonic integrated circuits.

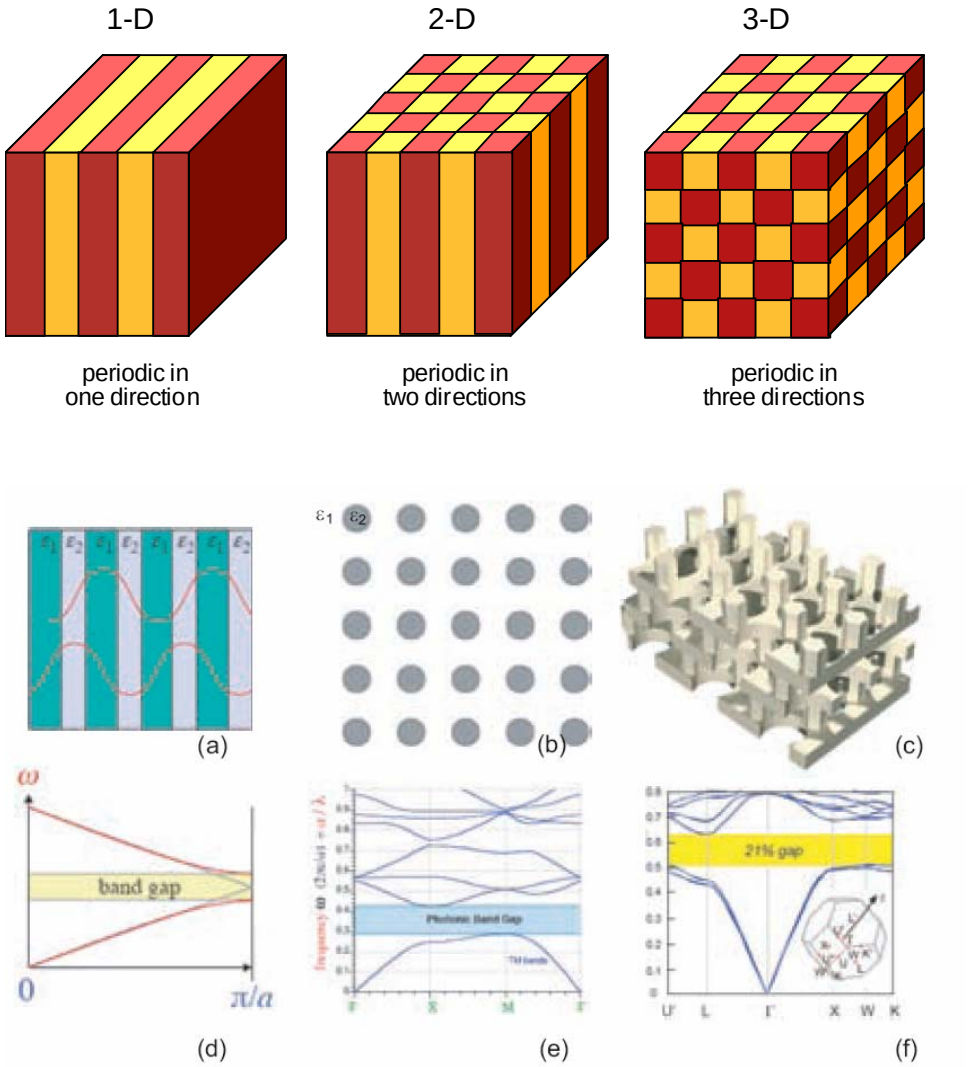

Fig.3.6. Examples (a-c) of 1D, 2D and 3D photonic crystals and (d-f) corresponding band structures.

If the periodicity in the refraction index holds only in one direction (i.e. 1D photonic crystal), only light travelling perpendicularly to the periodically arranged layers is affected.

In 2D case, light propagating in the plane perpendicular to the rods will be affected. In order to make a complete bandgap for any direction of light propagation, a 3D structure have to be constructed. Figure 3.6 illustrates 1D, 2D and 3D photonic crystals along with their band structures.

Many research groups have recently succeeded in controlling the pace of light emission using photonic crystals. In the process, they have verified a 20-year old

prediction of the American physicist Eli Yablonovitch that ignited a world-wide rush to build tiny "chips" that control light beams. Many other potential uses arise, not only as a tool for controlling quantum optical systems, but also in efficient miniature lasers for displays and telecom, in solar cells, and even in future quantum computers.

3.3.4. Cholesteric Liquid Crystals as 1D Photonic Crystals.

The layered structure of the cholesteric phase of liquid crystals is similar to that of nematic liquid crystals. However, because it is composed of chiral molecules, which can be either left or right handed, the lowest energy configuration is achieved with a rotation by a small fixed angle between consecutive molecular layers [21,22]. Since the dielectric constant of a particular layer and of a layer rotated by 180 are the same, the structure has double helix symmetry. As a result, the pitch of the structure, which is the distance in which the director rotates by 360, is twice the period of the cholesteric structure, as seen in Fig.3.7. The energy of the twist is smaller than the energy associated with in-layer interaction by a factor of order 10^5 [23]. As a result, a helical structure is created once the liquid crystal is placed between two glass substrates along which the CLC layers have a preferential orientation. This is achieved by coating both substrates with a polymeric layer giving planar alignment for the liquid crystal molecules.

Figure 3.7 illustrates the molecular ordering of a CLC. The rod-shaped molecules are arranged approximately parallel to each other. The average direction of the long molecular axis in the plane is called the director. The refractive indices for light polarized parallel and perpendicular to the director are the extraordinary and ordinary indices, n_e and n_o respectively.

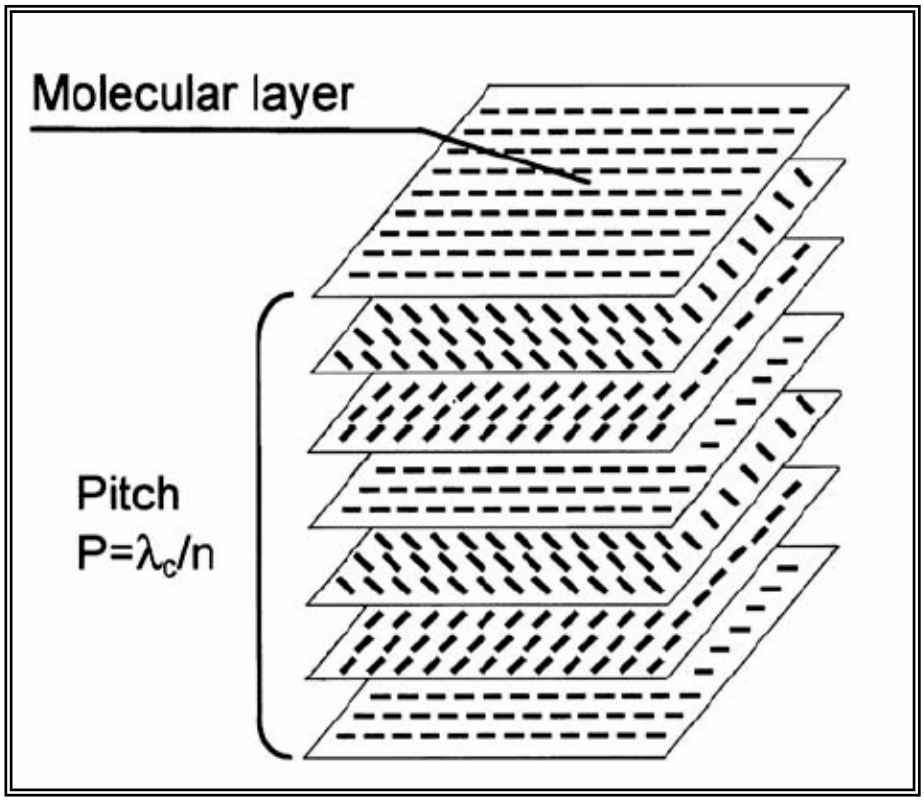

Fig.3.7. Molecular structure of cholesteic liquid crystals (CLC). The dashes indicate the orientation of the director.

For sufficiently thick films, the reflectance of normally incident, circularly polarized light with the same sign of rotation as the CLC structure is nearly complete within a band centered at a wavelength within the medium equal to the pitch of the structure. This corresponds to a vacuum wavelength $\lambda_c = n_{avg}\ \lambda_0 = n_{avg} p$ where n_{avg} is the average refractive index of the cholesteric planes which have a birefringence of $\Delta n = (n_e - n_o)$ and p is the pitch of the cholesteric helix [22]. A typical reflection spectrum from CLC film is shown in Fig.3.8 [24]. The reflected light has the same sign of circular polarization as the incident beam. This is in contrast to light undergoing Fresnel reflection from an isotropic medium for which the sense of circular polarization is reversed. Modeling the sample as a series of thin rotated anisotropic layers, de Vries [22] showed that the width of the reflection band is given by $\Delta\lambda = (n_e - n_o)\ p$. The band structure of a CLC at oblique incident angle was calculated in Ref. [25].

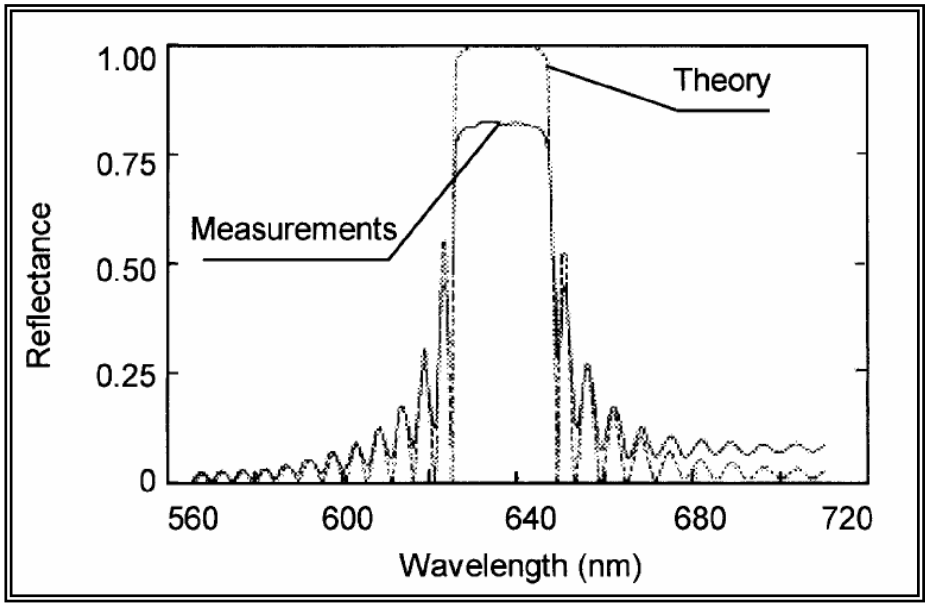

Fig.3.8. Reflection spectrum from a monodomain of CLC.

The birefringence and natural ability to form periodic structures make chiral liquid crystals interesting one-dimensional photonic bandgap materials. Because of the possessed helical superstructure chiral liquid crystals (CLC) show a 1D spatial modulation of the refractive index giving rise to Bragg selective reflection for circularly polarized light having the same handedness as the LC structure.

3.4. General principles of lasing operation

The word ”LASER” is an acronym for Light Amplification by Stimulated Emission of Radiation. The main principles involved in lasing are stimulated emission, population inversion and feedback.

The three basic elements of a laser are: (i) a laser medium consisting in of an appropriate collection of atoms, molecules, ions etc; (ii) a pumping process to excite these atoms into higher quantum-mechanical energy levels in order to realize the

population inversion, so that the stimulated emission is the dominant mechanism in the process; (iii) suitable optical feedback elements, such as optical cavities.

The output of a laser is a highly-coherent monochromatic (in a very ideal case) radiation, which can be pulsed or beamed in a visible, infrared or ultraviolet range.

The power of a laser can vary from several milliwatts (mW) up to megawatts (MW).

The main component of a laser is its active medium, which can be a solid, gas, liquid or semiconductor. In thermodynamic equilibrium nearly all atoms, ions or molecules (depending on the particular laser) of the active medium occupy their lowest energy level or ”ground state”. To produce laser action, the majority of atoms/ions/molecules should be ”pumped” up into higher energy level, creating so called population inversion. The energy required to achieve population inversion is provided by pumping the laser medium by an external energy source. This external source can be another laser, a flash lamp or an electrical discharge.

Typical three-level structure is given in Fig.3.9a. Pump energy here excites atoms from the ground state to the short-lived level, which rapidly decays to the longlived state. At random times, some of these excited atoms/ions/molecules will decay to the ground state on their own. Each decay is accompanied by emission of a single photon propagating in a random direction (spontaneous emission).

However, if one of these photons encounters an excited atom/ion/molecule, it will drop down to a lower energy state and emit a new photon with exactly the same wavelength, phase, direction and polarization. This is called stimulated emission.

When a photon is emitted nearly parallel to the long side of the cavity (Fig. 3.9b) it will travel down to one of the mirrors and be able to get reflected back and forth many times. Along its way, it hits excited atoms/ions/molecules and ”stimulates” them to emit up new photons. The process acts as an avalanche caused by a single photon which produces more and more photons via this stimulated emission process.

The material features gain if the net number of photons increases (i.e. more photons are generated than lost). If the chain reaction in a gain material is caused by a photon created by a spontaneous decay one speaks of Amplified Spontaneous Emission (ASE). ASE is spectrally broader than lasing as there is no mode selection through feedback and spontaneous emission can occur throughout the entire gain spectral region.

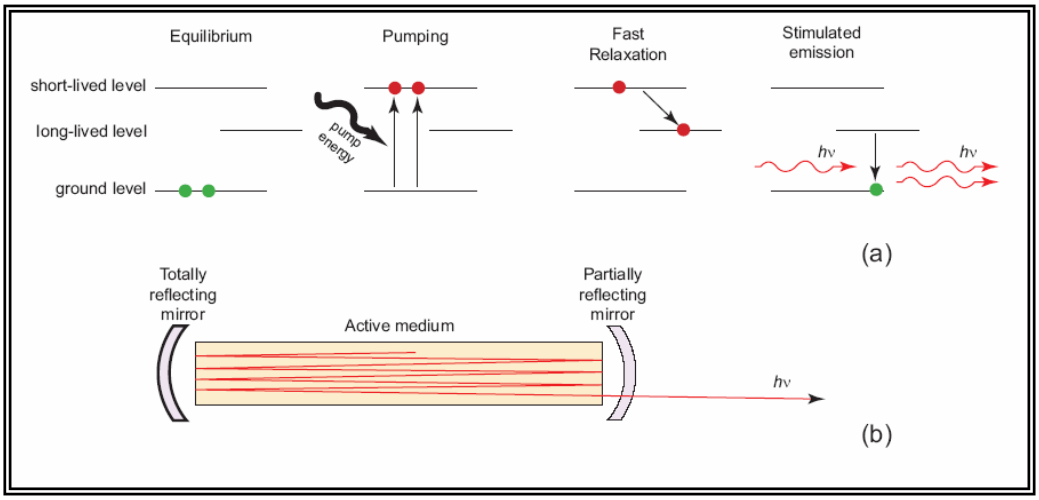

Fig.3.9. (a)Three-level diagram of a lasing system. (b) Lasing cavity.

Unfortunately, photons emitted by stimulated or spontaneous emission can also be reabsorbed by the laser material. This process, reabsorption, is a loss process: the photon is no longer available to stimulate an emissive process. Due to re-absorption lasing is not possible in a two-level system (i.e. a system where the upper and lower states are the first excited state and the ground state). The reason for this is that in any system that is in equilibrium with its surroundings the rate at which energy is absorbed must equal the rate at which it is emitted. Therefore, the absorption rate and decay rate are equal and population inversion is impossible. This issue is overcomed in three-and four-level systems.

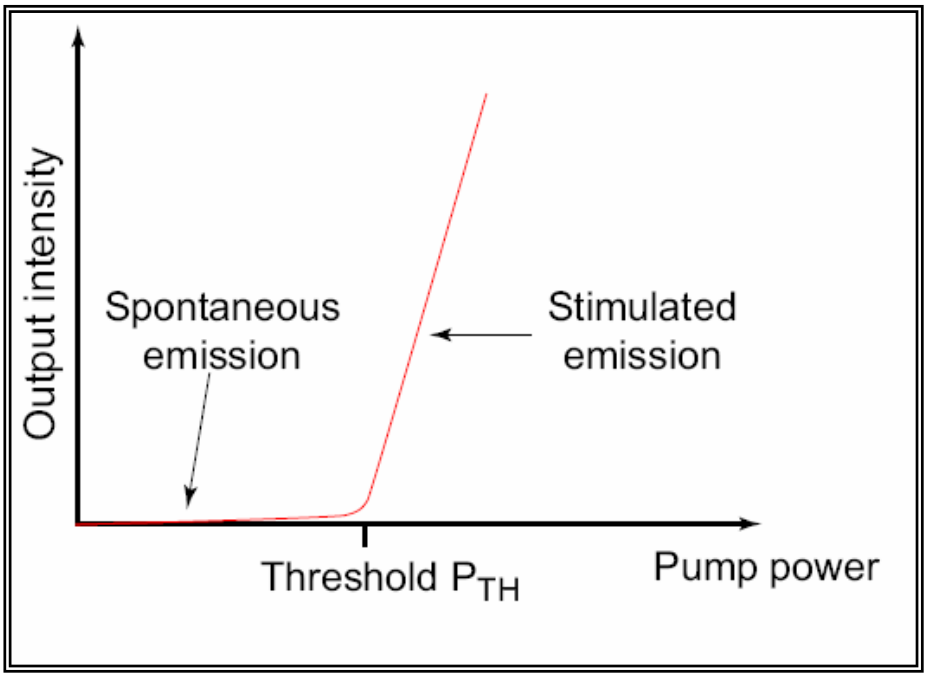

Fig. 3.10. Threshold behaviour of a laser.

In case of stimulated emission, when the energy of the photon beam becomes enough to make the beam escape a partially reflecting mirror, a highly monochromatic and coherent ray goes out. Depending of the type of a cavity the beam can be well collimated or appears to originate from a point/plane source.

One of the most important parameters of lasers is the threshold P_{TH}, that can be defined as the ”critical” pumping power that corresponds the initiation of the stimulated emission (Fig.3.10).

The threshold is proportional to the threshold population difference (i.e. the minimum positive difference in population between the long-lived and ground levels):

$$N_T = N_u - N_g \approx \frac{1}{c\tau_p} = \frac{\omega_0}{cQ} \qquad (3.6)$$

where c is the speed of light, τ_p is a photon lifetime, ω_0 is the resonant frequency

of a lasing mode and Q is the quality factor of a laser cavity. The main goal is, obviously, to minimize threshold, therefore maximize the photon lifetime and cavity quality factor.

The Q-factor is strongly determined by the cavity design [26], several representative examples are given in figure 3.11.

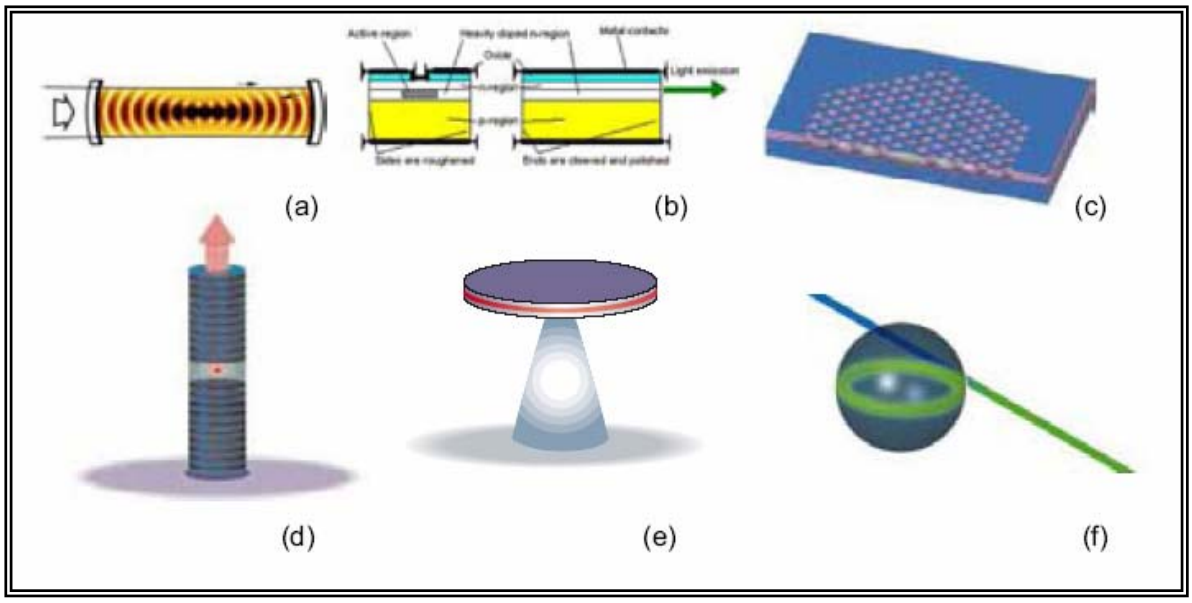

Fig.3.11. Different types of lasing cavities. (a) Confocal resonator. Employed in a variety of gas, solid-state and chemical lasers. Two confocal mirrors (one of them is partially reflecting) create a collimated beam parallel to the long side of the cavity. (b) Laser diode. The cavity is created by finely polished side walls of the structure. (c) Photonic-crystal cavity. The cavity is created by point inhomogeneity in a photonic-crystal lattice. (d) Fabry-Perot resonator. A set of stacked Bragg mirrors provides cavity confinement. (e) Whispering-gallery disk microcavity. The ray of light is trapped inside the cavity, undergoing multiple "bounces" against side wall due to the effect of total internal reflection. (f) A spherical whispering-gallery droplet.

3.5. Distributed Feedback (DFB)

Stimulated emission is enhanced by feedback as the stimulated photons are sent through the medium multiple times, stimulating more photons, before being emitted out of the laser. The number of round trips is proportional to quality factor Q of the laser.

Feedback for lasers can be provided by a wide range of resonators, such as Fabry-Perot cavities, ring resonators and photonic gratings (as presented in Fig.3.11). Resonance is only achieved for modes that satisfy the resonance condition of the cavity, leading to emission with narrow line widths as only one of a few modes are enhanced by feedback. By tuning the reflection of the mirrors with a wavelength-selective feedback mechanism like a grating, mode selection is possible.

In a distributed feedback (DFB) laser the laser modes receive feedback at one specific wavelength (and to a smaller extent, its harmonics), determined by the grating period of the structure. While the mode is propagating along the structure a small part of its energy is reflected (i.e. coupled into the counter-propagating mode).

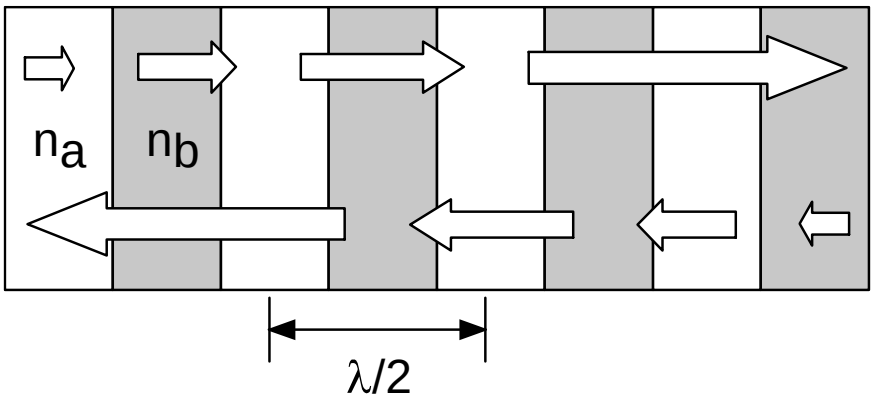

Fig.3.12. Scheme of the DFB mechanism in a 1D periodic structure.

The coupling strength, parameterized by the coupling constant κ, is influenced by the grating geometry and the refractive index contrast between substrate and waveguide material. The feedback is proportional to κL, where L is the coupling length. The coupling strength thus determines how large the corrugated area has to be to achieve

the feedback required for lasing: A small value for κ has to be compensated by larger coupling length L.

Kogelnik and Shank [27] were the first to report laser action in mirrorless periodic Bragg DFB structures. Laser action in chiral liquid crystals was predicted by Goldberg and Schnur in 1973 [28] and firstly observed by Il'chishin et al. in 1981 [29] being explained using the distributed feedback theory [27].

3.6. Dye Lasers and Laser Dyes

Dye lasers are "the fulfillment of an experimenter's pipe dream that was as old as the laser itself: To have a laser that is easily tunable over a wide range of frequencies or wavelengths" (Schaefer, 1977). Dye lasers can be pumped by incoherent or laser sources, both pulsed and CW, and offer the possibilities of broad wavelength control, multijoule pulsed operation, ultranarrow linewidths, or ultrashort pulses. They are conveniently divided into three broad technological categories:

(i) Continuous-wave jet-streamed dye lasers can provide narrow CW bandwidths and can be synchronously pumped or passively modelocked to generate short pulses.

(ii) Flashlamp -pumped dye lasers have a larger bandwidth and less wavelength stability than CW laser-pumped dye lasers. But, they have the advantage that large volumes of active dye medium can be pumped, yielding large output pulse energies and active powers.

(iii) Dye lasers that are pumped by Cu vapor, nitrogen or excimer lasers, or by the frequency-doubled or tripled output from pulsed Nd:YAG lasers, provide high peak powers. Also, the pulse duration of 4 to 60 nsec makes possible narrow bandwidths and a high spectral purity.

COMMERCIAL DYE LASER OUTPUT CHARACTERISTICS

Pump Source	Argon/Krypton Ion Laser		Flashlamp	Nd:YAG Laser	Excimer Laser
	CW	Mode-Locked/ Cavity Dumped			
Tuning Range [nm]	380-950	580-880	335-850	410-880	320-1.024
Average Power [W]	5	0.1	3	2	10
Repetition Rate [Hz]	CW	3.8M	2-30	10-40	1-500
Peak Power [kW]	-	10	7000	20,000	10,000
Energy/pulse [mJ]	-	0.01	3,500	10-120	40-120
Pulsewidth [nsec]	-	0.0001	260-600	5-10	7-250
Linewidth [GHz]	0.0005 to 40	Various	2	0.6	0.15

Fig.3.13. Typical output characteristics from commercial dye lasers.

Continuous-Wave Dye Lasers

CW laser systems consist of three major elements: the optical resonator, dye flow system and tuning element. The resonator is responsible for maintaining a rigid optical alignment of all cavity components. The dye flow system – the dye, circulation pump, and dye jet nozzle - must provide an optically flat stream of dye across the laser's optical axis. The tuning element allows the user to continuously tune to the required output wavelenght. Excitation in a CW dye laser is provided by an input pump beam from another CW light source, typically an ion laser. This beam is focused onto the dye stream and causes an extremely high level of fluorescence. The fluorescence is focused between two highly reflective concave mirrors that feed back the fluorescent light, initiating the lasing process.

The dye laser emission described above is broadband, typically exhibiting a 40-GHz linewidth. Many applications require narrow-linewidth singlefrequency operation. Meeting this requirement is possible by inserting one or two etalons into the dye laser cavity. A dye laser with an etalon, when coupled with electronic stabilization, can narrow the linewidth to less than 1 MHz.

Pulsed Dye lasers

Of the various pulsed dye lasers, two types tend to dominate because of their versatility, broad spectral coverage and high output power.

These are Nd:YAG (Neodimium doped : yttrium aluminium garnet) and excimer-pumped dye lasers.

The use of Nd:YAG and excimer pump lasers allows dye laser pulses to be produced at energy levels up to 100 mJ or more. Their performance is wavelength-dependent. At the long wavelengths more energy is provided by pumping with a frequency-doubled Q-switched Nd:YAG than with an excimer laser. However, UV-emitting excimer pumps allow dye lasers to operate directly at UV wavelengths down to 308 nm and at repetition rates of 500 Hz.

The strongest Nd:YAG lasing line is at 1,064 nm, which is unsuitable to pump dyes. Fortunately, its high peak power and near-diffraction-limited beam quality provides efficient frequency doubling, tripling and quadrupling. This provides suitable pump wavelengths of 532, 355 and 266 nm. Considerable engineering effort has gone into reducing the intensity fluctuations that are amplified by the inherent nonlinear frequency-doubling process. The tuning range can be covered by using one of these pump wavelengths and an appropriate dye.

The discovery of rare gas halide lasers - the "excimer“ laser - in 1976 introduced a new and powerful tool for dye laser pumping. It combines the advantages of the nitrogen system (high repetition rate, ease of operation, and low cost) with those of the Nd:YAG system (high peak power and sufficiently long pulse duration). Furthermore, the excimer laser is scalable to very high repetition rates (>1 kHz) and high pulse energies (>1 J). Excimer laser wavelengths range from 193 nm (ArF) to 351 nm (XeF). The strongest lines are at 248 nm (KrF) and 308 nm (XeCl). Most dyes have an absorption band at 308 nm. The result is that nearly the entire range of commercially available dyes can be pumped with a XeCl laser.

Dyes

Dyes, either as solutions or vapors, are the active medium in pulsed and continuous-wave dye lasers as well as ultrafast shutters for Q-switching and passive modelocking. They emit in a comparatively narrow spectral region (typically 30 nm); thus a variety of dyes is necessary in order to cover the entire (visible) spectral range.

The optical excitation of dyes corresponds to transitions of molecules in the singlet state, with the absorption $S_0 \rightarrow S_1$ being the strongest (Fig.3.14), and is specific for each dye molecule. For optimum pumping ($S_0 \rightarrow S_1$) of the various dyes, one would therefore need a number of pump-laser wavelengths.

Fortunately, nearly all dyes have additional absorption bands in the UV. These absorptions correspond to transitions to higher singlet states, from which fast internal relaxation processes lead to the upper laser level (S_1) with high quantum efficiency - the reason most dyes can be pumped by a single UV laser. However, this attractive excitation scheme – one pump laser for all dyes - brings other problems.

(i) The inner efficiency of dye lasers is lower as a result of excitation in higher S-states because a considerable part of the excitation energy is converted into heat (large Stokes shift). This disadvantage is more than compensated for, however, by the high efficiency of pulsed lasers.

(ii) A multiphoton excitation can lead to destruction of the cell and the solvent molecules. In this process, a previously excited molecule absorbs further photons (sequential absorption), or a molecule absorbs several photons “at the same time“. In these absorption processes the molecule can absorb so much energy that the binding energy is surpassed, and the molecule dissociates, or at least changes its structure. This process is more probable during excitation with UV light than with visible light. Thus, one must expect a reduced photostability of the dye when pumping with UV light.

(iii) Another problem results from the small absorption cross section at short wavelengths. To excite as many molecules as possible, a very high pump power density I_p (I_p being inversely proportional to the absorption cross section), or high dye concentrations is required. I_p is limited to values <30 MW/cm^2 due to the stability of most solvents.

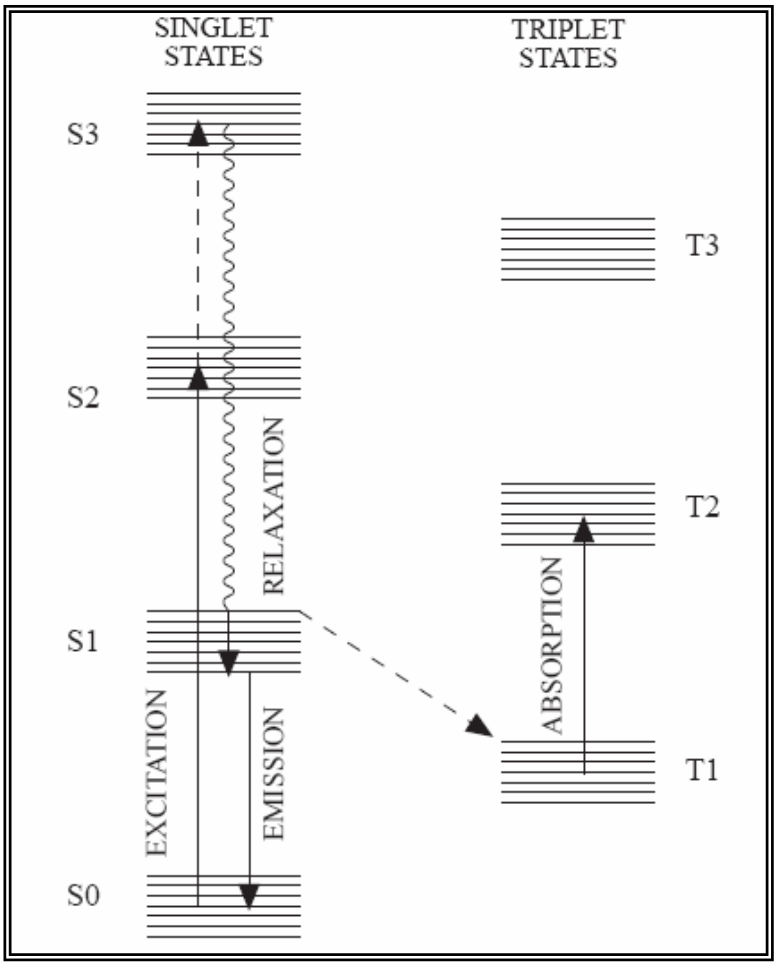

Fig.3.14. Schematic energy levels of a dye molecule.

The two most important laser dyes used in the experimens are:

- DCM (4-Dicyanmethylene-2-methyl-6-(p-dimethylaminostyryl)-4*H* –pyran)

- and Pyrromethene 597 - 4,4-Difluoro-2,6-di-t-butyl-1,3,5,7,8-pentamethyl-4-bora-3a,4a-diaza-s-indacene2,6-Di-t-butyl-1,3,5,7,8-pentamethylpyrromethenedifluoroborateComplex

Their optical and chemical characteristics are presented in the following tables [30].

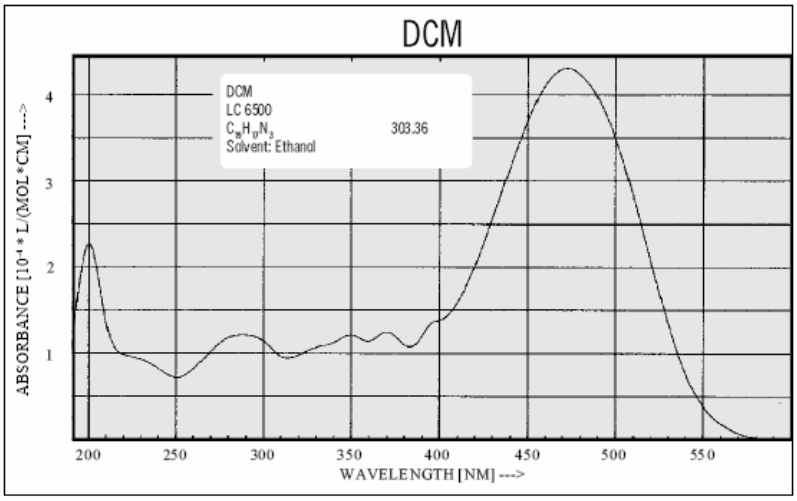

Constitution

4-Dicyanmethylene-2-methyl-6-(p-dimethylaminostyryl)-4*H*-pyran

$C_{19}H_{17}N_3$ · MW: 303.36

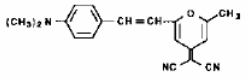

Characteristics

Lambdachrome® number:	6500
CAS registry number:	51325-91-8
Appearance:	red, crystalline solid
Absorption maximum (in ethanol):	472 nm
Molar absorptivity:	4.25 x 10^4 L mol^{-1} cm^{-1}
Fluorescence maximum (in ethanol):	644 nm

For research and development purposes only.

Lasing Performance

Efficient laser dye for pulsed and CW operation; tunable around 650 nm. DCM Special gives higher efficiency due to better solubility.

Pump		*Dye Laser Characteristics*					
Source	*Wavelength [nm]*	*Peak [nm]*	*Range [nm]*	*Effic. [%]*	*Conc. [g/l]*	*Solvent*	*Ref.*
XeCl-Excimer	*308*	*658*	*632 - 690*	*12*	*0.71*	*DMSO*	*1, 2*
Nitrogen	*337*	*659*	*626 - 703*	*rel.*	*0.50*	*DMSO*	*3*
Nd:YAG, 2nd	*532*	*639*	*615 - 666*	*27*	*0.50*	*PC*	*1, 4*
Cu-vapor	*510*	*644*	*598 - 677*	*14*	*0.61*	*Methanol*	*5*
Flashlamp	*-*	*655*	*610 - 710*	*-*	*0.76*	*DMSO*	*6, 7*
CW, Ar+	*VIS*	*660*	*-*	*-*	*0.45*	*Bz./Eg.*	*1, 8, 9, 10*

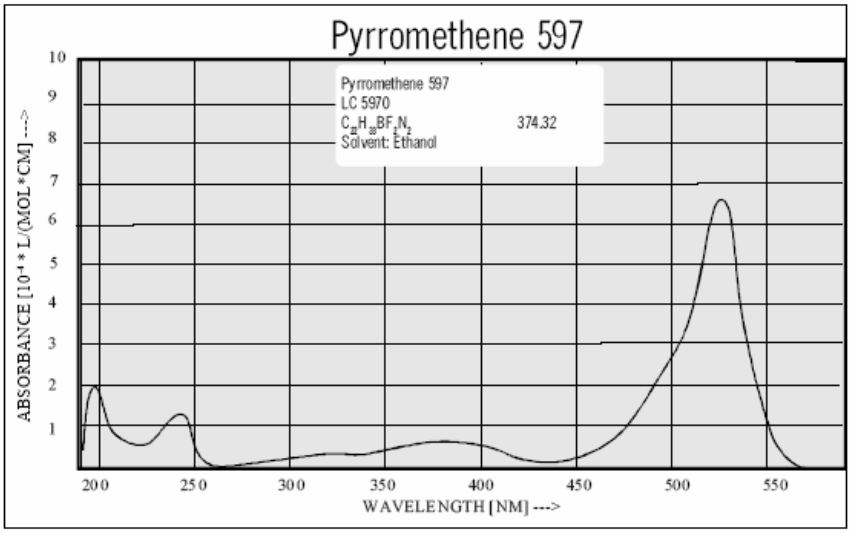

Constitution

4,4-Difluoro-2,6-di-t-butyl-1,3,5,7,8-pentamethyl-4-bora-3a,4a-diaza-s-indacene
2,6-Di-t-butyl-1,3,5,7,8-pentamethylpyrromethenedifluoroborate Complex

$C_{22}H_{33}BF_2N_2$ · MW: 374.32

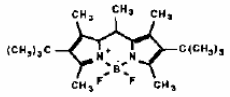

Characteristics

Lambdachrome® number:	5970
CAS registry number:	137829-79-9
Appearance:	red, crystalline solid
Absorption maximum (in ethanol):	524 nm
Molar absorptivity:	6.76 x 10^4 L mol^{-1} cm^{-1}
Fluorescence maximum (in ethanol):	557 nm

For research and development purposes only.

Lasing Performance

Laser dye for pulsed operation; tunable around 590 nm.

Pump		*Dye Laser Characteristics*					
Source	*Wavelength [nm]*	*Peak [nm]*	*Range [nm]*	*Effic. [%]*	*Conc. [g/l]*	*Solvent*	*Ref.*
Flashlamp	-	*593*	-	-	*0.08*	*Ethanol*	*1, 2*

3.7. Spontaneous Emission

3.7.1. Background

Spontaneous emission is a process in which an emission source, such as an excited atom or dye-molecule, loses energy under emission of a photon. Spontaneous emission is responsible for most of the light around us. Excited atoms will fall back to a lower energy level by emitting one or more photons. The term “spontaneous emission” was invented for this process when only the inadequate classical electromagnetic theory was around. In classical optics, if no light is present near the atom, the electric field is zero. An absent electromagnetic field can not be the external cause of the emission, which explains the word “spontaneous”. Einstein derived spontaneous-emission rates from classical theory by using energy-balance arguments, but a full understanding of spontaneous emission requires quantum optics. In quantum optics, atoms are surrounded by an omnipresent electromagnetic field. The field is always there, even when it is in its lowest energy state. In this vacuum state, no photons are present and no light can be detected. However, the electromagnetic field fluctuates even when in the vacuum state. Similar ground-state fluctuations occur for the position and momentum of an electron in a hydrogen atom: both the electromagnetic field operators and the atomic operators obey their respective Heisenberg uncertainly relations. An excited atom feels the fluctuations of the ground-state electromagnetic field. These fluctuations cause the atom to decay “spontaneously” to a lower state. In a semiclassical picture, exactly half of the spontaneous-decay rate of an atom can be attributed to these field fluctuations; the other half of the decay rate is caused by the electric field that the atom exerts on itself, the so-called radiation reaction. The process of spontaneous emission starts with an atom in an excited state and the field in the vacuum state. After the emission, the atom is in a lower-energy state and the field can be in any one-photon state that gives the same total energy before and after the emission.

3.7.2. Fermi's Golden Rule and the Photonic Density of States

It is now commonly accepted that spontaneous emission is not an immutable property of the emitter, but it depends on the density of modes of the light field at the location of the emitter. This dependence was originally noted by Purcell [1] and it is embodied in Fermi's Golden Rule [31]. The spontaneous emission or decay of a light source, depends strongly on the surrounding medium [1]. Experimental investigations demonstrated that the spontaneous emission rate can be enhanced or reduced with respect to vacuum by placing emitters in a high-quality resonant or non-resonant cavity, respectively [32-36].

Fermi stated already in 1932 that the decay can be treated as a transition between two states that depends on the strength of the coupling between these two states. His theory is now well-known under the name of Fermi's Golden Rule where properties of the material and the position of the source are included [31].

The radiative decay rate γ_{rad} of a transition from an initial to a final state at position *r* is described by Fermi's golden rule as:

$$\gamma_{rad} = \frac{1}{\tau} = \frac{2\pi}{h^2} \sum_f \left| \Psi_f H(\vec{r}) \Psi_i \right|^2 \delta(\omega_f - \omega_i) \tag{3.7}$$

where h is Planck's constant, Ψ_i and Ψ_f are the wavefunctions of respectively the initial and the final state, τ the excited state lifetime. H is a operator that contains the transition dipole moment $\vec{\mu}$ of the transition and the electric field $\vec{E}(\vec{r})$ of the surrounding medium at that position, $H = \vec{\mu} \cdot \vec{E}(\vec{r})$. The electric field $\vec{E}(\vec{r})$ depends on the frequency ω, dielectric contrast ε and volume V as $E \propto \sqrt{\frac{h\omega}{\varepsilon V}}$.

Fermi's golden rule sums over all available final states f. The delta function $\delta(\omega_i - \omega_f)$ describes the conservation of energy; a photon can only be emitted if its energy agrees with the energy difference between the final and initial state. If the coupling between the initial and final state is stronger, a transition will proceed more rapidly. This happens if there is more interaction between the dipole moment of the transition and the electric field of surrounding medium. In a material with a higher refractive index

(i.e. a larger electric field), the interaction between final and initial state will therefore be stronger, resulting in a shorter lifetime. It should be noted that Fermi's golden rule is not only applicable to fluorescence decay of light sources but also to for instance nuclear decay and many other physical transitions. Equation (3.7) can be rewritten in a part related to the atom itself and a part related to the position dependent field as:

$$\gamma_{rad} = \frac{1}{\tau} = \frac{2\pi}{h^2}\left|\Psi_f H \Psi_i\right|^2 \rho(\omega, r) \qquad (3.8)$$

where the part $|\Psi_f H \Psi_i|$ describes the coupling between the initial and final state (atom part) and $\rho(\omega, r)$ is the position dependent part also called local density of states (LDOS) [37,38]. This equation describes that not only the environment, included in $|\Psi_f H \Psi_i|$, determines the emission properties but also the spatial position of the light source plays a very important role. In particular the radiative lifetime is strongly determined by the density of available light modes at that specific spatial position, the LDOS. If the LDOS is large compared to the vacuum, the emission is enhanced since there are more modes for the excited state to decay. In the case of a small LDOS the reverse occurs; the emission is inhibited. Modification of the LDOS is therefore a very interesting subject for research since the spontaneous emission can be influenced. It is exactly the LDOS that is strongly modified in photonic crystals.

The effect of a modified LDOS in photonic crystals was first described by Suzuki and Yu and by Sprik et al. [39,37]. In photonic crystals the LDOS is changed in such a way that the emitted light from an embedded emission source is strongly modified; either enhanced or inhibited. In the case of a photonic band gap the LDOS is extremely modified and even goes to zero and spontaneous emission can be inhibited. Apart from inhibition or enhancement the light can also be localized. Localization of light occurs when the emission source is placed in a defect. In this way the light source can emit a photon but this photon cannot exit the defect. Since performing LDOS calculations for a photonic crystal is quite complicated, often total density of states (DOS) calculations are done. The total DOS in free space is equal to:

$$\rho(\omega) = \int dV \rho(\omega, r) = \omega^2 / \pi^2 c^3 \qquad (3.9)$$

where the LDOS is integrated over a volume V of an unit cell. A clear distinction should be made between LDOS and the (total) DOS. The total DOS is the averaged LDOS over one unit cell. Often the terms LDOS and DOS are randomly used but an unchanged total DOS is not necessarily an unaffected LDOS, so a crystal can still contain positions where the LDOS is going to zero, resulting in inhibited emission. At the position of the photonic band gap the DOS goes to zero. It can also be seen that near the edges of the photonic band gap the DOS is significantly increased.

Attenuation and enhancement of spontaneous emission was intensively studied by the use of cavities, investigated in the field of cavity quantum electrodynamics (QED) [32]. The essence of cavity QED is that an atom or atoms are stored in an enclosure which has dimensions comparable to emission wavelength of atoms. Therefore, compared to atoms in free space, the atoms couple to either smaller or larger electric field modes. If emission exists at the resonant wavelength the emission is greatly enhanced while off-resonance emission would be inhibited [9,12,26,40].

A typical cavity QED situation is shown in figure 3.15.

A first approach to study the modification of spontaneous emission is to replace the density of states for free space $D_{free}(\omega)$ phenomenologically with a cavity modified density of states $D_{cav}(\omega)$:

$$D_{cav}(\omega) = \frac{k}{2\pi V} \frac{1}{(k/2)^2 + (\omega_{cav} - \omega)^2} \qquad (3.10)$$

with the cavity damping rate k.

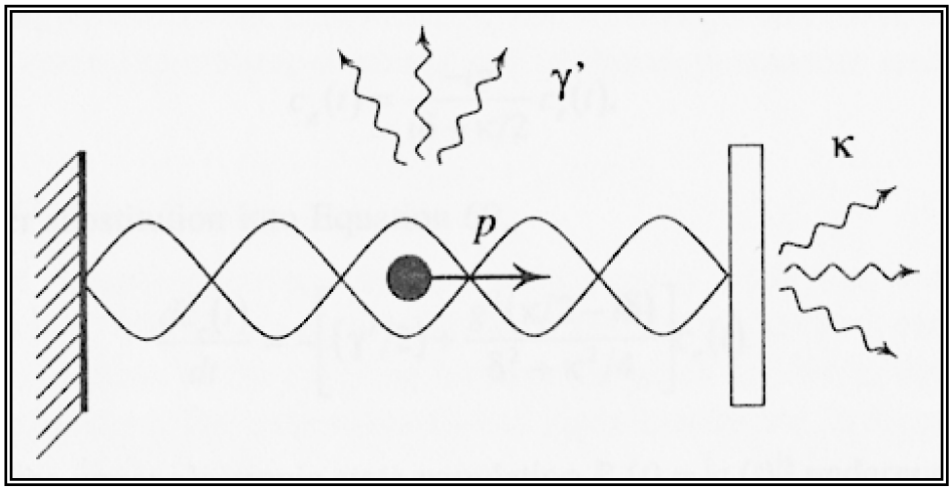

Fig.3.15. A typical cavity QED system: a single atom is inside a Fabry-Perot cavity.

With this expression one finds:

(i) the Enhanced Spontaneous Emission for an atom in resonance with the cavity:

$$\Gamma_{cav} = \Gamma_{free}\left(\frac{\lambda_0^3}{V}\right)Q \qquad \text{with} \quad \lambda_0 = 2\pi c/\omega \qquad (3.11)$$

(ii) the Suppressed Spontaneous Emission for an atom off-resonance with the cavity:

$$\Gamma_{cav} = \Gamma_{free}\left(\frac{\lambda_0^3}{V}\right)Q^{-1} \qquad (3.12).$$

Enhancement and suppression have been demonstrated for the first time in experiments by Kleppner [14].

3.8. The group velocity. Cavity quality factor

The phase velocity of a wave can be defined as the rate at which the phase of the wave propagates in space. This is the velocity at which the phase of any one frequency component of the wave will propagate. The phase velocity is given in terms of the wave's frequency ω and wave vector k by:

$$v_p = \frac{\omega}{k} \qquad (3.13).$$

The group velocity of a wave is the velocity with which the variations in the shape of the wave's amplitude propagate through space. The group velocity is defined by the equation:

$$v_g = \frac{d\omega}{dk} \qquad (3.14)$$

where ω is the wave's angular frequency and k is the wave number.
The quality factor of a mirrorless resonant cavity, Q, is defined as the resonant frequency multiplied the stored energy and divided by the dissipated power:

$$Q = \frac{\omega\varepsilon}{-d\varepsilon / dt} \qquad (3.15).$$

We have that $\frac{-d\varepsilon}{dt} = \frac{\varepsilon}{t_c}$, where t_c is the dwell time of the photons inside the cavity and is defined as:

$$t_c = \frac{2nl}{c\left[\frac{4\pi k}{\lambda}\right] - \ln R} \qquad (3.16).$$

One can notice that the dwell time of the photons is proportional to the length of the cavity. Here k is the extinction coefficient, λ is the wavelength, c is the speed of light , R is the cavity reflectance.
We obtain that the quality factor Q of the cavity is proportional to the dwell time of the photons inside the cavity [41]:

$$Q = \omega t_c \qquad (3.17).$$

So, the larger the quality factor is, the longer the radiation remains trapped inside the cavity resulting in a lower lasing threshold.

3.9. The Purcell Effect

Spontaneous emission is not an immutable property of the emitter, but it relies on the density of modes of the light field at the location of the emitter. It was predicted by Purcell [1] that an atom in a wavelength-size cavity can radiate much faster than in the free space. A two level system will decay spontaneously by interaction with a vacuum continuum at a rate proportional to the spectral density of modes per volume evaluated at the transition frequency. Within a cavity, the density of modes is modified and large swings in its amplitude can occur. From the viewpoint of cavity modes (which in the presence of dissipation must be viewed as quasi modes, the maximal density of modes occurs at the quasi-mode resonant frequencies and can greatly exceed the corresponding freespace density. Purcell [1] arrived at this conclusion by noting that a single (quasi) mode occupies a spectral bandwidth n/Q within a cavity of volume *V*. Normalizing a resulting cavity-enhanced mode density per unit volume to the mode density of free space yields the 'Purcell' spontaneous emission enhancement factor [42], where refractive index, *n*, is a modern addition to this expression to account for emission within dielectrics [43]:

$$F_P = \frac{3}{4\pi^2}\frac{Q}{V}\left(\frac{\lambda}{n}\right)^3 \qquad (3.18).$$

An atom whose transition falls within the mode linewidth will experience an enhancement to its spontaneous decay rate given by the Purcell factor. More significantly, because the enhancement comes about from coupling to only those continuum modes that make up the corresponding quasi-mode of the resonator, the spontaneous emission is directed to this quasi mode [] and has great utility with regard to coupling spontaneous power. In certain spectral locations that are intermediate to modal resonance frequencies, the density of the modes can fall well below the density in free space. So, with proper cavity design for operation at these offresonance frequencies, spontaneous decay can also be suppressed (not only enhanced) [12,42,44].

Thus, the rate at which a dipole spontaneously emits radiation can be enhanced or suppressed by placing the emitter inside an opportune optical cavity. This phenomenon, known as the Purcell effect, has been verified by numerous experiments that involve atoms passing through cavities. Optical microcavities confine light spatially and temporally [45]; a microcavity's great potential is not only determined by the increased photon dwell time (or the equivalent quality-factor, Q), but also by the simultaneous achievement of a small modal volume (V). The above defined Purcell factor describes the amount by which the spontaneous emission rate is enhanced for an emitter on resonance with a cavity mode. This factor is proportional to the quality factor of the mode and is inversely proportional to the mode volume and these aspects must be taken into account when designing a cavity for trapping light.

It was demonstrated that the DOS in optical microcavities and near surfaces shows large changes and several research groups already observed large effects in emission decay rates.

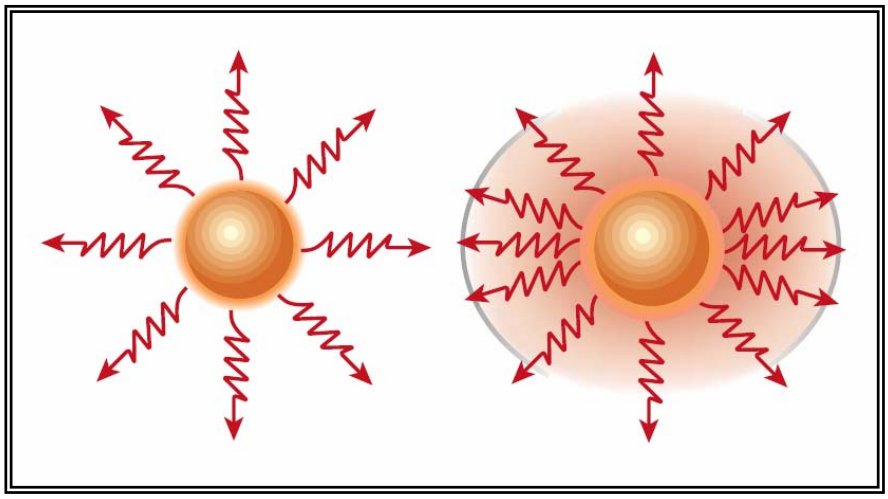

Fig.3.16. Purcell enhancement of spontaneous emission. Weak coupling to a cavity mode will enhance the spontaneous rate of emission by increasing the local density of modes (right) compared with their density in free space (left).

The control of spontaneous emission is a very interesting phenomenon. Enormous innovative advances can be made (thresholdless miniature lasers) [46,47]. If the density of states can be manipulated to the point that there is only one mode to decay there would be no decay into any other modes and lasing would occur into that one mode without loss.

3.10. Experimental Results

3.10.1 Colour-Tunable Organic Microcavity Laser Array Using Distributed Feedback

Overview and Motivation

The inclination toward miniaturization in the emerging generation of nanoscale optoelectronic devices leads to a growing interest in morphologically periodic photonic heterostructures like photonic bandgap materials and special microcavity geometries [48-50]. A relevant example is represented by the distributed feedback microstructures which play a fundamental role in confining and manipulating light for obtaining lasing in media with gain.

Helixed liquid crystals materials are self-organized mesophases which possess all the peculiar optical properties for achieving organic mirror-less optical resonant cavities. The birefringence and natural ability to form periodic structures make chiral liquid crystals interesting one-dimensional photonic bandgap materials. In fact, chiral liquid crystals (CLC) possess a helical superstructure which provides a 1D spatial modulation of the refractive index giving rise to Bragg selective reflection for circularly polarized light having the same handedness as the LC structure. In PBG microstructures light can be confined and manipulated by engineering quasi-ideal distributed feedback (DFB) micro-resonators [46,47]. In a CLC doped with fluorescent guest molecules, the spontaneous emission is suppressed for the reflection stop band and it is enhanced at the band edges where a series of narrow long-lived transmission modes are expected [51,52]. Within the bandgap, the wave is evanescent and decays exponentially, so that the density of states (DOS) within the gap vanishes in large structures. At the stop band edges the density of states is expected to diverge. The group velocity v_g is real, and at the photonic band edge tends to zero, while the photon dwell time is greatly increased, so that the gain is significantly enhanced at these spectral positions [53]. This gain enhancement together with distributed feedback mechanism can give rise to low threshold mirror-less lasing at the band edge in a variety of liquid crystal materials. In chiral liquid crystals the index modulation is relatively low so that sufficient feedback can be achieved by increasing the length of the resonant cavity.

Thousands of periods are needed in order to obtain an optical cavity with a quite high quality factor, Q [54].

In this chapter it is presented a detailed physical characterization of a novel array of organic distributed feedback microcavity lasers possessing a high ratio between the quality factor Q of the resonant cavity and its volume V. This optical microcavity was obtained by confining self-organized mesophases doped with fluorescent guest molecules into holographically patterned polymeric microchannels. The employed single-step process in creating the microstructures imposed the orientation of the liquid crystal helical axis along the polymeric walls. The liquid crystal microchannels act as mirrorless cavity lasers, where the emitted laser light propagates along the liquid crystal helical axis behaving as Bragg resonator.

The presented geometry allows obtaining a number of periods which is about 2 orders of magnitude larger than conventional systems because it exploits the entire length of the microchannel in a waveguide regime instead of the sample thickness. In this way, each microchannel becomes an optical mirrorless microcavity with a very small volume V of only a few cubic micrometers. This is highly desirable since it enhances the factor of spontaneous emission and severely reduces the threshold of laser emission.

A series of significant physical advantages yield from adopting this type of configuration: increase of the optical cavity length, very small modal volume per each resonant microcavity (providing also minimization of the optical losses), directional control of the lasing emission, wavelength tunability and control over the emission intensity.

This miniaturization process allows obtaining a micro-laser array possessing an ultralow lasing threshold (25nJ/pulse) where the single channel might be selectively tuned or switched off.

Experimental Setup and Preliminary Considerations

To accomplish the objective various suitable combinations of liquid crystal host, fluorescent guest molecules, alignment technique, and pumping conditions were considered. An initial important matter was to find a helixed material which presents a good spectral overlapping of its photonic stop band edge and the high efficiency region of the dye fluorescence spectrum. This is a fundamental element in obtaining our proposed goal. Also, it is desired that the wavelength of the maximum absorbtion peak of the dye matches the pump laser emission wavelength.

This peculiar attribute was met (after several attempts) by the BL088 liquid crystal (Merck) in the cholesteric phase and the Pyrromethene 597 dye (Exciton). The exact superposition of the red edge of the photonic stop band and the high efficiency region of the dye fluorescence spectrum was achieved by adding a small amount of BL001 (Merck) nematic liquid crystal. This procedure generates a small unwinding of the cholesteric helix, consequently producing a low-energy shift of the bandgap edge. However, this procedure slightly decreases the orientational order parameter of the system producing a reduced feedback mechanism and for this reason this method was ruled out.

The experimental setup used for optically pumping and characterizing the systems is depicted in Fig.3.17. The pump is represented by a frequency-doubled (532 nm) Nd:YAG (Neodimium doped: yttrium aluminium garnet) laser (New Wave, Tempest 20). The pump beam was focused onto the sample by means of a cylindrical lens (f = 100 mm). The emission spectra were aquired with a spectral resolution of about 2 nanometers using a multichannel charge-coupled device (Jobin-Yvon CP200).

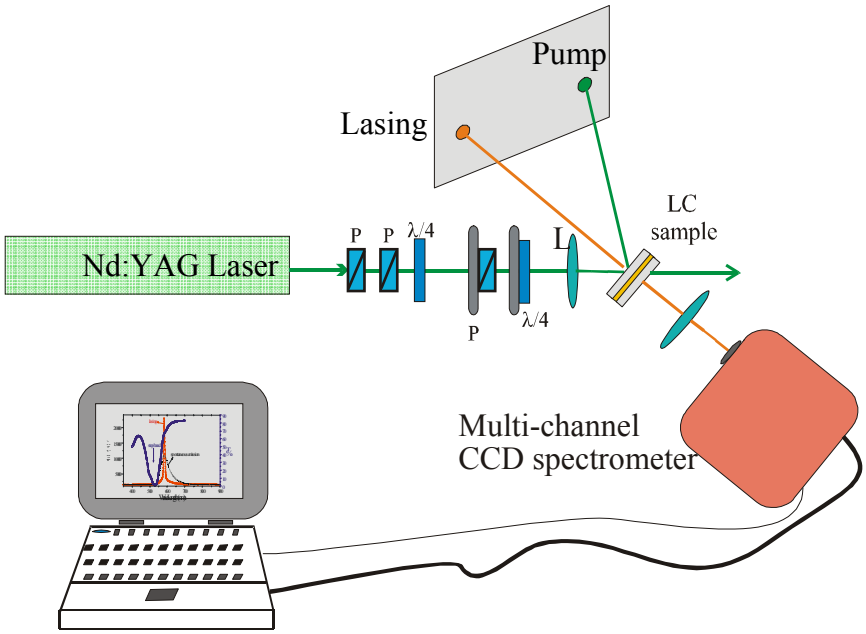

Fig.3.17. Experimental setup: the series of optical elements allows to select the state of polarization of the excitation pulses, and the emitted light is analyzed through a multi-channel CCD spectrometer.

The most interesting results were obtained by using a mixture containing 99.6 wt % of BL088 liquid crystal and 0.4 wt % of Pyrromethene dye. The mixture was confined between two indium tin oxide (ITO) parallel glass plates separated by 25 μm thick Mylar spacers.

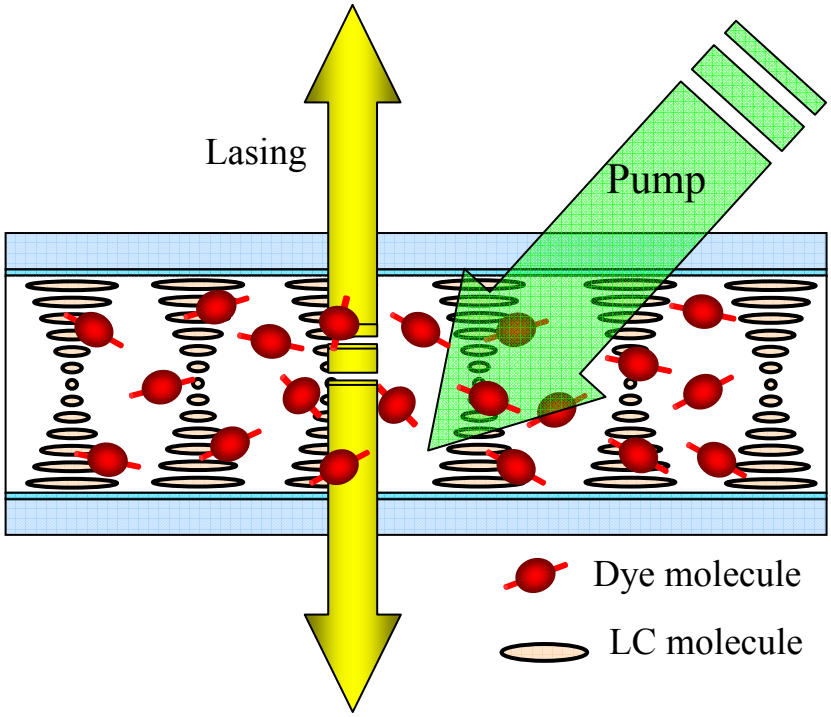

Fig.3.18. Diagram of Stimulated Emission process in a conventional cell.

The inner polyimide coated sides of the ITO glass give a planar alignment to the liquid crystal molecules inducing an orientation of the liquid crystal helical axis normal to the glass plates. The sample was optically pumped with 3 ns duration pulses, at a frequency of 10- 20 Hz, produced by the Nd:YAG laser (Fig.3.19).

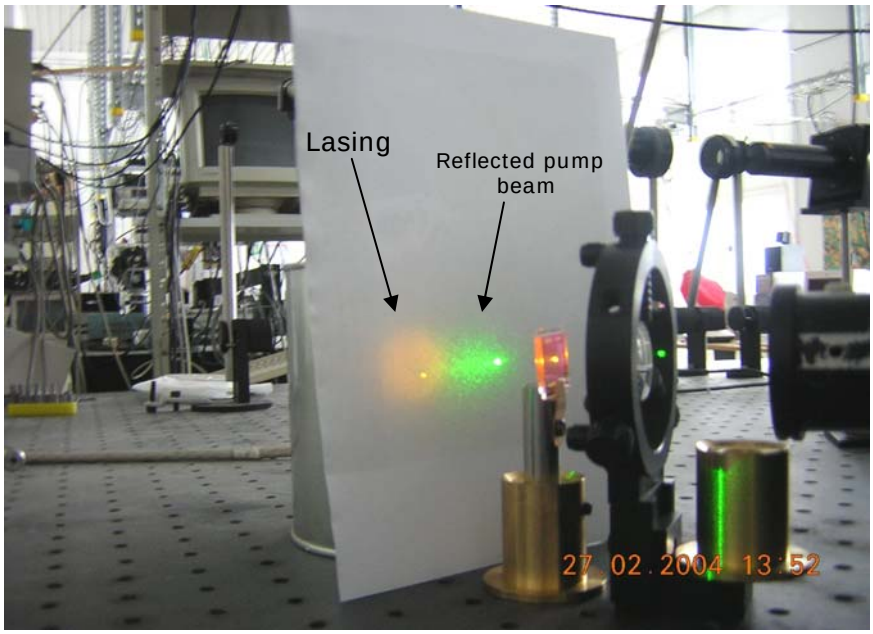

Fig.3.19. Digital photo illustrating the stimulated emission process in a conventional cell.

As expected, the photonic bandgap structure of the self organized chiral liquid crystal clearly modifies the fluorescence spectrum of the dye molecules: at low pump power a dip appears in the emission at the position of the stop band (Fig.3.20). By increasing the pump power above a certain limit, very intense stimulated emission radiation was obtained in a direction perpendicular to the ITO glass plates, along the helical structure (Fig.3.18). The lasing wavelength is about 580 nm and the reported FWHM is about 2 nm, limited by the resolution of the CCD spectrometer. Further investigations reveal a very stable system which presents an average lifetime for the gain medium of more than 6 months under normal pumping conditions.

The obtained results indicate the above mixture as the appropriate candidate for the principal stage of this study: to exploit the capabilities as optical microcavity of the novel polymeric configuration.

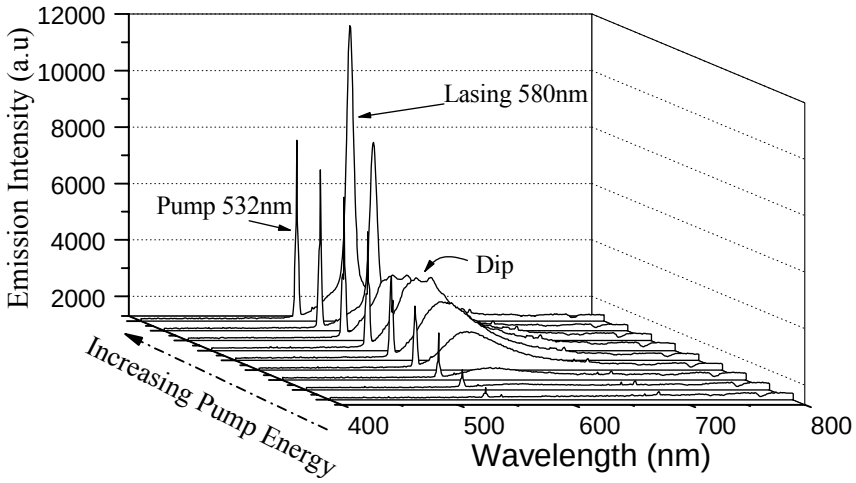

(a)

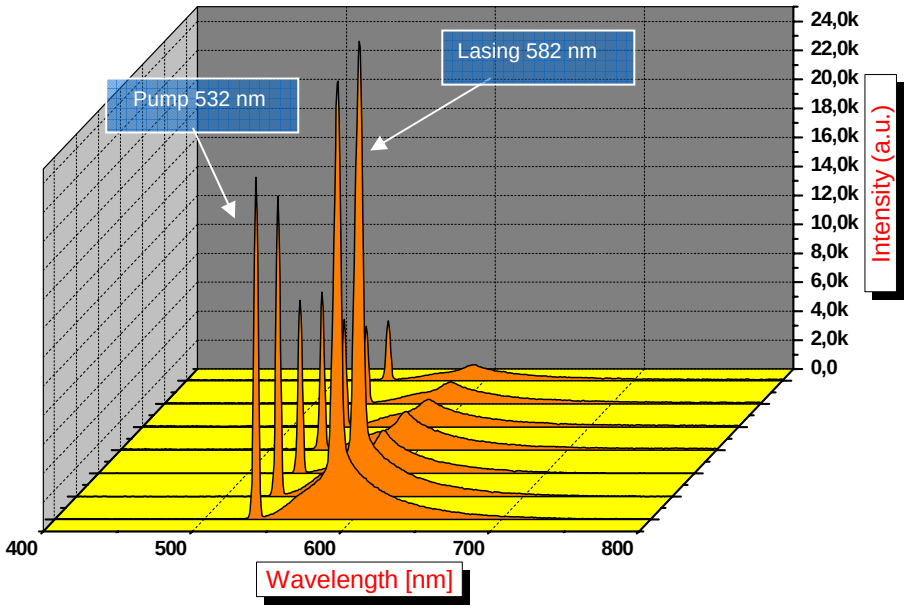

(b)

Fig.3.20.(a),(b) Emission Spectra as a function of the pump energy for a conventional cell.

Colour-Tunable Organic Microcavity Laser Array Using Distributed Feedback – Experimental Results

The engineered novel structure is known as PoLiCryPS (the abbreviation for POlymer LIquid CRYstal Polymeric Slides), the main difference with respect to the standard PoLiCryPS is the introduction of dye doped helixed liquid crystal material to create the PBG structure. Complete details regarding the fabrication process are present in several previous works [48,55].

Between two indium tin oxide (ITO) coated glass plates separated by 13.5 μm thick mylar spacers, we have confined a mixture of 29.9 wt%BL088 cholesteric liquid crystal (Merck), 69.3 wt% of NOA-61 monomer (Norland), 0.7 wt% of Irgacure 2100 and Darocur 1173 photoinitiators (1:1 wt%, Ciba Specialty Chemicals), and 0.09 wt%of Pyrromethene 597 dye (Exciton). The sample was then irradiated for approx. 17 min with the interference pattern produced by two UV laser beams (λ=351 nm, from an Innova-90C source, Coherent), at an intensity of 1.05 mW/cm^2 each. A series of side-by-side microchannels with a very sharp morphology was produced by a photopolymerization process which was locally induced by the sinusoidally modulated light intensity. The angle θ between the two interfering beams (~2º) was used to select a structure period Λ of 5 μm, according to the relation $\Lambda = \lambda/2\sin\theta$, where λ is the irradiation wavelength. However, this periodicity can range from 200 nm to some micrometers.

By means of a miniature oven (CaLCTec S.r.l.) it was possible to maintain the entire mixture at a fixed temperature (90 ºC), thus allowing the liquid-crystalline component to remain in the isotropic phase during the whole irradiation process. This approach increases the mass diffusion rate and prevents the formation of liquid crystal droplets encapsulated in the polymer as evidenced by the very low scattering exhibited by the sample. It is worth noting that the diffusion coefficient of the liquid crystal molecules is highly anisotropic due to their rodlike shape: diffusing from the polymer network, the molecules find an “easy way” aligning perpendicular to the polymeric walls. By slowly cooling the sample to room temperature (-0.5 ºCmin^{-1}) a self-organization process occurs owing to the isotropic-chiral liquid crystal phase transition. The system

tends to minimize its free energy by orienting the liquid crystal helices, on average, along the microchannels.

At the end of the whole process an almost complete phase separation was obtained, giving rise to helixed liquid crystal channels periodically separated by polymer walls.

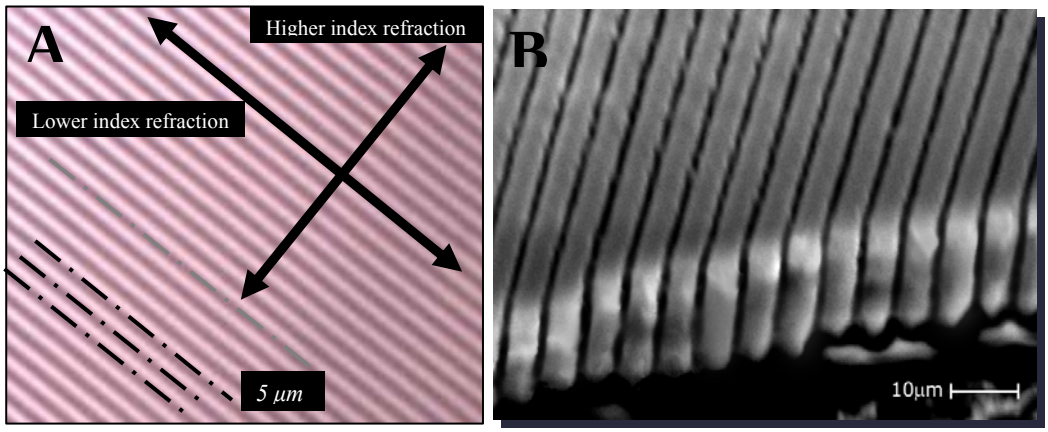

Fig.3.21. (a) Optical microscopy and (b) scanning electron microscopy images of the organic microcavity reveal a very well-defined morphology consisting in a string of side-by-side polymeric microchannels. Spatial periodicity of the structure of about 5 μm with the microcavity width of 1.5 μm.

A thorough structural analysis of the system was performed by using the optical (Fig.) and scanning electron microscopy (Fig.3.21) techniques. The study reveals a very welldefined morphology consisting in a string of side-by-side polymeric microchannels which act as optical microcavities by confining the active matrix of chiral liquid crystals doped with fluorescent guest molecules. The presented experimental results refer to a measured periodicity of the structure of about 5 μm with the microcavity width of 1.5 μm. A series of optical investigations (tilting compensator and photopolarimetry) confirmed the fact that the LC's helix orientation is along the polymeric channels.

This complex system was optically pumped with the second harmonic (532nm) of a Nd:YAG laser. The laser beam was focused onto the sample by means of a cylindrical

lens (f =100mm) which produces an elliptical profile (with a short axis of approximately 50 μm).

The long axis of the section was oriented perpendicularly to the orientation of the polymeric walls, therefore, the obtained profile (long axis of approx. 5 mm) assured the simultaneous excitation of multiple microchannels (Fig.3.22).

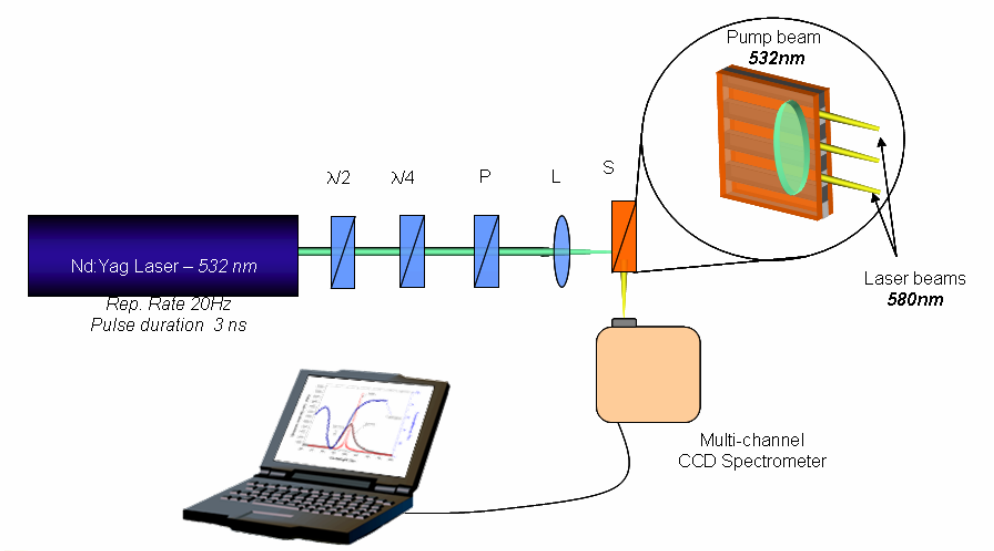

Fig.3.22. Experimental setup for Lasing in Policryps System.

Above a certain pump power, stimulated emission was achieved emerging from the microcavities in a direction parallel to the glass plates and along the microchannel structure. At this position highly sensitive spatial distribution emission measurements were performed in a restricted cone angle of about 0.1 rad. The sketch in figure 3.23 shows this lasing scenario of the micro-laser array. The stimulated emission emerging from the microchannels was circularly polarized demonstrating that the distributed feedback mechanism is behind the observed phenomenon. The LC microchannel behaves as a miniaturized mirrorless cavity laser, where the emitted laser light propagates in the waveguide defined by the chiroselective liquid-crystalline medium.

The spectral position of the lasing line (580 nm) was not importantly modified with respect to the conventional cell, indicating that the mixture, in particular the helix of the liquid crystal was slightly affected by the confinement process.

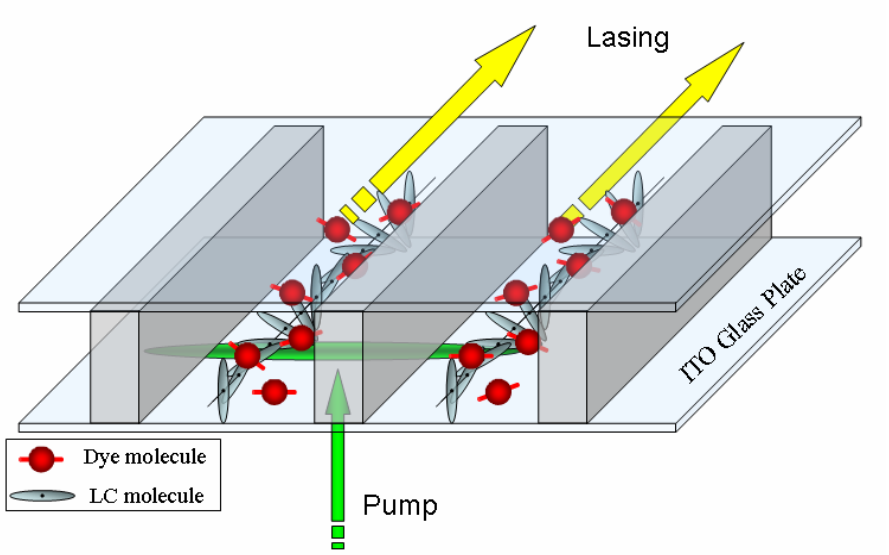

Fig. 3.23. 3D sketch describing the micro-laser array scenario. Highly directional and intense stimulated emission is achieved emerging from the microcavities in a direction parallel to the glass plates and along the microchannel structure.

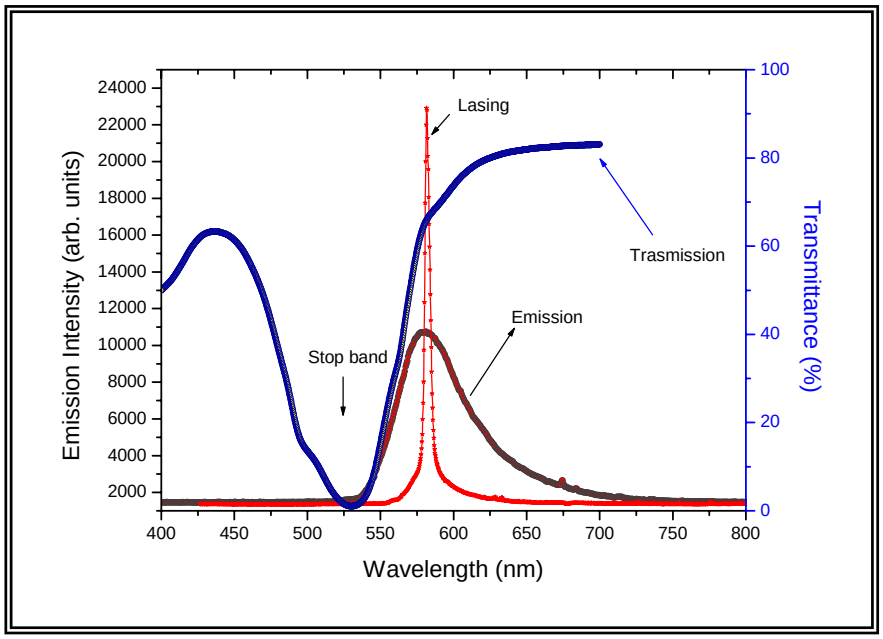

Fig.3.24. Transmission, fluorescence, and lasing spectra are reported. Highly directional laser action was observed along the microchannels within a limited cone angle (0.2 rad).

Lasing was obtained at red-edge of the photonic bandgap, where the photonic density of states is expected to diverge, the group velocity approaches zero and the resulting long dwell time of the emitted photons highly supports stimulated emission.
The lowest obtained FWHM of the lasing spectra was at the limit of our multi-channel charged coupled device (3 nm). One can also notice the remarkable spectral overlapping of the high efficiency of the dye fluorescence spectrum and the low energy edge of the stop band.
The photonic density of states ρ is defined as the inverse slope of the dispersion relation:

$$\rho = \left| \frac{d}{d\omega} \mathrm{Re}(K) \right| \qquad (3.19).$$

In an isotropic medium with refractive index n, the DOS is $\rho_{iso} = n/c$, where c is the speed of light in vacuo. By considering a birefringent chiral liquid crystal confined in long microcavities (LMC) where effects due to multiple reflections at the interfaces can be neglected, the DOS are calculated as follows:

$$\underset{R}{\overset{LMC}{\rho}} = \frac{1}{p}\left(\frac{d\tilde{k}}{d\tilde{\lambda}} \frac{d\tilde{\lambda}}{d\omega} \right) \qquad (3.20)$$

where $\tilde{\lambda} = \lambda / n_{avg} * p$, $\tilde{k} = kp$.

By deriving the quantities on the right-hand side of Eq. 3.20 and by inserting the relative dielectric anisotropy α and the reduced index of refraction $\tilde{n}$,

$$\tilde{n} = 1 + \tilde{\lambda}^2 - \left(4\tilde{\lambda}^2 + \alpha^2 \right)^{1/2} \qquad (3.21)$$

one finally obtains the DOS:

$$\rho_R^{LMC} = \frac{n_{avg}\tilde{n}}{c} - \frac{n_{avg}\tilde{\lambda}^2}{\tilde{n}c}\left(1 - \frac{2}{\sqrt{4\tilde{\lambda}^2 + \alpha^2}}\right) \qquad (3.22).$$

The calculated DOS diverges as the edges of the PBG is approached, matching very well with the experimental spectral position of the lasing emission in microcavities. Figure shows the graphic for the calculated density of states (DOS) function of our right handed chiral liquid crystals in the case of long microcavity (LMC) confinement, where one can ignore the multiple reflections at the boundary interfaces.

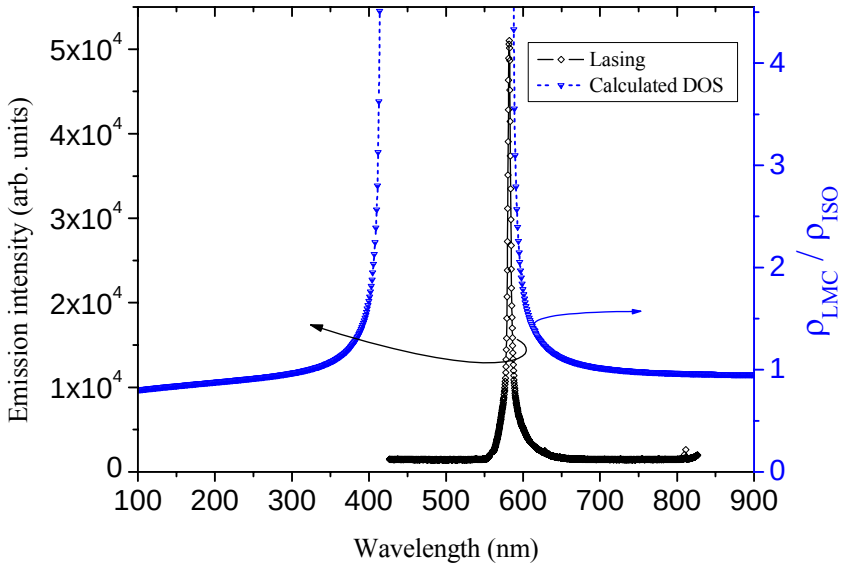

Fig.3.25. The calculated DOS are reported together with the band edge lasing emission.

The dependence of the emission intensity and spectral linewidth (FWHM) on the input pump energy are reported in figure 3.26. At low excitation energies, both the emission intensity and the linewidth show a quasi linear dependence as function of the pump energy. Above a characteristic threshold, the pump energy per excited sample area was about 5 mJ/cm^2 which corresponds to about 25 nJ/pulse, the emission intensity suddenly starts to increase nonlinearly.

Also, above this energetic pump limit, the emission linewidth break off from the previous tendency and begins to significantly decrease.

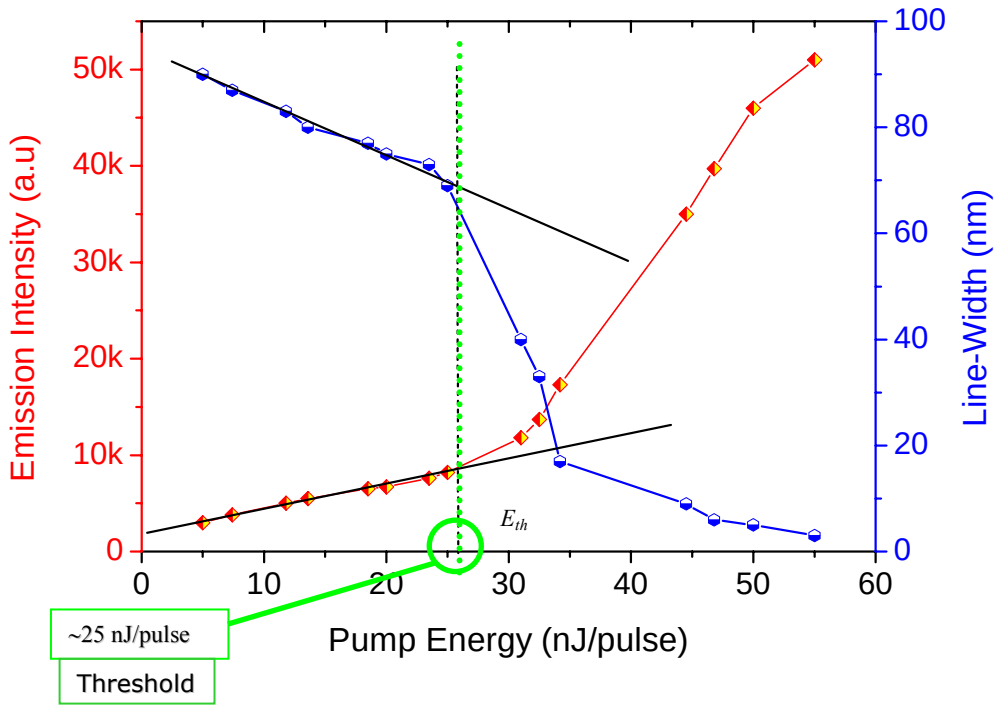

Fig.3.26. Emission intensity and line-width dependence on the pump energy. Above a threshold of 25nJ/pulse the reported curves change from initial regimes while lasing occurs.

The observed pump energy value for which the explosion and narrowing effects occur (25 nJ/pulse) is an order of magnitude lower than in the case of other conventional dye doped systems in a similar environment and under the same pumping conditions.

Polarized fluorescence measurements put into evidence a strong dependence of the emission intensity (spontaneous emission) on the pump polarization, as it shown in the polar plot of figure 3.27. By maintaining the pump energy fixed, a four fold increase in the spontaneous emission intensity was recorded by rotating a linear state of polarization from parallel to the microchannels (0 deg) up to a perpendicular one (90

deg) and by analyzing the emitted light along the direction of the excitation polarization.

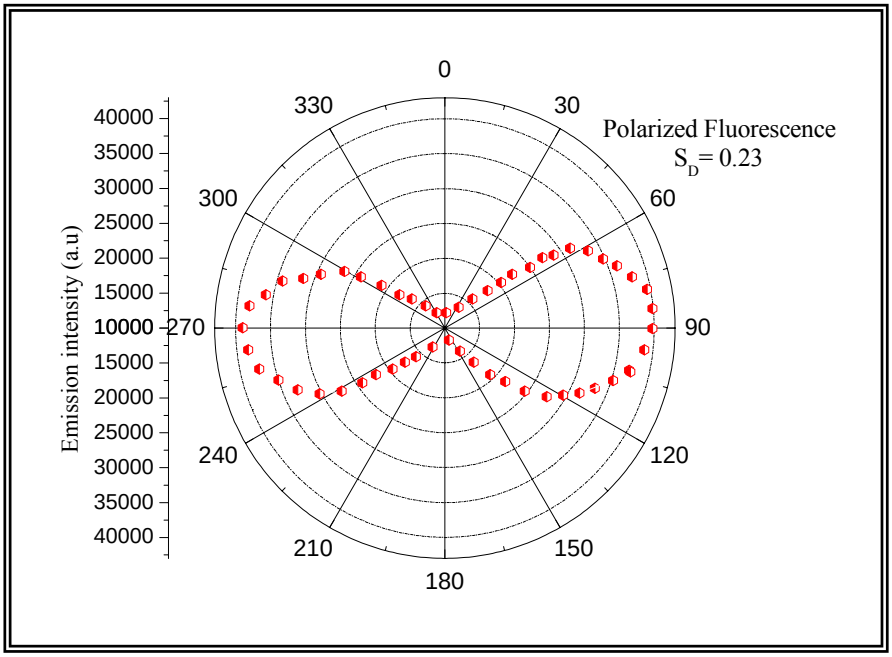

Fig.3.27. Polarized fluorescence measurements suggest an anisotropic orientational distribution for the dye transition dipole moments. Calculated order parameter value is SD=0.23.

This suggests that the PM 597 dye molecules possess an anisotropic orientational distribution of the transition dipole moments because of the strongly anisotropic environment in which has been dissolved, with a dye order parameter S_D = 0.23 calculated as follows [56]:

$$S_D = \frac{\left(\frac{F_\perp}{F_{//}}\right)^{1/2} - 1}{\left(\frac{F_\perp}{F_{//}}\right)^{1/2} + 2} \qquad (3.23)$$

where $F_{//}$ and $F_{\perp}$ are fluorescence intensities polarized parallel and perpendicular with respect to the microchannel polymeric walls.

The most interesting aspect of this lasing system is that optical and geometrical parameters can be modified by applying weak external fields (temperature, electric field, mechanical stress, and optical field), resulting in a direct control of lasing features (wavelength, bandwidth, and emission intensity). These properties were found to be fully reversible.

By means of a miniature oven (CaLCTec S.r.l.) we changing the system's temperature value from 25 °C up to 80 °C allowing to obtain a fine-tuning of the laser emission wavelength. An average red-shift of 0.2 nm/°C was recorded in the spectral range 580-590 nm. It is demonstrated that the period of the chiral liquid crystal, the pitch p, changes with temperature variations [50], in this case, producing a red shift of the stop band edge where lasing is expected.

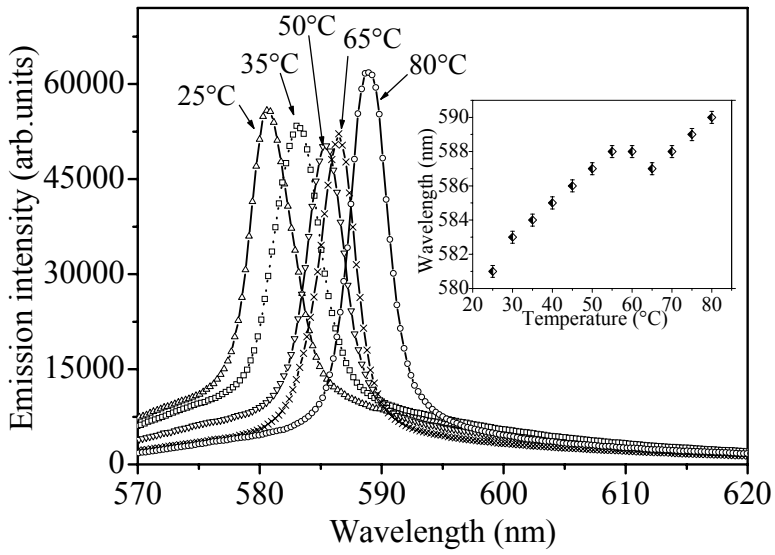

Fig.3.28. Stimulated emission spectra as function of temperature. A fine tuning (0.2 nm/°C) of the lasing wavelength is achieved for the spectral range 580-590 nm. The inset shows the lasing wavelength dependence on temperature.

The experimental evidence definitely proves that the distributed feedback mechanism, provided by the dielectric tensor modulation of the helixed liquid crystal, is behind the observed effect. The inset of Fig.3.28 shows the quasi linear dependence of the lasing wavelength on temperature. The peculiar behaviour around 60 °C is attributed to a sudden unwind of the helical superstructure, a discharge of the surplus elastic energy accumulated upon increasing the temperature.

A very interesting feature of the presented system is the possibility to control the stimulated emission intensity by applying an electric field (Fig.3.29). A sinusoidal voltage (1 kHz) was applied to the sample between the two glass-ITO plates. By maintaining fixed the pump energy and by varying the voltage from 0 up to $50V_{RMS}$ a significant decrease of the lasing intensity was observed. In addition, above a given field threshold the micro-laser switches off.

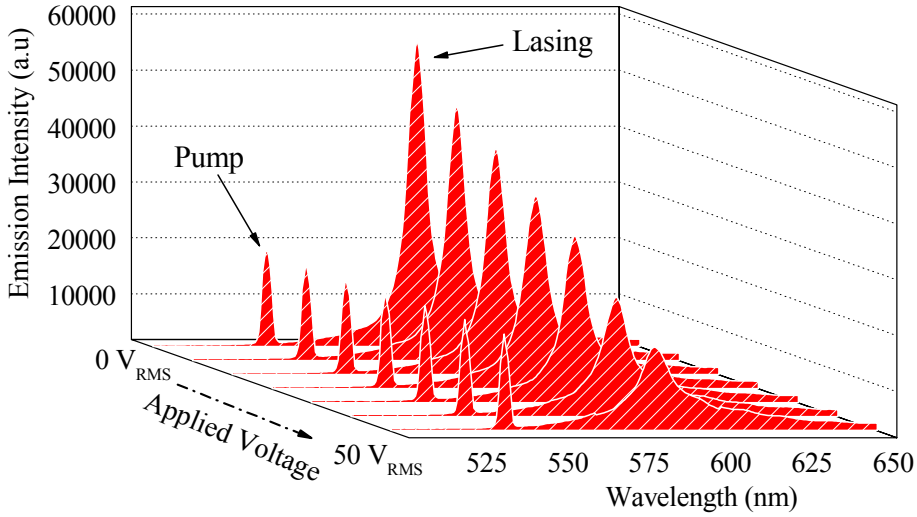

Fig.3.29. Lasing emission intensity dependence on the applied voltage. While keeping a fixed pump energy a four fold lowering of the stimulated emission intensity is achieved by applying an external voltage in the range 0 - 50 V_{RMS}.

Taking into account that the BL088 chiral liquid crystal possesses a positive dielectric anisotropy, the applied electric field perpendicular to the helical axis produces a local

distortion of the periodic structure. Liquid crystal molecules tend to align along the electric field producing modifications in the sinusoidal modulation of the refractive index which assumes a low efficiency rectangular profile [57,58]. The overall result is a diminishing of the DFB mechanism, therefore a decrease in the lasing intensity is observed.

By further increasing the field, the regions where the molecules are energetically favorably oriented (locally nematic) keep expanding until a certain threshold value is reached and the chiral helix completely unwinds and the structure becomes nematic. The critical electric field Ec for this transition is:

$$E_c = \frac{2\pi^{5/2}}{P_0}\left(\frac{K_2}{\varepsilon_a}\right)^{1/2} \tag{3.24}$$

where K_2 is the Frank's twist elastic modulus, ε_a is the dielectric anisotropy and P_0 is the unperturbed chiral pitch. The estimated critical field results several timed larger than the electric field applied at the presented system. Therefore, by working in a low field regime the slight helical distortion is sufficient to greatly reduce the optical feedback process.

A striking scenario is presented in figure 3.30 showing the spatial distribution of the laser emission emerging from the microcavity laser array. A high sensitivity and resolution (1390 X 1024 12bit PixelFlyQe by PCO) imaging CCD camera was employed in order to check the near-field modal profile for the stimulated emission. The images were acquired by scanning in the proximity of the output edge of our sample cell, in a direction perpendicular to the micro channels. The mapped intensities profile hereby obtained indicates that the maxima lasing intensities have a spatial recurrence. The periodicity of the organic micro-laser array is found to be about 5 μm, this value being in perfect agreement with the initial tailoring configuration (i.e. the distance between the polymeric walls).

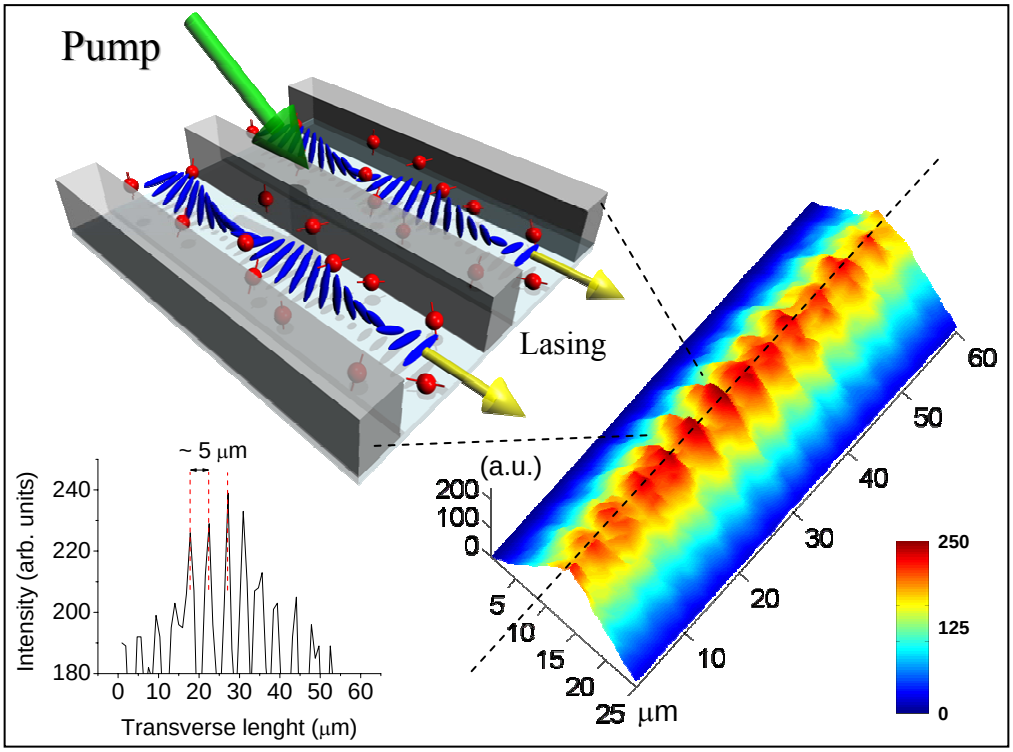

Fig.3.30. Spatial distribution of the laser emission emerging from the mirrorless microcavity laser array. The periodicity of maximum intensities is 5 μm. This value is consistent with the tailoring distance between the polymeric microchannels.

The LC microchannels act as miniaturized mirror-less cavity lasers, where the emitted laser light propagates along the liquid crystal helical axis behaving as Bragg resonator.

In addition, by considering a single channel emission intensity profile chart (Fig.3.31) and transposing it into the two main directions, transverse (X) and longitudinal (Y), we obtained that each single resonant mode have an elliptic Gaussian beam profile. The calculated ellipticity is about 7.

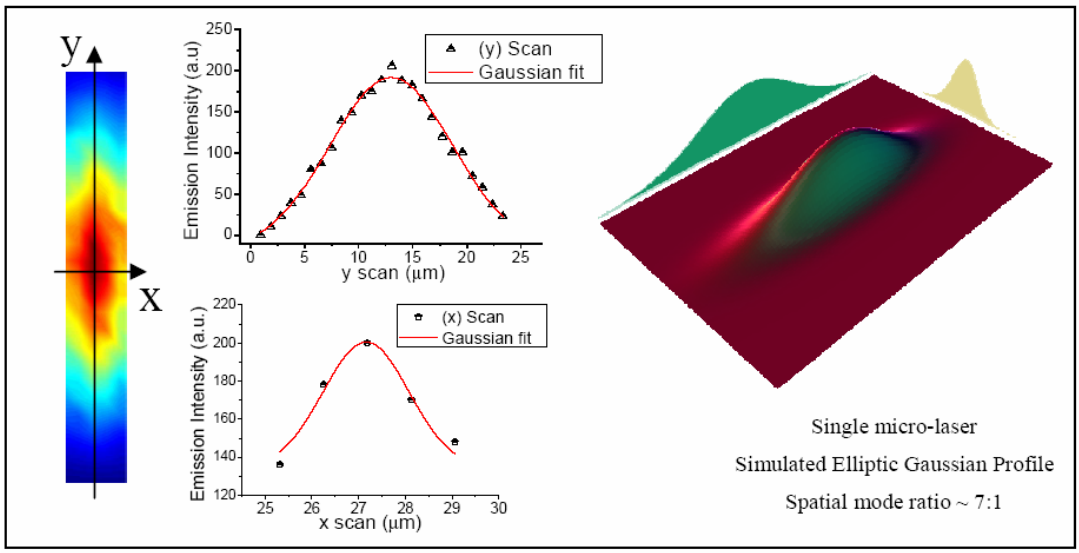

Fig.3.31. The intensity profile of a selected spatial mode of the laser array. The longitudinal and transversal intensity scan is fitted with a Gaussian curve. The simulated intensity profile for the presented astigmatic cavities shows an elliptic Gaussian profile revealing a remarkable agreement with the emitted spatial modes.

The microlasers of the array are intrinsically phase locked because they are simultaneously stimulated by the same laser pump. Furthermore, tailoring a proper array of electrodes which enables the application of a local electric field would give rise to electrically programmable phase holograms with interesting light polarization properties.

Conclusions & Remarks

An ultralow-threshold colour-tunable microlaser array was created by embedding dye-doped helixed liquid crystals in holographically sculptured polymeric microchannels (Policryps). The unique optical and electrical properties of chiral liquid crystals play a determining role in the mirror-less cavity limited by polymeric walls. The laser action was observed at the low energy edge of the bandgap where a sharp increase of the photonic density of states (DOS) is expected. In fact, the calculated DOS was found to

diverge at the spectral position where lasing was observed and the emitted light was circularly polarized corroborating the idea that distributed feedback is behind the presented lasing effect. The investigation of the spatial distribution of the emitted light shows a laser array where each microchannel acts as an astigmatic resonant cavity producing an elliptic Gaussian beam. This level of integration might lead to new photonic chip architectures and devices, such as zero-threshold microlaser, phased array, discrete cavity solitons, filters, and routers.

3.10.2. Band Edge and Defect Modes Lasing Due to Confinement of Helixed Liquid Crystals in Cylindrical Microcavities

Overview

In this chapter it is presented the study of the light emission properties from novel fiber-like cylindrical microcavities hosting helixed liquid crystals doped with fluorescent guest molecules.

The level of confinement ensures an increase of the axial resonant cavity length, while maintaining a small modal volume.

Cylindrical geometry favors the existence of a very complex structure of the chiral liquid crystal as evidenced by optical and structural investigations. The long-range periodicity guarantees the enhancement of distributed feedback mechanism which is behind the observed axial and radial low-threshold tunable lasing action. The aim of this study was to gain understandings about the role played by the number of helical periods, the influence of the CLC bulk volume and various surface treatments on the quality factor of the periodic mirrorless resonant system. This level of confinement allows obtaining interesting emission properties: laser action is exhibited both in the axial and radial directions at different spectral positions indicating that waveguide effects are not responsible of the multidirectional emission.

A striking point is represented by the spontaneous reconstruction of the helixed liquid crystal superstructural configuration inside the cylindrical microcavity, giving rise to a novel three dimensional (3D) multidirectional lasing system. By analogy to the nematic LC phase, a model is proposed for this cylindrical geometry where the axial orientation of the helix is preponderant close to the boundary substrates, while in the bulk region the radial configuration is preferred.

This complex system keeps the advantage of a 3D blue phase-like matrix while providing a wider thermal operating range and laser action wavelength tenability [46].

Experimental Results

The hosting cylindrical microcavities are represented by capillary glass tubes with various diameter values ranging from 15 up to 200 μm. Several chemical treatments were applied to the inner surface of the cylindrical microcavities in order to induce a privileged molecular alignment for the liquid crystal. These include mixtures of DMOAP (0.1% wt N,N-dimethyl-N-octadecyl-3-aminopropyltrimethoxysilyl chloride in isopropanol), orthochromic mixture (20% wt $K_2Cr_2O_7$ in H_2SO_4), ACM72 (0.1% wt in water), lecityne and polyimide which were used in different concentrations to induce axial alignment of the chiral liquid crystal helix in the proximity of the boundary surface (i.e., the helical structure is oriented parallel to the cylindrical main axis). Experimental investigations show that polyimide treated cylindrical capillary tubes provide the strongest surface-liquid crystal interaction and alignment for the liquid crystal.

The micro tubes were filled by capillarity with a mixture (*M*1) of 99.7 wt % BL094 right handed cholesteric liquid crystal (Merck) and 0.3 wt % of PM597 Pyrromethene dye (Exciton). The confined cholesteric liquid crystal had a birefringence Δn=0.21 and showed an optical bandgap which spans from 525 to 585 nm. The high efficiency region of the dye fluorescence spectrum and the red-edge stop band of BL094 present very close spectral positions (580 and 585 nm) which maximizes the gain in the case of stimulated emission.

Since this spectral overlapping could present the inconvenient of confusing the eventual amplified spontaneous emission effect with laser action, a second mixture (*M*2) was prepared by adding a small percentage of BL001 nematic liquid crystal (Merck). As a result, the low-energy band edge redshifted to 607 nm.

The cylindrical microcavity was optically pumped (Fig.3.32) with 3 ns pulses produced by a frequency-doubled (532 nm) Nd YAG: yttrium-aluminum-garnet laser (NewWave, Tempest 20). The pump beam was focused by means of a spherical lens (*f* =100 mm) perpendicular to the axial sample direction. The experimental setup is presented in figure 3.33.

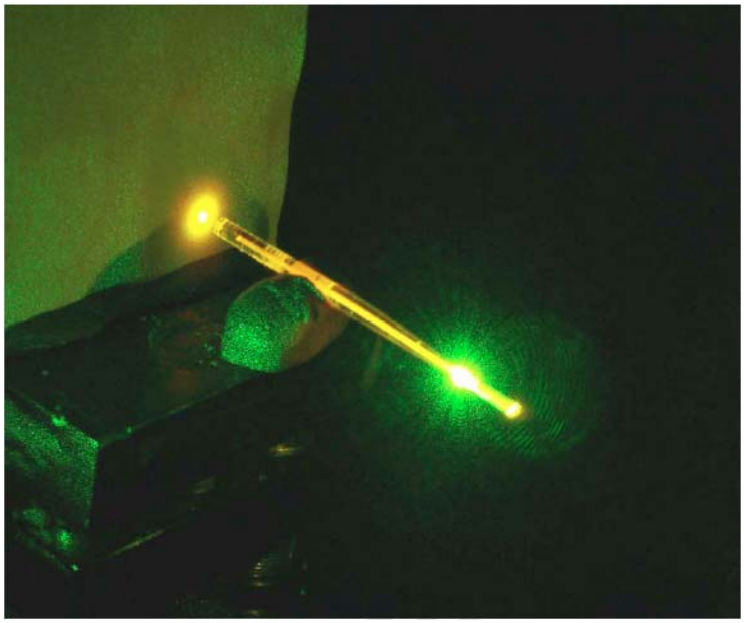

Fig.3.32. Lasing action from optically pumped (532nm) cylindrical microcavity. Intense highly directional axial stimulated emission (at 587 nm) is observed on the background screen.

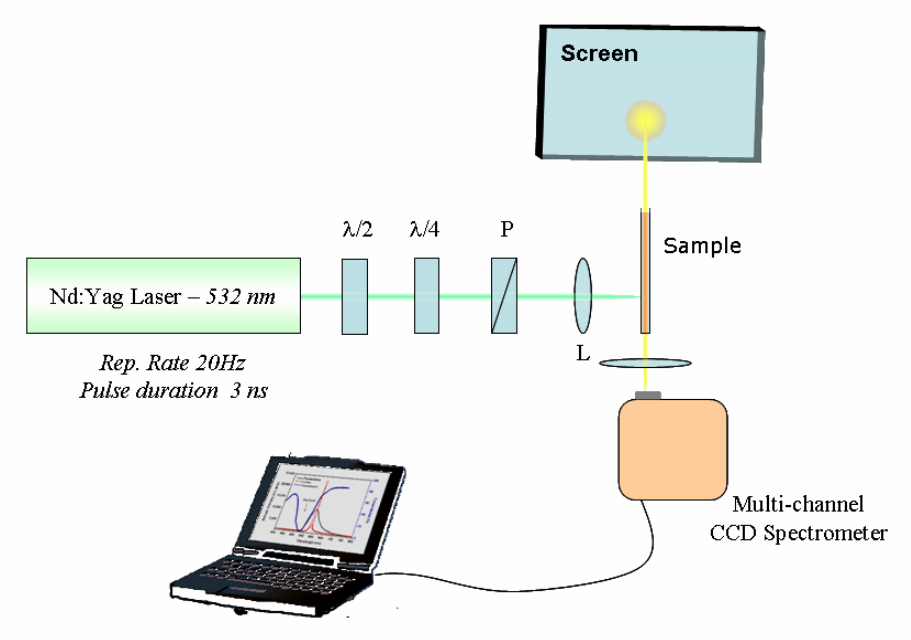

Fig.3.33. Experimental setup line.

The radial and axial emission were collected within a restricted cone angle of 0.2 rad by using a multichannel charge-coupled device (CCD) (Jobin-Yvon, Micro-HR).

The PBG structure of the self-organized liquid crystal material severely modified the fluorescence spectrum of the laser dye molecules: at low pump energies a dip in the spontaneous emission spectra occurred at the position of the stop band.
By increasing the pump energy above a certain threshold value, a highly directional laser action was observed at the red edge of the stop band both axially and radially. The laser emissions were found to be circularly polarized, which indicates that distributed feedback mechanisms take place through circular Bragg reflection.

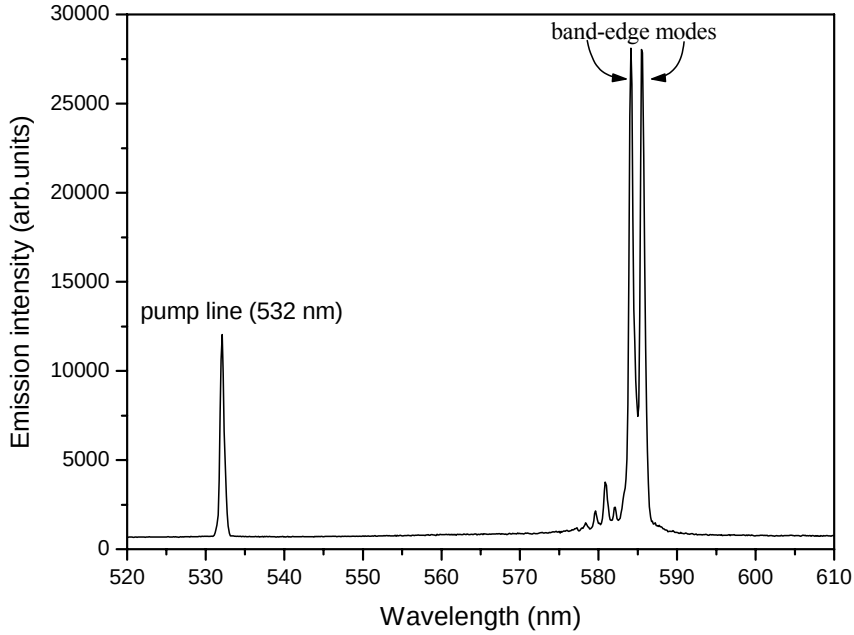

Fig.3.34. Stimulated emission spectrum depicting axial lasing of dye-doped CLC confined in microcylindrical cavity.

The LC microcylinder acts like a miniaturized mirrorless cavity laser, where the emitted laser light propagates along the liquid crystal helical axis which behaves as a Bragg resonator.

Recorded radial and axial lasing spectra present slightly different wavelength positions and linewidths full width at half maximum (Fig.3.35). The displayed lasing lines have a spectral position which correspond to the low-energy edge of the PBG and exhibit a very narrow stimulated emission peak of only 0.5 nm (limited by the resolution of the CCD spectrometer). The lowest measured lasing threshold was 250 nJ/ pulse for the radial direction and 500 nJ/ pulse for the axial one.

We experimentally found that the ratio r / p, with r as the internal radius of the cylinder and p as the pitch of the chiral liquid crystal, is the parameter which controls the arrangement of the helical superstructure. Low pump energy simultaneous radial and axial lasing indeed occurs when r / p < 50, indicating that the interplay of the strong boundary conditions and the symmetry of the microcavity is responsible for the observed effect. In fact, the length ξ over which extends the influence of the surface depends on the inner alignment layer, and generally is about 1 μm which corresponds to a few pitch lengths. Therefore, the competition between the double-twist

arrangement of the bulk region and the axial organization of the surface region finds a balance position for low *r* / *p* ratio.

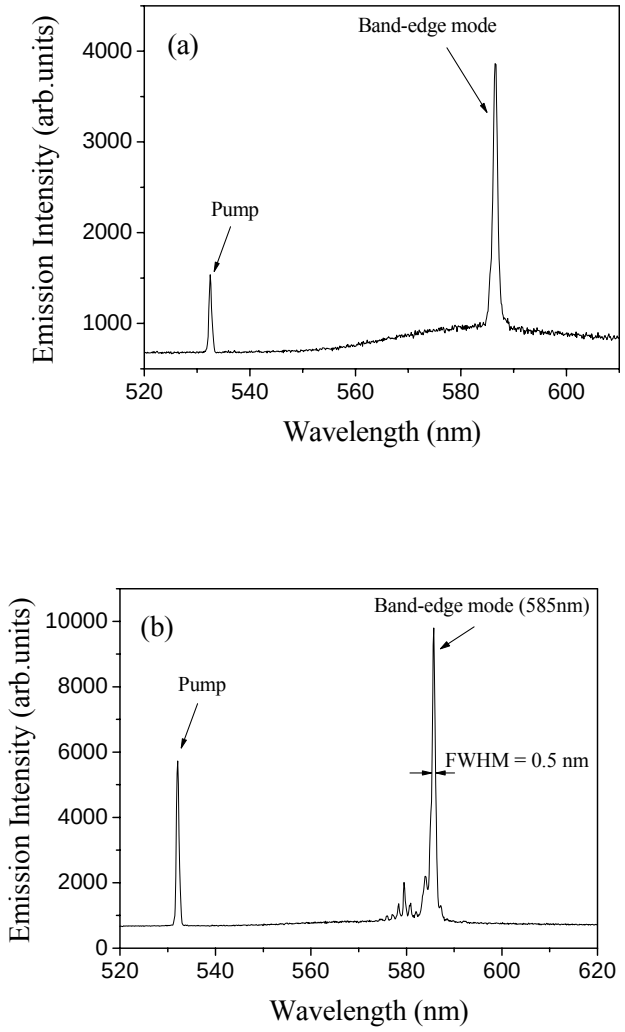

Fig.3.35. Axial (a) and radial (b) lasing spectra for a microcylinder with r/p ≈250.

In addition to the expected band edge lasing modes, lowthreshold defect lasing modes which occur within the selective reflection band gap have been observed (Fig.3.36). Defect mode laser action has been previously mentioned in layered chiral liquid crystal polymer networks as a consequence of the induced phase jump in the optical field or dislocations, being responsible for opening spectrally narrow transmission modes within the stop band. Lasing is facilitated at these wavelengths since the photon dwell

time is enhanced, giving ample opportunity for amplification by stimulated emission since the excitation energy will not be drained by spontaneous emission into modes other than the lasing mode, as predicted by Kopp [59] and Yablonovitch [12]. In the case of the presented cylindrical microstructure, the spontaneous rearrangement of the local director fields produces particular helical axis configurations which spans from planar (axial) to escaped twisted radial geometry. This structural organization materializes in the appearance of point defect modes [60]. The local alteration of the sample which disrupts the periodicity of the structure leads to long-lived and, hence, spectrally narrow laser defect modes within the gap, observed both axially (Fig.3.36a) and radially (Fig.3.36b). It is worth to notice that lasing wavelength on axial and radial defect modes are slightly different, since the resonant wavelength for the defect mode depends on the total phase slip which is given by the twist defect characteristics. Hence, the resonant wavelength undergoes important shift within the entire band gap by slightly changing either the defect layer thickness or the helical phase jump of the twist defect.

An important feature of the system is represented by the possibility of temperature tuning process of the lasing wavelength for the band edge modes. This effect is completely reversible. The period of the helix increases by increasing the temperature, producing an overall displacement of the spectral region where the circular Bragg reflection takes place.10 As a result of the thermal elongation of the pitch, a shifting of the stop band edge where the laser action occurs is obtained. Experimental measurements emphasize two different trends for lasing wavelength peak position in function of temperature for the radial and axial situations. A continuous temperature tuning of the lasing wavelength was obtained in the interval 585–595 nm by varying the temperature from 25 up to 50 °C (Fig.3.37a). We recorded a linear increase of 0.3 nm/ °C for axial and 0.45 nm/ °C for radial stimulated emissions (Fig.3.37b).

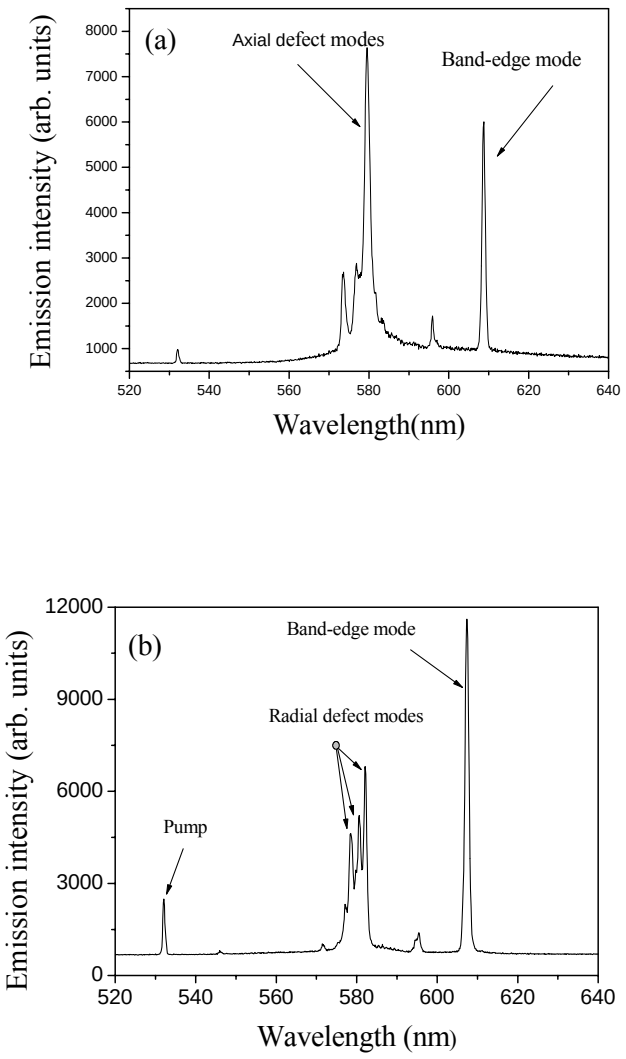

Fig.3.36. Axially (a) and radially (b) spectrally narrow laser defect modes are present within the band gap central region. M2 mixture is used, thus the lasing action occurs at 609 and 607 nm for axially and radially recorded stimulated emissions, respectively. microcylinder with r/p ≈50.

This dependence indicates that the axially oriented helical superstructure responds in a reduced way to an applied temperature gradient, with respect to the radial oriented helix. This different behaviour is strongly related to the confinement, in other words the interfacial region offers a much stronger constraint at the helical superstructure than the free bulk region. Belyakov theoretically investigated the cholesteric pitch

changing under the action of external perturbation, in particular which has been shown the strong dependence of the anchoring energy on the structural behaviour leading to a different response of the helical superstructure for interfacial and bulk regions of the cholesterics [61].

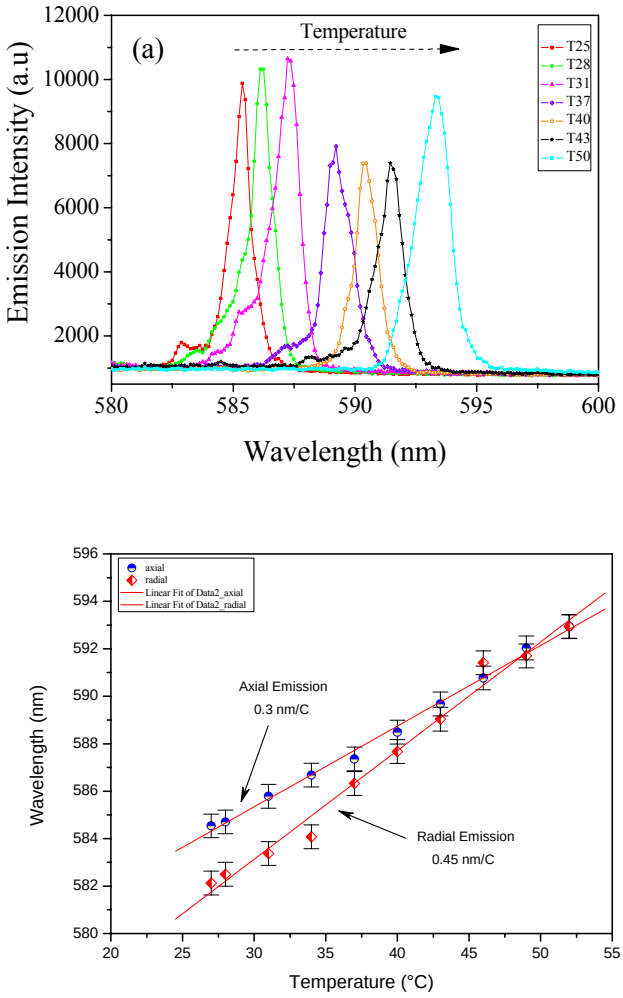

Fig.3.37. Temperature control of the lasing wavelength in self-organized helical mesophases confined in cylindrical microresonators. (a) A redshift of 0.3 nm/ °C for axial and 0.45 nm/ °C for radial stimulated emissions were recorded by increasing the temperature from 25 up to 50 °C resulting in a fine tuning of the lasing action. (b) The different temperature dependence of the wavelength for the axial and radial stimulated emissions suggests the presence of two discrete DFB Bragg resonators.

By analogy to the nematic LC phase, taking into account the experimental evidences, we suggest a model for this confined cylindrical LC configuration (Fig.3.38). Owing to

the surface treatments we propose preponderant orientation of the helical axis along the cylinder axis in the proximity of the boundary substrate, while in the bulk region the radial configuration is preferred. These two domains are connected through a narrow defect layer which ensures the passage from axial to radial helices alignment. This layer can be responsible for the observed lasing defect modes.

In the bulk region, because of the double-twist effect, a core interlinking zone has to be considered. Here, the local director is oriented along the cylindrical main axis, having a nematic-like structural configuration (see Fig.3.38). This model is in good agreement with the experimental observations, explaining the existence of the two main DFB resonant configurations (axial and radial) and the presence of the defect modes lasing spectra within the stop band.

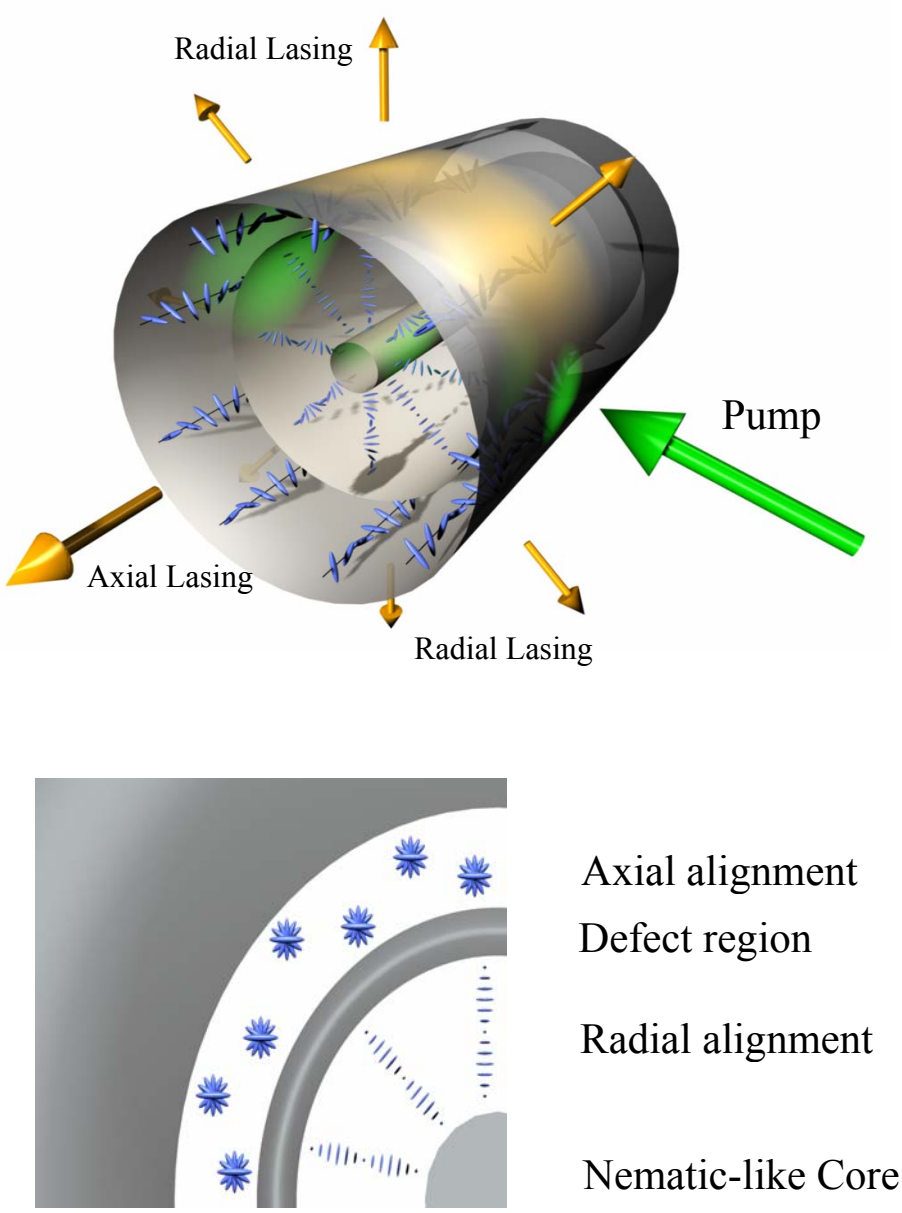

Fig.3.38. Schematic of the chiral LC configuration inside the microcylinder. Axial organization of the helical structure in proximity of the boundary substrate is suggested, while in the bulk region a radial orientation is preponderant. The bulk organisation implies a double twist configuration together with a nematic-like order for the core region.

Conclusions

The confinement of dye doped helixed liquid crystal in cylindrical microcavities gives rise to a 3D periodical superstructure where the two naturally preferred helical directions (axial and radial) create spontaneously. Low-threshold highly directional laser action was demonstrated both radially and axially. Along with the expected band edge mode we report the existence of long-lived spectrally narrow laser defect modes within the central region of the stop band. The defect modes are due to local dislocations of the chiral structure which yields optical phase jumps and weak light localization effects. Fine temperature tuning of the stimulated emission wavelength was achieved for both lasing situations. Experimental evidences suggest the existence of two main DFB resonant configurations (axial and radial) which are behind the demonstrated temperature tunable multidirectional (3D) lasing system. Novel photonic architectures and optical devices could be engineered by using this level of confinement of periodic and quasiperiodic photonic crystals.

References

[1]. E. M. Purcell, Phys. Rev. 69, 681 (1946).

[2]. M. Born and E. Wolf, Principles of optics. Electromagnetic theory of propagation, interference and diffraction of light, Cambridge University Press, Cambridge, (1999).

[3]. R. W. James, The Optical Principles of the Diffraction of X-Rays, G. Bell & Sons, London, (1954).

[4]. A. Yariv and P. Yeh, Optical Waves in Crystals: Propagation and Control of Laser Radiation, JohnWiley & Sons, New York, (1983).

[5]. K. Ohtaka, Phys. Rev. B 19, 5057 (1979).

[6]. P. St. J. Russell, Phys. B 39, 231 (1986).

[7]. P. St. J. Russell, , Physics World 5, 37 (1992).

[8]. P. St. J. Russell, T. A. Birks, and F. D. Lloyd-Lucas, Confined Electrons and Photons, edited by E. Burstein and C.Weisbuch, Plenum, New York, (1995).

[9]. J. D. Joannopoulos, R. D. Meade and J. N.Winn, Photonic Crystals: Moulding the Flow of Light, Princeton University Press, Princeton, NJ, (1995).

[10]. S. Spillane, T. J. Kippenberg and K. J. Vahala, "Ultralow-threshold Raman laser using a spherical dielectric microcavity," Nature 415, 621 (2002).

[11]. O. Painter, R. K. Lee, A. Scherer, A. Yariv, J. D. O'Brien, P. D. Dapkus and I. Kim, Science 284, 1819 (1999).

[12]. E. Yablonovitch, Phys. Rev. Lett. 58, 2059 (1987).

[13]. S. John, Phys. Rev. Lett. 58, 2486 (1987).

[14]. D. Kleppner, Phys. Rev. Lett. 47, 233 (1981).

[15]. D. Wiersma, Nature, 406, 132 (2000).

[16]. J. S. Foresi, P. R. Villeneuve, J. Ferrera, E. R. Thoen, G. Steinmeyer, S. Fan, J. D. Joannopoulos, L. C. Kimerling, H. I. Smith, and E. P. Ippen, Nature Lett. 390, 143 (1997).

[17]. H. Finkelmann, S. T. Kim, A. Munoz, P. Palffy-Muhoray, and B. Taheri, Adv. Mater., 1069 (2001).

[18]. J. Schmidtke, W. Stille, H. Finkelmann, and S. T. Kim, Adv. Mater., 746 (2002).

[19]. W. L. Vos, R. Sprik, A. van Blaaderen, A. Imhof, A. Lagendijk, and G. H. Wegdam, Phys. Rev. B 53, 16231 (1996).

[20]. W. L. Vos, M. Megens, C. M. van Kats, and P. B¨osecke, J. Phys.-Condens. Matter 8, 9503 (1996).

[21]. M.C. Mauguin, Bulletin de la Societe Francaise de Mineralogie et de cristallographie, 34 (1911).

[22]. H. de Vries, Acta Crystallographica 4, 219 (1951).

[23]. S. Chandrasekhar, Liquid Crystals, Cambridge University Press, Cambridge, (1977).

[24]. R. Dreher, G. Meier, A. Saupe, Mol. Cryst. and Liq. Cryst. 13, 17 (1971).

[25]. C. Elachi, C. Yeh, JOSA 63, 840 (1973).

[26]. K. J. Vahala, Nature, 424, (2003).

[27]. H. Kogelnik and C. V. Shank, Appl. Phys. Lett. 18, 152 (1971).

[28]. L. S. Goldberg, J. M. Schnur, U.S. Patent No. 3,771,065 (1973).

[29]. I.P. Il'chishin, E.A. Tikhonov, V.G. Tishchenko, M.T. Shpak, JETP Letters 32, 27 (1981).

[30]. U. Brackmann, Laser Dyes Book, Lambda Physik, Germany, (2000).

[31]. E. Fermi, Rev. Mod. Phys. 32, 87-132 (1932).

[32]. D. J. Heinzen, J. J. Childs, J. E. Thomas, and M. S. Feld, Phys. Rev. Lett. 58, 1320-1323 (1987).

[33]. W. Jhe, A.Anderson, E.A.Hinds, D.Meschede, L.Moi, and S.Haroche, Phys. Rev. Lett. 58, 666-669 (1987).

[34]. S.Haroche, Fundamental systems in quantum optics, North-Holland, Amsterdam, (1992).

[35]. P. T. Worthing, R.M. Amos, and W. L. Barnes, Phys. Rev. A 59, 865-872 (1999).

[36]. F. De Martini, G. Innocenti, G. R. Jacobovitz, and P. Mataloni, Phys. Rev. Lett. 59, 2955-2958 (1987).

[37]. R. Sprik, B. A. van Tiggelen, and A. Lagendijk, Europhys. Lett. 35, 265 (1996).

[38]. K. Busch and S. John, Phys. Rev. E 58, 3896 (1998).

[39]. T. Suzuki and P. K. L. Yu, J. Opt. Soc. Am. B 12, 570 (1995).

[40]. W. L. Barnes, J. Mod. Opt. 45, 661 (1998).

[41]. V.I. Kopp et al., Progress in Quantum Electronics, 27, (2003).

[42]. Haroche S., Kleppner D., Phys. Today 42, 24–30 (1989).

[43]. Gerard J. M., Gayral B. J., Lightwave Tech., 17, (1999).

[44]. Chang R. K., Optical Processes in Microcavities, World Scientific, Singapore, (1996).

[45]. T. J. Kippenberg, S. M. Spillane and K. J. Vahalaa, Appl. Phys. Lett. 85, 25 (2004).

[46]. W. Cao, A. Munoz, P. Palffy-Muhoray and B. Taheri, Nature Mat. 1, 111 (2002).

[47]. J. Schmidtke, W. Stille, H. Finkelmann and S.T. Kim, Adv. Mat. 14, 746 (2002).

[48]. G. Strangi, V. Barna, R. Caputo, A. de Luca, C. Versace, N. Scaramuzza, C. Umeton, R..Bartolino and G.Price, Phys. Rev. Lett. 94, 063903 (2005).

Editor ‘s choice for Virtual Journal of Nanoscale Science and Technology 11, 8 (2005).

Barna V., Caputo R., De Luca A., Scaramuzza N., Strangi G., Versace C., Umeton C. , Bartolino R., Price G. N. Optics Express, Vol.14, 7, (2006).

[49]. V. Barna, S. Ferjani, A. De Luca, R. Caputo, N. Scaramuzza, C. Versace and G. Strangi, Appl. Phys. Lett. 87, 221108 (2005).

[50]. M. Ozaki, M. Kasano, D. Ganzke,W. Haase, and K. Yoshino, Adv. Mater. 14, 306 (2002).

[51]. J. Schmidtke and W. Stille, Eur. Phys. J. B 31, 179 (2003).

[52] . R. C. McPhedran, L. C. Botten, J. McOrist, A. A. Asatryan, C. M. de Sterke and N. A. Nicorovici, Phys. Rev. E 69, 016609 (2004).

[53]. V.I. Kopp, Z.Q. Zhang and A.Z. Genack, Phys. Rev. Lett. 86, 1753 (2001).

[54]. A. Yariv, Quantum Electronics, CBS College Publishing, New York, (1985).

[55]. R. Caputo, L. De Sio, A. V. Sukhov, A. Veltri and C. Umeton, Opt. Lett 29, 1261 (2004).

[56]. S.T. Wu and D.K. Yang, Reflective Liquid Crystal Displays, John Wiley & Sons, Chichester, (2001).

[57]. P. G. de Gennes and J. Prost, The Physics of Liquid Crystals, Oxford University Press, New York, (1993).

[58]. L. M. Blinov and V. G. Chigrinov, Electrooptic Effects in Liquid Crystal Materials , Springer-Verlag, New York, (1994).

[59]. V. I. Kopp and A. Z. Genack, Phys. Rev. Lett. 89, 033901 (2002).

[60]. H. S. Kitzerow, B. Liu, F. Xu, and P. P. Crooker, Phys. Rev. E 54, 568 (1996).

[61]. V. A. Belyakov, Mol. Cryst. Liq. Cryst. 410, 219 (2004).

Chapter IV

Random Lasing and Weak Localization of Light in Dye Doped Nematic Liquid Crystals

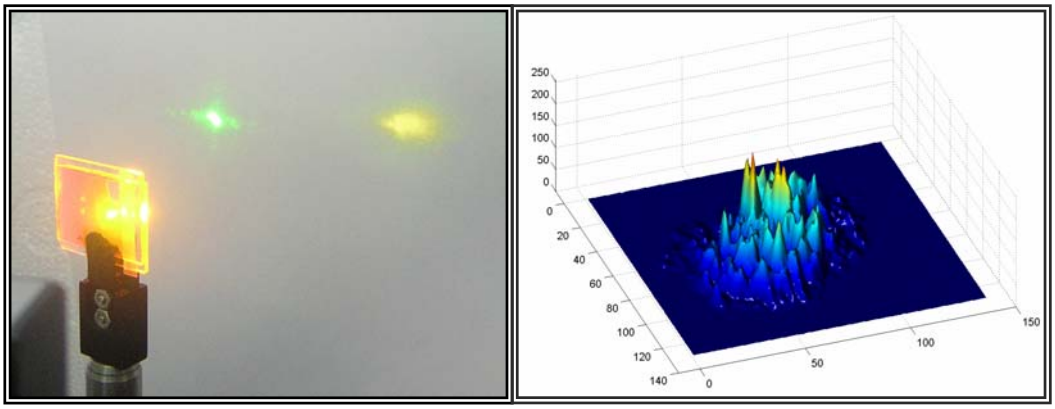

Chapter IV

Random Lasing and Weak Localization of Light in Dye Doped Nematic Liquid Crystals

4.1. Introduction

Light propagates along straight lines and with constant intensity. This statement is only true as long as the radiation does not encounter obstacles. Objects can either absorb part of the light, or can change its direction of propagation. The latter phenomenon is called “scattering”. When scattering is efficient for all colors, the object will look white. When absorption is efficient for all colors, it will look black. The origin of light scattering is often caused by refraction, which is - in its simplest form - described by the well-known Snell’s law.

“Multiple scattering” will set in when light propagation is influenced by more than one obstacle. Its occurrence is determined by both absorption and scattering of the individual particles. As a rule, one might say that multiple scattering of a wave is most likely to occur in the presence of a high concentration of obstacles that each have a large scattering efficiency and hardly absorb any intensity. In a medium where multiple scattering of light fully determines the energy transport, the so-called regime of radiative transfer, the underlying wave character of light seems to be eliminated.

What remains, appears to be a diffuse intensity pattern with hardly any interesting wave physics involved.

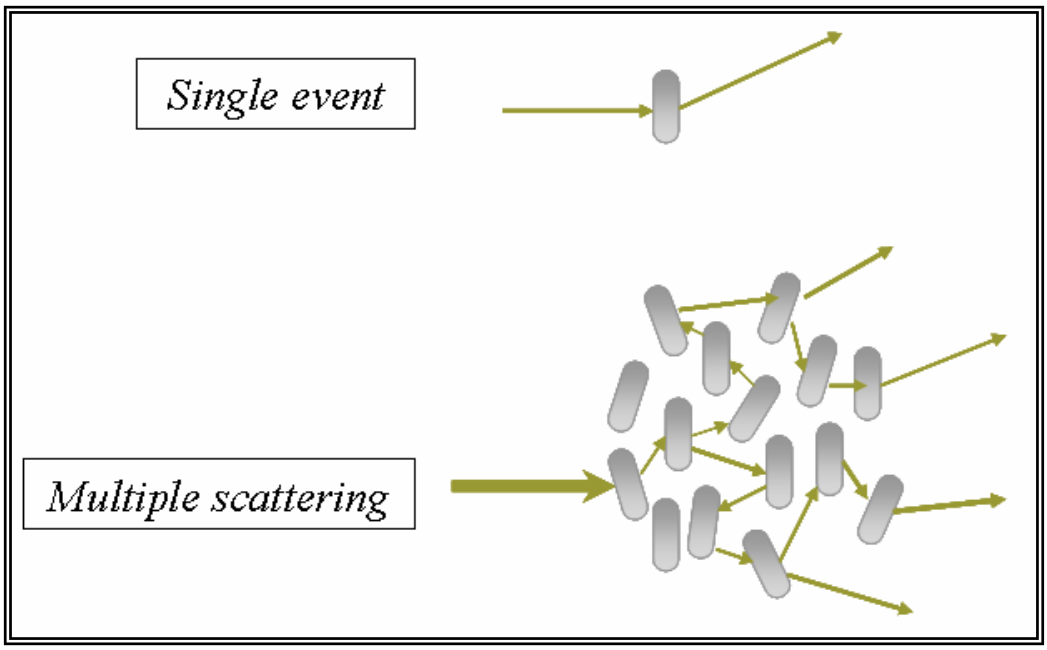

Fig.4.1. Events of single and multiple scattering of light.

In the past, experiments involving optics tried to avoid multiple scattering as much as possible. The phenomenon was considered to be unexciting and disregardable. It was not until the late fifties that the first indications showed that multiple scattering is full of rich and fundamental phenomena. However, these advances were not made by addressing multiple scattering of light, but by studying multiple scattering of electrons in the solid state. Electrons scatter from a local variation in potential just like light scatters from a local variation in dielectric constant. The resistivity of metals at low temperatures is to a large extent determined by multiple scattering of electrons from the potentials of impurities.

But, in order to explain the diffuse motion of an electron caused by scattering off impurities in the crystal it is not necessary to incorporate the interference of the electronic wave function in this scattering process. The new developments in condensed matter focused on the role of interference of the electron wave function in

multiple scattering. Among the many new concepts that were introduced, “Anderson Localization” is for sure one of the most fascinating. It describes the vanishing of propagation in the regime of very strong multiple scattering due to interference and was suggested as a model for metal-insulator transitions [1].

If electron propagation can be inhibited by interference, why not also the propagation of light?

This question was posed only about 25 fifteen years ago. Since then, optimizing multiple scattering of light has become an active area of research, with localization of light as its major goal. The scattering of light from one individual dielectric particle can be optimized by tuning the wavelength of light right into a scattering resonance. In order to set a scatterer into resonance its size should be matched to the wavelength of the light. This balancing of length scales together with a suitable shape will turn the particle into a resonator for light. In fact, in search for localization of light, the study of resonant multiple scattering has become a very interesting and large topic by itself.

4.2. Single Scattering

Light propagation inside a homogeneous material is simple - light propagates in straight trajectories. Eventually, optical absorption may occur and the light intensity decays exponentially as the wave travels in the medium. If the wave encounters an inhomogeneity it is scattered, which means that its direction of propagation changes. An inhomogeneity or scatterer can be an atom with polarizability φ, or a particle of refractive index n, or a density fluctuation in a liquid or gas. The scattering cross section of the scatterer σ_s is defined as the amount of light removed from the incident beam by scattering.

Depending on the size of the scatterer r relative to the wavelength λ_o, the scattering can be classified in three different types: Rayleigh scattering [2-4], Mie scattering [5-7], and geometrical-optics scattering.

Rayleigh scattering is the scattering by particles much smaller than the optical wavelength, like for instance atoms and molecules. In this regime the scattering is very inefficient and the cross section is given by [4]:

$$\sigma_S = \frac{8}{3}\pi\varphi^2 k_0^4 \qquad (4.1)$$

where φ is the polarizability and the wave vector in vacuum is given by $k_o = 2\pi/\lambda_o$.

If the size of the scatterer is of the order of the wavelength then σ_s is maximal. This regime is known as Mie scattering. The determination of the Mie cross section is far from trivial and it was calculated numerically for objects with a high degree of symmetry, as spheres or cylinders [4]. In general, σ_s is larger when the refractive index contrast *m* between the scatterer and the surrounding medium is higher.

If the size of the scatterer is much larger than the wavelength then its scattering cross section is equal to two times its geometrical cross section. This is the geometrical-optics regime, and the scattering is described by Snell's law [5].

4.3. Multiple Scattering and Light Localization

The scattering mean free path, l_s , in a medium, is defined as the average distance between two consecutive scattering events. If the medium is larger than l_s the single scattering approximation is not valid. Multiple scattering takes place. Depending on the arrangement of the scatterers, two limiting cases of multiple scattering media can be distinguished: crystals on one side and random or disordered media on the other. A disordered medium has a random distribution of scatterers. The photonic or scattering strength in a disordered scattering medium is described by the inverse of the localization parameter kl_s (also known as the Ioffe-Regel parameter [8]):

$$kl_S = \frac{2\pi}{\lambda_0} n_e l_S \qquad (4.2)$$

where k is the wave vector in the medium, and n_e is the effective refractive index of the medium.

The scattering mean free path is, to a first approximation (independent scattering approximation), given by:

$$l_S = \frac{1}{\rho \sigma_S} \qquad (4.3)$$

where ρ is the density of scatterers and σ_s is the average scattering cross section.

In a weakly scattering medium we have $kl_s >> 1$. The photonic strength can be increased by reducing l_s, which is achieved by maximizing the scattering cross section.

In the weak scattering limit, that is when the scatterers density is low, and/or when the scattering cross section is small, the transport of light is well described by the diffusion equation. The wave diffuses in the medium as electrons do in a disordered metal. The main approximation of the diffusion approach is to neglect any interference of the wave propagating along different paths. When the scattering becomes strong, interference plays an important role.

By using the diffusion equation a great simplification is achieved in the macroscopic description of the wave propagation [9] (i.e. on length scales larger than l_s). The main approximation that the diffusion approach does is to neglect any interference effect.

The main aspect of the diffusion approximation can be considered by looking at the average intensity I_{AB} in a point Q produced by a source located in a point P, as shown in Figure 4.2.

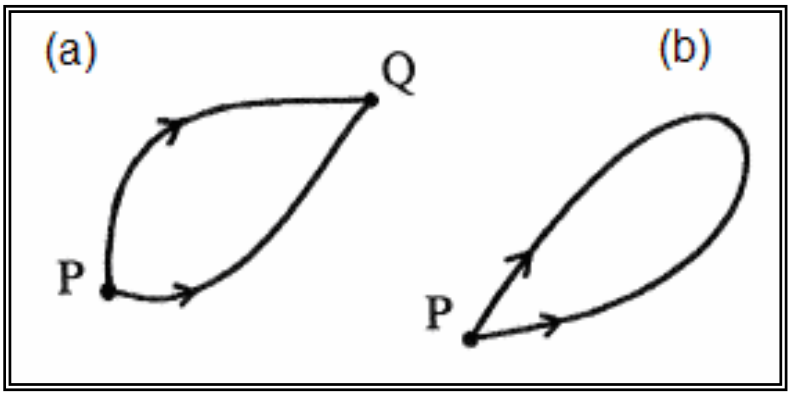

Fig.4.2. (a) The intensity at point Q due to a source in P is given by the sum of intensities of all possible paths leading from P to Q. (b) If Q is overlapped with P an interference contribution appears.

By average intensity is meant the ensemble average or the intensity averaged over all possible positions of the scatterers.

The wave can propagate along many different optical paths, but for simplicity, only two of these paths are represented. The lines representing the optical paths in Fig.4.2. correspond to the wave vector of the scattered waves.

Inside any multiple scattering medium, the intensity a the point Q [10] is given by the square of the sum over a suitably normalized amplitudes of waves following all possible scattering paths connecting P to Q

$$I = \left| \sum_i A_i (P \to Q) \right|^2 \qquad (4.4).$$

Since each path gives a different phase shift to the wave, on average, the cross terms in the square will cancel and the intensity at Q will be given by the sum of the squared amplitudes (meaning that the interference contribution is absent)

$$I = \sum_i \left| A_i (P \to Q) \right|^2 \qquad (4.5).$$

In the case for which Q coincides with P, the scattering path can be crossed in opposite direction. A wave traversing the path in one direction will interfere constructively with a wave crossing the path in the other direction, which doubles the total intensity at P. Thus, the probability to return to the initial position is twice as large as one would expect (without interference taken into account).

In a real system there are many possible optical paths, and the interference term leads to the characteristic speckle pattern that can be observed on the transmitted or reflected light. Speckles are the bright and dark spots formed by the scattered light and they give to the transmission and reflection its granular aspect [11-14]. If the intensity is averaged over all possible realizations of the disorder, the interference term, or speckle, vanishes. This vanishing of the speckle occurs because on average the interference term cancels out since the contribution of constructive and destructive interference are equal. When neglecting the interference term is the sum of the intensities of the waves diffusing along different paths. Therefore, the diffusion approximation does not make any distinction between diffusing particles or wave intensities. The wave diffuses in a 3D medium with a diffusion constant

$$D_B = \frac{1}{3} v l_B \qquad (4.6)$$

where v is the energy velocity or the rate at which the energy is transported [15,16], and l_B is the Boltzman mean free path or the length over which the direction of propagation of the wave is randomized by scattering in the absence of interference.

However, in a random medium there is always an interference contribution that survives (even for weakly scattering media) the averaging over different configurations of the disorder. This interference originates from closed paths (Fig.4.2.). For each closed path a wave emitted at the source P can return to the same point after propagating along two reversed paths, I and II. These paths are called time-reversed paths. This effect is called weak localization, since it is believed to be the precursor of Anderson localization or strong localization.

Similar to photonic crystals, direct and inverse random media can be realized. A direct medium or disordered opal consists of a powder of particles in air; while an inverse

random media is a sponge like material in which air voids are surrounded by the material with high refractive index.

4.4. Anderson Localization

Localization was introduced by Philip W. Anderson in 1958 in the famous article "*Absence of diffusion in certain random lattices"* [1]. Anderson predicted a transition in the diffusive transport of electrons in metals, in particular, in lattices where disorder was introduced as impurities. The transition changes the electrons transport from classic diffusion (i.e. what happens in a copper wire) to the absence of diffusion. Anderson localization brings classical diffusion to a complete halt. Thus, this transition can be defined as $D = 0$ or equivalently $l = 0$. That is, on increasing the amount of scattering beyond a critical value, the material makes a transition into a localized state (Fig.4.3.). Experimental evidence of this prediction was found in the following years when studying this transition in conducting materials. The electric conductivity σ decayed exponentially with the length of the system when the Anderson localization regime was reached [1,17,18].

The Anderson transition means that a conductor becomes an insulator, because the wave function of electrons is localized inside the sample, stopping the classic diffusion. The same effect is present for photons in strongly disordered dielectrics, with the great advantage that no interaction is present for photons with respect to electron-electron interaction in the electronic case [19]. This fact can make photonic systems more suitable for studying Anderson localization than electronic ones. On the contrary, obtaining the same scattering efficiency with respect to electronic solids is not so easy in dielectrics. The proposal of John for photonic crystals derived from the necessity to design a strongly scattering dielectric system to study Anderson localization of photons.

This transition can best be observed in the transmission properties of the system. In the localized state, the transmission coefficient decreases exponentially instead of linearly

with the thickness of a sample. At the transition, the transmission coefficient is expected to have a power-law dependence on the inverse thickness.

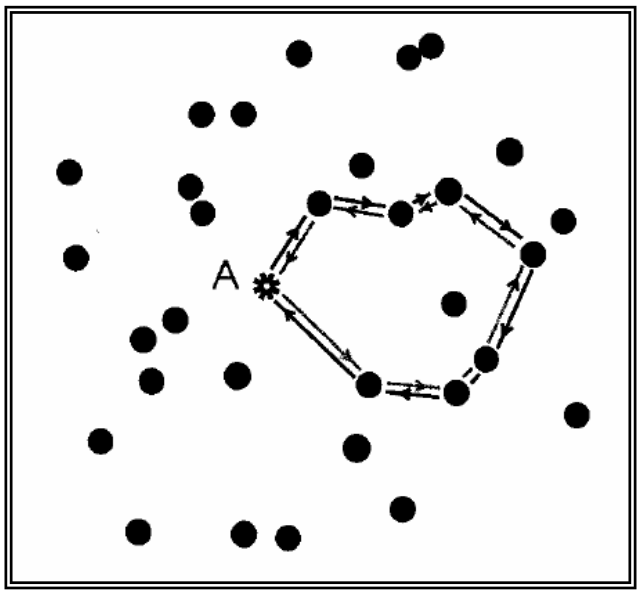

Fig.4.3. Anderson localization of waves in disordered systems originates from survival of the interference in multiple elastic scattering. A random light path that returns to the light source (A) can be followed in two opposite directions. The two waves which propagate in opposite directions along this loop will acquire the same phase and therefore interfere constructively in A. This leads to a higher probability of the wave coming back to A and consequently a lower probability of propagating away from A. On decreasing the mean free path l, the probability for such looped paths increases and at strong enough scattering the system makes a phase transition from the normal conducting state into a localized state, due to interference. In the localized regime, the system behaves as a non-absorbing insulator. Light which is incident on would be almost completely reflected and the remaining transmission would decrease exponentially with the slab thickness.

Anderson localization of electrons in a disordered system has become a prominent part of contemporary condensed matter physics, and remains an active subject of theoretical and experimental research.

Following the discussion of the preceding section, localization occurs when the diffuse transport breaks down due to interference of waves propagating along time-reversed paths (i.e. when the wave returns to the source). When a wave is localized, its ensemble average intensity decays exponentially with the distance to the source L and

with a characteristic length given by the localization length ξ (the critical dimension for a sample to have localized states)

$$I \propto \exp(-L/\xi) \qquad (4.7).$$

Anderson localization is a phase transition between propagating states and localized states. Because wavelength is the important length scale for interference effects , A.F. Ioffe and A.R. Regel proposed that when the scattering mean free path (l) is comparable to λ it should not be possible to describe classically the wave transport [8]. They established that the transition between the extended and localized states in a 3D infinite system formed by isotropic scatterers occurs when

$$kl \sim 1 \qquad (4.8)$$

where $k=2\pi/\lambda$ is the wave vector.

This equation is known as the Ioffe-Regel criterion for localization. The validity of the Ioffe-Regel criterion has been confirmed with more rigorous theories [20-23].Localization is expected for $kl < 1$, which is known as the (modified) Ioffe–Regel criterion. This criterion can be understood intuitively if one realizes that below $kl = 1$, the electric field can not even perform one oscillation before the wave is scattered again.

If one considers a point source inside a strongly scattering medium, subject to the Ioffe-Regel condition, two waves that propagates in opposite directions along this loop will acquire the same phase shift and so they interfere constructively. Far from the localization [24-32], loops of this type have very low probability to exist and classical diffusion dominates.

An important characteristic of classical waves is absorption. Since the number of electrons is conserved, absorption is absent in electronic systems. Absorption preserves the phase coherence of the wave. Therefore, it has been argued that absorption only introduces trivial effects and does not alter the essential behaviour of the transport. However, since absorption removes paths that are longer than the absorption mean free

path, preventing them to interfere, it is believed that it strongly affects the localization of classical waves and ultimately destroys it.

It is certainly very interesting the study of the competition between localization and absorption, but special care has to be taken in absorbing systems since experiments can be misinterpreted. For instance, a transmission that decays exponentially with the sample thickness can be due to strong localization in a nonabsorbing medium, or to classical diffusion in an absorbing medium, or to a combination of both effects.

4.5. Enhanced Backscattering

As pointed out in the paragraph 4.3, a laser beam incident on a random scattering medium produces a spatial speckle pattern of high and low intensities. If the scatterers in the sample are able to move, or if the sample itself is moving, the points in space where the light interferes constructively and destructively are changing position and the speckle pattern averages out if one observes it at a long enough timescale. There is however one interference effect that will survive: there will be an increased intensity in a small solid angle around the direction of pure backscattering.

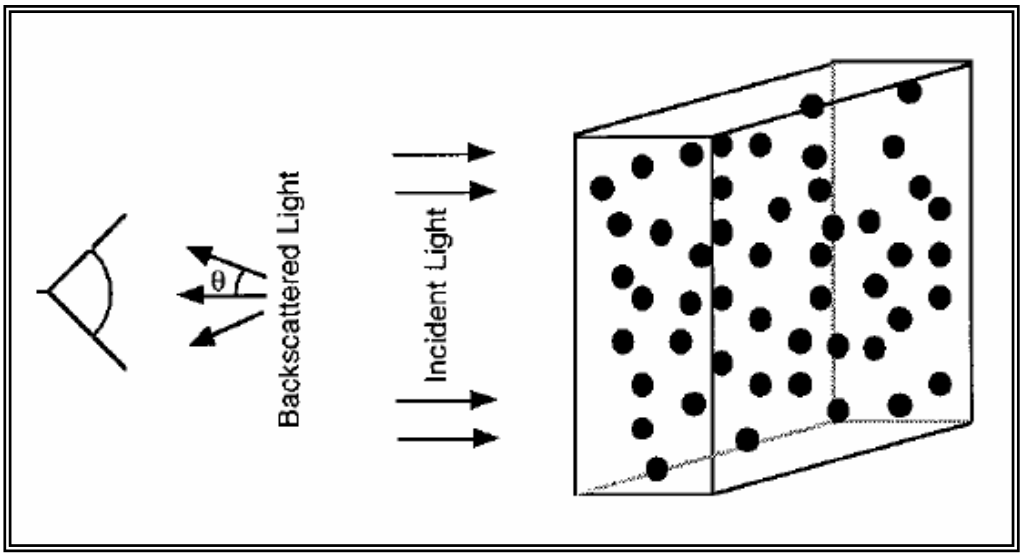

Fig.4.4. Schematic representation for light backscattering.

This effect is referred to in literature as enhanced backscattering, sometimes as weak localization, or coherent backscattering. The first theoretical analysis of this effect was found in radar backscattering. Enhanced backscattering of light has been confirmed experimentally in the mid-eighties [33,24-27]. This phenomenon is the result of interference of counter propagating waves which is always constructive in the direction of the incident wave.

Let us consider that light is going into a medium at a certain point A, then it is multiple scattered and leaves the medium at some point B. We can see that a wave traveling along this path in the opposite direction, entering at B and leaving the sample at A, has exactly the same path length and thus the same phase upon leaving the sample (Fig.4.5). The two waves interfere constructively in the exact backscattering direction and their amplitudes add up.

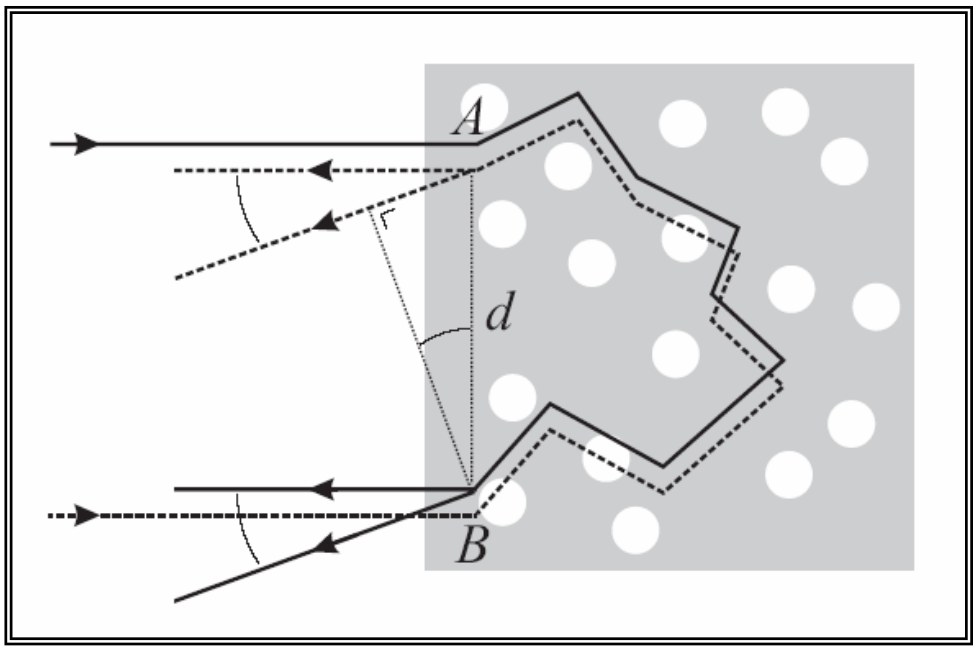

Fig.4.5.Schematic picture of enhanced backscattering. One light path is traveled in opposite directions and the outcoming waves interfere. For the exact backscattering direction this interference is constructive because the paths of the waves are equal and so are their phases. Light that comes out at an angle θ acquires a phase difference because of the difference in path length of Δl = d sin θ and the resulting intensity is an oscillating function of θ.

Assuming an equal amplitude for the counter-propagating waves ($A_1 = A_2 = A$) we can see that the resulting intensity is twice the intensity then in the case when there is no interference:

$$I = (A_1 + A_2)^2 = A_1^2 + 2A_1A_2 + A_2^2 = 4A^2 \quad \text{- constructive interference}$$

$$I = A_1^2 + A_2^2 = 2A^2 \quad \text{- no interference.}$$

When we look slightly off-axis, a difference in path length is produced and the corresponding phase difference will make the interference less constructive. Again, assuming equal amplitudes, the angular dependent intensity becomes:

$$I(\vartheta) = I_0\left(1 + \cos\frac{2\pi d \sin\vartheta}{\lambda}\right) \tag{4.9}$$

where d is the distance between the points where the light path enters the medium and the point where it leaves, λ the wavelength of the light and I_0 the intensity where there no interference effects exist. One can see that the intensity is a goniometric function of the exit angle (Fig.4.6).

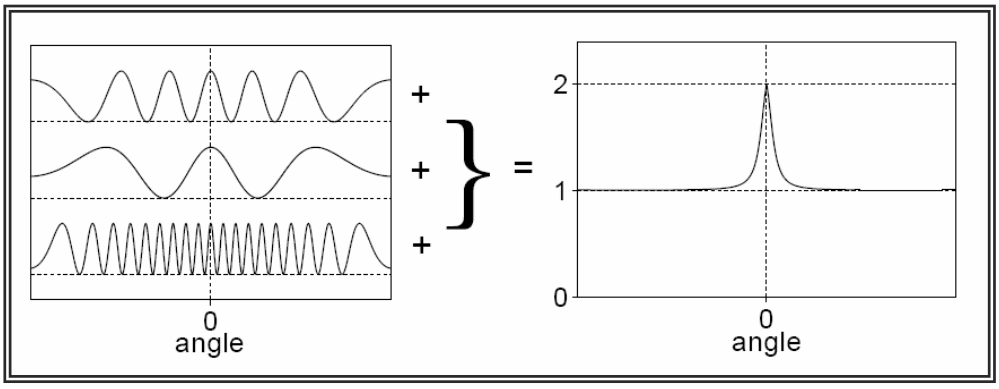

Fig.4.6. (left) The interference patterns of light coming from the exit points of a light path and its counter propagated path. Patterns are shown for three values of the distance between the exit points, d. (right) When for a realistic system all interferences are added, the result is a characteristic peak - the enhanced backscattering cone.

Of course, there are multiple light paths and they all contribute to the backscattering intensity. Different paths will have different starting and ending points, which will yield different values for the distance between them, d. As can be seen from equation (4.9), these distances will determine the periodicity of the intensity profile. Large d will produce fast oscillations and small d slow ones. Although differing in period, all oscillating contributions have their maximum value for $\theta = 0$. If we sum many of them with different d, contributions around $\theta = 0$ add and the rest averages out. We find a characteristic peak, the so-called enhanced backscattering cone, that has a strong dependence on the exit angle (Fig.4.6). In fact, if we would make the addition for any d, all contributions having the same weight, the result would be a δ function.

But this is not what one observes. A δ function is not obtained because of several reasons. First, d cannot grow infnitely, because it is limited to the beam diameter. Furthermore, the weights of contributions from different d are not equal. The value of the distance d between the starting and ending points of a light path is related to the total length of this light path s: long paths will on the average end up at a large distance from their starting point, short paths will leave the medium in the vicinity of their starting point. Therefore the probability distribution for the distance d is determined by the path length distribution P(s) of light in the system. If, for example, short paths are favoured over long ones, slowly oscillating contributions with small d will be more important and the backscattering cone will be wide.

In an ordinary (non-absorbing and non-amplifying) multiple scattering medium P(s) is indeed large for short paths and small for long paths. This can be understood if we consider the diffusive process as a three-dimensional (3D) random walk, where one of the half-spaces represents the sample. The probability to make long paths with a large transverse displacement is small because of the increasing probability to end up in the wrong half-space and thereby having left the sample. Since in non-absorbing media contributions of path lengths up to infity have to be summed, the peak of the backscatter cone is not exactly at $\theta = 0$.

The presence of absorption is an important factor reducing the probability of long paths. Absorption puts longer paths at a disadvantage because the intensity has an

exponential dependence. This will drastically suppress the fast oscillating contributions to the backscattering cone, which will result in a rounded peak at θ = 0.

Apart from this, there are a number of other influences on the shape of the backscattering cone (like localization of light) which are not to be presented here.

The main factors determining the shape of the cone were presented above, but something more can be said – what about about its height? Assuming that the incident laser beam has a flat transverse intensity profile we can say that the constructive interference at θ = 0 of one pair of counter-propagating waves will result in an intensity that is exactly twice the intensity if there were no interference. However, this does not hold for the case in which light is scattered back immediately by one single scatterer. Then, there is no doubling of the intensity since the incoming and outgoing paths coincide and no interference takes place. We have to treat multiple and single scattered light differently and separate the total backscattered light in a multiple scattered and a single scattered component. So, the total backscattered intensity can be written as:

$$I_{tot}(\theta)=I_d+I_c(\theta)+I_S \qquad (4.10)$$

where I_d and $I_c(\theta)$ represent the constant term and the angle dependent term from equation 4.9 respectively, both summed for appropriate values of d. The sum of I_d and I_c is the multiple scattering component of the backscattered light. I_s is the single scattering contribution. If we divide $I_{tot}(0)$ by its value for large enough θ, for which the interferences of the multiple scattering component have averaged out and $I_c = 0$ (we can call this value the background intensity), we can find the enhancement factor of the backscattering cone.

$$E = \frac{I_{tot}(\vartheta = 0)}{I_{tot}(\vartheta >> 0)} = \frac{I_d + I_c(0) + I_S}{I_d + I_S} \qquad (4.11).$$

In the above discussion, the components I_d and I_s were considered angle independent. This is not actually correct because they do show a dependence on θ, which is due to the projection of the spherically symmetric emission of the source on a plane in which

the emission is measured. This dependence usually does not show up in the limited angular region where the backscattering cone is measured and is therefore neglected. Since $I_c(0) = I_d$, we can write for the enhancement factor:

$$E = \frac{2I_d + I_S}{I_d + I_S} = 2 - \frac{I_S}{I_d + I_S} \qquad (4.12).$$

From this we can see that the enhanced backscattering cone has a height of twice the background intensity minus the single scattering component. For isotropic scatterers without absorption the single scattering contribution is about 12%, which yields an enhancement factor of about 1.89. The enhancement factors considered here are the theoretical maximum values.

Since the first experimental observation of coherent backscattering from colloidal suspensions [24-26], the phenomenon has been successfully studied in strongly scattering powders [34,35], cold atom gases [36,37], two-dimensional random systems of rods [38], randomized laser materials [39], disordered liquid crystals [41,41], and even photonic crystals [42,43].

Liquid crystals in the nematic phase exhibit multiple light scattering, but, in contrast to most disordered materials, are orientationally ordered. The simplest consequence of orientational anisotropy in multiple scattering is manifest in light diffusion. Theory predicts [44-46] and experiments confirm [47-50] that monodomain nematic liquid crystals are characterized by an anisotropic light diffusion constant. The resulting diffusion coefficients for a nematic liquid crystal are on the order of $D_\perp$ = 0.98 x 109 cm^2/s and $D_{//}$ = 1.43 x 109 cm^2/s which results in $D_{//}/D_\perp = 1.45$.

It is interesting to speculate about the possible survival of anisotropy effects in interference phenomena such as weak and strong localization. For weak localization, the width of the backscattering cone depends on the transport mean free path rather than the light diffusion constant. Mean free path anisotropy should therefore be

manifest in angular anisotropy of the backscattering cone, even at very high orders of scattering.

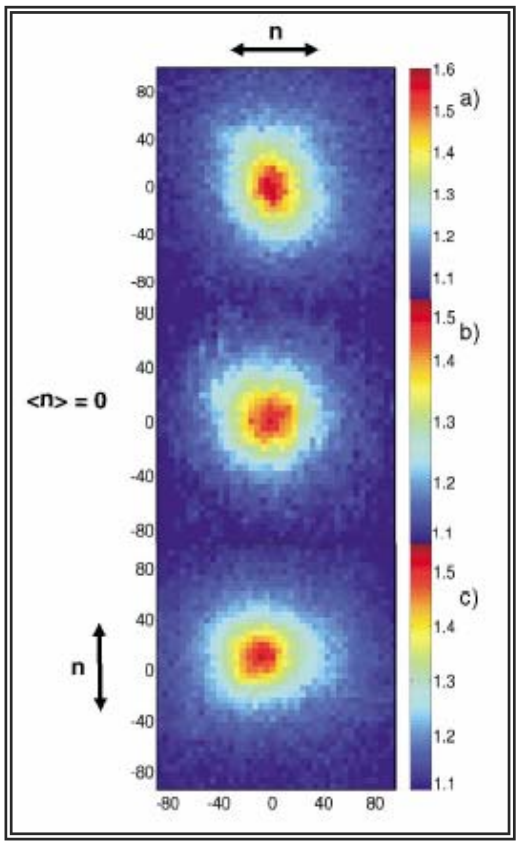

Fig.4.7. Coherent backscattering cones in polar colour plots from nematic liquid crystal for three cases of the nematic director. (a) nematic director in x; (c) director in y; (b) polydomain phase. The polarization is in the x direction in all cases.

While pioneering experiments on coherent backscattering from monodomain liquid crystals have been performed [51], measurements of the transport mean free path length or backscattering cone anisotropy remain to be investigated. Thus, important questions are still open about how weak and strong localization are influenced by anisotropic multiple scattering. Recently, observations of anisotropic weak localization of light in nematic liquid crystals [52] revealed that the backscattering cone profile exhibits an angular anisotropy - dependence on the direction of the nematic director (Fig.4.7).

A quantitative model description of the cone shape will not be discussed here.

Also, enhanced backscattering in an amplifying system is quite different from the case presented above and adjustments have to be made to include gain coeffcients into the diffusion and backscattered intensity profile equations.

4.6. Random Lasers

Optical scattering in a random medium may induce a phase transition in the photon transport behaviour. When the scattering is weak, the propagation of light can be described by a normal diffusion process. With an increase in the amount of scattering, recurrent light scattering events arise. Interference between the counter propagating waves in a disordered structure gives rise to the enhanced backscattering, also called weak localization. When the amount of scattering is increased beyond a critical value, the system makes a transition into a localized state. Light propagation is inhibited due to interference in multiple scattering. Since Anderson localization is completely based on the interference effect, and interference is a common property of all wave phenomena, it is natural to extend electron localization to photon localization in disordered dielectric media.

Apart from the remarkable similarities, there are striking differences between electron transport and photon transport in a disordered medium. For example, the number of electrons is always conserved, while the number of photons is not in an amplifying (or absorbing) random medium. A fascinating phenomenon, which would never occur in an electronic system, is laser action in a disordered gain medium [53-57]. In the case of strong scattering and gain, recurrent scattering events could provide coherent feedback and results in lasing [58-60]. When the scattering mean free path becomes equal to or less than the wavelength, light may return to a scatterer from which it was scattered before, and thereby forming closed loop paths. If the amplification along such a loop path exceeds the loss, laser oscillation could occur in the loop which serves as a laser resonator. The requirement of the phase shift along the loop being equal to a multiple of 2π determines the oscillation frequencies. Such a laser is called a “random laser”.

Random laser represents a non-conventional laser whose feedback is mediated by random fluctuation of dielectric constant in space. Since the pioneering work of Letokhov and coworkers [61] in 1968 which predicted that the combination of multiple scattering and light amplification would lead to a form of laser action, lasing in disordered media has been a subject of intense theoretical and experimental studies [62-69]. Random lasers have been realized in various material systems, from semiconductor nanoparticles, ceramic powder to polymers, organic materials and biological tissues. Their low fabrication cost, sample specific lasing frequency, small size, flexibleshape, and substrate compatibility lead to many potential applications.

There are two kinds of feedback for random lasing: one is intensity or energy feedback, the other is field or amplitude feedback. The field feedback is phase sensitive (i.e. coherent), and therefore frequency dependent (i.e. resonant). The intensity feedback is phase insensitive (i.e. incoherent) and frequency independent (i.e. non-resonant). Based on the different feedback mechanisms, random lasers are classified into two categories: (i) random laser with incoherent and non-resonant feedback, (ii) random laser with coherent and resonant feedback.

Lasing with nonresonant feedback occurs in the diffusive regime. In a disordered medium, light is scattered and undergoes a random walk before leaving the medium. In the presence of gain, a photon may induce the stimulated emission of a second photon. When the gain length is equal to the average length of light path in the medium, the probability that a photon generates a second photon before leaving the gain medium approaches one. Thus the photon density increases. From the theoretical point of view, the solution to the diffusion equation, including optical gain, diverges. This phenomenon is similar to neutron scattering in combinations of nuclear fission. When optical scattering is strong, light may return to a scatterer from which it is scattered before, and thereby form a closed loop path. When the amplification along such a loop path exceeds the loss, laser oscillation could occur in the loop which serves as a laser resonator. The requirement that the phase shift along the loop is equal to a multiple of 2π determines the oscillation frequencies. This is a random laser with coherent feedback. Of course, the picture of a closed loop is intuitive but naive. The light may come back to its original position through many different paths. All of the backscattered light waves interfere and determine the lasing frequencies. Thus, a

random laser with coherent feedback is a randomly distributed feedback laser. The feedback in this case is provided by disorder induced scattering.

The first experimental evidences of this effect are dated 1993-1994, while later on outstanding research in this field was done by A. Lagendijk [14,15,30,39,67,69], D. Wiersma [35,49,63,70-74] and H.Cao [54-57,75-79].

A random laser is a sort of mix of a standard laser and a light bulb. Figure 4.8 shows the comparison between a "classic" laser and a random laser. On the left side a traditional laser cavity is depicted. It is simply formed by two mirrors and by an active medium that amplifies the light. The output is a coherent beam, monochromatic and directional. On the right side of the figure a random laser is shown. The cavity does not exist and the gain medium is dissolved in the scattering dielectrics. It is the multiple scattering that in a certain way replaces the optical cavity. One might question how laser action occurs in a disordered material, given that it lacks a real cavity? The answer is simple. The condition for lasing comes from a careful balance between gain and loss. The light is trapped inside the medium by multiple scattering and during the scattering it is amplified by the gain medium. The output radiation can be roughly monochromatic, but without coherence and it is emitted over the whole solid angle. The emission properties of random lasers are not so different from the traditional ones. In particular random laser exhibit a threshold behaviour. When the gain overcomes the losses the system goes above threshold. The losses are proportional to the total sample surface and the gain to its volume, so the threshold criterium can be expressed in terms of a critical volume V_{cr} above which the system lases [61].
There are many ways to obtain a random amplifying medium: nanoparticle suspension of TiO_2, laser crystals , Ti:Sa , ZnO powders for high scattering and gain and many others [61-79]. From the point of view of the random laser the crucial parameter is the transport mean free path, that is a measure of the scattering strength of the system. Most of the systems studied are in the diffusive regime, where $\lambda << l_t << L$.
Some experiments were also performed in the Anderson localization regime.

Cao et al. [79] used a high scattering semiconductor powder as a random laser. The emitted light had the same behavior as a diffusive random laser, except for the fact that the spectrum exhibited ultranarrow spikes.

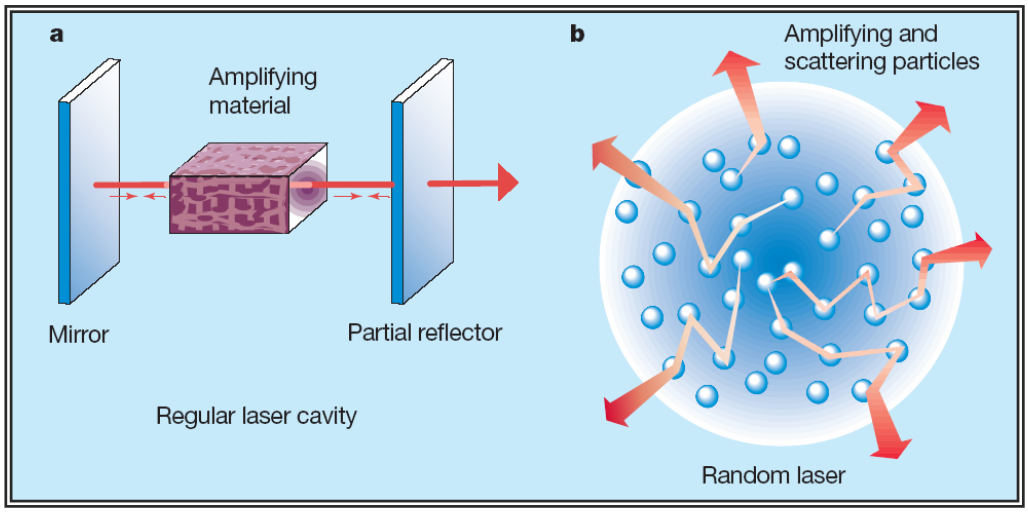

Fig.4.8. (a) Traditional laser cavity. (b) Random laser; the light is retained in the sample by multiple scattering and it is amplified at the same time.

The random laser not only becomes a new member of laser family, but also provides a new path to study localization phenomena [80-82]. Unlike the conventional lasers, the modes of random lasers are formed by random scattering instead of designed reflection. Because random lasing modes come from the eigenstates of disordered systems [80], they open a special door to study the interplay between localization and amplification.

4.7. Partially Ordered Systems and Lasing in Dye Doped Nematic Liquid Crystals

The diffusion and transport of light waves in complex dielectric structures have encouraged a wide series of experimental and theoretical investigations, revealing one of the most challenging and exciting scientific area of the past decade. The propagation of electromagnetic waves in periodically structured dielectric systems (i.e. photonic bandgap materials) and the linear and non linear optical phenomena in completely disordered systems doped with gain media represent two opposite sides of this promising scientific branch. The literature demonstrates that much has been done in these extreme areas, but the huge intermediate world constituted by the partially ordered systems still remains almost unexplored. The laser emission study in ordered and periodic systems has known an extraordinary revival in the last years; even because of the remarkable development of experimental techniques which allow to scale the photonic crystal structures down to the nanoscale with the aim to mould the flow of light [83]. Surprisingly, active random media repeatedly proved to be suitable for obtaining diffusive laser action, mainly based on the resonant feedback mechanisms in multiple scattering. Light localization and interference effects which survive to multiple scattering events have been invoked to explain the random lasing observed in many exotic and complex systems [71,84-86]. In fact, when the diffusive photon transport in completely disordered systems encounters the condition $kl \sim 1$, k is the magnitude of the local wave vector and l is the transport mean free path, an almost complete localization of light waves should occur.

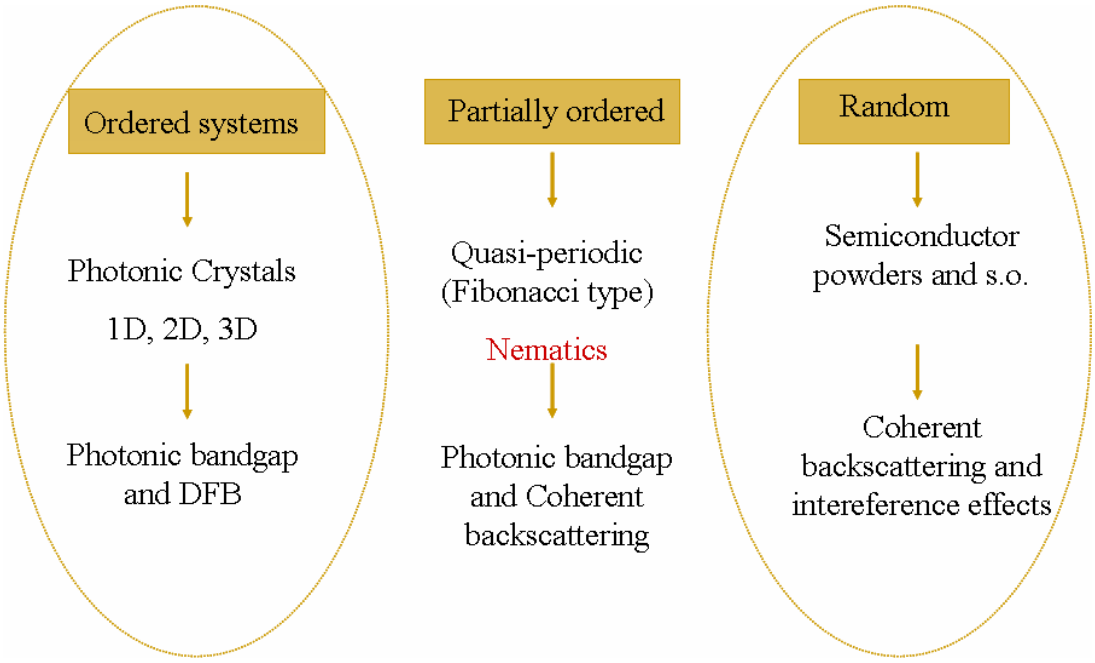

Fig.4.9. Electromagnetic waves propagation in periodically structured and in completely random systems doped with gain media represent two challenging fields of research. In-between, the partially ordered systems which, so far, are practically unexplored.

Weak localization of light waves is considered as a particular case of interference effects which were predicted and observed in random media and in partially ordered systems for $kl_t > 1$ [8].

Recently, coherent backscattering experiments performed with high accuracy apparatus manifested weak localization of light even in tensorial systems characterized by high optical anisotropy, like nematic liquid crystals [51]. These experiments show how the recurrent multiple scattering events exactly back enhance the scattered intensity giving rise to an anisotropic backscattering cone [87].

Nematic liquid crystals (NLC) are uniaxial fluids with rod-like molecules aligned on average along a local anisotropy axis which is represented by the unit vector n(r,t), the molecular director.

The spontaneous fluctuations of the director represented by $n(r,t) = n_0 + \delta n(r,t)$ lead to fluctuations in the local dielectric tensor $\varepsilon_{\alpha,\beta} = \varepsilon_\perp \delta_{\alpha\beta} + (\varepsilon_{//} - \varepsilon_\perp) n_\alpha n_\beta$ which is the main effect responsible of the recurrent multiple scattering events as a light wave is propagating through the NLC medium. The scattering of visible light by NLC is higher, by a factor of the order of 10^6, than the scattering by conventional isotropic fluids [88]. The fluctuations of $\varepsilon_{\alpha\beta}$ come from two different sources: (i) fluctuations in $\varepsilon_\perp$ and $\varepsilon_{//}$ due to small, local, changes in the density, temperature, etc.; (ii) fluctuations in the orientation of n - this being the dominant effect which is specific of nematic liquid crystals.

When the scattering is increased beyond a critical value, the system makes a transition in a localized state, where light propagation is inhibited owing to interference in multiple scattering. The weak localization of light in an amplifying scattering medium supports stimulated emission through resonant and nonresonant optical feedback. Such laser action is usually called diffusive or random lasing.

In this chapter we primarily consider the multiple scattering of spontaneously emitted photons within the gain medium. These photons are characterized by different initial states of polarization which does not depend on the excitation polarization. The polarization of the excitation pulses and the scattering intensity is considered only in terms of quantum yields and photons available to be radiated into the lasing modes.

In this chapter it is presented the first experimental observation of random laser action in a partially ordered and highly anisotropic nematic liquid crystals doped with fluorescent guest molecules [89,90].

The study of laser emission in such a system emphasizes the peculiar behaviour of diffusive laser action, randomness of laser emission was observed in time, space and frequency. In fact, the spatial distribution of the emitted light is speckle-like accompanied by strong intensity fluctuations and slight shifts of the resonant peaks occur for each pump pulse. The random laser relevant length scales (i.e. the scattering mean path length l, the gain length l_g and the sample size) are found to be in good agreement with the random laser theory. In fact, the gain length at the onset of lasing is $l_g \sim V^{2/3} / l \sim 3.5 \times 10^{-2}$ mm, is in reasonable agreement with the value found experimentally at the lasing threshold pump intensity (4.4×10^{-2} mm).

In addition, the scattering mean path length was measured to be about an order of magnitude longer than the gain length providing ample opportunities for triggering the lasing effect.

4.8. Experimental Setup and Confinement Geometries

The nematic liquid crystal, BL001 provided by Merck, having the following bulk phase sequence Cr. – -10°C – Nematic – 63°C – Iso, was doped with 0.3 wt% of Pyrromethene 597 dye (Exciton). We used two different types of geometries for confinement: wedge cells or cylindrical glass capillaries. The wedge is constituted by two glass-ITO plates separated by Mylar spacers, with a thickness of 100 μm at one edge and 1.5 μm at the other one. The inner side of the plates were covered with rubbed polyimide alignment layers in order to induce a homogeneous (planar) alignment of the NLC molecules at the interface. Then, the wedge cell was filled by capillarity with the flow direction along the rubbing direction and normal with respect to the wedge. Upon observing the sample under a polarized microscope, it shows a planar alignment with the optical axis which lies in the plane of the cell parallel to the rubbing direction.

The pyrromethene dye molecules dissolved in the NLC at very low concentration (0.3-0.5% by wt), proved to be completely miscible as evidenced by the almost complete absence of micro droplets of dye embedded in the nematic phase. The same mixture was confined also in cylindrical capillaries, without any surface treatment, having inner diameters of 200 and 500 μm.

The samples were optically pumped with 3-5 ns pulses produced by a frequency-doubled (532 nm) Nd:YAG laser (NewWave, Tempest 20).

The pump beam was focused onto the sample with a spherical lens (f = 100 mm), yielding a beam waist of about 30 μm at the focus position. The experimental set-up (Fig.4.10) presents a combination of optical elements (quarter-wave plates, half-wave plates and Glan-Thompson polarizers) in order to select all the states of polarization of the pump beam.

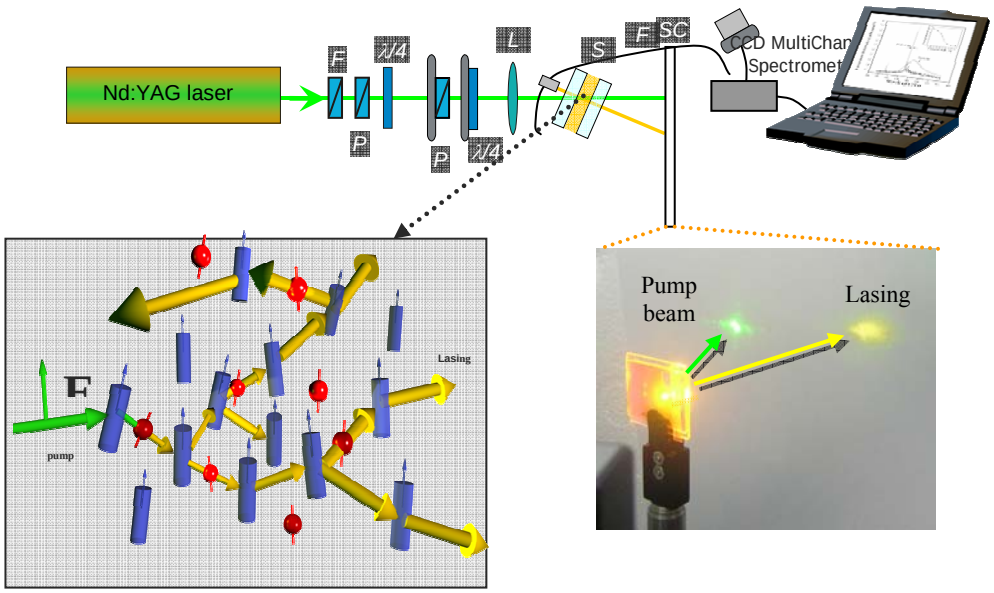

Fig.4.10. Schematic diagram of the experimental set-up: the picture shows the pump beam and the diffusive laser emission projected on the screen. Recurrent multiple light scattering in dye doped nematics provides the feedback for laser oscillations.

A multichannel CCD spectrometer with a high spectral resolution (0.5 nm) and with a fiber termination was used to capture the emission spectra within a limited cone angle of 0.05 rad. The speckle-like pattern of the emission spot was imaged on a screen while simultaneously the emission spectrum was captured by means of the CCD spectrometer.

Experiments have been performed on empty cells (in the case of both geometries) by checking the transmission and reflection spectra collected by using a high sensitivity spectrophotometer (UV-visible-near-infrared Cary 500 by Varian) in order to rule out any cavity effect due to multiple reflected light waves at the boundaries. In addition, it was calculated the free spectral range by assuming a cavity effect and it was found to be absolutely incompatible with the wavelength region of the lasing modes and with the spectral spacing of the modes.

4.9. Experimental Results

The input pump energy was varied, and we spectrally analyzed the resulting emission, using a high resolution optical multi channel charge coupled device (CCD) spectrometer (Jobin-Yvon).

At low pump power, the emission spectra show the typical spontaneous emission curve of pyrromethene dye, indicating that NLC does not considerably modify the fluorescence spectrum (Fig.4.11). Upon increasing the pump power above a given threshold value (about 900 nJ/pulse), discrete sharp peaks emerge from the residual fluorescent spectrum and the output energy was found to be about 150 nJ/pulse at room temperature. The line width of these sharp peaks was less than 0.5 nm. When the incident pump energy exceeds the threshold value, the peak intensity increases much more rapidly with the pump power and more sharp peaks appear, because now the balance gain-loss of these lossiest modes become positive (see Fig.4.11).

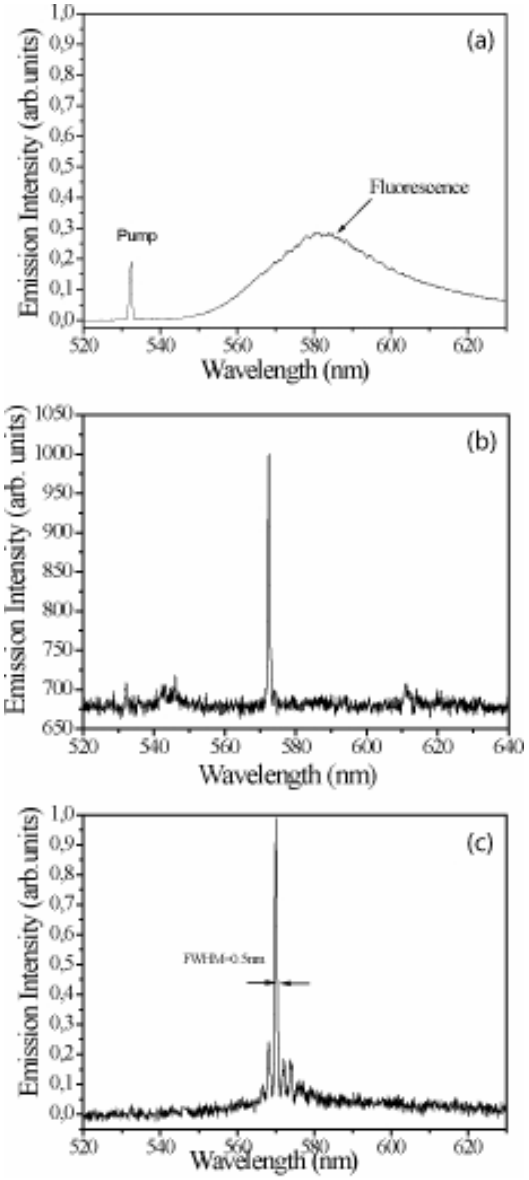

Fig.4.11. Fluorescence (a) and lasing spectra (b,c) for a wedge cell upon increasing the pump energy. Discrete sharp peaks emerge from the residual spontaneous emission for pump energy of about 1 μJ/pulse.

Hence, diffusive lasing occurs in dye doped nematics by recurrent light scattering and the lasing frequencies are determined by phase relationship of the counter-propagating scattered light waves. In fact, the weak localization of light waves owing to the strong optical scattering gives rise to reciprocal paths within the gain medium.

When the phase accumulation in reciprocal path is equal, constructive interference occurs among the backscattered amplitudes. Therefore, it is believed that blue shift

(Fig.4.11) of the laser emission with respect to the fluorescence maximum is determined by interference effects which introduce coherence and feedback, leading to lasing action.

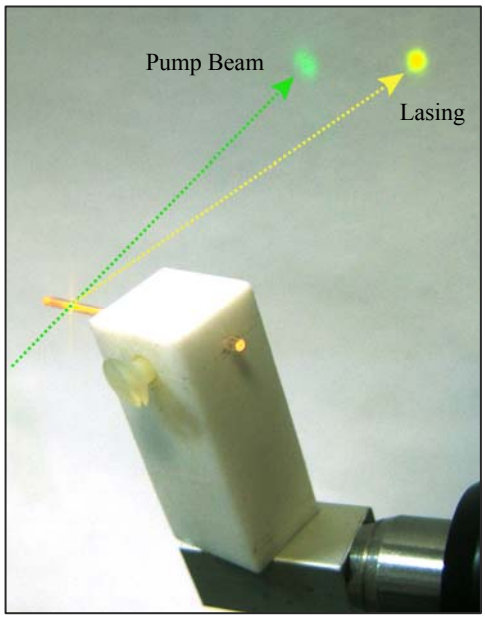

Fig.4.12. Image of diffusive lasing from optically pumped cylindrical capillary. Intense stimulated emission is observed on the background screen.

The stimulated emission sharp peaks prove that lasing effect does not depend on the size and the geometry of the boundary conditions, but the key role is played by the bulky dye doped nematics.

Furthermore, the emitted light by the cylindrical capillary was redshifted with respect to the wedge cell - this was due to phase relationships which depend on the boundary constraints.

The lasing intensity undergoes a five-fold lowering when the pump light is polarized perpendicularly to the NLC director (o-wave) compared with the light polarized parallel to the director (e-wave). The polarization dependence of the scattering intensity and the coupling of the optical field with the gain medium have to be taken into account for the observed anisotropy. The former effect is mainly due to polarization dependence of the diffusion constant D for the emitted photons. Indeed a

larger diffusion constant for the e-wave compared to the o-wave is generally measured. The latter aspect can be analyzed by considering the Fermi's Golden Rule which clearly states that the molecular transitions and the rate of emission strongly depend by the coupling of the pump electric field E and the transition dipole moment d of the dye molecules.

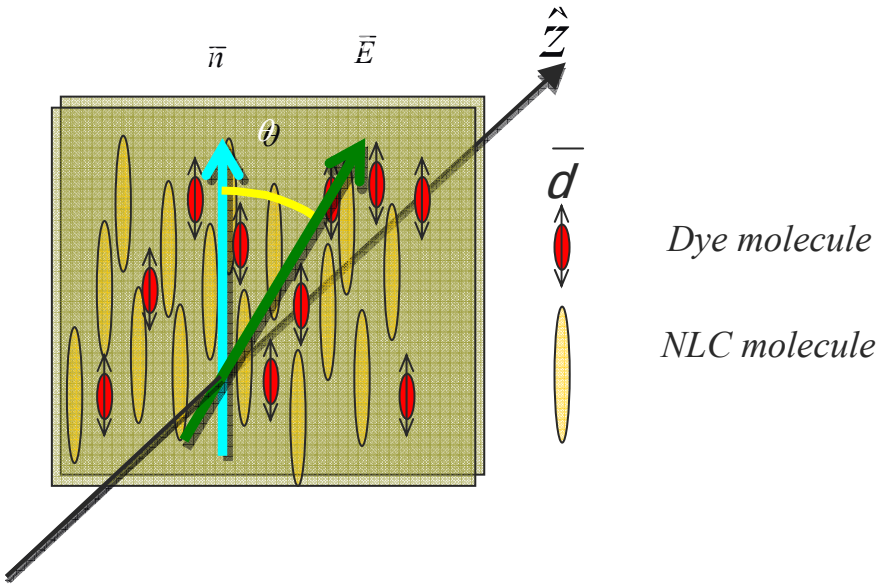

Fig.4.13. Scheme showing the proposed preferential orientation of the dye molecules inside a wedge cell. θ is the angle between the direction of the local molecular director and the input polarization direction of the pump beam.

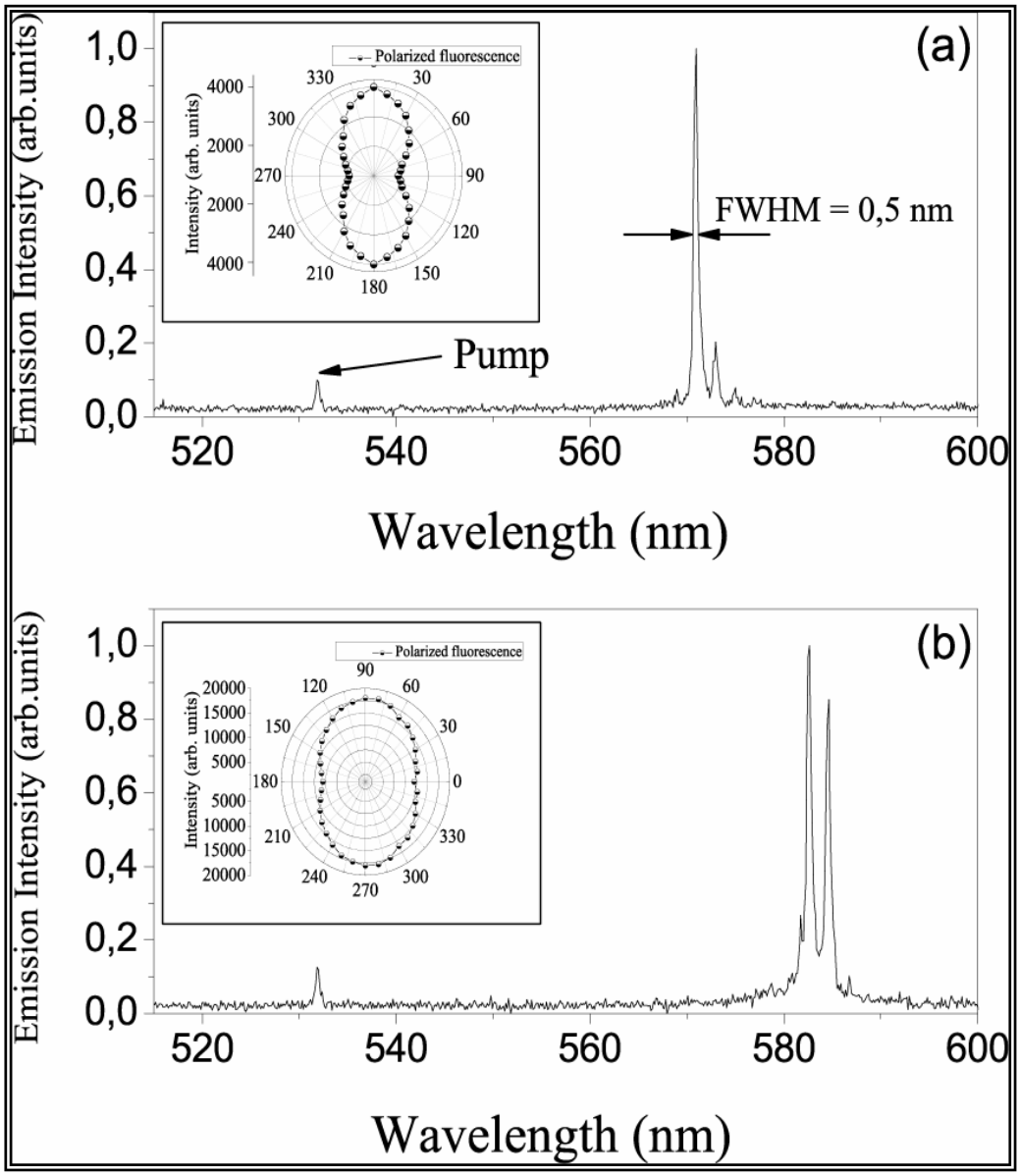

Fig.4.14. Wedge cell (a) and capillary tube (b) emission spectra show different lasing wavelengths and numbers of lasing modes. The insets show the dependence of the polarized fluorescence on the angle θ between the linearly polarized light and the local nematic director orientation for the two confining geometries.

Therefore, these processes are governed by the projection $E \circ d$. In addition, the experimental results emphasize that the fluorescent molecules adopt to some degree the local nematic order of the liquid crystal solvent, which results in an anisotropic orientational distribution of the transition dipole moment. Polarized fluorescence measurements (insets of Fig.4.14) show a more pronounced anisotropy for the wedge

cell. This clearly indicates that the dye molecules adopt to some degree the higher order parameter and the alignment of the nematic phase confined in the wedge cell with respect to the degenerate alignment within the untreated cylindrical capillary.
The dye order parameter S_D can be calculated as follows:

$$S_D = \frac{\left(\frac{F_\perp}{F_{//}}\right)^{1/2} - 1}{\left(\frac{F_\perp}{F_{//}}\right)^{1/2} + 2} \qquad (4.13).$$

Here $F_{//}$ and $F_\perp$ are fluorescence intensities polarized parallel and perpendicular to the NLC director, respectively.
Therefore, this confirms that the dipolar coupling modifies the quantum yield for fluorescence and plays an important role for the light amplification process; some states of polarization of the pump pulses provide a larger number of spontaneously emitted photons which are radiated in the lasing modes.
It is worth to point out that the maximum of the lasing intensity was obtained for linearly polarized pump pulses with *E* oriented along the local director ($\theta = 0°$), being in good agreement with the polarized fluorescence results as well as the polarization dependence of the scattering intensity.

The lasing threshold for the two types of confinement is quite different. Experimental results show that for the wedge cell the lasing threshold is lower than in the case of the microcylinder.

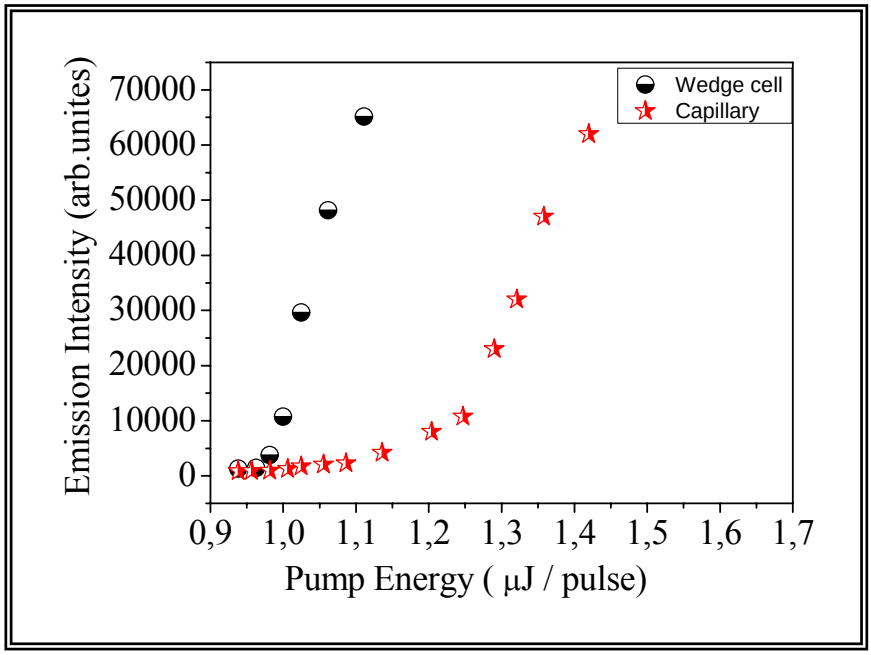

Fig.4.15. Emission Intensity vs Pump Energy for the wedge cell and capillary glass microtube.

In order to gain further understanding on the diffusive laser action observed in this partially ordered system, a comparative study of the emission properties of systems with different order degree was performed. We investigated the input-output characteristics and evaluated the β-factor of the following systems: (i) self-ordered dye doped helixed liquid crystals confined in conventional sandwich type cells [91-93]; (ii) laser dye solution containing ZnO or TiO_2 nanoparticles [94]; (iii) dye doped nematic liquid crystal confined in a wedge cell.

While the first two systems have been widely investigated showing a lasing action with a well known input-output behaviour, the unexplored presented system presents a peculiar intermediate behaviour.

In a conventional laser, β is defined as the ratio of the rate of spontaneous emission into the lasing modes to the total rate of spontaneous emission ($0 \leq \beta \leq 1$) and determines the sharpness of the laser threshold [95]. In the science of cavity laser this parameter is of great interest because of the promise of "thresholdless laser" with β=1, in which all the spontaneous emission is radiated into the lasing modes.

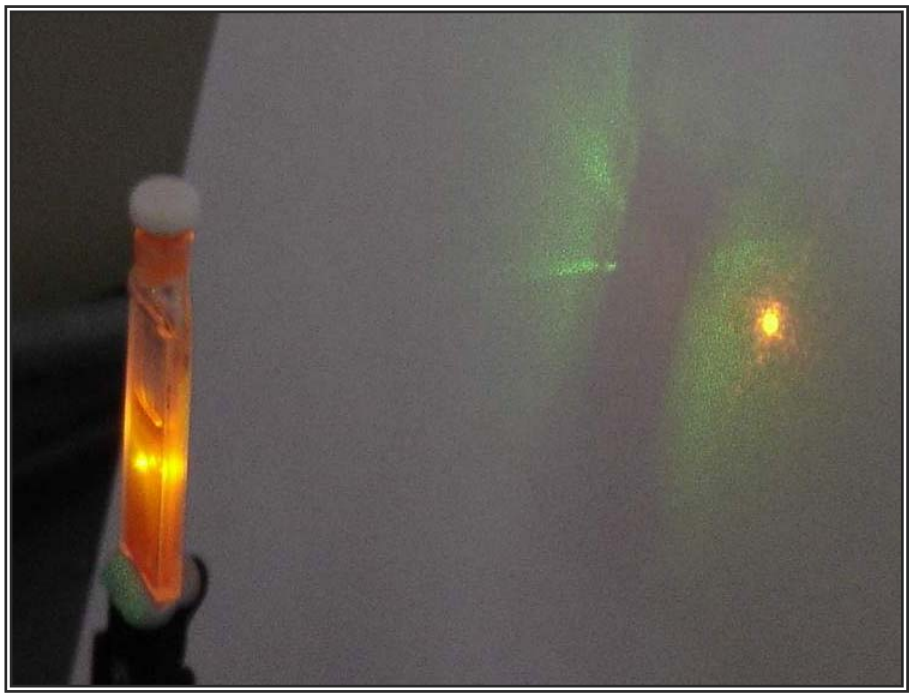

Fig.4.16. Random lasing in a solution of TiO_2 nanoparticles and PM597 dye.

In the figure 4.17. it is presented the integrated emission intensity as function of the input pump energy for the investigated systems characterized by different order degrees. Unlike the sharpness of the lasing threshold observed in the selfordered cholesteric cells ($\beta \sim 0.01$), in which a super-linear increase of the emission intensity is measured above the threshold, the input-output curve measured in the totally random medium shows a stretched-exponential behaviour characterized by $\beta \sim 0.2$. The partially ordered nematic sample exhibits an intermediate behaviour between these two extremes (highly ordered and random systems). In fact, the output energy increases almost exponentially with the pump power ($\beta \sim 0.08$). The presented behaviour suggests that a large part of the spontaneous emission is radiated into the lasing modes because of the sufficient optical feedback provided by the anisotropic coherent backscattering medium.

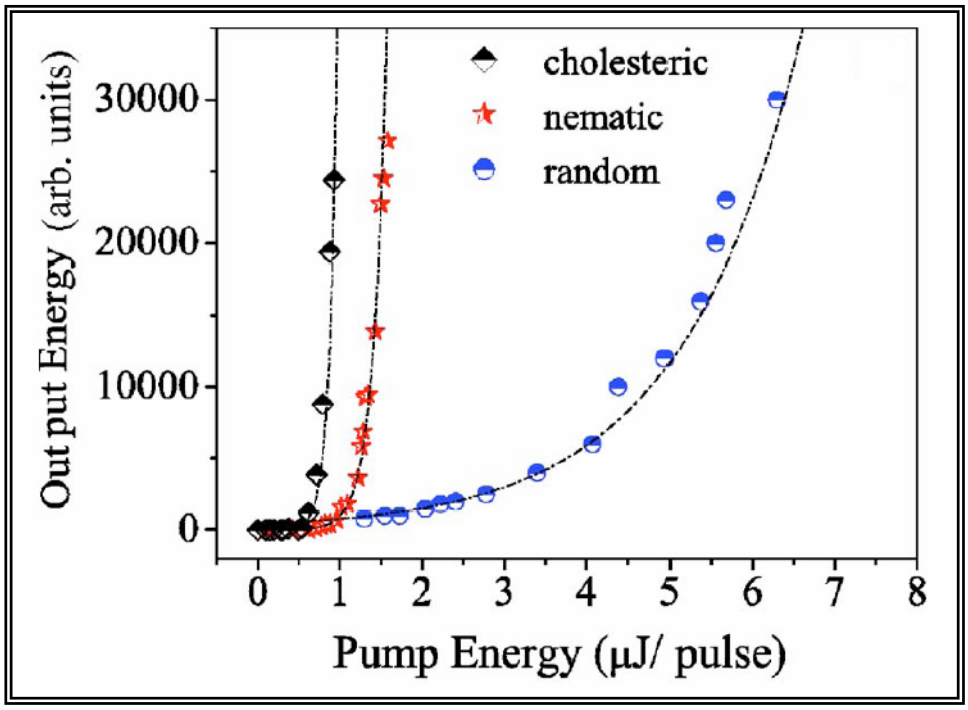

Fig.4.17. Input-output energy curves for the three systems with different order degrees: chiral LC, nematic LC, and nanopowdered dye solution.

This radiative transfer is regulated by the order of the system, as clearly evidenced by the curves reported in Fig.4.17.

Interestingly, upon increasing the temperature of the nematic sample, the diminished nematic order parameter results in a smoother lasing threshold, approaching the threshold behaviour of the fully disordered nanopowdered system (Fig.4.18). The thermally induced disorder comes from an enhancement of the director fluctuations and strong gradients of concentration of the cyanobiphenyl components of the E7 mixture. The enhanced scattering shifts the balance gain-loss because a larger number of spontaneously emitted photons are needed to act as seeds for the stimulated emission process. Thus, increasing the temperature results in having a lasing threshold behaviour similar to the typical stretched exponential curve of the nano-powdered dye solutions.

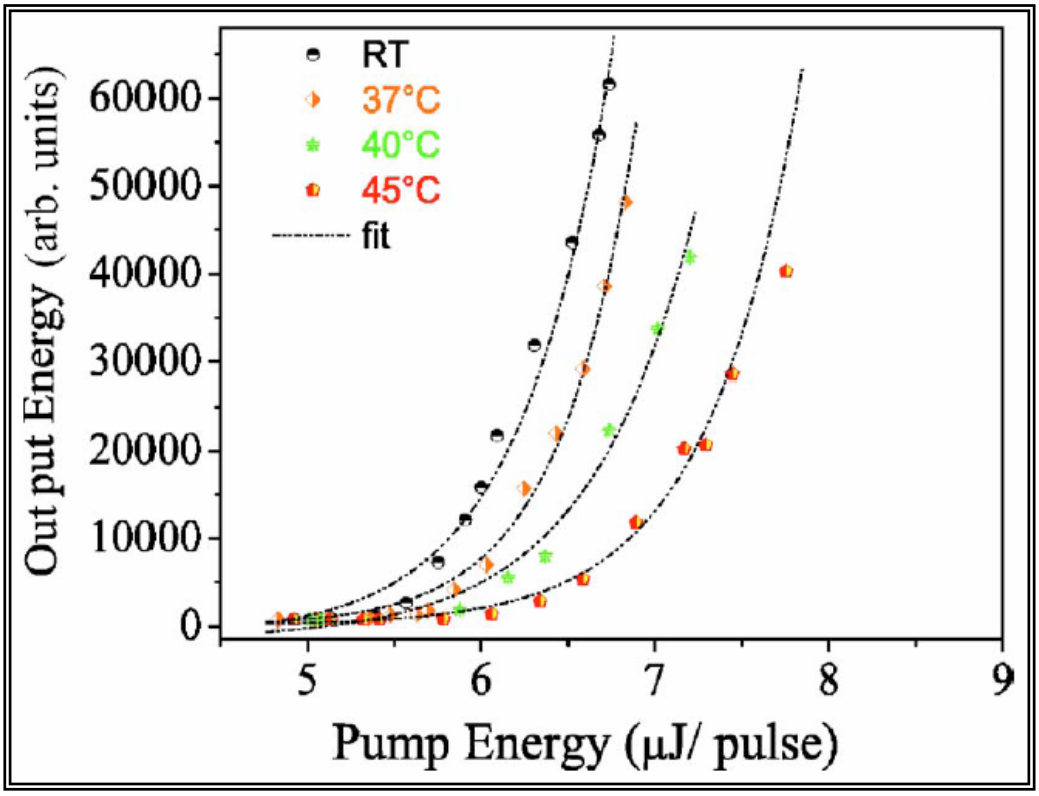

Fig.4.18. Thermal behavior of the β factor for a dye doped nematic liquid crystal sample. Upon increasing the temperature the β factor approaches the value demonstrated for a fully disordered system (TiO_2 nanopowders).

In addition, the thermal analysis of the emission spectra reveals an unexpected behaviour; the emitted light drops off as the temperature approaches 50 °C and reappears in the proximity of nematic-isotropic transition (around 63 °C). This effect is accompanied by a strong scattering of the pump beam during the temperature range over which the lasing is absent, indicating that a cascade of scattering regimes occurs as the temperature varies upward and downward the nematic phase.

We also analyzed the eventual temporal fluctuations in emission intensity in the case of the highly ordered cholesteric and also for the partially ordered nematic samples. The obtained results are depicted in Fig.4.19.

For a fixed input pump energy the cholesteric system shows very small variations in the lasing output intensity (the pump energy was kept at a value which is over the cholesteric sample lasing threshold).

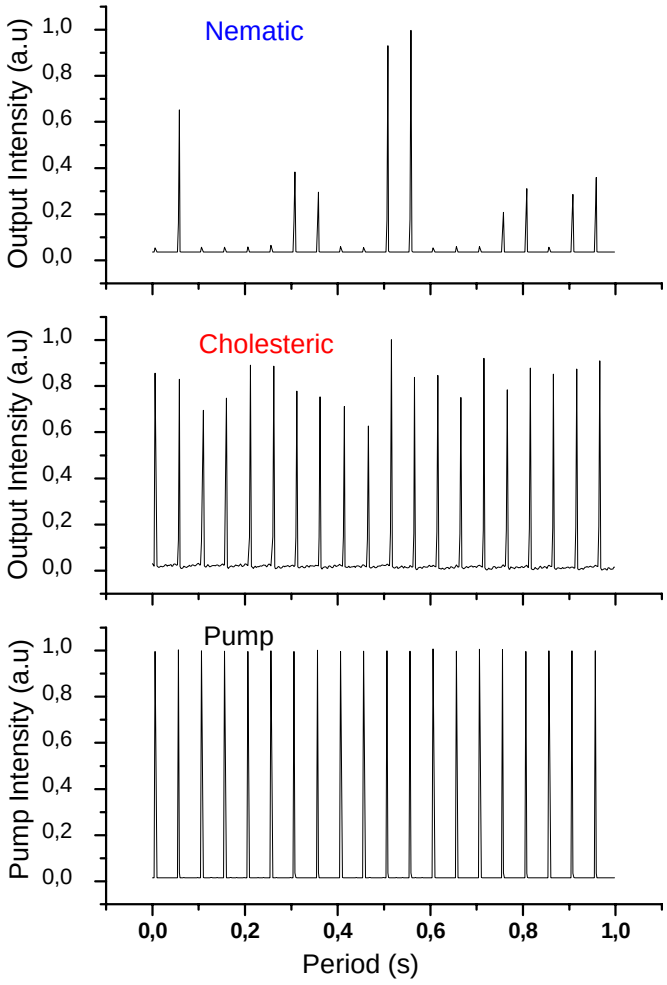

Fig.4.19. Pump and output emission intensities from both cholesteric and nematic dye doped samples as function of time.

Essentially, for each shot of the pump beam the system was in the ON state. A totally different scenario is revealed in the case of the nematic dye doped system, where one can observe that very high oscillations of in the emission intensity are present (even for pump intensities above the lasing threshold). Intermittent OFF and ON states demonstrate a characteristic behaviour for a random laser. Since the condition for lasing comes from a careful balance between gain and loss, it is clear that in this case

not for every pump pulse the random walk inside the anisotropic medium gathers enough gain for the system to lase.

Finally, the far field spatial distribution of the emitted light was analyzed. Lasing emission was captured in a limited cone angle (~0.1 rad) by means of a high resolution CCD camera (1390 X 1024 12bit PixelFlyQe by PCO). This reveals a series of bright tiny spots spatially overlapped creating a richly structured pattern. In Fig.4.20 the spatial distribution is compared with the expected pseudo-Gaussian lasing profile obtained for a well ordered helixed liquid crystal creating a one-dimensional photonic band gap structure.

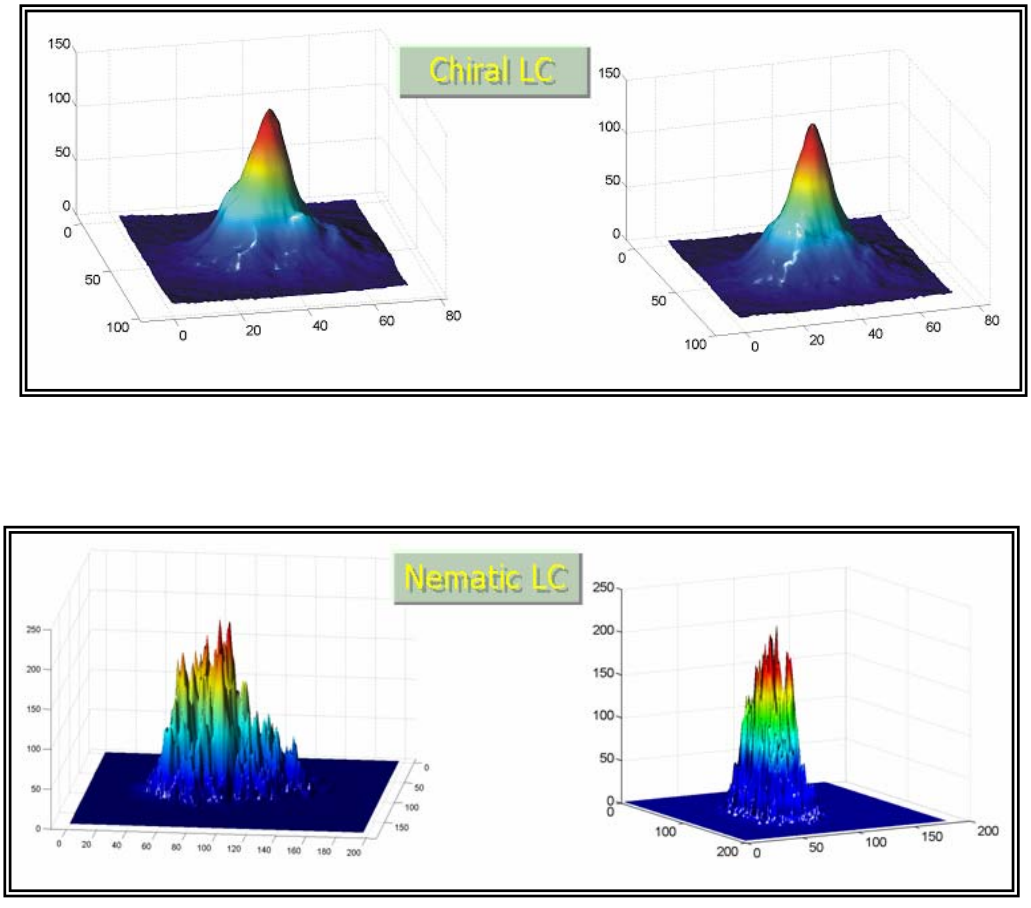

Fig.4.20. Intensity spatial distribution showing a Pseudo-Gaussian profile obtained for a well ordered helixed liquid crystal sample (top) is compared with (bottom) the laser emisssion for a dye doped NLC wedge cell. Bright tiny spots spatially overlapp describing a richly structured emission pattern typical of diffusive laser action.

This emission mechanism is based on the diffusive process of spontaneously emitted photons by fluorescent guest molecules launched at random directions from random positions (Fig.4.21). These photons are involved in a weak localization process within the gain medium because of recurrent multiple scattering.

The entrapment of the emitted photons for enough time gives rise to reciprocal paths providing the optical feedback. In fact, the reciprocal paths are responsible of interference effects which survive in multiple scattering, because generally the phase accumulates equally in such paths.

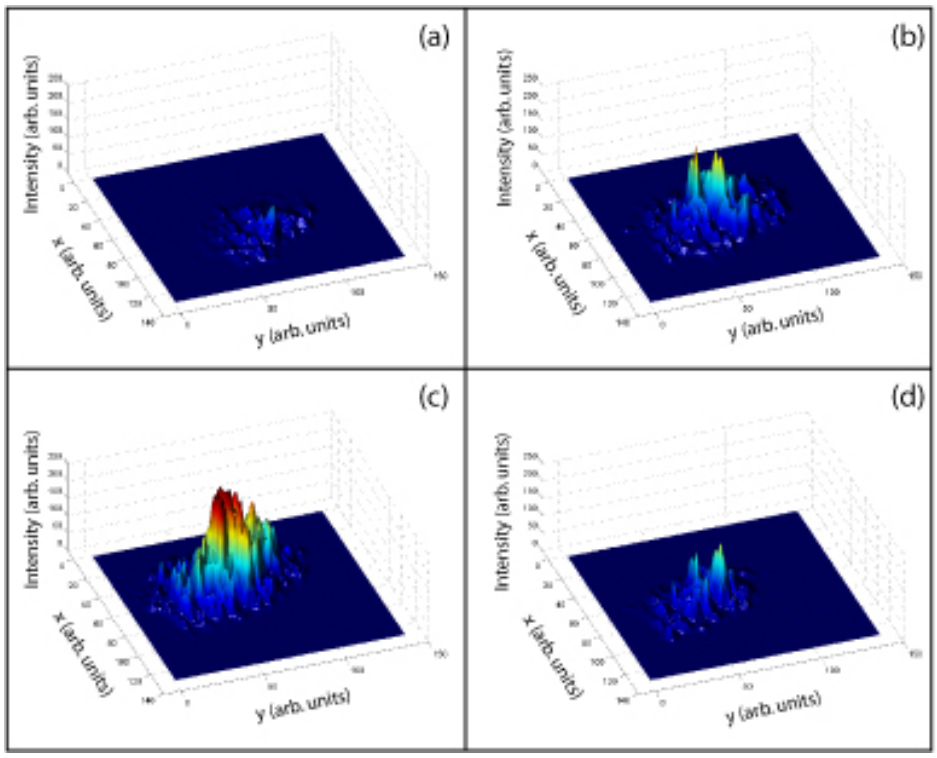

Fig.4.21. Spatial distribution of the intensities profile in a wedge NLC sample in the case of four succesive (a,b,c,d) pump beam pulses (f = 10Hz) demonstrate an intermittent behaviour – both spatial and temporal – of the emission.

4.10. Random Lasing in Free Standing and Freely Suspended Dye Doped Nematic Liquid Crystals

Recently we started investigating the behaviour of free standing (e.g. a drop of material on a glass surface) and freely suspended (e.g. thin film of material holding to a bounding support by surface tension) dye doped nematic liquid crystals. With great enthusiasm we found out that these systems lase when optically pumped with an excitation laser.

We briefly introduce the first experimental evidence of random lasing in free standing and freely suspended dye doped nematic liquid crystals together with an experimental overview of some of the most interesting results.

Lasing action has been previously mentioned in cholesteric liquid crystalline elastomers, PDLC systems but never before in a freely suspended dye doped liquid crystalline film.

The active mixture consists of nematic liquid crystal, BL001 provided by Merck (*Cr*. – -10°C – *Nematic* – 63°C – *Iso*) doped with 0.3 wt% of Pyrromethene 597 or Pyrromethene 650 dye (Exciton). A small amount from this mixture was then spread on top of a rectangular network (l=2-3mm, depth=0.2-0.5mm) by means of a spatula. In this way we tailored a simple system where we have several parallelepipedic "holes" filled with a thin film of active material, as depicted in the figure. Other geometries (disk, rectangular) of various sizes have also been used for moulding the shape of thin films.

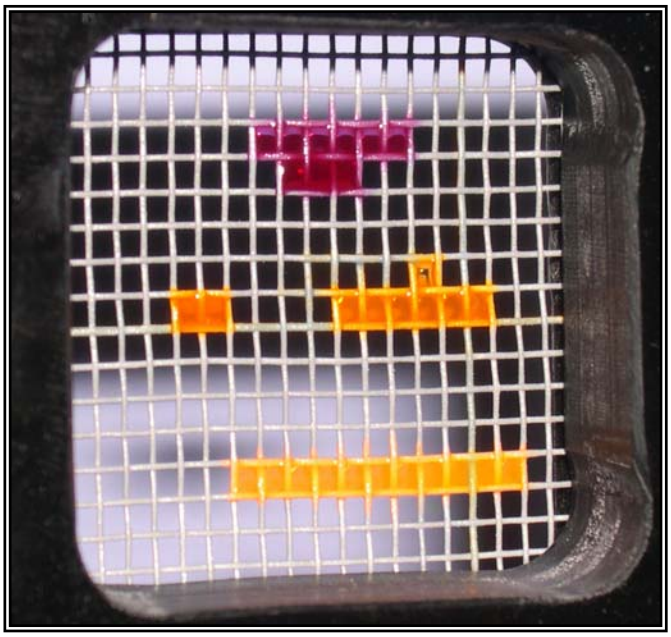

Fig.4.22. Network containing several freely suspended thin films of dye doped nematic liquid crystal.

The system was then optically pumped with 3-5 ns pulses (f= up to 20 Hz) produced by a frequency-doubled (532 nm) Nd:YAG laser (NewWave, Tempest 20).

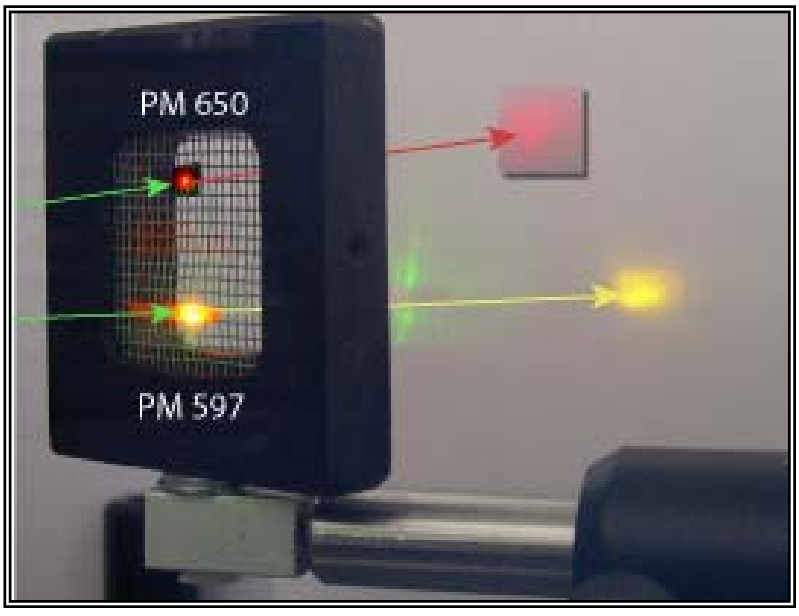

Fig.4.23. Random lasing in freely suspended thin films of dye doped nematic liquid crystal.

Figure 4.23 presents the obtained intermittent speckle like pattern of granular aspect. By investigating the emission spectra we can clearly acknowledge that random lasing occurs above a given input threshold value for which the coherent backscattering is sufficient enough to promote the gain inside the active material.

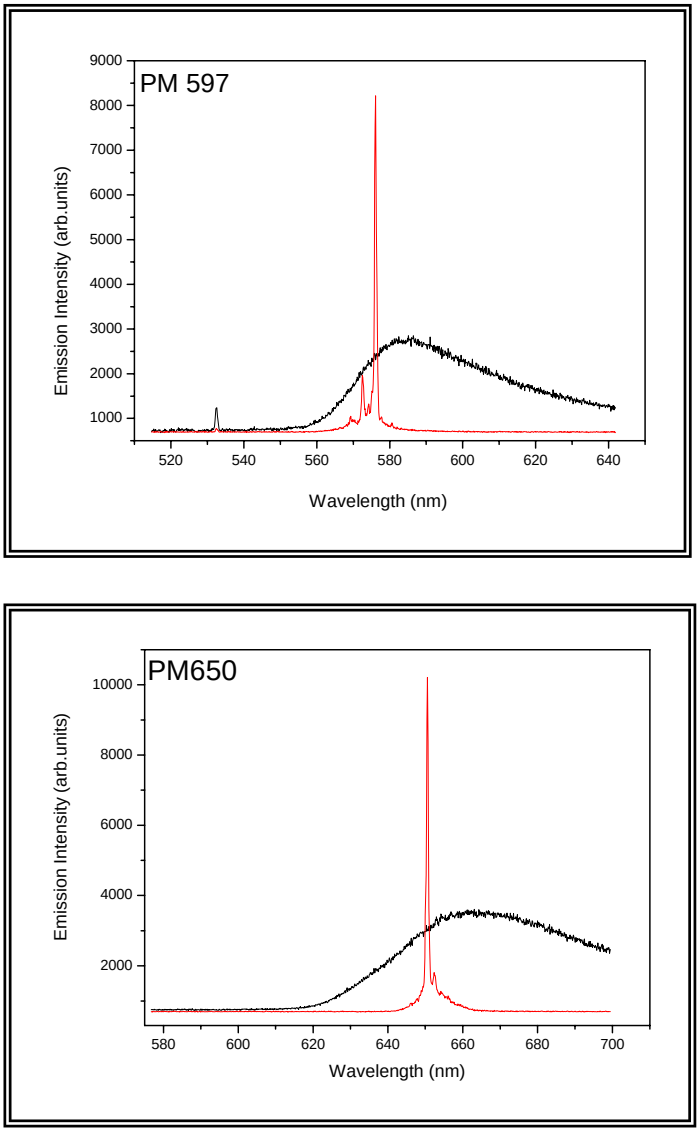

Fig.4.24. Fluorescence and lasing spectra in thin films of freely suspended NLC doped with (top) Pyrromethene 597 and (bottom) Pyrromethene 650.

Measured lasing FWHM is about 0.5 nm, limited by the resolution of the CCD detector. Detailed future investigations were planned for fully characterizing these novel lasing systems.

4.11. Conclusions

For the first time, it was observed and characterized the process of random laser action in confined dye doped nematics - under diverse boundary conditions (i.e., geometry, size, and surface treatment).

The underlying mechanism is mainly based on interference effects which survive to recurrent multiple scattering driven by nematic director fluctuations. Coherent backscattering experiments performed on similar systems have already proven that interference effects leads to weak localization of light waves.

Weakly localized light waves into dye doped nematic sample are responsible for amplification while the resonance frequencies are selected through interference phenomena of the counter-propagating light waves within the localized loops. For simplicity, photons spontaneously emitted by the fluorescent guest molecules are launched at random directions from random positions within the excited volume. Because of the recurrent multiple scattering the probability to trace reciprocal paths by these photons is not null, as demonstrated by coherent backscattering experiments, thus resulting in equal phase accumulation during these open loops. While the gain length is comparable with the transport mean free path the emission of other photons is stimulated before the recurrently scattered photons leave the sample, triggering a coherent chain reaction. When the balance gain-loss becomes positive the optically excited dye doped nematic start to lase. Unlike distributed feedback mirror-less laser, this system can be considered as a cavity-less microlaser where the disorder unexpectedly plays the most important role, behaving as randomly distributed feedback laser. We found that the dye transition dipole moments adopt in some degree the orientational order parameter of the nematic director, resulting in a control of the emission intensity by varying the polarization of the pump beam. In addition, the evaluated β-factor for the presented system yields an intermediate value with respect to

the random and fully ordered systems, suggesting that the order parameter drives the amount of spontaneous emission radiated into the lasing modes. The thermal behavior of the laser action is an example in this way.

Many further studies will be needed in order to gain full understandings of the diffusive laser action in nematic samples. For this, a wide series of experiments, simulations and extensive investigations have been planned.

References

[1]. P.W. Anderson, Phys. Rev. 109, 1492 (1958).

[2]. J.W.S. Rayleigh, Philos. Mag. 41, 107, 274 (1871).

[3]. J.W.S. Rayleigh, Philos. Mag. 41, 447 (1871).

[4]. C. F. Bohren and D. R. Huffman, Absorption and scattering of light by small particles, John Wiley & Sons, New York, (1983).

[5]. H. C. van de Hulst, Light scattering by small particles, Dover, New York, (1981).

[6]. G. Mie, Ann. Phys. (Leipzig) 25, 377 (1908).

[7]. Y.-L. Geng, X.-B. Wu, L.-W. Li, and B. R. Guan, Phys. Rev. E 70, 056609 (2004).

[8]. A.F. Ioffe and A.R. Regel, Prog. Semicond. 4, 237 (1960).

[9]. M.B. van der Mark, Propagation of Light in Disordered Media, PhD. Thesis, (1990).

[10]. D.E. Khmel'nitskii, Physica 126 B, 235, (1994).

[11]. G. Parry, Opt. Comm, 12, 75 (1974).

[12]. N.Garcia, A.Z.Genack, Phys. Rev. Lett.63, 1678 (1989).

[13]. M. Tomita, M. Matsuok, Phys. Rev. B, 43, 13579 (1991).

[14]. A Lagendijk, Bart A. van Tiggelen, Physics Reports 270, (1996).

[15]. M. P. van Albada, B. A. van Tiggelen, A. Lagendijk, and A. Tip, Phys. Rev. Lett. 66, 3132–3135 (1991).

[16]. P. Sheng, Introduction to wave scattering, localization, and mesoscopic phenomena, Academic Press, New York, (1995).

[17]. P.A. Lee and T.V. Ramakrishnan, Rev. of Modern Phys. 57, 287 (1985).

[18]. B.L. Altshuler, A.G. Aronov, D.E. Khmel'nitskii, and A.I. Larkin, Quantum Theory of Solids, MIR Publishers, Moskva, (1983).

[19]. S. John, Phys. Rev. Lett. 53, 2169 (1984).

[20]. D. Vollhardt and P. Wolfle., Phys. Rev. Lett. 45, 842 (1980).

[21]. D. Vollhardt and P. Wolfle Phys. Rev. B 22, 4666 (1980).

[22]. D. Vollhardt and P. Wolfle Phys. Rev. Lett. 48, 699 (1982).

[23]. E.N. Economou, C.M. Soukoulis, and A.D. Zdetsis, Phys. Rev. B 31, 6483 (1985).

[24]. Y. Kuga and A. Ishimaru, J. Opt. Soc. Am. A 8, 831 (1984).

[25]. M.P. van Albada and A. Lagendijk, Phys. Rev. Lett. 55, 2692 (1985).

[26]. P.E. Wolf and G. Maret, Phys. Rev. Lett. 55, 2696 (1985).

[27]. E. Akkermans, P.E. Wolf, and R. Maynard, Phys. Rev. Lett. 56, 1471 (1986).

[28]. R. Dalichaouch, J. P. Armstrong, S. Schultz, P. M. Platzman and S. L. McCall, Nature 354, 53 (1991).

[29]. A.Z. Genack and N. Garcia, Phys. Rev. Lett. 66, 2064 (1991).

[30]. D.S. Wiersma, P. Bartolini, A. Lagendijk, and R. Righini, Nature 390, 671 (1997).

[31]. M.P. van Albada, J.F. de Boer, and A. Lagendijk, Phys. Rev. Lett. 64, 2787 (1990).

[32]. P. Sebbah, B. Hu, A. Z. Genack, R. Pnini, and B. Shapiro, Phys. Rev. Lett. 88, 123901 (2002).

[33]. K. M. Watson, J. Math. Phys. 10, 688–702 (1969).

[34]. M. Kaveh et al., Phys. Rev. Lett. 57, 2049 (1986).

[35]. D. S.Wiersma et al., Phys. Rev. Lett. 74, 4193 (1995).

[36]. G. Labeyrie et al., Phys. Rev. Lett. 83, 5266 (1999).

[37]. Y. Bidel et al., Phys. Rev. Lett. 88, 203902 (2002).

[38]. I. Freund et al., Phys. Rev. Lett. 61, 1214 (1988).

[39]. D. S.Wiersma, M. P. van Albada, and A. Lagendijk, Phys.Rev. Lett. 75, 1739 (1995).

[40]. D.V. Vlasov et al., Pisma Zh. Eksp. Teor. Fiz. 48, 86 (1988).

[41]. L.V. Kuzmin, V. P. Romanov, and L. A. Zubkov, Phys. Rev. E 54, 6798 (1996).

[42]. A. F. Koenderink et al. Phys. Lett. A 268, 104 (2000).

[43]. J. Huang et al., Phys. Rev. Lett. 86, 4815 (2001).

[44]. V. P. Romanov and A. N. Shalaginov, Opt. Sectrosc. 64, 774 (1988).

[45]. B. A. van Tiggelen, R. Maynard, and A. Heiderich, Phys. Rev. Lett. 77, 639 (1996).

[46]. H. Stark and T. C. Lubensky, Phys. Rev. Lett. 77, 2229 (1996).

[47]. M. H. Kao et al., Phys. Rev. Lett. 77, 2233 (1996).

[48].H. Stark et al., J. Opt. Soc. Am. A 14, 156 (1997).

[49]. D. S. Wiersma et al., Phys. Rev. Lett. 83, 4321 (1999).

[50]. P.M. Johnson et al., Phys. Rev. Lett. 89, 243901 (2002).

[51]. H. K. Vithana, L. Asfaw, and D. L. Johnson, Phys. Rev. Lett. 70, 3561 (1993).

[52]. R.Sapienza et al., Phys. Rev. Lett. 92, 3 (2004).

[53]. S.V. Frolov, Z.V. Vardeny, K. Yoshino, A. Zakhidov, and R, Baughman., Phys. Rev. B 59, R5284 (1999).

[54]. H. Cao, Y.G. Zhao, S.T. Ho, E.W. Seeling, Q.H. Wang, and R.P.H. Chang, Phys. Rev. Lett. 82, 2278 (1999).

[55]. H. Cao, J.Y. Xu, E.W. Seeling, and R.P.H. Chang, Appl. Phys. Lett. 76, 2997 (2000).

[56]. H. Cao et al., Phys. Rev. Lett. 84, 5584 (2000).

[57]. H. Cao, Y. Ling, J.Y. Xu, C.Q. Cao, and P. Kumar, Phys. Rev. Lett. 86, 4524 (2001).

[58]. A. Mitra and R.K. Thareja, J. Appl. Phys. 89, 2025 (2001).

[59]. S.V. Shkunov, M.C. Dalong, M.E. Raikh, Z.V. Vardeny, A.A. Zakhidov, and R.H.
Baughman, Synthetic Met. 116, 485 (2001).

[60]. G. van Soest. Experiments on random lasers, PhD. thesis, University of Amsterdam

(2001).

[61]. V.S. Letokhov, Sov. Phys. JETP 26, 835 (1968).

[62]. W.L. Sha, C.-H. Liu, and R.R. Alfano, Opt. Lett. 19, 1922 (1994).

[63]. D.S.Wiersma, M.P. van Albada, and A. Lagendijk., Phys. Rev. Lett. 75, 1739 (1995).

[64]. M. Siddique, R.R. Alfano, G.A. Berger, M. Kempe, and A.Z. Genack, Opt. Lett. 21,
450 (1996).

[65]. P.C. de Oliveira, A.E. Perkins, and N.M. Lawandy, Opt. Lett. 21, 1685 (1996).

[66]. G.A. Berger, M. Kempe, and A.Z. Genack, Phys. Rev. E 56, 436 (1997).

[67]. G. van Soest, M. Tomita, and A. Lagendijk, Opt. Lett. 24, 306 (1999).

[68]. X. Jiang and C.M. Soukoulis, Phys. Rev. Lett. 85, 70 (2000).

[69]. G. van Soest, F.J. Poelwijk, R. Sprik, and A. Lagendijk, Phys. Rev. Lett. 86, 1522 (2001).

[70]. D.S. Wiersma , Nature 406, 132 (2000).

[71]. D.S. Wiersma and S. Cavalieri, Nature 414, 709 (2001).

[72]. D.S. Wiersma , M. P. Albada and A. Lagendijk, Nature 373, 203 (1995).

[73]. D.S Wiersma and A. Lagendijk, Phys. Rev. E 54, 4256 (1997).

[74]. D.S. Wiersma and A. Lagendijk, Phys. World 10, 33 (1997).

[75]. H. Cao et al., Phys. Rev. E 66, R25601 (2002).

[76]. H. Cao et al., Appl. Phys. Lett. 75, 1213 (1999).

[77]. H. Cao et al., Phys. Rev. B 59, 15107 (1999).

[78]. H. Cao et al., Appl. Phys. Lett. 73, 3656 (1999).

[79]. H. Cao et al., Phys. Rev. Lett. 82 ,2278 (1999).

[80]. X. Jiang and C.M. Soukoulis, Phys. Rev. E 65 (2002).

[81]. M. Patra, H. Schomerus, and C.W.J. Beenakker, Phys. Rev. A 61, 023810 (2000).

[82]. H. Cao, X. Jiang, Y. Ling, J.Y. Xu, and C.M. Soukoulis, Phys. Rev. B 67, 161101 (2003).

[83]. J. D. Joannopoulos, R. D. Meade, and J. N.Winn, Photonic Crystals:Moulding the Flow of Light, Princeton University Press, Princeton, NJ, (1995).

[84]. V. M. Markushev, V. F. Zolin and Ch. M. Briskina, Sov. J. Quantum Electron. 16, 281 (1986).

[85]. C. Gouedard, D. Husson, C. Sauteret, F. Auzel and A. Migus, J. Opt. Soc. Am. B 10, 2358 (1993).

[86]. M. A. Noginov, N. E. Noginov, H. J. Caulfield, P. Venkateswarlu, T. Thompson, M. Mahdi, and V. Ostroumov, J. Opt. Soc. Am. B 13, 2024 (1996).

[87]. R. Sapienza, S. Mujumdar, C. Cheung, A. G. Yodh, D. Wiersma, Phys. Rev. Lett. 92, 033903 (2005).

[88]. P. G. deGennes, The Physics of the Liquid Crystals, Oxford University Press, New York, (1974).

[89]. Strangi G., Ferjani S., Barna V., De Luca A., Scaramuzza N., Versace C., Umeton C., Bartolino R. Optics Express, 14, 17, 7737-7744 (2006).

[90]. Ferjani S., Barna V., De Luca A., Scaramuzza N., Versace C., Umeton C., Bartolino R., Strangi G. Applied Physics Letters 89, 121109 (2006).

[91]. J. Schmidtke, W. Stille, H. Finkelmann, and S.T. Kim, Adv. Mater. 14, 746 (2002).

[92]. M. Ozaki, M. Kasano, D. Ganzke, W. Haase, and K. Yoshino, Adv. Mater. 14, 306 (2002).

[93]. G. Strangi, V. Barna, R. Caputo, A. De Luca, G. N. Price, C. Versace, N. Scaramuzza, C. Umeton, and R. Bartolino, Phys. Rev. Lett. 94, 063903 (2005).

Editor's choice for the 2005 Virtual J. Nanoscale Sci. Technol., 11 (8) (2005).

[94]. H. Cao, J. Y. Xu, E. W. Seelig, and R. P. H. Chang, Appl. Phys. Lett., 76, 2997 (2000).

[95]. G. V. Soest and Ad Lagendijk; Phys. Rev. E, 65, 047601 (2002).

Perspectives

During the three years of the Ph.D course I was involved in a succession of very captivating physical research activities. Throughout this period I gained knowledge and practical experience in the fields of Polymers and Plasma Polymerization, Electro-Optics of Liquid Crystals, Photonic Crystals, Mirror-less Liquid Crystal Lasers.
Subjects like ultra-fast electro-optic switching in nematic liquid crystals; Design, fabrication and characterization of organic microcavities for confining light; Laser action in ordered, partially ordered and random media are just few examples of topics of great interest for today's research.
The experimental results together with the proposed models are self-consistent and they open also new horizons for the field of applied physics. The prospective realization of LCD panels without TFTs, tunable micro laser arrays for photosensitive drug delivery systems or high precision surgery, integrated waveguide optical systems, liquid crystal lenses can now be considered as near-future intentions.
Nevertheless, these concepts can be moulded and further developed as they could represent an exceptionally promising route of potential fundamental studies for the fields of polymers, condensed matter, opto-electronics and photonics.

Acknowledgements

I am deeply grateful to my Parents, my Teachers, my Colleagues and to all of my Friends at UNICAL.

List of Publications

The Ph.D research work described in this thesis has been published in the following papers:

"Fast electro-optic switching in nematic liqiud crystals"
A.L.Ionescu, A.Ionescu, E.S.Barna, **V. Barna**, N. Scaramuzza,
Applied Physics Letters Vol 84(1) pp. 40-42. January 5, (2004)

"Molecular simulation of the free surface order in NLC samples"
N. Scaramuzza, C.Berlic, **V. Barna**, E.S.Barna, G.Strangi, A.Ionescu,
J.Phys.Chem.B, 108(10), 3207-3210, (2004)

"Role of delocalized electrons in polyaniline – nematogen cyanobiphenyls interaction"
A.L.Ionescu, A.Ionescu, E.S.Barna, **V.Barna**, N. Scaramuzza,
J.Phys.Chem.B 108(26), 8894-8899, (2004)

"Color-Tunable Organic Microcavity Laser Array Using Distributed Feedback"
G. Strangi, **V. Barna**, R. Caputo, A. de Luca, C. Versace,
N. Scaramuzza, C. Umeton, R..Bartolino, G.Price
Physical Review Letters 94, 063903, (2005)

"Color-Tunable Organic Microcavity Laser Array Using Distributed Feedback"
Strangi G., **Barna V**., Caputo R., De Luca A., Versace C.,
Scaramuzza N., Umeton C. P., Bartolino R., Price G.
Editor's choice for Virtual Journal of Nanoscale Science and Technology,
Vol. 11, n.8, (2005)

"Band-Edge and Defect Modes Lasing Due to Confinement of Helixed Liquid Crystals in Cylindrical Microcavities"

Barna V., Ferjani S., Strangi G., De Luca A.,Versace C., Scaramuzza N.

Published as article in Appl. Phys. Lett. 87, 221108 (2005)

Published as cover in Applied Physics Letters November 2005 Issue.

"Distributed FeedbackMicro-Laser Array: Helixed Liquid Crystals Embedded in Holographically Sculptured Polymeric Microcavities"

Barna V., Caputo R., De Luca A., Scaramuzza N., Strangi G., Versace C., Umeton C. , Bartolino R., Price G. N.

Optics Express, Vol.14, 7, pp 2695-2705, April 2006

"Random Lasing and Weak Localization of Light in Dye-Doped Nematic Liquid Crystals"

Strangi G., Ferjani S., **Barna V.**, De Luca A., Scaramuzza N., Versace C., Umeton C., Bartolino R.

Optics Express, 14, 17, 7737-7744 (2006)

"Thermal Behaviour of Random Lasing in Dye Doped Nematic Liquid Crystals"

Ferjani S., **Barna V.**, De Luca A., Scaramuzza N., Versace C., Umeton C., Bartolino R., Strangi G.

Applied Physics Letters 89, 121109 (2006)